Adipocyte-derived extracellular vesicles: characterisation and function

by

Katherine Diana Connolly

A thesis submitted for the degree

DOCTOR OF PHILOSOPHY

Institute of Molecular and Experimental Medicine

Wales Heart Research Institute

Cardiff University School of Medicine

2016

DECLARATION

This work has not been submitted in substance for any other degree or award at this or any other university or place of learning, nor is being submitted concurrently in candidature for any degree or other award.

Signed ………………………………………… (candidate) Date …………………

STATEMENT 1

This thesis is being submitted in partial fulfilment of the requirements for the degree of PhD

Signed ………………………………………… (candidate) Date …………………

STATEMENT 2

This thesis is the result of my own independent work/investigation, except where otherwise stated. Other sources are acknowledged by explicit references. The views expressed are my own.

Signed ………………………………………… (candidate) Date …………………

STATEMENT 3

I hereby give consent for my thesis, if accepted, to be available online in the University's Open Access repository and for inter-library loan, and for the title and summary to be made available to outside organisations.

Signed ………………………………………… (candidate) Date …………………

*To my parents and family, for their constant love*

and support

Acknowledgements

My sincere thanks go to my supervisors, Professor Phil James and Dr Aled Rees. I can't thank you enough for the opportunities, help and advice you've given me throughout my PhD.

A special thank you to Dr Aled Clayton and his group at Velindre, particularly to Mr Vincent Yeung. Also to Dr Irina Guschina, Dr Keith Morris and Mr Nurudeen Hassan, Professor Marian Ludgate and Dr Mohd Shazli Draman, Dr Chris Von Ruhland, Dr Kristin Ladell, Professor Maurice Hallet, and Dr Andy Devitt and Miss Parbata Chauhan for their help and support with this work.

Thank you to my friends and colleagues, past and present, Dr Jessica Tiplady, Dr Ewelina Sagan, Dr Gareth Willis, Dr Laurence Thornhill, Miss Megan Curzon, Dr Rebecca Wadey, Dr Joanne Welton, Dr Fairoz Abdul, Dr Justyna Witzcak, Mr Nicholas Burnley-Hall, and Miss Donna Mathew. A further thank you to my friends, Miss Jessica Davis, Miss Rhiannon Roberts, Miss Sami Jennings, Dr Monika Seidel, Dr Kirsten Smith, Miss Libby Ellins, and Miss Luned Badder.

A final thank you to Miss Joni Quintanilla and Mrs Hannah Taylor for your love and friendship.
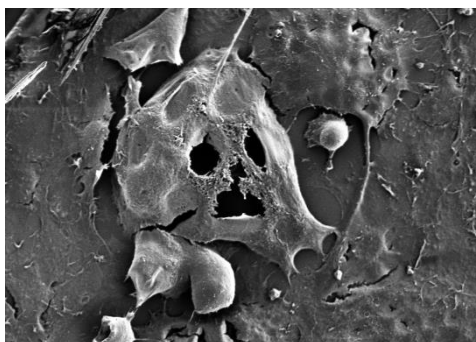
Scaredy fat: A scanning electron microscope image of a 3T3-L1 mature adipocyte.

"It does not do to dwell on dreams and forget to live"

JK Rowling via Albus Dumbledore

Table of Contents

Summary

Extracellular vesicles (EVs) are submicron vesicles released from cells as intercellular communicators. EV research is hindered by a current lack of standardisation. However, mounting evidence suggests a role for EVs in both physiological and pathophysiological processes. Little is known about adipocyte-derived EVs despite the recognition of adipose tissue (AT) as an endocrine organ and the role of dysfunctional AT in disease. Obese AT develops regions of hypoxia and inflammation, leading to obesity-associated metabolic complications. The aim of this thesis was to explore EVs as novel adipocyte communicators, characterising their release under physiological and disease-like conditions.

Nanoparticle tracking analysis (NTA) and tunable resistive pulse sensing (TRPS) were assessed for their accuracy and usability for EV quantification. NTA and TRPS both accurately quantified EVs though NTA was more user-friendly. The choice of anticoagulant, filtering and storage of EVs all affected EV concentration.

Physiological EV release from 3T3-L1 adipocytes was characterised pre- and post-adipogenesis. EV generation increased prior to adipogenesis and EVs were enriched in pro-signalling fatty acids and proteins characteristic of the original cell. Therefore, EVs may aid the initiation of adipogenesis. Hypoxia was then used to pathologically generate EVs to mimic adipocyte obesity. Adipocyte EV release increased in hypoxia; these EVs were enriched in pro-signalling fatty acids and monocyte chemoattractant protein-1. Hypoxic EVs were then analysed for their interaction with macrophages (Mϕ). Hypoxic EVs may increase Mϕ migration and promote an anti-inflammatory Mϕ phenotype; further repeats are needed to confirm this.

Finally, adipocyte markers were detected in plasma EVs suggesting the presence of circulating adipocyte-derived EVs *in vivo*. Plasma EVs were also reduced in hypercholesterolaemia patients by routine apheresis treatment.

In conclusion, adipocytes release EVs which may assist intercellular communication in both physiological and disease-like conditions. Adipocyte-derived EVs can be detected *in vivo* and may provide novel biomarkers of obesity-associated diseases.

Abbreviations

A

ABC	ATP-binding cassette
ACD	Acid citrate dextrose
ADRF	Adipose-derived relaxing factor
AFM	Atomic force microscopy
AMPK	Adenosine monophosphate-activated protein kinase
APS	Ammonium persulphate
AT	Adipose tissue
AT-BF	Adipose tissue blood flow/perfusion
ATP	Adenosine triphosphate

B

BAT	Brown adipose tissue
BBB	Blood-brain barrier
BCA	Bicinchoninic acid
BMI	Body mass index
BOLD-MRI	Blood oxygen level-dependent magnetic resonance imaging
BP	Blood pressure
BSA	Bovine serum albumin

C

Ca^{2+}	Calcium
CAD	Coronary artery disease
cAMP	cyclic adenosine monophosphate
CAT	Calibrated automated thrombography
CD	Cluster of differentiation
C/EBP	CCAAT/enhancer binding protein
cGMP	cyclic guanosine monophosphate
CLS	Crown-like structure

CRP	C-reactive protein
CTAD	Citrate-theophylline-adenosine-dipyridamole
CVD	Cardiovascular disease

D

DC	Dendritic cell
DLS	Dynamic light scattering
DMEM	Dulbecco's modified eagle medium
DMSO	Dimethyl sulphoxide
DNA	Deoxyribonucleic acid

E

EDTA	Ethylenediaminetetraacetic acid
EGFR	Epidermal growth factor receptor
ELISA	Enzyme-linked immunosorbent assay
EM	Electron microscopy
EPA	Eicosapentaenoic acid
EPC	Endothelial progenitor cells
ESCRT	Endosomal sorting complex required for transport
EV	Extracellular vesicle

F

FABP	Fatty acid binding protein
FAME	Fatty acid methyl ester
FC	Flow cytometry
FCS	Foetal calf serum
FFA	Free fatty acid
FH	Familial hypercholesterolaemia
FMI	Forward migration index

G

GAPDH	Glyceraldehyde 3-phosphate dehydrogenase

GC	Gas chromatography
GC-FID	Gas chromatography with flame ionisation detection
GC-MS	Gas chromatography-mass spectrometry
GLUT	Glucose transporter
GTP	Guanosine triphosphate

H

HDL	High density lipoprotein
HIF	Hypoxia-inducible factor
hPSC	human pluripotent stem cell
HSP	heat shock protein
HUVEC	human umbilical vein endothelial cells

I

ICAM	Intercellular adhesion molecule
IEC	Intestinal epithelial cell
IL	Interleukin
ILV	Intraluminal vesicle
IR	Insulin resistance
ISEV	International Society of Extracellular Vesicles

K

kDa	kilodaltons

L

LAMP	Lysosomal-associated membrane glycoprotein
LDL	Low density lipoprotein
LR	Leptin receptor

M

MCP	Monocyte chemoattractant protein
MFG-E	Milk fat globule-epidermal growth factor
MHC	Major histocompatibility complex

mIR	micro ribonucleic acid
mL	millilitre(s)
μL	microlitre(s)
mm	millimetre(s)
μm	micrometre(s)
mM	millimolar
μM	micromolar
mmHg	millimetres of mercury
MMP	matrix metalloproteinase
Mϕ	Macrophage(s)
mRNA	messenger ribonucleic acid
MSC	Mesenchymal stem cell
MUFA	Monounsaturated fatty acid
MVB	Multivesicular body

N

nm	nanometre(s)
nM	nanomolar
NTA	Nanoparticle tracking analysis

O

O_2	Oxygen

P

PAI	Plasminogen activator inhibitor
PBS	Phosphate-buffered saline
PC	Phosphatidylcholine
PCOS	Polycystic ovary syndrome
PCR	Polymerase chain reaction
PDGF	Platelet-derived growth factor
PE	Phosphatidylethanolamine

PET	Positron emission tomography
PFP	Platelet-free plasma
PI	Phosphatidylinositol
PI3K	Phosphoinositide 3-kinase
PMA	Phorbol-myristate-acetate
PMN	Polymorphonuclear neutrophil
PO_4	Phosphate
PPAR	Peroxisome proliferator-activated receptor
PPP	Platelet-poor plasma
PREF	Preadipocyte factor
PS	Phosphatidylserine
PUFA	Polyunsaturated fatty acid

Q

qRT-PCR	quantitative real-time polymerase chain reaction

R

RA	Rheumatoid arthritis
RAS	Renin-angiotensin system
RhoK	Rho-kinase
RIPA	Radioimmunoprecipitation assay
RISC	Ribonucleic acid-induced silencing complex
ROS	Reactive oxygen species

S

SC	Subcutaneous
SCD	Stearoyl CoA desaturase
SDS-PAGE	Sodium dodecyl sulphate-polyacrylamide gel electrophoresis
SEC	Size exclusion chromatography
SEM	Scanning electron microscopy
SFA	Saturated fatty acid

SSC	Side scatter
T	
TDZ	Thiazolidinedione
TEM	Transmission electron microscopy
TF	Tissue factor
TFF	Tangential flow filtration
TGF	Transforming growth factor
TLC	Thin layer chromatography
TNF	Tumour necrosis factor
TRF	Time resolved fluorescence
TRPS	Tunable resistive pulse sensing
TSG	Tumor susceptibility gene
T2D	Type 2 diabetes
U	
UCP	Uncoupling protein
V	
VAMP	Vesicle-associated membrane protein
VEGF	Vascular endothelial growth factor
VSMC	Vascular smooth muscle cell
W	
WAT	White adipose tissue

Fatty acid index

Shorthand notation	Common name
C14:0	Myristic acid
C14:1	Tetradecenoic acid
C15:0	Pentadecanoic acid
C16:0	Palmitic acid
C16:1n9	*cis*-7-hexadecenoic acid
C16:1n7	Palmitoleic acid
C18:0	Stearic acid
C18:1n9	Oleic acid
C18:1n7	*cis*-vaccenic acid
C18:2n6	Linoleic acid
C18:3n3	α-linolenic acid
C20:0	Arachidic acid
C20:1n9	Eicosenoic acid
C20:2n6	Eicosadienoic acid
C20:3n3	Eicosatrienoic acid
C20:4n6	Arachidonic acid
C20:5n3	Eicosapentaenoic acid
C22:1n9	Erucic acid
C22:0	Docosanoic acid
C22:2n6	Docosadienoic acid
C22:3n3	Docosatrienoic acid
C22:5n3	Docosapentaenoic acid
C22:6n3	Docosahexaenoic acid
C24:0	Lignoceric acid
C24:1n9	Nervonic acid

Shorthand and common names for fatty acids detected and discussed within this thesis.

Publications

Connolly KD, Guschina IA, Yeung V, Clayton A, Draman MS, Von Ruhland C, Ludgate M, James PE, Rees DA (2015). Characterisation of adipocyte-derived extracellular vesicles released pre- and post-adipogenesis. *Journal of Extracellular Vesicles*. 24 (4): 29159.

Willis GR, Connolly K, Ladell K, Davies TS, Guschina IA, Ramji D, Miners K, Price DA, Clayton A, James PE, Rees DA (2014). Young women with polycystic ovary syndrome have raised levels of circulating annexin V-positive platelet microparticles. *Human Reproduction*. 29 (12): 2756-63.

Connolly KD*, Willis GR*, Datta DB, Ellins EA, Ladell K, Price DA, Guschina IA, Rees DA, James PE (2014). Lipoprotein-apheresis reduces circulating microparticles in individuals with familial hypercholesterolemia. *Journal of Lipid Research*. 55 (10): 2064-72.

Connolly KD*, Witzcak J*, Wadey RM, Ludgate M, Rees DA, James PE (in preparation). Is there evidence for adipocyte-derived extracellular vesicles *in vivo*?

Connolly KD, Hassan N, Morris K, James PE, Rees DA (in preparation). The effect of hypoxic adipocyte-derived extracellular vesicles on macrophage phenotype and chemotaxis.

Published abstracts

Connolly KD, Guschina IA, Chauhan P, Devitt A, Hassan N, Morris K, Clayton A, Rees DA, James PE (2015). Extracellular vesicles secreted from adipocytes exposed to hypoxia and their effects on macrophage chemotaxis and phenotype. *Journal of Extracellular Vesicles*. 4: 27783; P-VIII-16.

Connolly K, Morris K, Willis GR, Rees DA, James PE (2014). Do conditions of freezing and time-in-freezer really matter? *Journal of Extracellular Vesicles*. 3: 24214; P8B-301.

Willis GR, Connolly K, Ladell K, Guschina IA, Miners K, Price DA, Clayton A, James PE, Rees DA (2014). Women with PCOS have increased circulating annexin V positive microparticles, which are predominantly platelet-derived. *Endocrine abstracts*. 31: P218.

Presentations

Oral presentations

University Graduate College "Speaking of Science" (Cardiff University, Cardiff, UK, June 2015).

UK Extracellular Vesicle Forum (Royal Veterinary College, London, UK, December 2014).

Postgraduate Research Day (Cardiff University, Cardiff, UK, December 2014).

IZON Science annual research symposium (University of Oxford, Oxford, UK, September 2014).

Institute of Molecular and Experimental Medicine monthly meeting (Cardiff University, Cardiff, UK, July 2014)

Cardiovascular Biology and Metabolism seminar (Cardiff University, Cardiff, March 2013).

Poster presentations

International Society of Extracellular Vesicles (Washington D.C, MD, USA, 2015).

International Society of Extracellular Vesicles (Rotterdam, Netherlands, 2014).

Cardiff University Postgraduate Research Day (Cardiff, UK, December 2013).

Awards

University Graduate College "Images of Research" – People's Choice Award (Cardiff University, Cardiff, UK, December 2015).

IZON Science invited speaker (University of Oxford, Oxford, UK, September 2014).

Postgraduate Research day – Oral presentation prize (Cardiff University, Cardiff, UK, December 2014).

1. General Introduction

The emergence of extracellular vesicles (EVs) as novel cellular communicators and potential biomarkers has led to an exponential growth in EV research. Similarly to the history of adipocyte research itself, the study of adipocyte-derived EVs is somewhat behind the rest of the EV field. Data presented in this thesis describes the physiological and potential pathophysiological characteristics of adipocyte-derived EVs.

It is important to state that from the onset of this thesis, the EV field has been rapidly and continually changing in suggested protocols and methods. Therefore in order to keep up with the dynamics of the field, methods may differ slightly with progression through the chapters; though consistency was maintained wherever possible. In particular, the methods and protocols employed in *Chapter 8* (which was conducted at the beginning of my PhD) were based on those recommended at the time. Therefore, some of these methods such as the use of FC without beads or instead of time resolved fluorescence to phenotype EVs are now regarded suboptimal. Though frustrating, it provides an important insight into ever changing field of EV research, which is described in detail below.

1.1 EXTRACELLULAR VESICLES

Extracellular vesicles (EVs) are cell-derived submicron vesicles. EVs are spherical, ranging from 30 nm to 1 μm in size, and are contained by a phospholipid bilayer. The following section provides a detailed account of the current classification, functions and potential clinical relevance of EVs.

1.1.1 History

The first visual evidence of EVs was published in 1967 by Peter Wolf (1). In this study, plasma EVs were visualised by electron microscopy (EM) and termed "platelet dust". Wolf's study aimed to explain a study from 1946 where platelet-free plasma (PFP) had been shown to possess thrombin generation capacity and that this could be reduced by high speed centrifugation (2). This was in fact, the first experimental evidence for the existence and functional capacity of EVs, though the visual evidence of this was not supplied until 20 years later by Wolf. In 1970, Webber and Johnson eloquently illustrated the blebbing of particles from activated platelets by EM (**Figure 1.1.1 A**).

Concurrently, the works of George Palade and in later years, James Rothman, helped to delineate the role of vesicles in the secretory pathway of intracellular protein transport, largely in relation to the secretion of enzymes, hormones and neurotransmitters (3–6). However, it also provided important evidence for: a role of vesicles in the transfer of cellular material; fusion of vesicles with the plasma membrane; and discharge of intravesicular contents into the extracellular space. It was later demonstrated that reticulocytes package the transferrin receptor into vesicles to allow for maturation into erythrocytes (7). The authors later proved this shedding of the transferrin receptor was specifically mediated by exosomes (8) (**Figure 1.1.1 B/C**). Over the next few decades, EV research was slow to progress, and only in the last 15 years has the EV field seen a rapid expansion.
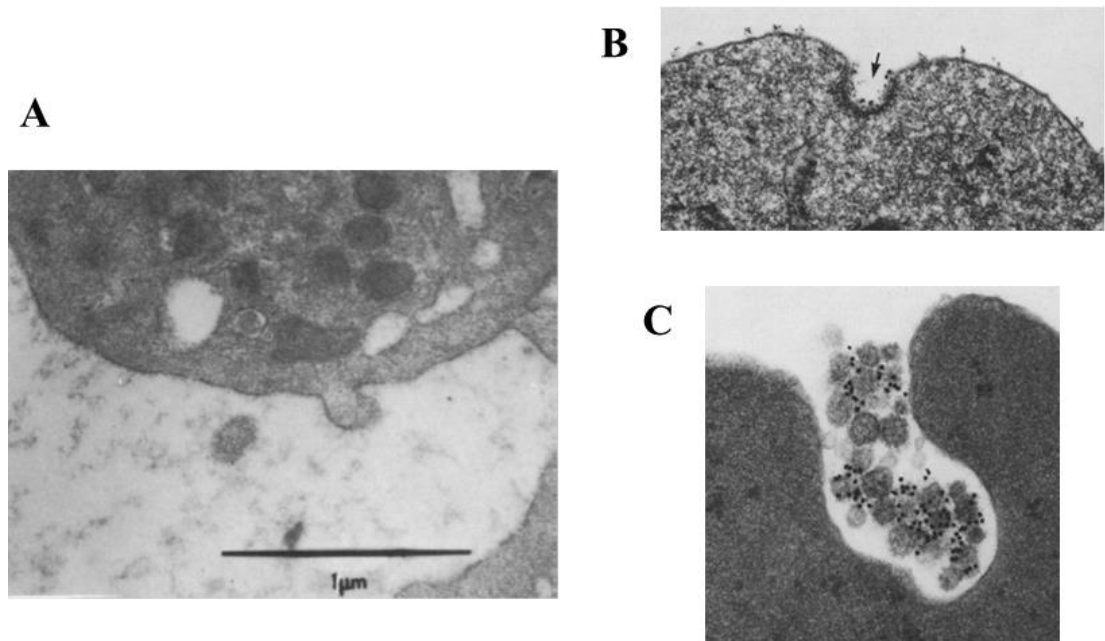
Figure 1.1.1: Early evidence of EVs. Transmission EM images of EV release. (**A**) Activated platelets releasing submicron vesicles via a direct blebbing of the plasma membrane. (**B**) Invagination of the plasma membrane of reticulocytes leads to packaging of the transferrin receptor into intracellular vesicles contained within a larger vesicle which fuses with the plasma membrane to release the vesicles from the cell via exocytosis (**C**). Image A is reproduced with permission from (9) © 1970, American Society for Investigative Pathology. Published by Elesevier Inc. All rights reserved. Images B and C are reproduced with permission from Rockefeller University Press, ©Pan et al. Journal of Cell Biology (8).

1.1.2 Nomenclature

Whilst the interest in and impact of the EV field has boomed over recent years, it has been accompanied by a varied use of terminology (10). Unfortunately, this causes confusion within the field and the published literature as to the precise nature and classification of the vesicles being studied. The varied nomenclature has primarily arisen from the vast subject areas of EV researchers, who have named the vesicles after the cell from which they originate (11). For example: tolerosomes (intestinal epithelial cells) (12), oncosomes (cancer cells) (13), prostasomes (prostate cancer cells) (14) and matrix vesicles (bone cells and cartilage) (15). In addition to cell-specific terminology, terms referring to the mechanism of biogenesis such as "exosomes", "microvesicles", "microparticles" and "apoptotic bodies" are often used interchangeably, and often mean different things to different researchers. Thus, in 2014, the International Society of Extracellular Vesicles (ISEV) produced a position paper to unify these discrepancies. The statement encourages the use of "EVs" as an umbrella term to encompass all secreted vesicles and requests that authors in the field provide complete clarity in reporting the defined EV population(s) of study (10,16). Secreted vesicles that fall under the generic EV umbrella and their typical characteristics are summarised in **Figure 1.1.2**. It should be noted that **Figure 1.1.2** summarises characteristics of EVs that are generally accepted by the field. However, some of the specific characteristics are not strictly evidenced, for example, some exosomes may be >100 nm and some microvesicles may be <100 nm (17). Specificity and further characterisation is likely to be improved in future years.

Extracellular vesicles

	Exosomes	Microvesicles	Apoptotic bodies
Size range	30 – 100 nm	100 – 1000 nm	1 – 5 μm
Origin	Intracellular processing and recycling	Plasma membrane	Plasma membrane
Markers	Tetraspanins: *CD9, CD63, CD81* Other: *TSG101, Alix, GM1*	PS binding: *Annexin V, lactadherin* Cell surface proteins	PS binding: *Annexin V* Nuclear material: *Propidium iodide*
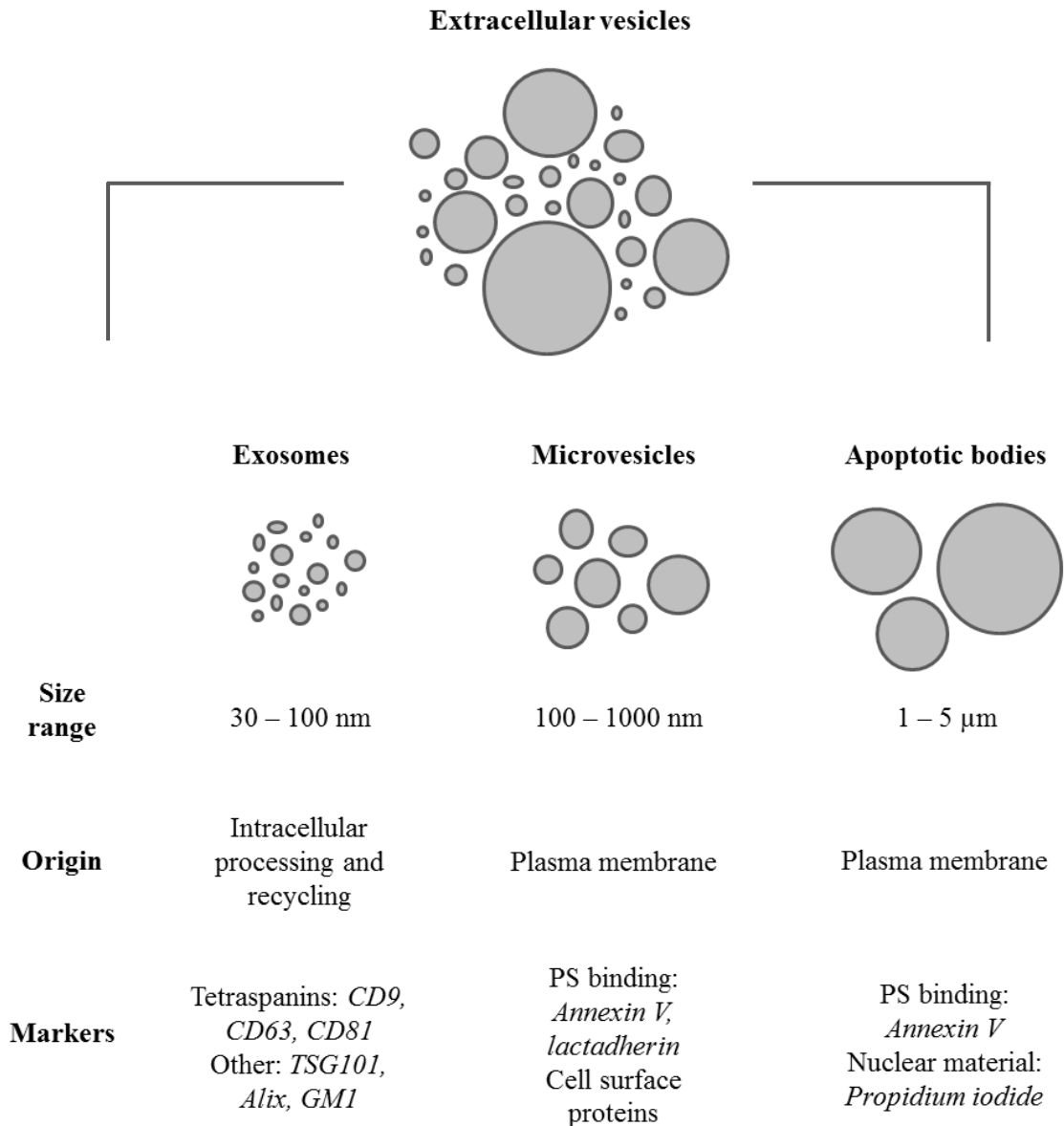
Figure 1.1.2: Summary of EV nomenclature. The term "EV" is used as a generic term to encompass all cell-derived secretory vesicles. This includes exosomes, microvesicles and apoptotic bodies. CD = cluster of differentiation; GM1 = monosialotetrahexosylganglioside; PS = phosphatidylserine; TSG101 = tumour susceptibility gene 101.

As the name indicates, apoptotic bodies are released by cells undergoing apoptosis (18) and therefore do not represent EVs from viable cells. Thus, the term EV in this thesis refers to both exosomes and microvesicles but does not include apoptotic bodies.

1.1.3 Formation

EV biogenesis is categorised into two pathways: the classical pathway for exosome formation, and the direct pathway for microvesicle budding (**Figure 1.1.3**); although, EVs may not be limited to these pathways of biogenesis. Exosome-like vesicles with a diameter, density and tetraspanin expression akin to those of exosomes have been shown to be released via the direct pathway (19). However, it is not yet possible with current technology to discriminate between EV subtypes with similar sizes (10).

1.1.3.1 The classical pathway

The mechanisms of the classical pathway are part of those in the endocytic pathway. The endocytic pathway primarily regulates the expression of cell surface receptors, which can be internalised and degraded or recycled depending on the needs of the cell (20). Indeed, the endocytic formation of exosomes was first illustrated as a novel mechanism of receptor recycling (8). However, exosomes are now considered to play a major role in intercellular communication and hence, this pathway has now been widely studied with respect to exosome formation.

The process begins with the invagination of the plasma membrane and endocytosis of membrane proteins and surrounding material to form an intracellular vesicle (**Figure 1.1.3 A**). Intraluminal vesicles (ILVs) are then formed from an inward budding of the intracellular vesicle membrane. ILV generation is governed by the endosomal sorting complex required for transport (ESCRT) of which there are 4 main complexes (21). ESCRT complexes 0, I and II recognise and ubiquitinate endocytosed proteins in the intracellular vesicle membrane (22). The ESCRT III complex (including alix and TSG101) then orchestrates the inward budding and scission of the ILV to form multi-vesicular bodies (MVBs). ESCRT-derived MVBs may then be degraded in lysosomes or secreted as exosomes. Knockdown of ESCRT complex proteins such as TSG101 impairs, but does not abolish exosome secretion (23) suggesting an alternative pathway for MVB formation. Furthermore, the differential targeting of MVBs for either lysosomal degradation or exocytosis is suggestive of subtle alterations in the compositions of ILVs and MVBs that determine the fate of the MVBs and their contents.
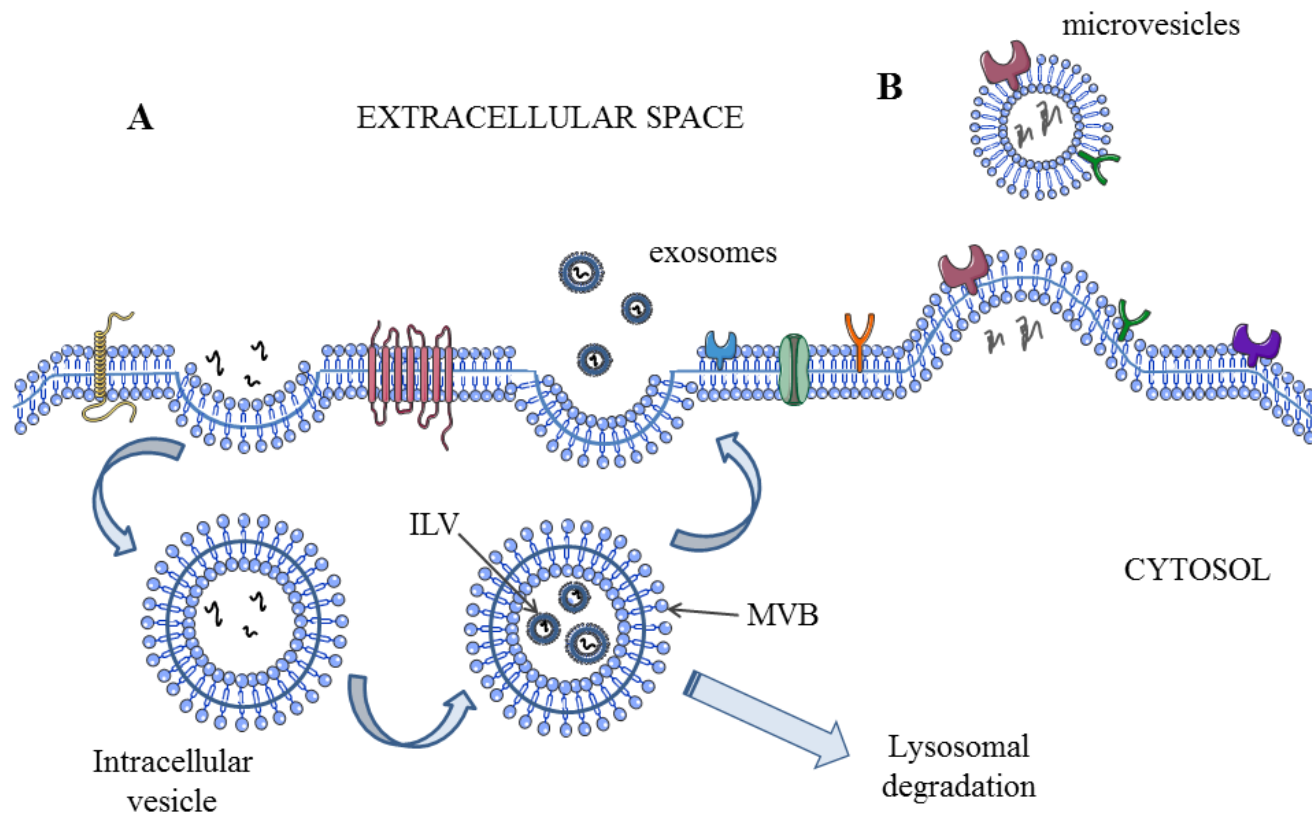
Figure 1.1.3: Schematic of EV biogenesis. The two main pathways for EV biogenesis are summarised. (**A**) The classical pathway: inward budding of the plasma membrane creates intracellular vesicles which process endocytosed material forming intraluminal vesicles (ILV). ILV are contained within multivesicular bodies (MVB) which may then be targeted for lysosomal degradation or fuse back with the plasma membrane to release ILV as exosomes. (**B**) The direct pathway: alterations in plasma membrane asymmetry cause an outward budding of the membrane directly into the extracellular space producing microvesicles that contain surface proteins of the parent cell. Image created using Servier Medical Art (Servier, France).

The precise processing of MVB subpopulations is currently unknown, though data is accumulating for a role of lipids in an ESCRT-independent process. MVBs that were cholesterol rich were found to be destined for release as exosomes (24). Furthermore, association of exosomal proteins with lipid-raft microdomains was found to segregate MVBs for exosome secretion rather than lysosomal degradation (25). Ceramide was also detected within exosomes, which is hydrolysed from the phospholipid sphingomyelin by sphingomyelinase enzymes. Addition of exogenous sphingomyelinases to cells induced aggregation of lipid-raft microdomains in intracellular vesicles and inward budding, producing ILVs. Furthermore, inhibition of sphingomyelinases reduced secretion of exosomal markers such as tetraspanins and TSG101 (26) suggesting a role for ceramide in the production of ILVs destined for exosome secretion. However, others have shown that inhibition of sphingomyelinases has little or no effect on exosome secretion (27) suggesting this process may be cell-specific. Tetraspanins, particularly CD63, have also been proposed as ESCRT-independent stimulators of ILV formation and exosome secretion (27,28) and are known to be enriched in ILVs and exosomes (29). Phospholipase D2 (PLD2) which is highly enriched in exosomes, is necessary for the formation of CD63-containing ILVs (30,31). PLD2 targets phosphatidylcholine (PC) in the plasma membrane to yield phosphatidic acid which, similarly to ceramide, has been implicated in the formation of MVBs. Recently, ESCRT-dependent and − independent mechanisms were shown to form ILVs of different sizes (32), providing a potentially simple method of distinguishing ILV populations.

The majority intracellular vesicle trafficking is controlled by Rab GTP (guanosine triphosphate)-ases, a family of conserved, small cytosolic proteins (33). Several Rab GTPases have been implicated in exosome secretion, particularly Rab 27. These Rabs have been shown to play a fundamental role in exosome secretion by directing MVBs to the plasma membrane and assisting their docking for fusion and exocytosis (34). Inhibition of Rab 27A in cancer cells prevented exosome secretion *in vitro* and also reduced tumour metastasis *in vivo* (35,36).

The final stage of the classical pathway involves fusion of MVBs with the plasma membrane and exocytosis of exosomes. The "SNARE hypothesis" (37) has been proposed as a mechanism for MVB fusion with the plasma membrane. The SNARE complex is formed between the attached vesicle and the plasma membrane by:

syntaxin and SNAP (soluble NSF (N-ethylmaleimide-sensitive fusion) attachment protein) which protrude from the cytosolic plasma membrane, and vesicle-associated membrane protein (VAMP) in the vesicle membrane. The folding of the SNARE proteins between the docking vesicle and the plasma membrane provides the thermodynamic energy to pull apart the membranes, creating a pore for exosomes release (38). The involvement of the SNARE complex in MVB fusion and exosome release has not yet been widely studied, though several groups have indicated SNARE and accessory proteins may be crucial to exosome secretion (39–42).

Though a plethora of research exists detailing the classical pathway, the exact mechanisms of exosome biogenesis are by no means clear. Currently, it seems that the endocytic pathway of exosome formation may involve several different proteins and share similarities between cell types, though some aspects may be cell-specific. **Figure 1.1.4** summarises the major current theories surrounding exosome biogenesis. Further investigation is needed to draw parallels between different cell types to further our understanding of how MVB heterogeneity can result from different mechanisms of ILV formation and hence impact upon exosome biogenesis.
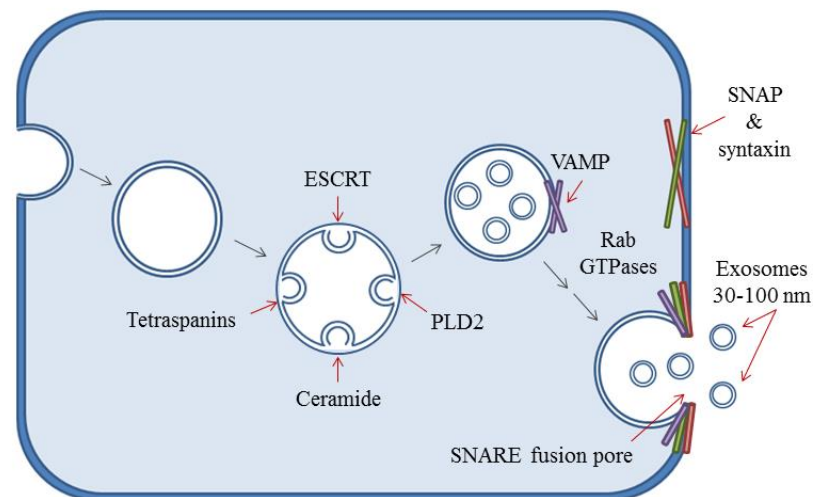
Figure 1.1.4: Summary of classical exosome biogenesis. A summary of the major steps and inducers of classical exosome biogenesis. ILV formation may arise from actions of the ESCRT complexes, ceramide, tetraspanins or PLD2 to form MVBs. RabGTPases then aid the translocation and docking of MVBs to the plasma membrane where the SNARE complex assembles. Energy created by the association of the SNARE complex pulls the docked vesicle and plasma membranes apart creating a fusion pore to allow for exosome secretion.

1.1.3.2 The direct pathway

During resting conditions where cells are unstimulated, the phospholipid bilayer exists in an asymmetric state (43). Aminophospholipids phosphatidylserine (PS) and phosphatidylethanolamine (PE) are preferentially situated on the cytoplasmic side of the bilayer whilst PC and sphingomyelin are positioned on the outer leaflet (44). This physiological asymmetry is generated by synthesis of phospholipids on a specific leaflet of the membrane and is maintained by three phospholipid translocase enzymes embedded in the plasma membrane. Flippase is an adenosine triphosphate (ATP)ase which causes rapid translocation of aminophospholipids to the inner membrane leaflet, with a higher affinity for PS. Floppase is also an ATPase and a member of the ATP-binding cassette (ABC) transporter family (45). It acts to move phospholipids to the outer membrane leaflet, but does so at a much slower rate than flippase when the cell is at rest (43). Scramblase does not require ATP and causes random bidirectional transport of phospholipids across the membrane. When the cell is at rest, transport of phospholipids between the membrane leaflets is slow and generally mediated by flippase.

Activation of the cell usually results in an increase in cytosolic calcium which causes concurrent activation of floppase and scramblase and inhibition of flippase (45). The resulting effect is a dissemination of phospholipid asymmetry with a profound exposure of PS on the outer membrane leaflet. Furthermore, increased cytosolic calcium concentrations also cause a disruption in the actin cytoskeleton (46). The proteolysis of the actin cytoskeleton may require the actions of several enzymes. Rho-kinase (RhoK)-II has been shown be essential for endothelial microvesicle production (46) and RhoK inhibitors are able to block microvesicle blebbing (47). Furthermore, the production of adipocyte-derived EVs has been shown to be dependent on RhoK following cleavage by caspase-3 (48). Caspases can also modulate the actions of calpain to cause cytoskeletal reorganisation and microvesicle blebbing in neutrophils (49) and macrophages (Mϕ) (50). Though a number of proteins have been implicated in microvesicle budding, the precise mechanism remains unclear and similarly to exosome biogenesis, is likely to vary between cells.

The resulting exposure of PS and cleavage of the actin cytoskeleton following cellular activation causes budding and shedding of the plasma membrane in the form

of microvesicles. Typically between 100 and 1000 nm in diameter, microvesicles often harbour surface antigens from their cell of origin in their own plasma membrane as well as specific lipid signalling molecules, messenger ribonucleic acid (mRNA), micro RNA (mIR) and soluble proteins (**Figure 1.1.5**).
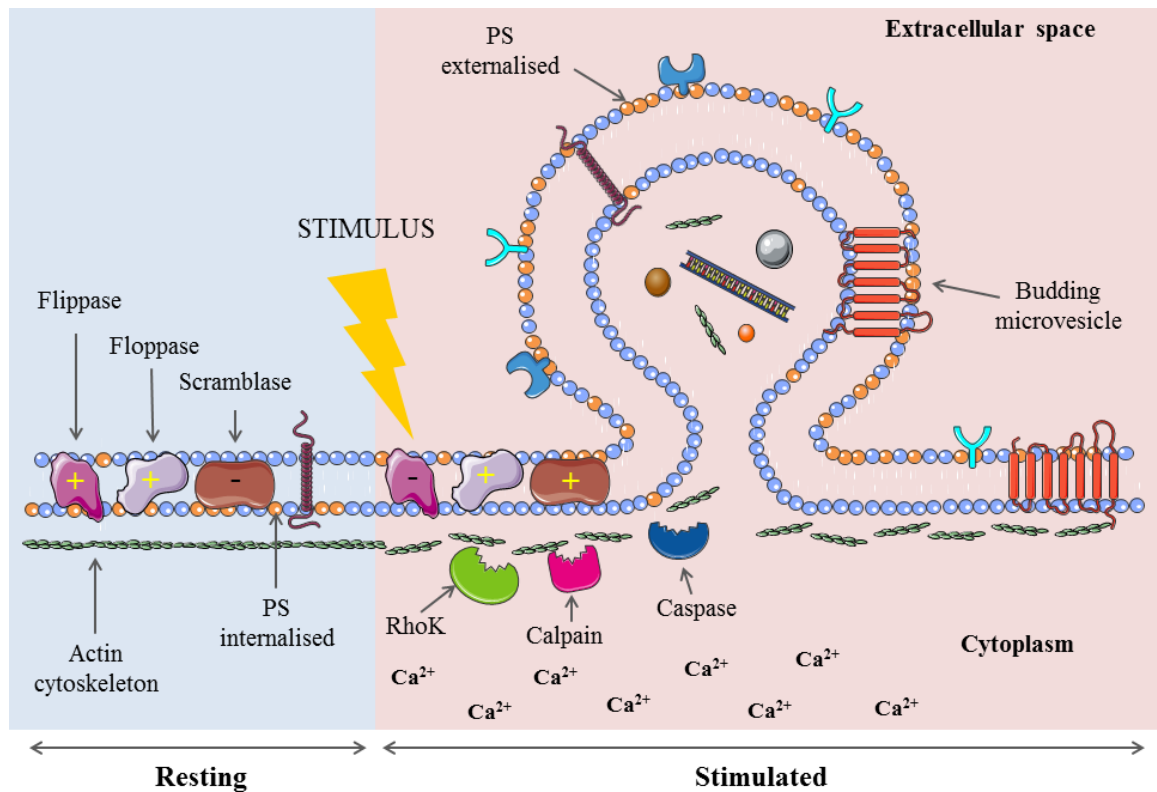
Figure 1.1.5: Summary of microvesicle formation. The membrane of resting cells has an asymmetric distribution of phospholipids which is primarily maintained by the action of the enzyme, flippase. This causes anionic phospholipids such as PS to remain facing the cytoplasm. Upon cellular activation and calcium (Ca^{2+}) influx, flippase is inhibited and scramblase is activated. This causes PS to be externalised to the outer membrane leaflet. Concurrently, increased cytosolic Ca^{2+} activates enzymes such as RhoK, calpain, and caspases which cleave the actin cytoskeleton. Together, this causes an external budding of the plasma membrane, into which surface receptors and antigens, and cytosolic enzymes, nucleic acids and lipids are incorporated. Image created using Servier Medical Art (Servier, France).

1.1.4 Composition of extracellular vesicles

Owing to their different methods of biogenesis, EV subtypes are likely to alter in composition despite originating from the same cell. Broadly, EVs have been shown to contain proteins (membrane-bound, secretory, cytosolic and enzymes), nucleic acids and lipids. The specific cargo of EVs is likely to reflect the originating cell but also may determine their eventual function.

1.1.4.1 Protein markers

Exosomes have been more intensely studied than microvesicles or EV fractions as a whole, and therefore much more data exists detailing their composition. The current canonical markers of EVs are largely associated with EV biogenesis and can be split into luminal (intravesicular) and membrane-associated markers. Intravesicular markers include cytoskeletal proteins such as actin, tubulin, and ezrin, endosomal trafficking proteins such as RabGTPases, ESCRT complexes, heat shock proteins (HSPs), Alix and TSG101 and enzymes such as glyceraldehyde 3-phosphate dehydrogenase (GAPDH). Membrane-associated EV markers include tetraspanins (CD9, CD63 and CD81), membrane trafficking proteins such as annexins, flotillin and milk fat globule-epidermal growth factor VIII (MFG-E8), lysosome-associated membrane glycoprotein (LAMPs) and major histocompatibility complex (MHC) I and II (21,51). EVs also harbour an array of cell-specific markers which assists in the identification of their cell of origin in complex biological fluids. The most commonly used markers are summarised in **Table 1.1.1**.

Proteomic analysis of plasma membrane-derived vesicles is beginning to reveal that markers previously regarded as "exosome specific" may also be present on microvesicles (52). For example, CD9 is frequently used to confirm the presence of exosome populations. Silencing of Rab27A reduced expression of classical exosome markers such as CD63, alix and TSG101 but had little effect on CD9. Furthermore, larger vesicles (as viewed by EM and separated at a different density to exosomes) were also found to be CD9 positive (53) suggesting CD9 may be more of a ubiquitous marker of EVs than other tetraspanins.

Cell type	Marker/antigen	Citations
B cells	B cell receptor, CD19	(51,54)
Dendritic cells	CD11c	(51)
Endothelial cells	CD31, CD62E, CD144, CD146	(54–60)
Erythrocytes	CD235a, CD236	(54–57,60,61)
Leukocytes	CD15, CD45	(54,57,61)
Monocytes	CD11b, CD14	(61,62) (60)
Platelets	CD41, CD42a, CD42b, CD61	(54–57,59–63)
Reticulocytes	CD71	(57)
T cells	CD2, CD3, CD86	(51,54)

Table 1.1.1: Cell-specific markers used for EV analysis. Common markers used in EV analysis of complex biological fluids to identify the cellular origin.

MFG-E8 has been historically associated with exosomes (64) though recent evidence suggests it may also be a more universal marker of EVs (35,65,66). MFG-E8 is able to bind PS, which has repeatedly been used to identify microvesicle populations due to the phospholipid rearrangement that occurs prior to their formation. PS exposure is frequently used to gate EV populations by flow cytometry (FC) and is usually quantified using annexin V or MFG-E8. However, the use of PS as a microvesicle marker has been contested in recent years as not all microvesicles appear to expose PS (63,67) and some exosomes seem to contain an enrichment of PS (21,68).

As more detailed proteomic analyses of EVs continue to be published, it is hoped that more ubiquitous markers of EVs and both cell- and subtype-specific markers will be identified. As such, a database of such proteins identified in EV populations (Vesiclepedia) has been compiled and is managed by members of the EV field (69).

1.1.4.2 RNA

It was not until relatively recently (2007) that EVs were conclusively shown to contain RNA (70). The original study of murine mast cell exosomes showed a number of important features:

1. Exosomes contained significant amounts of mRNA and mIR but no DNA or ribosomal RNA.
2. RNA was not susceptible to RNAse degradation and was therefore intravesicular.
3. RNA could be translated to functional proteins when incubated with protein machinery.
4. Exosomes could transfer RNA to human mast cells and be translated into protein.

Concomitant studies also showed that microvesicles from tumour cells (71) and embryonic stem cells (72) could also transfer functional mRNA to recipient cells. Since these key discoveries, countless studies have indicated the presence of mRNA and mIR in EVs from a variety of cell types. A recent study visualised the transfer of functional RNA contained within glioma-derived EVs to Mϕ *in vivo*, illustrating the subsequent effect on Mϕ gene and protein expression and modulation of the tumour microenvironment (73). EV-mediated transfer of mRNA has also been proposed between mother and neonate in breast milk (74) suggesting post-natal transfer of maternal genetic material via EVs. Cells infected with Epstein-Barr virus (EBV) were able to produce EVs packaged with mIRs that could selectively silence genes in B cells, thereby promoting and maintaining viral infection (75). Furthermore, circulating EVs in a cohort of young women with polycystic ovary syndrome (PCOS) had an altered profile of mIR compared to healthy controls (76) which might accelerate the progression of cardiovascular disease (CVD) in these individuals.

In EV therapeutics, dendritic cell exosomes were successfully loaded with short interfering RNA and systemically injected into mice. The exosomes harboured a protein that enabled them to translocate to the brain and silence specific genes including a gene target for Alzheimer's disease therapy (77). Therefore, the capacity of EVs to carry functional nucleic acids is an exciting prospect, not only in the identification of novel disease biomarkers but also for targeted therapy.

1.1.4.3 Lipids

Lipid signalling mediators are the least studied of the biochemical components of EVs despite being important precursors and mediators of a number of signalling pathways. Typically, lipid bilayers are ~ 5 nm thick, meaning >60% of the smallest EVs (~30 nm) are made of lipids (78). Compositional analysis of mast, dendritic, prostate cancer and B cell-derived EVs have all revealed the enrichment of sphingomyelin within EVs compared to cells (79–81) suggesting a higher reserve of ceramide which is required for exosome biogenesis. EV lipids are more tightly packed (79) with lipid rafts (80) and are more detergent-resistant (80) compared to the cells. The decreased membrane fluidity and resistance to detergents suggests EVs are more resistant to degradation in the circulation (79). The randomised distribution of PE observed in EVs indicates EV membranes retain the phospholipid reorganisation that precedes their biogenesis (79). Furthermore, the overall lipid composition of EVs bore both similarities and differences to the cell of origin (81); a concept also observed between circulating EVs and corresponding plasma (55,76).

Lipid analyses of EVs are gaining popularity with the increased accessibility of in-depth analysis techniques such as gas chromatography-mass spectrometry (GC-MS). For example, a recent lipidomic study using platelet EVs illustrated compositional differences in lipids between EV subpopulations (82). Increased knowledge of the type of lipids packed into EVs may help to elucidate alternative biological roles and biomarkers for EVs that are not based on proteomic or nucleic acid detection.

1.1.5 Uptake and trafficking of extracellular vesicles

1.1.5.1 EV internalisation

Much of the evidence for the internalisation of EVs arose from the presence of the EV cargo within recipient cells, however, the mechanism of uptake was not studied in parallel. Recognition and internalisation of EVs is likely to differ between cell types and perhaps also between EV subpopulations; as such, a variety of uptake mechanisms have been proposed.

The initiation of EV uptake by a cell is likely to involve a receptor-ligand interaction between the EV and the target cell. Evidently, this may be extremely cell-specific and depend upon the origin of the secreted EV and the target cell, though a number of less specific interactions have also been described. PS exposure on activated T cell EVs was recognised by the anti-PS receptor on Mϕ. Consequent EV internalisation resulted in the accumulation of cholesterol and tumour necrosis factor (TNF)-α in the Mϕ, which may initiate the transition towards a foam cell (83). However, inhibition of PS did not completely prevent EV uptake suggesting alternative methods of uptake. Integrins have also been implicated in the engulfment of EVs. The presence of α4β1 integrins on endothelial progenitor cell (EPC)-derived EVs were essential for uptake by endothelial cells (84) and uptake of dendritic EVs was partially blocked by the inhibition of αvβ3 (85). The latter study also illustrated a role for tetraspanins in EV-cell recognition as blocking antibodies to CD9 and CD81 reduced EV uptake (85). Interestingly, the tetraspanin Tspan8 was shown to form a complex with the integrin α4 in EV membranes, both of which were then required for exosome internalisation (86). These results suggest that tetraspanins and integrins may have both isolated and concomitant roles in EV uptake. Proteoglycans, lectins and immunoglobulins have all been implicated in EV-cell interactions, though in more cell-specific circumstances (87).

Following recognition of EVs by the target cells, internalisation ensues. The majority of studies analysing EV uptake suggest an active, endocytic mechanism of internalisation, of which, there are several pathways (87). The most studied of these pathways is clathrin-mediated endocytosis, which involves an intracellular accumulation of clathrin-coated vesicles in the target cell which assemble to cause invagination of the plasma membrane and endocytosis of the EV. Inhibitors of

clathrin-mediated endocytosis can stem EV uptake including chlorpromazine (88–90) which inhibits clathrin-coated pit formation, or silencing of dynamin 2, (90,91) a GTPase required for endocytic vesicle formation and cleavage.

Endocytosis of EVs can also be mediated by lipid raft-associated calveolae, which form small chasms in the plasma membrane (87). Knockdown of Calveolin-1, a key component of calveolae , suppresses internalisation of EVs (92). This study also showed that dynamin inhibition reduced EV uptake, though this may have been due to blockade of clathrin-mediated endocytosis.

Phagocytosis of EVs has also been proposed as a mechanism for EV internalisation, particularly of larger EVs (21) and more so by professional phagocytes (93). However, exosomes were rapidly internalised by Mϕ suggesting smaller vesicles may also be phagocytosed (93). Interestingly, this study also showed that dynamin 2 was required for exosome phagocytosis, illustrating the parallels between different endocytic mechanisms. Dendritic cells (DCs) have also been shown to phagocytose EVs as EVs were labelled and tracked to the phagosome of the target cell and the content of EVs was later detected in the cytosol (94).

Finally, endocytosis of EVs has been shown to occur via macropinocytosis, which is often utilised by the cell to sample the extracellular milieu. Macropinocytosis occurs in a phagocytosis-like manner, though the process is constitutive and not targeted (87). Microglia were shown to employ macropinocytosis to internalise oligodendrocyte EVs as inhibition of macropinocytosis-associated proteins, Rac-1 and the Na^+/H^+ exchanger, inhibited uptake of EVs.

Direct membrane fusion has also been suggested as a non-endocytic mechanism of EV internalisation in a process that may resemble the fusion of MVBs with the plasma membrane (*Section 1.1.3.1*). Metastatic melanoma cell EVs were internalised into melanoma cells by direct fusion, a process which was enhanced when EVs were isolated from acidic melanoma cells (95). This suggests the tumour microenvironment can release EVs which are more efficient in being internalised into cells and therefore have a greater metastatic potential. Furthermore, Mϕ-derived EVs were shown to fuse with activated platelets and induce coagulation via the transfer of tissue factor (TF) (96).

It seems that cells may utilise several different mechanisms to recognise and internalise EVs, though the significance of each particular mechanism is not currently understood. The pathway of internalisation may perhaps be determined by the initial interaction of the EV with the cell, which is likely to be affected by receptors and ligands carried by the EV.

1.1.5.2 Intracellular trafficking of EVs

With the exception of direct fusion of EVs with target cells, the uptake of EVs appears to leave the EV intact, and hence the EV cargo remains contained within the endocytosed EVs. Indeed, endothelial-derived EVs endocytosed by human umbilical vein endothelial cells (HUVECs) were visualised by confocal microscopy as intact vesicles (97). This suggests that the EV membrane undergoes intracellular degradation to liberate the delivered EV cargo. Fusion of EVs with the limiting membrane of endosomes has been illustrated using the lipid mixing probe R18, which quenches to form a fluorescent probe upon fusion with an unlabelled membrane (94,98). Furthermore, endocytosed tumour cell EVs were shown to demonstrate two distinct forms of intracellular translocation (98). The "confined mode" of movement was associated with diffusion into the cytoplasm whereas the "rapid directed mode" was associated with an active movement of EVs along microtubules or actin filaments. Transport of endocytosed glioblastoma EVs were also visualised along microtubules using live confocal imaging (99). Recent data presented at the ISEV annual meeting (100) (Washington DC, 2015) by Hartjes et al., (O-6C-1) demonstrated the uptake and translocation of individual fluorescently labelled exosomes via microtubules using high speed spinning disk microscopy.

The development and application of more sophisticated microscopy techniques to visualise the uptake and intracellular trafficking of EVs is likely to further our understanding of the fate of EVs within target cells. However, from the diversity of uptake mechanisms, it seems likely that intercellular communication via EVs is highly specific to the cell types involved.

1.1.6 Pre-analytical processing

The rapid growth of EV research proposes exciting functional prospects of EVs, but data must also be reviewed with a degree of circumspection. The diversity of biological fluids analysed combined with different levels of experience in working with EVs and the variety of isolation procedures employed, highlights the lack of consistency in pre-analytical processing of EVs. Consequently, a position statement from ISEV was issued in 2014, highlighting a need for researchers to meet a set of "minimal requirements" for the classification of an EV population (16). The requirements include the presence and absence of particular markers and techniques that should be used in combination to claim the presence of EVs (**Table 1.1.2**).

1.1.6.1 Sample collection and handling

Sample collection for EV processing will ultimately depend on the starting biological fluid. Due to the nature of data presented in this thesis, only the processing of blood and culture medium will be covered in detail, though processing of EVs from other biological fluids has been reviewed elsewhere (17).

Blood is a complex biological fluid and therefore, there are many stages at which variation could be introduced. Before blood is drawn from a patient or individual, a full history should be taken to collect information on age, sex, ethnicity, medications, health complications and potentially anthropometric and biochemical measurements such as weight, height, blood glucose etc. depending on the study. The fasting or fed state of the individual may be important to establish, due to postprandial elevations in circulating lipoproteins and chylomicrons, which fall within the same size range as EVs. A postprandial increase in EV concentration has also been observed (101,102) suggesting a fasted state may be better for EV isolation to avoid a false overestimation of EV concentration. The time of sample collection may also be important to consider as the activation of platelets, one of the major sources of EVs in the blood, varies throughout the day (103). Interestingly, TF[+] EVs follow the same pattern of variation throughout the day, peaking at 9am (104). Therefore, EV samples should be collected after this time to minimise false estimations of platelet-derived EVs.

Requirement	Examples
Evidence of transmembrane or lipid-bound proteins derived from extracellular membranes (Present or enriched in EV fractions)	Tetraspanins (CD9, CD63, CD81) Integrins or cell adhesion molecules Growth factor receptors Heterotrimeric G-proteins Phosphatidylserine-binding proteins (MFG-E8, annexin V)
Evidence of cytosolic proteins with membrane- or receptor-binding capacity (Present or enriched in EV fractions)	Endosomal proteins (TSG101, Alix, Rab GTPases) Signal transduction or scaffolding proteins (syntenin)
Lack of non-endocytic intracellular proteins (i.e. proteins not directly related to EV biogenesis, associated with other intracellular compartments)	Endoplasmic reticulum proteins (Grp94, calnexin) Golgi proteins (GM130) Mitochondrial proteins (cytochrome c) Nuclear proteins (histones, argonautes, RISC complexes)
Cell-specific extracellular proteins that may bind specifically or non-specifically to EV membranes (Variable association with EVs depending on cell type)	Acetylcholinesterases Serum albumin Extracellular matrix proteins (fibronectin, collagen) Soluble and secretory proteins (cytokines, growth factors, matrix metalloproteinases)
Indication of heterogeneity	Electron microscopy or atomic force microscopy images of individual EVs and multiple EVs
Size distribution measurements	Nanoparticle tracking analysis or tunable resistive pulse sensing measurements of the size and concentration distributions of EVs to correlate with microscopy images

Table 1.1.2: ISEV minimal requirements. Details of the minimal requirements outlined by ISEV for the classification of an EV population.

The processing of blood for EV isolation presents a number of important considerations, primarily because circulating platelets are easily activated, causing a release of EVs *in vitro*. The type of needle, vacutainer and time between collection and processing may all influence EV concentration. Shear stress may be higher in smaller gauge needles due to an increased pressure, however, no differences were observed between 19 and 21G needles on EV concentration (60) and these diameters are frequently used in the literature. A slow, gentle removal of blood into a syringe is recommended to minimise shear stress activation of platelets and the first 2-3 mL of blood are then usually discarded to avoid contaminating factors resulting from vascular injury (60). Previously used anticoagulants for EV isolation have included protease inhibitors such as heparin sulphate and hirudin, and calcium chelators such as sodium citrate, ethylenediaminetetraacetic acid (EDTA), acid citrate dextrose (ACD) and citrate-theophylline-adenosine-dipyridamole (CTAD). Unfortunately, only 2 studies have directly compared the effects of anticoagulants on EV concentration. Both studies found an increased concentration of EVs with the use of protease inhibitors compared to chelating anticoagulants (59,60). However, the authors of each study reached different conclusions as to the observed difference in EV concentration. Jayachandran et al., concluded that chelating anti-coagulants caused EVs to bind to platelets in whole blood, resulting in fewer EVs in the plasma that was later analysed for EVs (following depletion of platelets) (59). Conversely, Shah et al., hypothesised that the anticoagulant properties of chelating anticoagulants were superior to those of protease inhibitors, resulting in a greater platelet activation and *ex vivo* generation of EVs in blood collected in protease inhibitor anticoagulants (60). The correct conclusion remains a mystery as neither of the authors provided evidence for their theory. However, Jayachandran et al., did observe a reduction in endothelial-derived EVs with chelating agents but not with protease inhibitors. Endothelial cells are not present in the circulation and therefore, *ex vivo* generation of endothelial EVs is unlikely, suggesting protease inhibitor anticoagulants may provide a truer reflection of circulating EVs than chelating agents. The use of heparin for downstream EV analyses has however, been advised against (17). Heparin sulphate has inhibitory effects on the polymerase chain reaction (PCR) (105) and is therefore unsuitable for mRNA and mIR analysis using blood-derived EVs. Moreover, heparin sulphate was an effective inhibitor of EV internalisation into recipient cells (106), suggesting heparin sulphate should not be used if functional

interactions of EVs with target cells are being studied. Additional comparisons of the effects of anticoagulants on EVs are needed to decipher the optimal reagent. These comparisons should be accompanied by functional evidence of the negative effects of other anticoagulants (e.g. proof of EV-platelet binding with calcium-chelating anticoagulants) and should preferably not use FC for enumeration of EVs (see *Section 1.1.7.2*).

The length of time following collection of blood should also be considered. A time-dependent increase in EV concentration has been reported following blood collection which was attributed to *ex vivo* microvesiculation of blood cells (107,108), however others have observed no differences in EV counts (59,109). Despite conflicting results, it may be best to process samples immediately after venepuncture to avoid the risk of misleading data. At the very least, the time between sample collection and processing should be kept consistent between samples and experiments.

EVs isolated from cell lines in culture are released directly into the surrounding medium and therefore provide a pure source of EVs from a specific cell type. However, there are a number of important points to consider when using cultured cells for EV analysis. Firstly, the time of incubation used to generate EVs. Twenty-four hour incubation with fresh medium is the most widely used incubation time as this is often optimal in allowing enough time for sufficient EV generation; though, both shorter and longer incubation times have been used (110–112). Secondly, the modification or exclusion of foetal calf serum (FCS) or other serum from the media for the incubation period is commonly used as serum contains an abundance of EVs that are morphologically similar to EVs analysed with EM and nanoparticle tracking analysis (NTA) (113). Serum-derived EVs not only contaminate the EV population of the cultured cells but may also affect downstream functional assays using EVs. FCS-derived EVs stimulated migration of lung epithelial cancer cells (113). However, serum-depleted or –starved media has been shown to reduce cell growth (114) and to change the size, concentration and protein composition of EVs (115,116). Therefore, it is important to first establish that serum-deprived or –free media has no effect on cell viability to ensure cellular stress is minimised. Cells that do not survive in serum-depleted or –free media may be supplemented with 1% (w/v) bovine serum albumin (BSA) (117).

1.1.6.2 Methods of EV isolation

A number of techniques are currently employed to isolate EVs including differential centrifugation, density gradient ultracentrifugation, size exclusion chromatography (SEC), immunoaffinity capture assays, filtration and commercially available products such as ExoQuick™; or a combination of several of these methods. The method employed usually reflects the EV population being studied and/or the downstream application.

Differential centrifugation requires a number of sequential centrifugation steps (often with increasing centrifugal force) and is one of the most popular techniques for EV isolation. The number and speed of centrifugation steps may vary between groups and especially between biological fluids. Typical differential centrifugation of EVs from blood and conditioned culture medium are summarised below (**Figure 1.1.6**).
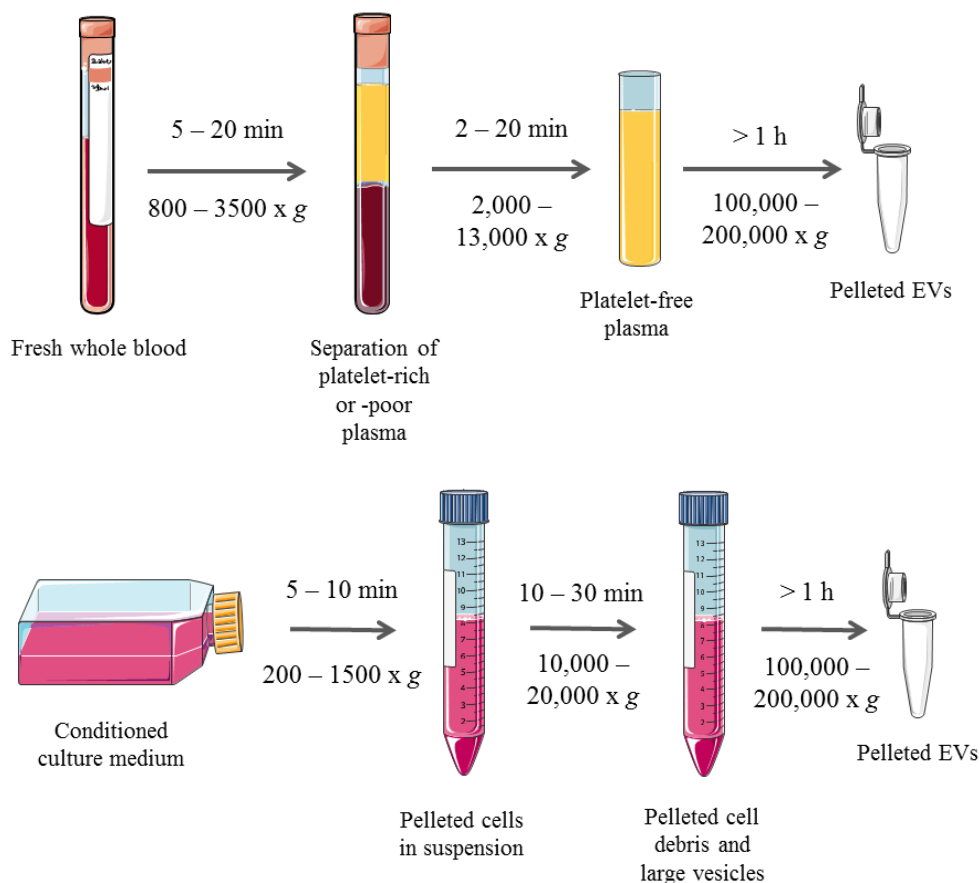
Figure 1.1.6: Differential centrifugation. Typical differential centrifugation steps used to isolate EVs from blood and conditioned culture media. Number of steps, centrifugal force and times may vary between groups and biological fluids.

The popularity of differential centrifugation as an isolation technique may be due to its simplicity and short preparation time. However, several limitations are associated with differential centrifugation. For instance, the final ultracentrifugation step may pellet some soluble material in the remaining supernatant. Therefore the preparatory spins prior to ultracentrifugation are crucial to remove contaminating artefacts such as platelets and cell debris. Supernatants, particularly those derived from blood, are likely to contain a mixture of lipoproteins and soluble proteins as well as EVs (21,118,119) which may co-pellet following ultracentrifugation. Ultracentrifugation may also alter the physical properties of EVs by inducing EV aggregation with protein complexes (117,120), fusion with other EVs (11,121), and increasing PS exposure (122) which may lead to erroneous results. Therefore, differential centrifugation is proposed as an enrichment method rather than a purification method for EV analysis. Calculating the ratio between the number of vesicles and the amount of protein detected in the EV sample was recently suggested as a simple method of determining EV sample purity (123).

Alternatively, successive filtration of EVs has long been used as a less vigorous method of purification (124). A number of studies have applied the use of simple submicron filters to remove larger vesicles and protein aggregates (58,59,110,117,123). However, it is unknown whether any interaction occurs between the EV and the filter and whether the higher concentrations of EVs observed post-filtration are due to increase purity, or deformation and disintegration of EVs by the filter. More sophisticated filtering systems have used to separate free protein from EVs such as tangential flow filtration (TFF), in which samples are passed through a hollow fibre 500 kDa filter (124,125) or ultrafiltration which combines centrifugation and filtration (typically a 100 kDa filter) (126,127). Filtration is often then combined with other techniques such as differential centrifugation or density centrifugation to aid purification.

Density gradient ultracentrifugation is regarded as the current "gold standard" EV isolation technique as it allows EVs to be separated from protein contaminants which are denser, and EVs can also be validated to their expected density (1.13 – 1.19 g/mL for exosomes (128) and 1.03 – 1.08 g/mL for microvesicles (129)). EVs sediment at the point where their density is equal to that of the surrounding media. Each density fraction can then be probed for EV markers to confirm enrichment (**Figure 1.1.7**)

and then be pooled for further analysis. Sucrose (64,66,74,128,130) or iodixanol (106,131,132) are often used as mediums for density ultracentrifugation of EVs. The process is typically longer than differential centrifugation (**Figure 1.1.6**) taking up to 16 hours (117) and is usually performed overnight (17). Interestingly, EVs separated by density gradient ultracentrifugation have usually first been pelleted by differential centrifugation. Density separation is then used to improve the purity of the EV sample for downstream analyses. However, lipoproteins have similar densities to EVs, suggesting EVs isolated by density ultracentrifugation may still be contaminated with lipoproteins. Moreover, EVs are still exposed to the initial ultracentrifugation and therefore may have been fused or damaged before loading onto the density gradient. Pooling of specific EV fractions may also introduce a selective bias towards a certain EV population, causing others to be discarded.
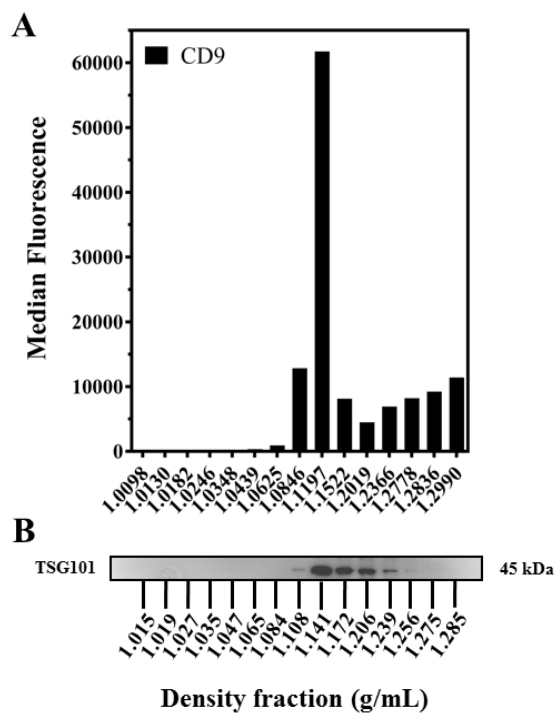
Figure 1.1.7: Density ultracentrifugation enrichment of EV markers. Example data of EVs separated by density ultracentrifugation and probed for (**A**) the generic EV marker, CD9, using FC and latex beads and (**B**) for the exosomal marker, TSG101 using Western blot. Data are courtesy of Dr Joanne Welton (Cardiff Metropolitan University).

The application of SEC as a novel EV isolation technique has been relatively well received as prior ultracentrifugation processing may not be required. SEC, also termed gel filtration, separates particles based on their relative size to porous polymer beads packed into a column (133) (**Figure 1.1.8**).

SEC columns have been tested for plasma-derived EV isolation by directly adding isolated plasma to columns packed with Sepharose CL-2B (118,119,134–136), Sepharose CL-4B, Sephacryl S-400 (134) or the commercial qEV column (126) (IZON Science, NZ). Most columns used a 10 mL bed volume collecting 500 μL elution fractions following loading of 1-1.5 mL plasma (depleted or free of platelets). All studies found SEC successfully separated EVs in distinct fractions to the majority of serum proteins such as albumin by enrichment of tetraspanins, cleaner transmission EM (TEM) images and good particle to protein ratios. Two studies also illustrated a successful separation of lipoprotein makers (118,135) from EVs following SEC, however this was not reproducible in other studies that measured lipoprotein markers (119) and in our own pilot experiments (unpublished observations). Muller et al., observed that SEC had no effect on the ability of cancer exosomes to immuno suppress CD4^{+} T cells (136) indicating EVs isolated by SEC retain their functionality. This is also important to demonstrate the effect is due to the EV itself rather than co-pelleted contaminants. The relative potential of SEC for EV isolation is reflected in the marketing of two commercial SEC columns specifically for EV isolation: Exo-Spin™ Midi Columns (Cell Guidance Systems, UK) and qEV™ (IZON Science, NZ). However, further optimisation of SEC is needed to improve separation from lipoproteins and to design a repeatable workflow. The labour-intensiveness and time of fraction collection could be reduced following optimisation, by pooling fraction collection into larger volumes (119,135,136). However, this may also introduce bias through the selection of specific fractions and EV populations. Due to the relatively small volume loaded in comparison to the bed volume, dilution of signal could be a limitation of SEC, particularly for less abundant markers. Welton et al., experienced difficulties in concentrating eluted fractions back up for subsequent analysis (119). Furthermore, dilution of signal in combination with the pooling of fractions may make it difficult to relate the measured concentration of EVs to that in circulating plasma.
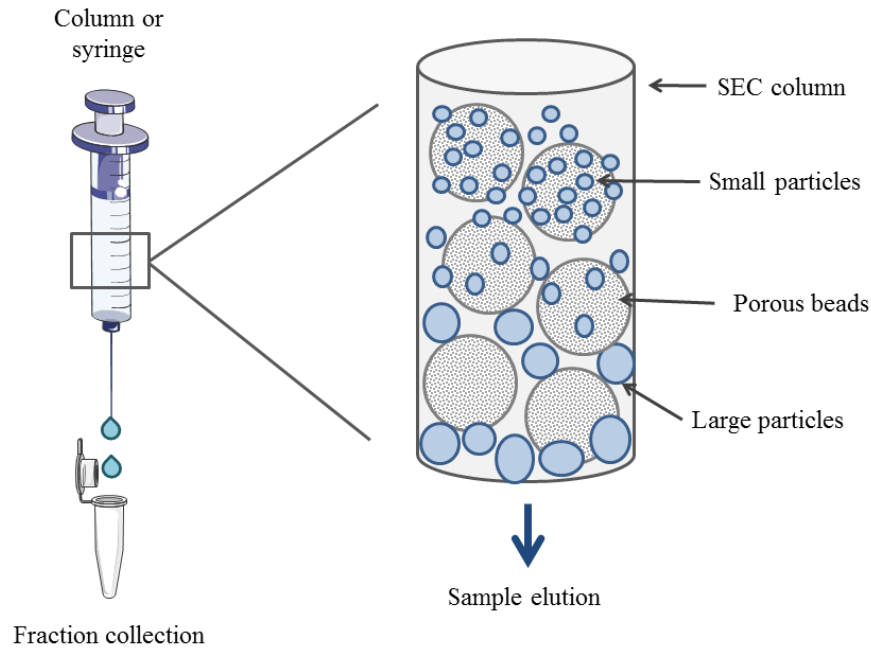
Figure 1.1.8: Principle of SEC: SEC columns are usually prepared in 10 mL syringes by pouring the matrix (commonly Sepharose) and allowing it to pack under gravity. Complex biological fluids such as plasma containing a heterogeneous mix of EVs, proteins and lipoproteins can then be added directly onto the SEC column. Larger particles are unable to pass through the pores in the beads and so pass quickly through the column, whereas smaller particles are able to pass through the pores, therefore taking longer to elute. Fractions can then be collected at set intervals (volume or time) and analysed for protein markers, EV concentration and lipoprotein markers to monitor the progress of the sample through the SEC column.

Immunoaffinity isolation of EVs involves the coupling of an antibody of interest to magnetic beads (or beads that are pelleted at relatively low centrifugal forces). The beads are then incubated with EVs which bind to the antibody-bead complex and the beads can be subsequently removed from unbound EVs and contaminants by a magnet or low speed centrifugation. The technique is well characterised for cells and was first demonstrated for EV isolation using exosomes bearing MHC II in 2001 (137). Despite the demonstration of successful isolation of EVs without the need for high-speed centrifugation using a quick, simple method, the use of immunoaffinity isolation has been slow to catch on in the EV field. Recently, magnetic beads were used to isolate TF$^+$ EVs from plasma (138) and annexin V positive EVs isolated by

immunoaffinity were then used for downstream analysis of EV RNA (139). Antibody-coated beads have also been used to capture EVs for flow cytometric measurements as often the bead is ~1 – 10 μm in diameter (140). This overcomes the major limitations of using FC for EV measurements (*Section 1.1.7.2*) and also allows for dual staining of EVs. However, immunoaffinity assays isolate specific populations of EVs and may therefore bias towards certain EV subsets. Furthermore, recovery may not be 100% efficient and therefore downstream analyses may be underestimated.

Commercial techniques for EV isolation are also available including SEC-based methods, ExoSpin™ and qEV™, and the precipitation technique, ExoQuick™ (System Biosciences, USA). The exact mechanism of action of ExoQuick™ has not been disclosed though the process uses a polymer to precipitate exosomes directly from biofluids such as plasma using a mixture of specific reagents and low speed centrifugation (141). ExoQuick™ has been reported to provide superior isolation of exosomal RNA and proteins compared to ultracentrifugation, SEC and immunoaffinity-based methods (142) however, other studies have indicated low enrichment of EV markers and high contamination of non-EV protein with ExoQuick™ isolations (126,141). Therefore, commercial isolation techniques such as ExoQuick™ should not be used without prior validation of sufficient EV purification.

A summary of the methods outlined above with respective advantages and disadvantages is given in **Table 1.1.3**. Irrespective of the protocol used for EV isolation, the method must first be validated for the biological fluid and shown to fulfil the minimal requirements outlined by ISEV to confirm the isolation of a true EV population (16).

Method	Subpopulation isolated	Advantages	Disadvantages
Differential centrifugation	Exosomes Microvesicles EVs	→ Fast → Little training required → Enriches EV markers → Can be adapted to remove larger microvesicles/isolate only exosomes	→ Crude separation of EVs (contamination from soluble protein and lipoprotein) → May cause EVs to fuse → May increase PS exposure
Filtration (including tangential flow filtration (TFF))	Exosomes EVs	→ Fast and simple → Remove protein contaminants (TFF)	→ Unknown interaction of EVs with filter → May require additional purification steps
Density gradient	Exosomes Microvesicles EVs	→ Separation from protein contaminants → EVs can be verified by density	→ Lengthy procedure → Requires training → May not separate lipoproteins → May require additional processing
Size exclusion chromatography (including qEV™ and ExoSpin™)	Exosomes Microvesicles EVs	→ Fast and simple → Requires minimal pre-processing → Separation from protein and potentially lipoprotein contaminants	→ Labour-intensive → Sample diluted by column so may require concentration afterwards → Workflow needs refining and further validation of homemade and commercial columns needed
Immunoaffinity	Exosomes Microvesicles EVs	→ Fast and simple → Allows isolation of specific sub population	→ Recovery may not be 100% → May bias towards specific population → Needs further validation
ExoQuick™	Exosomes	→ Fast and simple	→ Impure isolation → Low enrichment of exosomes

Table 1.1.3: Summary of methods of EV isolation. Current methods employed for EV isolation and their respective advantages and disadvantages.

1.1.6.3 Storage of isolated EVs

For EVs to serve as clinical biomarkers in large-scale studies or routine diagnostic analyses, storage of EV samples is paramount. Therefore, optimal storage vessels, medium, method and length must be established to minimise changes in EV profiles. Though a number of studies have reported differences in EVs when varying storage parameters, results are often conflicting and as such, no standardised protocols are in place for EV storage. Furthermore, many of these studies have been undertaken using FC to enumerate EVs, which as discussed in *Section 1.1.7.2*, is sub-optimal.

The material of the storage vessel has been proposed to affect EVs as certain plastics may cause EV aggregation and adherence to the vessel. Silicone storage vessels have been suggested as an alternative (17), however no physical evidence exists in the literature demonstrating the effect of storage material on EV characteristics. The most widely-used medium for EV resuspension and storage is phosphate buffered saline (PBS) (117). Recent advice suggests the PBS must be completely free of calcium to avoid formation of calcium phosphate complexes (16), which are in the same size range as EVs and may therefore skew size and concentration analyses. Other solutions have also been used to store EVs, including 4-(2-hydroxyethyl)-1-piperazineethanesulphonic acid (HEPES), water, dimethyl sulphoxide (DMSO) and glycerol (16). DMSO and glycerol, commonly used in the cryo-freezing of cells, reportedly cause partial lysis of EVs (143); however, our own observations with glycerol do not marry with this (P8B-301) (144). Storage mediums should also be filtered (using a 0.22 μm filter) to remove any EV-sized contaminants prior to resuspension of EVs, or a commercial sterile medium should be purchased.

Analysis of EV samples on the same day as isolation is often not feasible, particularly if a lengthy isolation procedure is used. Therefore, it is important to understand the impact of the method and of short- and long-term storage on EV characteristics. Although a number of studies have analysed the effects of storage on EVs, much of the data are contradictory, making it difficult to interpret the "best option". Studies have illustrated that EV isolation from the biofluid before storage is optimal, particularly with blood-derived samples. Plasma frozen prior to EV isolation contained a greater contamination of protein aggregates in subsequent EV isolations (136). Additionally, storage of platelets at -80°C resulted in an increased

concentration of platelet-derived EVs with a reduced diameter and a greater thrombin-generation (procoagulant) capacity (145,146).

Currently, most studies store samples at -80°C in PBS (17). Concentration, functionality (143) and EV diameter were shown to be unchanged following storage at -80°C and repeated freeze-thaw cycles also had no effect on EV size (147) suggesting stability of EVs at this storage temperature. Furthermore, small RNAs within EVs were stable following 1 month of storage at room temperature and also following 20 freeze-thaw cycles at -80°C (110). The size, concentration and morphology of EVs from conditioned culture medium, platelet and erythrocyte concentrates and urine were also unaffected by storage at -80°C (109).

Conversely, others report that storage of EVs at -80°C resulted in an immediate decrease in diameter of EVs and a gradual (>2 months storage) degradation of EV RNA (148). Ayers et al., observed increases in annexin V and platelet-positive (CD41+/CD31+) plasma EVs following 1 month storage at -80°C (107), supported by Yuana et al., who reported an increase in lactadherin-positive EVs following storage at -80°C (109). Storage of EVs at -80°C with repeated freeze-thaw cycles also reduced the EV RNA (139). Long-term storage was also detrimental to the concentration of plasma-derived EVs which was significantly decreased between 1 (59) and 2 years of storage at -80° C (107). Storage of EVs at temperatures above freezing has also been shown to have conflicting effects on EV characteristics. Storage of EVs at 20°C or 4°C for >1 week resulted in decreased EV concentration and a loss of functional activity (143). The diameter of EVs was also rapidly reduced following storage at 37°C, and to a lesser extent at 4°C (147). However, others have observed stability in EV concentrations following storage at room temperature for 4 days (59).

There are evidently many problems regarding the pre-analytical processing of EVs and few concrete solutions to these issues from which to design a protocol. Until more is known about the effects of EV processing steps, consistency between samples and experiments and complete clarity in reporting methods are paramount to enable comparisons with the rest of the field.

1.1.7 Measurement

A variety of optical and non-optical techniques are available for the measurement of EVs, and the chosen technique often reflects the desired outcome or application. TEM is commonly used to determine the ultrastructure, FC to analyse surface phenotypic makers, and NTA to quantitate the size and concentration of EVs (149).

1.1.7.1 Methods for determining EV morphology

The minimal requirements outlined by ISEV (16) (**Table 1.1.2**) indicate a need for visual evidence of individual and multiple EVs in samples. TEM is the most widely-used technique to visualise EV structure; originally described as a "cup-like morphology" though this has since been shown to be an artefact of TEM preparation (117). Heavy metals such as uranyl acetate allow staining of lipid membranes, and these are visualised following fixation and dehydration onto grids (17). EVs can also be stained with antibodies (such as CD63) coupled to nano-gold particles to allow further confirmation of an EV population (150). Cryo-EM may relinquish the need for dehydration and fixation by fast-freezing EV samples, and has recently identified a number of different EV structures such as "vesicle-within-vesicle" structures (151).

Atomic force microscopy (AFM) is also used to visualise EV structures by scanning the surface of EVs without contact, using deflections of a directed laser beam to build a 3D image with nanometre resolution (108,152). EVs are bound to a flat surface onto which antibodies can also be conjugated, allowing the application of immuno-detection to analyse specific EV populations (152).

Though size distributions and structures of EVs can be visualised by TEM and AFM, EV concentration cannot be calculated and experiments may take hours to conduct.

1.1.7.2 Phenotyping EVs

Perhaps the most interesting aspect of EV research is the analysis of the markers carried by EVs, and particularly how these may change in disease. Once again, the ISEV minimal requirements outline the need for analysis of EVs to show the presence of certain markers and the absence of others (**Table 1.1.2**). FC is the most

widely used technique for both qualitative and quantitative EV measurements. Samples are introduced into the system surrounded by a fluid sheath which then directs the sample through a laser beam (**Figure 1.1.9**). The constituents of the sample (usually cells) scatter light forwards depending on their size (forward scatter) and sideways depending on their granularity (side scatter). Both scatter profiles are collected by detectors and used to create a dot plot from which samples can be gated to allow enumeration of particles within the sample. Additionally, specific antibodies can be used bearing a fluorochrome which is excited by a certain laser to allow quantification and phenotyping of subpopulations. Multiple antigens can be analysed simultaneously by using different lasers and antibody-fluorochrome combinations, providing fluorochrome emission spectra do not overlap.

Unfortunately, the use of FC for EV analysis is hampered by a number of limitations. Many conventional flow cytometers are unable to detect EVs <300 nm in diameter, which is the range in which most EVs fall (120). This is due to the low refractive index of EVs (149) meaning the majority of EVs fall within the noise of the cytometer. Furthermore, the gating of EV populations is usually based on the forward and side scatter properties of submicron polystyrene beads (17,149). The refractive index of a 200 nm polystyrene bead can be up to 15 times higher than that of an EV of equal diameter (149) leading to false comparisons of size between beads and EVs, as EVs would scatter less light and appear to be smaller. Silica beads reportedly have a refractive index more akin to that of EVs than polystyrene and may be more representative for EV gating (153). The limited diameter of EVs also prevents the flow cytometer from efficiently sorting EVs into a single particle stream for individual analysis, meaning individual EV counts may be the result of "swarm" detection (multiple EVs) (154).

Steps have been taken to improve the flow cytometric detection of EVs such as high resolution FC which may detect EVs ~100 nm in diameter (155) though this requires expensive machinery and an experienced user. Alternatively, similarly to immunoaffinity isolation (*Section 1.1.6.2*), EVs can be conjugated to latex beads (>1 µm in diameter) carrying an antibody to a marker of interest (117), e.g. CD9. EVs bound to the beads are then within a detectable range for analysis and can be probed with further antibodies.
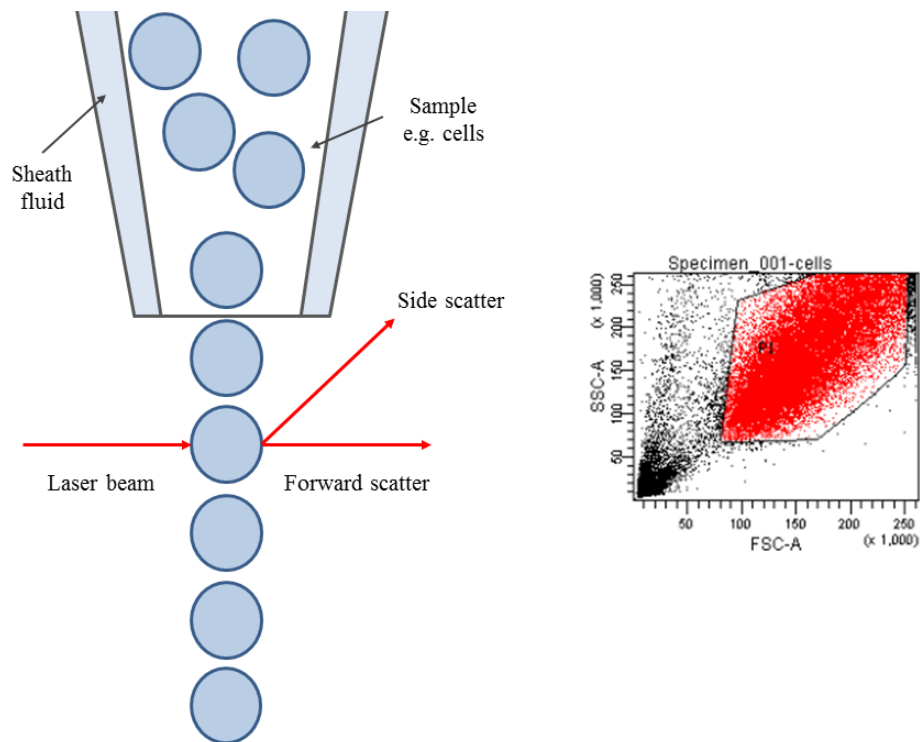
Figure 1.1.9: Flow cytometry. A schematic illustrating the mechanism of FC. The sample (e.g. cells) is drawn into the machine and surrounded by sheath fluid. The fluid and the shape of the tube allow the hydrodynamic focusing of the sample into a stream of single cells. Individual cells then pass through a laser and the resulting forward and side scatter are collected by positioned detectors. Scatter profiles can then be plotted and gated (right).

Western blotting and quantitative real-time (qRT)-PCR are also useful techniques for analysing the protein and RNA content of EVs. Western blots are frequently presented alongside density ultracentrifugation data to provide evidence for enrichment of EV proteins in the correct density fractions (**Figure 1.1.7**). More sensitive proteomic techniques (primarily using MS) can be applied to EVs that are able to simultaneously analyse an array of proteins to highlight potential biomarkers (156–158). Microarray analysis can also be used to analyse a wide variety of RNA species in EV samples to highlight potentially interesting changes in specific mRNAs and mIRs (76). Lipid species (lipidomics) of EVs can be identified using GC alone (55,76,159) or combined with MS (GC-MS) (78). Generally, large-scale analyses of EVs are useful to analyse a range of markers within EVs and may highlight potential biomarkers of interest for further study. However, due to the amount of data generated by these methods, great care should be taken with data

interpretation and an experienced user should be consulted. Markers of interest should then be validated using Western blot or qRT-PCR to confirm results. These types of techniques are usually expensive and time-consuming.

Immunophenotyping of EVs has been proposed as an alternative method to Western blotting that allows analysis of multiple antigens in synchrony (119,158). The principles of EV immunophenotyping are shown in **Figure 1.1.10**. EVs are settled onto high-binding enzyme-linked immunosorbent assay (ELISA) plates and probed for antibodies of interest. EVs may also be partially permeabilised to analyse antigens within EVs as well as surface markers. A biotinylated secondary antibody then allows binding of streptavidin-europium conjugates. The bound europium probe can then be dissociated from the streptavidin and excited at 340 nm by a series of flashes. The resulting fluorescence emission is monitored using time resolved fluorescence (TRF) and a narrow emission peak is produced with a large Stokes' shift and long decay time, thereby giving a good signal-to-noise ratio. The technique has been successfully applied to measure markers within prostate cancer EVs (158), plasma-derived EVs (119) and by ourselves in adipocyte-derived EVs (159). Though the technique requires initial efforts to validate EV and antibody concentrations, it is a promising simple and rapid technique for phenotyping multiple markers on the surface of and within EVs.
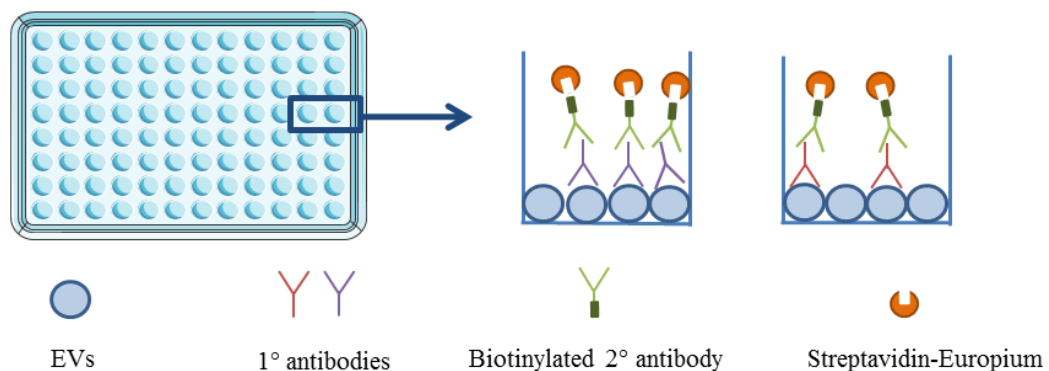
Figure 1.1.10: Immunophenotyping of EVs. EV immunophenotyping is performed on high-binding ELISA plates. A primary antibody of choice can be added to the well and the same sample can be probed with other antibodies using remaining wells. A biotinylated secondary antibody is then added which allows binding of a streptavidin-europium conjugate. Flash excitation of wells allows generation of fluorescence which can then be measured in a plate reader with TRF settings.

1.1.7.3 Quantification of EVs

The enumeration and accurate sizing of EV populations may also be important in comparing EVs between healthy and disease states. Several techniques have been used to determine the size and concentration of EV samples, each with their own advantages and limitations. Dynamic light scattering (DLS) measures the light scattered from EVs in suspension (i.e. under Brownian motion) and uses the information to determine EV size and concentration (143,160). However, the scattering of EVs is collected by a single detector (160,161), meaning the signal is averaged for the whole EV population. Therefore larger EVs scattering more light bias the average signal and potentially overestimate the overall size. For monodisperse populations such as exosomes however, DLS may produce relatively accurate size and concentration data.

NTA is a technique which incorporates the principles of DLS but uses additional video tracking of EVs over time for detection. This overcomes the shortfalls of DLS by tracking the light scattering and Brownian motion of individual EVs over time to calculate EV size and concentration distributions. However, large EVs will still scatter considerably more light than smaller EVs, and hence may still dominate recordings. Analytical software settings have the potential to introduce subjectivity into EV analysis with NTA, though a recently published technical report provides advice on how to minimise sources of variation (162). Due to its simplicity and the relatively short sampling time, NTA is one of the most popular techniques for EV quantification. The addition of a syringe pump and more advanced software which can be programmed to continuously introduce samples into the viewing chamber allows measurement of replicates in quick succession (162) and reduces the input time of the user. NTA is also moving towards the measurement of fluorescently labelled EVs using different laser and camera attachments (161,163). A current limitation of NTA and other EV quantification methods is the inability to distinguish EVs from contaminating material such as protein complexes and lipoproteins. Although fluorescence NTA is not yet in routine use, it has great potential in combining the direct labelling of EVs with accurate size and concentration data.

Tunable resistive pulse sensing (TRPS) is a non-optical method for determining EV size and concentration. TRPS measures the disruption in current generated by EVs as

they pass through a tunable nanopore that is suspended between two wells of electrolyte buffer (164). EVs are measured on a particle-by-particle basis, allowing data to be recorded for each EV traversing the pore. The magnitude of the blockade event (disruption in current) is proportional to the EV size and the frequency of blockade events is proportional to the concentration of EVs. TRPS has been used to accurately quantify EVs in a variety of biological fluids (55,165); however, issues with pore clogging and the need for multiple nanopores to cover the EV size range have perhaps prevented TRPS becoming as widely used as NTA. Furthermore, sample analysis is much more labour intensive than NTA as continuous monitoring is needed to identify pore blockages and (especially less concentrated) samples may take up to 10 minutes to record per replicate. However, a unique ability of TRPS is the measurement of EV surface charge from the duration of the blockade event (166). This may have interesting applications in the phenotyping of EVs based on changes in surface charge. Aptamers are single strands of nucleic acids (DNA or RNA) with high specificity and affinity to a target (e.g. protein) (164,167). Aptamers conjugated to beads and incubated with thrombin were shown to traverse the nanopore differently due to a change in surface charge from binding of thrombin to the aptamer-bead complex (167). This work was then extended using two aptamers (for vascular endothelial growth factor (VEGF) and platelet-derived growth factor (PDGF)) conjugated to beads of different sizes allowing multiplexing of samples (168). The combined use of aptamers for specific EV markers and TRPS may allow for simultaneous analysis of size, concentration and surface markers of EVs.

Currently no "gold standard" technique exists for measurement of EVs, and the chosen technique is often dictated by the desired outcome. As with EV isolation, it seems that complete clarity in the methods used to analyse EVs is needed to enable comparison with the rest of the field. Users must also have a good understanding and be aware of the advantages and limitations of each analytical technique to avoid erroneous results. Clearly, most of the measurement techniques used for EVs are striving to improve their methods and capabilities, so it is hoped in the future that standardisation of EV measurements will be achieved.

1.1.8 Physiological roles of extracellular vesicles

EVs from a variety of sources can be detected in a number of biological fluids of healthy individuals and have been recognised as important cell-cell communicators. The field has been dominated by pathological roles of EVs in disease, though it is clear that EVs are also important homeostatic mediators (**Figure 1.1.11**).

1.1.8.1 Biodistribution of EVs

The biodistribution of circulating EVs is dependent upon the ratio between EV biogenesis and EV clearance (169). Little is known about the half-life of circulating EVs, though a number of studies indicate the rapid clearance (within 30 minutes) of exogenously isolated EVs following re-introduction (170–172). EVs bearing a MFG-E8-luceriferase label were cleared from the circulation within 2 minutes of injection (173). *In vivo* studies however, reported a much slower clearance from the circulation (~6 hours). EV internalisation by cells is likely to account for the majority of clearance, which is a cell-specific process, depending on the cellular origin of the EV and the target cell (*Section 1.1.5*).

1.1.8.2 Role of EVs in haemostasis

One of the most studied functions of EVs is their contribution to the coagulation cascade; primarily the role of platelet-derived EVs. Some of the earliest studies into EVs insinuated a procoagulant effect of platelet-derived EVs (1,2) and platelet-derived EVs were recently shown to enhance thrombin generation *in vitro* (174,175). The exposure of PS on platelet-derived EVs provides a platform for the assembly of factors of the coagulation cascade such as Factors VII and X and prothrombin (176). However, flow cytometric analyses of PS exposure of platelet-derived EVs using annexin V or MFG-E8 indicates that not all EVs expose PS at their surface (63,177). TF is a potent stimulator of coagulation and has also been shown to be present in EVs (169). Interestingly, platelet-derived EVs seem to contain very little TF (169) suggesting EVs derived from other cell types contain procoagulant TF. Indeed, procoagulant EVs have been shown to be released from leukocytes, endothelial cells, monocytes (169), erythrocytes (178) and vascular smooth muscle cells (179). The

presence of TF within these EVs seems to be the reason for their procoagulant characteristics (176). Some studies suggest the presence of EVs with anticoagulant properties in the circulation, harbouring inhibitors of the TF pathway (180,181) and also those with a fibrinolytic phenotype (182). Interestingly, these subsets of EVs were not of platelet origin, indicating many of the haemostatic properties of EVs are not regulated by platelet-derived EVs. Furthermore, non-blood derived EVs such as those derived from saliva and urine, possess procoagulant properties. Salivary EVs were found to contain TF and were able to initiate coagulation in EV-free plasma. The authors hypothesised that the presence of procoagulant EVs in our saliva may explain why we lick wounds, in order to enhance coagulation and sealing of the wound from pathogens (183).

The regulatory role of EVs in coagulation is illustrated by individuals with Scott Syndrome, who have lower levels of circulating platelet-derived EVs (184). A scramblase enzyme in the plasma membrane of platelets is mutated, preventing PS externalisation (185). These individuals are at an increased risk of severe bleeding due to a reduced ability of platelets and platelet-derived EVs to initiate coagulation.

1.1.8.3 Role of EVs in angiogenesis

EVs derived from a number of cell types regulate vascular cell growth. Endothelial cells were shown to generate EVs containing the Notch signalling ligand, delta-like 4 (Dll4) which is crucial for the regulation of angiogenesis (186). These EVs were then shown to induce sprouting and branching of endothelial cells *in vitro* and *in vivo*. Platelet-derived EVs were also shown to contain pro-angiogenic lipids and VEGF which could induce endothelial cell proliferation and capillary sprouting *in vivo* (187). The transfer of phosphoinositide 3-kinase (PI3K) protein and mRNA from EPCs can stimulate angiogenesis in endothelial cells (84). Furthermore, EVs derived from hypoxic placental mesenchymal stem cells (MSCs) were shown to aid the adaptation of the placental vasculature to low oxygen (O_2) concentrations by enhancing endothelial cell angiogenesis (188).

1.1.8.4 Role of EVs in the immune system

EVs are also implicated in modulating cells of the innate and adaptive immune system. Polymorphonuclear neutrophils (PMNs) secrete EVs that promote an anti-inflammatory phenotype in DCs and monocytes (189) and control the phagocytosis of apoptotic PMNs to promote resolution (190). Additionally, PMN-EVs impaired leukocyte adhesion and infiltration to endothelial cells, preventing subsequent leukocyte extravasation and initiation of tissue inflammation (191,192). EVs are also involved in antigen presentation. Intestinal epithelial cell-derived EVs harbouring MHC class I and II are able to transfer orally ingested antigens from the apical lumen to antigen presenting cells at the basolateral membrane of the gut epithelia (193,194). Antigen presenting cells can also secrete EVs carrying MHCs class I and II to present the antigen to T cells (195) showing EVs are heavily involved in modulating immune responses. MSC EVs harbour the same anti-inflammatory and immunosuppressive properties as MSCs (169) and were shown to induce Mϕ polarisation towards an M2 (anti-inflammatory) phenotype and enhance T regulatory (Treg) cell production. (196).

1.1.8.5 Role of EVs in bone formation

The role of EVs in bone formation was first documented over 40 years ago, providing one of the earliest examples for a physiological role for EVs (197). These EVs are often referred to as matrix vesicles, and they are required for the initiation of mineralisation (198). Matrix vesicles are secreted from chondrocytes in response to retinoic acid (199) and are enriched in Ca^{2+}-binding proteins to promote transport of Ca^{2+} into the vesicle lumen and phosphatases to liberate phosphate (198). Accumulation of Ca^{2+} and phosphate within matrix vesicles leads to the formation of calcium-phosphate complexes (hydroxyapatite) (200). EVs then release hydroxyapatite into the extracellular matrix where further hydroxyapatite formation can occur in clusters around matrix vesicles and between collagen fibres leading to mineralisation (198).
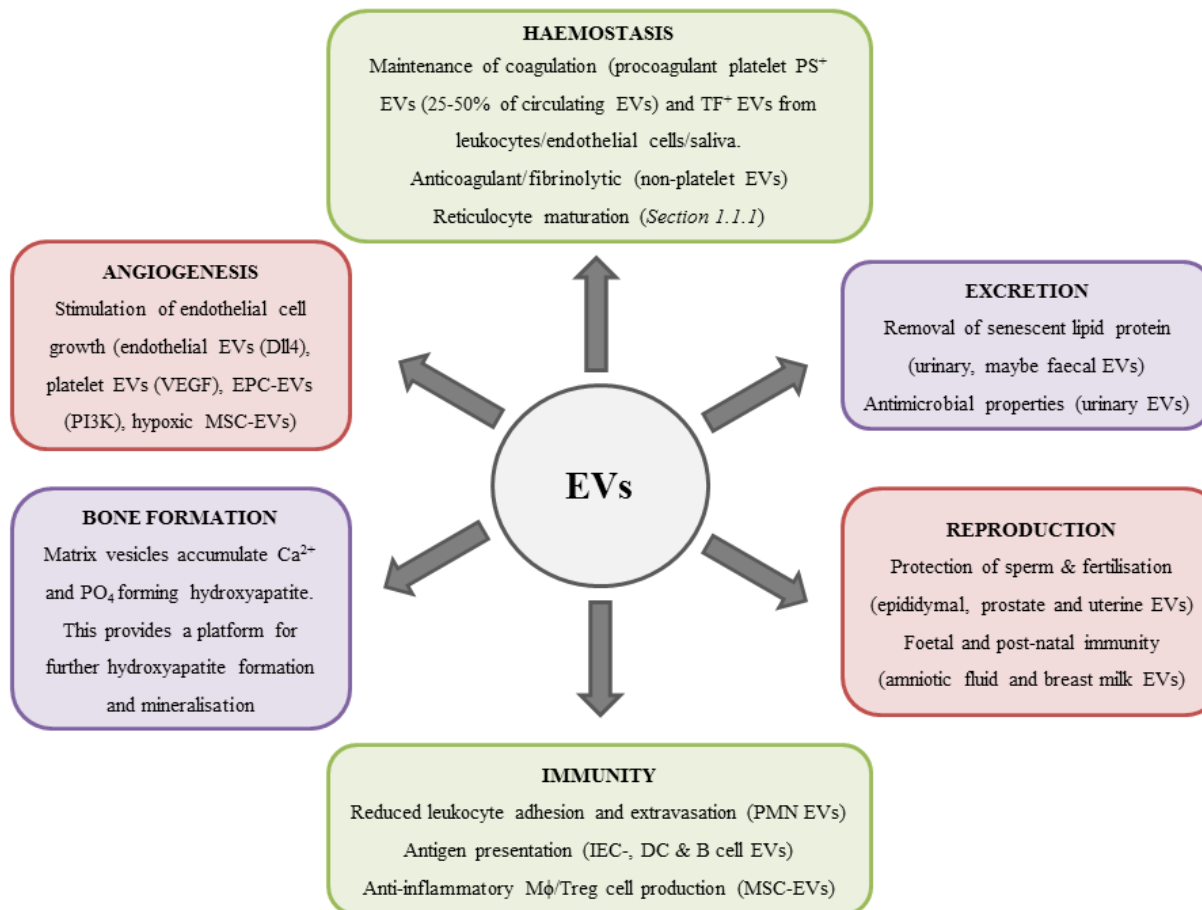
Figure 1.1.11: Physiological roles of EVs. A summary of documented physiological roles of EVs *in vivo*. Ca^{2+} = calcium; DC = dendritic cell; Dll4 = delta-like 4; EPC = endothelial progenitor cell; IEC = intestinal epithelial cell; MSC = mesenchymal stem cell; Mϕ = macrophage; PI3K = phosphoinositide 3-kinase; PMN = polymorphonuclear neutrophil; PO_4 = phosphate; PS = phosphatidylserine; TF = tissue factor; VEGF = vascular endothelial growth factor.

1.1.9 Pathophysiological roles of extracellular vesicles

Despite the diversity of physiological roles for EVs, the vast majority of EV research is centred on the role of EVs in pathology. Altered concentrations and differences in biochemical composition in disease states make EVs promising biomarkers.

1.1.9.1 EVs in cardiovascular diseases

CVD is the global leading cause of mortality, accounting for over 30% of deaths worldwide in 2012 (201). CVD is an umbrella term for a number of disorders that afflict the heart and vasculature such as coronary artery disease (CAD). CVDs are multifaceted and often present alongside co-morbidities such as diabetes mellitus. EVs have been implicated in a plethora of CVDs and co-morbidities, a number of which are outlined below.

In CAD, coronary arteries are occluded by fatty deposits in the artery wall, increasing the risk of myocardial infarction. Studies have found elevations in endothelial EVs in CAD (202,203), perhaps reflecting the underlying endothelial dysfunction. Endothelial EVs also displayed a procoagulant phenotype (202) and contained elevated CD144 (vascular endothelial cadherin) (204) which may indicate changes in endothelial cell permeability in patients with CAD. Endothelial EVs have also been shown to possess anti-inflammatory mIRs; mIR-216, involved in vascular repair, and mIR-222, which is able to reduce endothelial cell expression of intercellular adhesion molecule (ICAM)-1 and hence reduce leukocyte adhesion to endothelial cells (205). However, these mIRs were reduced in hyperglycaemic conditions, thus enhancing leukocyte adhesion and extravasation. Furthermore, EVs from hyperglycaemic endothelial cells induced endothelial dysfunction and increased Mϕ infiltration leading to subsequent development of atherosclerosis *in vivo* (206). EVs derived from atherosclerotic plaques were rich in ICAM-1 which could then be transferred to healthy endothelial cells to induce leukocyte adhesion and atherosclerotic plaque formation (207). Taken together, alterations in endothelial EV concentration and composition may provide an indication of CVD status. Indeed, endothelial EVs correlated with a subset of diabetic patients with no symptomatic evidence of angina, but with evidence of CAD on angiography (204). The

concentration of endothelial EVs from patients with high risk coronary lesions was over twice that of patients with low risk lesions. However, concentrations of endothelial EVs in patients with severe occlusions of the coronary artery were comparable with healthy controls (208). This suggests that endothelial EVs may be useful biomarkers of early CAD, before the development of severe stenosis.

Age- or disease-related arterial stiffening increases the risk of CVD and mortality (209). Vascular calcification plays a major role in arterial stiffening and is often found in association with atherosclerotic plaques. Vascular smooth muscle cells (VSMCs) have been heavily implicated in calcification as they are able to transition towards a phenotype associated with bone formation (210). Physiological VSMCs release EVs enriched with osteogenic inhibitors such as matrix Gla protein (211) and fetuin-A (212). In conditions of endothelial dysfunction and/or conditions of elevated extracellular Ca^{2+}/PO_4, VSMC EV release is altered (213). These EVs contain low amounts of osteogenic inhibitors and high levels of Ca^{2+}-binding annexins and PS that can initiate nucleation of hydroxyapatite (213,214). These EVs also contain specific mIRs that target markers of osteogenic differentiation (215) and matrix metalloproteinase-2, which assists calcification via degradation of elastin fibres (214). Therefore vascular calcification is mediated by EVs as in chondrocyte calcification and bone formation. However, VSMCs release EVs via the classical pathway (*Section 1.1.3.1*) as EVs contain exosomal markers and arise from MVBs whilst chondrocyte-derived EVs arise from a direct budding of the plasma membrane (216). Mϕ within atherosclerotic lesions are also capable of releasing EVs that promote local microcalcification (217). Interestingly, these Mϕ were also shown to possess an M1-like phenotype (217) suggesting a proinflammatory role for Mϕ in addition to calcifying capabilities. Microcalcification within atherosclerotic plaques causes the plaque to become unstable, hence increasing the risk of rupture and subsequent MI or stroke (218). A recent review of EV-mediated vascular calcification suggested that calcifying EVs are "erroneously caught in the ECM" and inadvertently induce microcalcification in vessel walls due to being trapped in the ECM (219). In light of the data presented here, this notion seems unfounded as it appears EVs produced by changes in the extracellular environment are specifically packaged with a cargo to deliberately induce an osteogenic phenotype in vessels.

Obesity is a major risk factor for CVD and has also been associated with an altered profile of circulating EVs. Studies have found increases in circulating EVs in "healthy" obese women (with no clinical presentation of CVD or diabetes) compared to healthy lean women (220,221). Increases in specific subsets of EVs such as platelet-EVs (220,222,223) and endothelial EVs (220,223–225) were also found in healthy obese subjects versus healthy lean controls. An increase in platelet-EVs was also observed in obese women with PCOS compared to age- and body mass index (BMI)-matched controls (226). However, this increase may not be due to obesity as others have found increases in annexin V positive EVs and platelet-derived EVs in PCOS women over a range of BMIs compared to age/BMI-matched controls (76,227). A number of studies have also observed reductions in platelet- and endothelial-derived EV concentrations in obese subjects following weight loss accompanied by a reduction in procoagulant markers (222,228,229) suggesting weight loss in apparently "healthy" but obese subjects, may have cardiovascular benefits. Further work is needed to analyse EVs associated with obesity, particularly those from other cellular sources. For example, our own group is currently analysing circulating EVs carrying inflammatory and adipocyte markers in a group of subjects across a range of BMIs.

1.1.9.2 EVs in cancer

The intercommunication of tumour cells with non-tumour cells via EVs is an intensely studied area of EV research. Tumour cells utilise EVs to promote tumour survival and progression through evasion of the immune system, modulating the tumour microenvironment and promoting angiogenesis for metastases.

Remodelling of the extracellular milieu allows the tumour to control the microenvironment so that tumour growth, proliferation and angiogenesis are supported (230). Tumour cells can both release EVs and modulate the EV release of MSCs to reduce tumour suppression and promote tumour growth (231). Tumour cell EVs also assist tumour progression and angiogenesis by driving the transition of stromal fibroblasts towards a myofibroblast phenotype via transfer of transforming growth factor (TGF)-β and induction of α-smooth muscle actin expression (232).

Tumours also use EVs to avoid immune recognition, helping to establish the tumour in the early stages of growth. Tumour cells shed the ligand for the natural killer group 2D (NKG2D) receptor via EVs to reduce recognition and destruction of tumour cells by cytotoxic NK and CD8$^+$ T cells (233). Transfer of TGF-β within tumour-derived EVs plays an important role in immune evasion by preventing dendritic cell antigen presentation (234) and encouraging the transition of CD8$^+$ cytotoxic T cells towards a regulatory T cell phenotype (235). Additionally, tumour EVs express Fas ligand on their surface which is able to bind to Fas$^+$ lymphocytes and suppress their response (236), and induce lymphocyte apoptosis (237).

The ability of tumours to induce neovascularisation enables tumour growth and enhances metastatic potential. EVs facilitate tumour-mediated angiogenesis through a number of mechanisms, usually by targeting VEGF expression. As described in *Section 1.1.8.3*, the Notch ligand Dll4 is carried by endothelial EVs and is essential for angiogenesis (186). Tumour EVs also harbour Dll4 and VEGF which stimulate local angiogenesis (238). Alternatively, tumour EVs were shown to carry a mutated, but functional form of the epidermal growth factor receptor (EGFR) (239). The mutated EGFR could be transferred to other tumour cells via EVs, increasing VEGF expression and oncogenic activity in these cells (240). These EVs could also be detected in the serum of glioblastoma patients, illustrating the mobility and metastatic potential of these EVs once in the systemic circulation. A major stimulus for tumour-mediated angiogenesis *in vivo* is hypoxia which results from rapid tumour growth. Secretion of EVs enriched in angiogenic proteins and mIRs is enhanced in hypoxic cancer cells in a hypoxia-inducible factor (HIF)-dependent manner (241). HIF proteins are able to regulate Rab22a which is involved in EV release. Inhibition of Rab22a abrogated tumour metastasis, highlighting the role of hypoxic-derived EVs in the co-ordination of tumour progression.

1.1.9.3 EVs in inflammatory diseases

In stark contrast to the immunosuppressive role of EVs in cancers, the general role of EVs in inflammatory disorders is immune-activating, highlighting the diversity of biological functions of EVs. EVs have been shown to possess auto-antigens that trigger and/or aid the progression of a number of autoimmune diseases such as

Rheumatoid arthritis (RA), systemic lupus erythematosus and multiple sclerosis (242). RA is an autoimmune disorder characterised by chronic inflammation of joints. Platelet-derived EVs have been strongly implicated in RA as circulating concentrations are elevated compared to healthy controls and the number of platelet EVs correlates with the severity of disease (243). However, very few platelet-derived EVs are detected within the synovial fluid of arthritic joints (244), suggesting a more systemic role for platelet-derived EVs in RA, perhaps by increasing the risk of CVD. Leukocyte EVs, particularly those derived from granulocytes were found to be the predominant EV population in RA synovial fluid (244,245). These EVs were highly annexin V positive and thrombogenic, suggesting a role in stimulating local coagulation and fibrin formation (244). Furthermore, these EVs enhanced the secretion of proinflammatory cytokines interleukin (IL)-8 and IL-6, and cytokines including monocyte chemoattractant protein (MCP)-1, soluble ICAM-1 and VEGF from synovial fibroblasts in an autologous fashion (245). Therefore, leukocyte EVs within synovial fluid may mediate and sustain inflammation within the arthritic joint.

EVs were also shown to exacerbate inflammation caused by infectious diseases. Mϕ infected with *Mycobacterium tuberculosis* release EVs containing microbial antigens and pathogen-associated molecular patterns that induce an inflammatory response in uninfected Mϕ via toll-like receptor activation (246). Also, cells infected with the malaria parasite produce EVs that strongly stimulate Mϕ activation and TNF-α secretion, contributing to the systemic inflammation associated with malaria (247). Systemic inflammation from sepsis is also associated with increases in circulating platelet and endothelial-derived EVs. Injection of EVs from septic patients into mice induces proinflammatory cytokine production and oxidative stress, further highlighting the potential immune-activating roles of EVs (248).

Evidently, EVs have a variety of different roles in the induction, progression and maintenance of disease pathology. Those covered here are summarised in **Figure 1.1.12**.
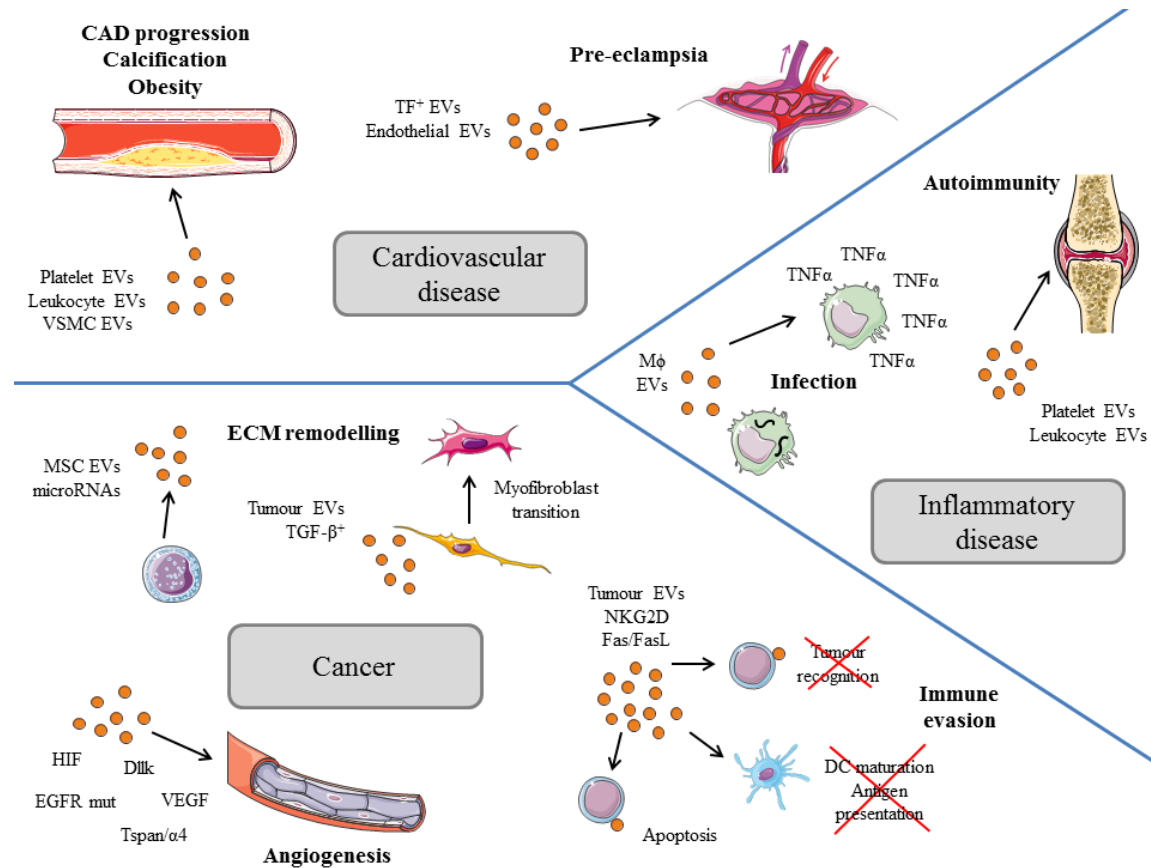
Figure 1.1.12: Roles of EVs in disease. A summary of the potential roles of EVs in cardiovascular diseases, cancers and inflammatory diseases. CAD = coronary artery disease; DC = dendritic cell; Dll4 = Delta-like 4; EGFR = epidermal growth factor receptor; HIF = hypoxia inducible factor; Mϕ = macrophage; MSC = mesenchymal stem cell; NKG2D = natural killer group 2D; TF = tissue factor; TGF-β = transforming growth factor-β; TNF-α = tumour necrosis factor-α; VEGF = vascular endothelial growth factor; VSMC = vascular smooth muscle cell

1.1.10 Therapeutic applications of extracellular vesicles

The biological properties of EVs and their roles in cell-cell communication has prompted research into their potential use as therapeutic agents, and also, their capacity to be altered in disease has highlighted EVs as potential circulating biomarkers. The potential clinical applications of EVs as therapeutic agents and biomarkers of disease are outlined below.

1.1.10.1 EV therapeutics

EVs can be used as delivery vehicles for pharmacological agents, but also nucleic acids such as mIRs. EVs have been shown to be superior to liposomes in this respect as the lipid and protein content are more compatible than synthetic liposomes. MSCs genetically modified to produce mIR-143 were shown to produce EVs containing the transfected mIR which could then go on to inhibit the migration of osteocarcinoma cells (249). Similarly, DCs modified to overexpress IL-10 were shown to produce IL-10 containing EVs which were capable of suppressing the onset of collagen induced arthritis in a mouse model (250). Alternatively, other methods have exploited the native antigens expressed on EVs to generate therapeutic agents. For example, pulsing of antigen presenting cells with tumour-derived EVs isolated from ascites resulted in the presentation of the tumour antigen. This was then shown to prime a set of leukocytes specifically targeted to the tumour for expansion (251). EVs produced from microbe-infected cells have also been used effectively as vaccines (252). A further example of using unmodified EVs for therapy is the use of stem cell EVs. Stem cell therapy has received a great deal of attention in previous years as a novel therapeutic strategy for a wide variety of conditions. However, potential issues include the proliferation of undifferentiated stem cells towards an oncogenic phenotype and the poor survival of transplanted stem cells (253). Stem cell EVs may help to circumvent these problems by eliminating the need for cellular transplantation. For example, *in vivo* delivery of EVs from cardiac progenitor cells to a mouse model of myocardial infarction diminished caspase activation and subsequent apoptosis of cardiomyocytes (254). Finally, EVs themselves could be targeted to attenuate cell-cell communication. For example, inhibition of heparin

sulphate proteoglycans required for EV uptake was shown to reduce migration of cancer cells (255).

1.1.10.2 EVs as biomarkers of disease

The application of more in-depth analyses such as proteomics and lipidomics to EVs has allowed for identification of a number of novel biomarkers in a range of diseases, particularly using cancer EVs. For example, myeloma EVs were shown to express CD44 which was shown to be prognostic for disease progression (156). Prostate cancer EVs have also been shown to express prostate specific membrane antigen which indicates the progressive status of the tumour (256). Less laborious methods have also been suggested for the use of EVs as biomarkers. For example, circulating levels of TF^+ EVs may be useful in predicting the risk of venous thrombosis (176).

EVs offer a non-invasive approach to diagnostics due to their presence in a number of biological fluids. However, the field is currently hindered by a lack of standardisation of nomenclature and pre-analytical processing that makes inter-study comparison a challenge. As our understanding of the composition and roles of EVs in homeostasis and disease continues to expand, the therapeutic manipulation and targeting of EVs is likely to be an extremely important and exciting area of research. In parallel with these developments however, standardisation of pre-analytical protocols is essential for the progression of the EV field towards clinical diagnostics and therapeutics.

1.2 ADIPOSE TISSUE

In the early 1970's, adipose tissue (AT) was shown to possess aromatase activity for the enzymatic conversion of circulating reproductive hormones (257). Despite such evidence for the participation of AT in endocrine signalling and a known association of obesity with cancers of the female reproductive tract, AT was long regarded as a latent storage tissue. It was over 20 years later before AT became firmly established as an endocrine organ through the identification of the "fat gene" and adipocyte-derived protein, leptin (258). In the past 20 years, over fifty different proteins have been shown to be produced by adipocytes within AT, termed 'adipokines', with diverse biological functions (259). This section will examine AT in more detail, with a specific focus on adipocytes and their role in physiology and disease.

1.2.1 Types of adipose tissue

There are currently 3 distinguishable types of AT: white AT (WAT), brown AT (BAT) and the more recently discovered beige AT (260). The composition and characteristics differ between types of AT (**Figure 1.2.1**), and consequently, the tissues serve different functions.

1.2.1.1 White adipose tissue

WAT is commonly stored subcutaneously (more so in women) and within the peritoneum (visceral, more so in men), forming the major reserve for surplus energy intake from the diet. In addition to storage of energy, WAT also provides basic insulation and cushioning of internal organs, including blood vessels (perivascular AT). White adipocytes are the primary constituents of WAT though preadipocytes, adipocyte progenitors (such as MSCs), immune cells and endothelial cells (261) also form a major part of WAT. White adipocytes are histologically simple, consisting of a unilocular triglyceride lipid droplet with a small number of mitochondria. In fact, triglycerides constitute more than 85% of WAT mass (262) and lipid droplets can comprise up to 90% of cellular volume (263), illustrating the dominance of lipid storage in white adipocytes. Adipokines such as leptin and adiponectin are released from white adipocytes allowing proximal and distal endocrine signalling of WAT.

White adipocytes are also capable of expansion (hypertrophy) to cater for increases in triglyceride influxes and are typically between 50 and 100 μm in diameter (264) but can reach up to 200 μm in diameter in obese AT (265,266). If the storage capacity of the adipocyte is exceeded, tissue-resident preadipocytes and adipocyte progenitors are induced to differentiate into mature adipocytes (hyperplasia) to accommodate the extra lipid. This allows WAT to safely store lipid and prevent ectopic lipid deposition and lipotoxicity in other organs. Hypertrophy and hyperplasia of white adipocytes may allow the indefinite expansion of WAT, as demonstrated in morbidly obese patients where WAT can account for over 50% of total body weight (261).

1.2.1.2 Brown adipose tissue

BAT is essential for thermogenesis in neonates and is thought to be progressively lost into adulthood as skeletal muscle and other thermogenic mechanisms develop (267). However positron emission tomography (PET) imaging studies have suggested regions of BAT are present in adults, predominantly located in cervical and supraclavicular locations (268). PET imaging also found BAT was more abundant in: women; the youngest and least obese individuals; and those with the lowest levels of fasting glucose (268). Brown adipocytes contain large amounts of mitochondria and very few, multilocular lipid droplets (263). This abundance of mitochondria (which are usually large with multiple cristae) is responsible for the utilisation of fat by BAT as opposed to the storage of fat in WAT. The expression of uncoupling protein (UCP)-1 on the inner mitochondrial membrane of brown adipocytes drives oxidative phosphorylation of cellular respiration away from ATP production, towards the dissipation of energy as heat (261). BAT is densely vascularised with capillary networks and innervated by noradrenergic fibres. Under cold conditions, sympathetic nerve stimulation of BAT via noradrenaline and β_3 adrenoreceptors activates lipolysis of triglycerides, liberating free fatty acids (FFAs) which in turn activate thermogenesis (267). Interestingly, ablation of UCP-1 in mice not only leads to a lack of thermogenic control, but also to obesity (269). Furthermore, BAT is reduced in obese subjects (263,268). Together, this suggests that activation of BAT is triggered by changes in temperature and diet and the

reduction in BAT in obesity may aid weight gain in order to restore the thermogenic balance.
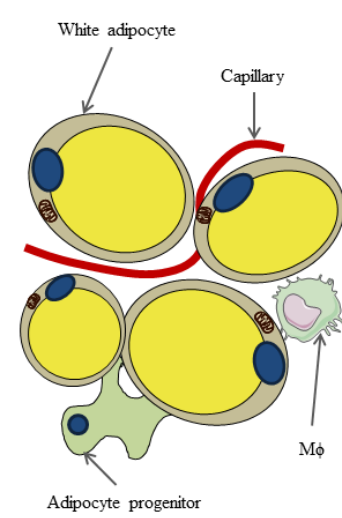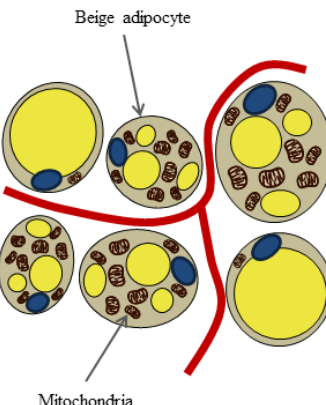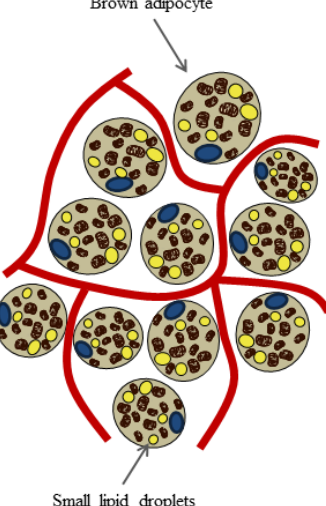
1.2.1.3 Beige adipose tissue

Beige adipocytes are so called due to their intermediary morphology between white and brown adipocytes. They are also referred to as "brite (brown-in-white)" or "paucilocular" adipocytes and are generally found within WAT (263). Similarly to brown adipocytes, beige adipocytes contain high numbers of mitochondria and express UCP-1 (270). Unstimulated beige adipocytes also share similarities in gene expression with white adipocytes, including fatty acid binding protein (FABP) 4, adiponectin, and peroxisome proliferator-activated receptor (PPAR) γ (271). In addition to the shared similarities with white and brown adipocytes, beige adipocytes are enriched in distinct genes such as *TBX1* and surface markers including CD137 (271). Several factors are implicated in the browning of WAT, including cyclic guanosine monophosphate (cGMP) as stimulation of the β_3 adrenoreceptor leads to downstream increases in cGMP levels (272,273). Prostaglandins and nitric oxide (NO) signalling pathways also converge on cGMP generation, both of which (NO via reduction from inorganic nitrate) were shown to stimulate browning of WAT (272,273). Roberts et al., also showed that the nitrate-induced beige phenotype was only achieved with differentiating adipocyte progenitors and not with mature adipocytes (273), suggesting beige adipocytes originate from adipocyte progenitors and not transdifferentiation of white adipocytes. Analysis of BAT from adult humans has shown gene expression patterns similar to those of beige adipocytes, suggesting that the presumed BAT in adults may actually be beige AT (271).

1.2.1.4 Adipocyte lineage

It is well established that white and brown adipocytes originate from different mesodermal lineages. White adipocytes derive from mesodermal stem cells that give rise to adipoblast progenitors, followed by preadipocytes and finally mature adipocytes (274). Conversely, BAT arises from a progenitor population of the mesoderm expressing $Pax7^+/Myf5^+$ genes which also give rise to skeletal muscle

cells (275). The transcriptional regulator PR domain-containing 16 (PRDM16) controls the fate of progenitor cells by activating PPARγ to induce adipogenesis and promote differentiation to brown adipocytes (275). The exact lineage of beige adipocytes is unclear though two theories have been proposed. The first suggests that white adipocytes may undergo transdifferentiation to beige adipocytes in response to cold environments or prolonged β₃ adrenoreceptor activation (263,276). However, recent evidence suggests that adipocyte progenitors within WAT respond to low temperatures and/or increased sympathetic activity by differentiating into beige adipocytes to increase thermogenesis and utilisation of energy stores to produce heat (270,273). It has also been hypothesised that beige adipocytes may be capable of transdifferentiation to white adipocytes in conditions of high energy influx (270). Therefore, the plasticity often associated with WAT may be attributed to the ability of adipocyte progenitors and subsequent beige adipocytes to respond to changes in the microenvironment.

Figure 1.2.1: Types of AT. A simplified summary of the 3 main types of AT and their typical characteristics.

1.2.2 Adipose tissue depots

In addition to total body fat, the distribution of adiposity is also an important determinant for metabolic health. The deposition of fat in specific anatomical locations and the association with metabolic disease and CVDs has been an area of great controversy in recent years. Depots of WAT can be visualised using imaging techniques such as computed tomography and are broadly grouped into subcutaneous (SC), visceral and perivascular, each of which seem to have specialised compositions and functions.

1.2.2.1 Subcutaneous AT

Typically, up to 85% of body fat is SC (277) most of which is stored in abdominal, gluteal and femoral regions. Women tend to have greater proportions of SC AT than men, perhaps to aid the continuous supply of energy to the foetus during pregnancy, as lipolysis in SC AT is slow and continuous (278). The lifespan of a typical SC white adipocyte is reportedly 8-10 years (279) illustrating the stability and slow turnover of adipocytes. Cells of the SC stromal vascular fraction (containing adipocyte progenitors and preadipocytes) show a high efficiency of differentiation (270) (usually in response to PPARγ) (280), suggesting SC AT expansion is mediated through adipocyte hyperplasia. The general size of adipocytes in SC AT is debated with some studies reporting high proportions of small adipocytes which are more insulin sensitive (281) and others arguing the presence of large diameter adipocytes that secrete the majority of adipokines (such as leptin) and adipocyte-derived oestrogens (from aromatase conversion of androgens) (280). SC AT deposition is generally regarded as physiological, as the primary function of adipocytes is "liposynthetic" characterised by high levels of insulin sensitivity (280). In fact, the obesity of SC AT that is not associated with metabolic syndrome may be characterised as "metabolically healthy" (282). This phenotype tends to be associated with gluteal and femoral SC adiposity as opposed to abdominal SC AT deposition which is associated with an increased risk of CVD and type 2 diabetes (T2D) (283).

1.2.2.2 Visceral AT

Visceral or intra-abdominal AT surrounds the internal organs and accounts for up to 10% of total body fat in women and up to 20% in men. Visceral AT is associated with a rapid energy release state, perhaps a conserved evolutionary mechanism to quickly liberate high amounts of energy for hunting (278). Visceral adipocytes are reportedly smaller in women, suggesting a reduced capacity for rapid calorie release (280). Visceral adipocytes are indeed highly lipolytic, due to a high level of triglyceride influx, sympathetic nerve fibre innervation and expression of β_3 adrenoreceptors (280). Increased catecholamine stimulation of visceral AT induces lipolysis and liberation of FFAs, which are drained into the circulation (via the liver) by the portal vein. Obesity with accompanying metabolic syndrome is associated with an increased circulating level of FFAs (284), suggesting visceral AT activity may play an important role. Furthermore, visceral adipocytes are much less sensitive to the anti-lipolytic effects of insulin than SC adipocytes (280) suggesting an increased mass and/or activity of visceral AT could contribute to the reduced sensitivity of insulin in metabolic syndrome and obesity. Unlike SC AT, adipogenesis within visceral AT is not induced by PPARγ and adipocytes predominantly expand by hypertrophy (285). Similarly to abdominal SC AT, visceral AT is associated with an increased risk of developing CVD and T2D (283).

1.2.2.3 Perivascular AT

Perivascular AT is a form of visceral AT surrounding blood vessels that is able to directly affect the responsiveness of the underlying vessel due to the absence of a fascial plane between the vessel and AT (286). Perivascular AT of resistance vessels is predominantly WAT whereas larger vessels are surrounded by a combination of WAT and BAT (286). *In vitro* isolated vessel experiments have traditionally removed perivascular AT prior to testing however, Soltis et al., showed the vasoconstriction of noradrenaline was attenuated when the perivascular fat was left intact (287). This effect was later attributed to a soluble substance, termed adipose-derived relaxing factor (ADRF), as transfer of bath solution from aortic rings with perivascular AT intact to aortic rings with fat removed induced rapid relaxation (288). The identity of ADRF is still unknown though adipocyte-derived vasodilators

have since been proposed (289) including adiponectin and angiotensin 1-7 which produce NO in an endothelium-dependent manner, and hydrogen peroxide which induces vasodilation in an endothelium-independent manner (290). Interestingly, perivascular AT has also been shown to enhance contractility of vessels via thromboxane A_2 (291). Variations in the composition of perivascular AT and the type of vessel may result in differences in regulation of vessel tone. Perivascular fat volume is higher in men and shows a positive correlation with BMI, regardless of gender (292). The anti-contractile properties of perivascular AT in lean individuals was completely absent in obese individuals (293). Furthermore, the vasodilatory effects of lean perivascular AT were lost by addition of inflammatory mediators (TNF-α and IL-6) and hypoxia. This suggests that dysfunctional perivascular AT in obesity (and obese-like conditions) is unable to regulate vascular tone, and hence may increase the risk of hypertension. Increased contractility of small arteries could deprive tissues downstream of nutrients and O_2, thus enhancing local inflammation and hypoxia (discussed in more detail in *Section 1.2.5*).

1.2.3 Methods of studying adipose tissue and adipocytes

With various roles in homeostasis and disease (discussed in *Sections 1.2.4* and *1.2.5* respectively), understanding adipocyte function is hugely important. Several methods exist to study adipocytes *in vitro* and *in vivo* including the use of preadipocyte cell lines, isolation of adipocytes from primary human explants and genetic mouse models.

1.2.3.1 Preadipocyte cell lines: 3T3-L1

Much of our current understanding of adipocyte biology comes from the use of preadipocyte cell lines (**Table 1.2.1**), primarily using 3T3-L1 cells. Preadipocyte cell lines have undergone determination from mesodermal precursors and can therefore either remain as preadipocytes, or can be differentiated to mature adipocytes (294). 3T3-L1 cells were the first preadipocyte cell line to be developed (295,296) and have been (and still are) used extensively to study adipocyte biology and adipogenesis (294). Differentiated 3T3-L1 cells possess the major hallmarks of mature adipocytes: lipid storage, insulin sensitivity and endocrine signalling.

Cell line	Origin	Characteristics
3T3-L1	Mouse	Sub-line of 3T3 embryonic fibroblasts (295,296)
3T3-F442A	Mouse	Sub-line of 3T3 embryonic fibroblasts (295,296)
AP-18	Mouse	Derived from sub-epidermis of ear skin from adult C3H/HeM mouse (297)
SGBS	Human	Derived from SC AT stromal cells from an infant with Simpson-Golabi-Behmel syndrome (298)
Ob 17	Mouse	Derived from epididymal fat pad of C57BL/6J *ob*/*ob* mouse (299)
HGFu	Mouse	Derived from epididymal fat pad of wild-type C57BL/6J mouse (300)

Table 1.2.1: Preadipocyte cell lines. Details of commonly used, established preadipocyte cell lines to study adipogenesis.

Upon confluency, 3T3-L1 preadipocytes are stimulated to differentiate using a simple cocktail of adipogenic inducers (**Figure 1.2.2**). Differentiation cocktails always include insulin to stimulate insulin-like growth factor signalling pathways, a glucocorticoid (e.g. dexamethasone) to enhance nuclear gene expression (e.g. CCAAT/enhancer binding proteins (C/EBP)-δ), an agent to increase intracellular cyclic adenosine monophosphate (e.g. 3-isobutyl-1-methylxanthine or indomethacin) to stimulate specific G-protein pathways and C/EBPβ, and serum (containing essential growth factors and cytokines) (294,301).
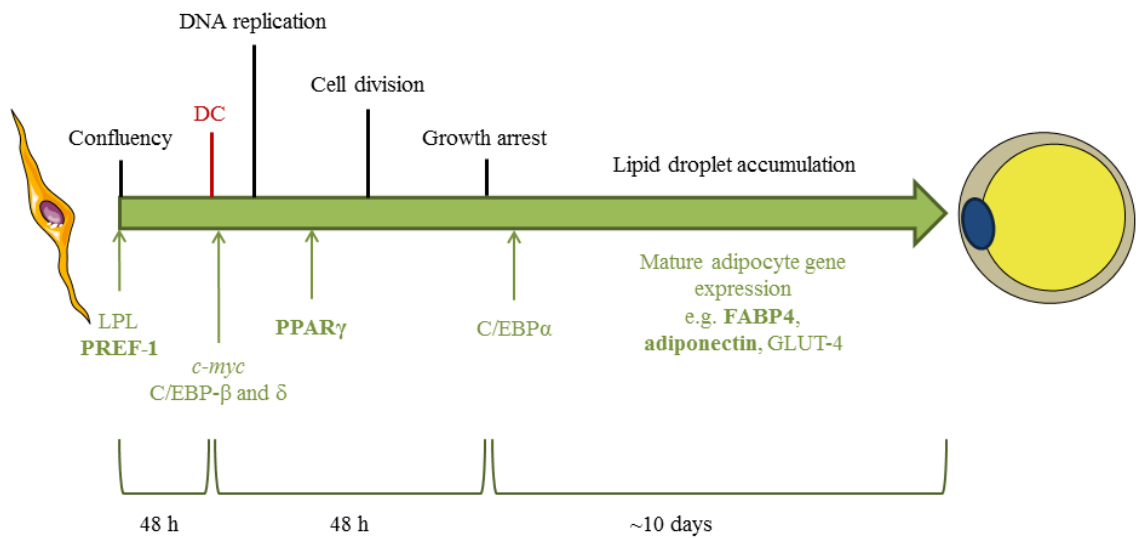
Figure 1.2.2: 3T3-L1 differentiation. Major stages and genes involved in 3T3-L1 differentiation from a preadipocyte to a mature adipocyte. Upon confluency, lipoprotein lipase (LPL) expression is induced, one of the earliest markers of differentiation. Around 48 hr post-confluency differentiation cocktail (DC) is added and genes including *c-myc* and C/EBPβ and δ are rapidly induced. *c-myc* induces clonal expansion of preadipocytes (~2 rounds of mitosis) before cellular growth arrest. C/EBP-β and δ enhance PPARγ and CEBP-α expression which induce the transcription of adipocyte genes such FABP4, adiponectin and GLUT-4 that generate and sustain the mature adipocyte phenotype. Markers highlighted in bold are used in this thesis to assess the stage of differentiation in 3T3-L1 cells and EVs.

Adipogenesis is a complex process of co-ordinated transcriptional activation to differentiate the fibroblast-like preadipocyte to a rounded cell containing lipid droplets. Differentiation is usually confirmed by morphological changes (i.e. rounding, lipid accumulation), observed using light microscopy and lipid droplet

accumulation, which can be visualised and measured (semi-quantitatively) using Oil Red O staining. Ideally, the above are performed in combination with qRT-PCR measurements of early adipogenic markers (e.g. preadipocyte factor (PREF)-1) and late adipogenic markers (e.g. FABP4) compared to housekeeping genes (e.g. GAPDH).

A recent study also demonstrated the capability of 3T3-L1 adipocytes to acquire a brown adipocyte phenotype upon stimulation with noradrenaline (302). The authors of this study suggest this is due to a previously unidentified plasticity of 3T3-L1 cells and that the differences in lineage between white and brown adipocytes may not be as straightforward as initially thought. Further characterisation of the 3T3-L1 brown adipocyte is needed, though this may point to an additional application of 3T3-L1 cells *in vitro*. Preadipocyte cell lines such as 3T3-L1 provide robust models from which to study adipocyte differentiation and biology. Their ease of use and accessibility make preadipocyte cell lines useful adipocyte research models.

1.2.3.2 Primary human adipocyte culture

Mouse and human primary adipocyte cultures have also been used as adipocyte research models. Excised AT can be digested using collagenase to separate adipocyte progenitor cells from free lipid and mature adipocytes. Preadipocytes can then be cultured *in vitro* and stimulated to differentiate for ~2 weeks to produce mature adipocytes (303). Mature adipocytes can also be separated using the collagenase digest (304,305), though their subsequent culture is tricky as the adipocytes float (and are therefore less likely to adhere) and are prone to bursting during isolation. The rate and extent of differentiation may differ between donors and AT depots, and may therefore introduce variation between experiments.

Isolated pre- and mature primary adipocytes are also available commercially (e.g. PromoCell, Lonza). These adipocytes are isolated and fully characterised by the vendor to ensure an adipocyte population. Adipocytes from specific depots including SC and visceral AT, and from different disease sets, including obese and diabetic patients can be purchased allowing analysis of specific adipocyte populations. Unsurprisingly, these cells are often expensive.

Culture of AT explants has also been used to study adipocytes (306–308). In this setting, intact sections of AT may be analysed *ex vivo* and may be used to compare AT function between depots. However, the explant contains a mixture of cells present within AT, making it difficult to pinpoint the origin of any observed effects.

1.2.3.3 Adipocyte progenitor cells

The mesodermal origin of adipocytes provides an alternative source of precursory adipocyte cells that can differentiate *in vitro* into preadipocytes and subsequently, mature adipocytes (**Figure 1.2.3**). MSCs and pluripotent stem cells (PSCs) have both been used to generate adipocytes *in vitro*. MSCs can be isolated from bone marrow or AT extracts and are multipotent cells, capable of differentiating into osteocytes, myocytes, chondrocytes and adipocytes (309). Commercially available MSCs are also frequently used, reducing the need for invasive tissue sampling. Differentiation of MSCs to adipocytes follows a similar timeframe and differentiation cocktail to that of 3T3-L1 cells. Although as a human source, MSCs may provide a more relevant adipocyte population compared to 3T3-L1 cells, their use is disadvantaged by a limited proliferative potential and varied adipogenic differentiation between sources (310).

Isolated human PSCs (hPSCs) can be cultured *in vitro* indefinitely whilst retaining their ability to differentiate along a variety of lineages, including adipocytes (311). Adipogenic medium requires the addition of a PPARγ agonist (e.g. Rosiglitazone) (311) to that described for 3T3-L1 cells. More recently, a lentiviral construct containing a PPARγ2 promoter has been shown to vastly improve the extent of hPSC differentiation (310). Interestingly, the use of a PRDM16 promoter-containing lentiviral construct could induce differentiation of hPSCs to a brown adipocyte population. Furthermore, when both hPSC-derived white and brown adipocytes were implanted *in vivo*, they were successfully incorporated and functional as brown and white AT (310). Culture *in vitro* to mature adipocytes typically takes ~3 weeks, and as described above, may require the use of more complex techniques to ensure sufficient adipogenic differentiation. However, the extent and variation of differentiation of hPSCs is superior to that of MSCs (310) and perhaps provides a more relevant adipocyte population compared to 3T3-L1 cells.
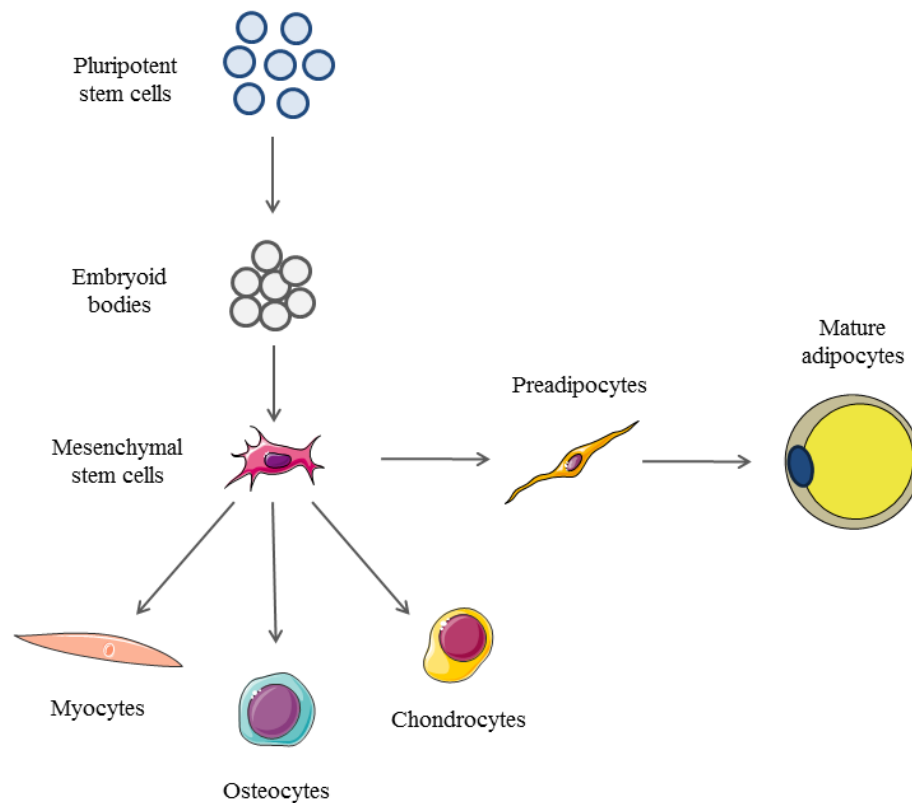
Figure 1.2.3: Mesodermal lineage of pluripotent stem cells. The mesodermal lineage; both pluripotent stem cells and mesenchymal stem cells can be used to generate adipocytes.

1.2.3.4 Genetic mouse models of obesity

Genetic mouse models have also been employed to analyse the *in vivo* role of AT. The most widely used mouse model is the *ob*/*ob* mouse carrying a mutation in the "obese" gene that encodes for the adipokine leptin, resulting in leptin deficiency (258). Mice with the *ob* mutation display a phenotype akin to that in morbid obesity, becoming profoundly obese, developing diabetes, demonstrating hyperphagia, and showing impairments in immune and reproductive function (258,312). Alternatively, *db*/*db* mice carry a mutation in the "diabetic" gene that encodes for the leptin receptor. These mice also become significantly obese and develop diabetes and dyslipidaemia (313). Furthermore, leptin mRNA increases ~20 fold in *db*/*db* mice (314). Though *ob*/*ob* mice are more frequently used *db*/*db* mice may provide a more accurate representation of obesity, as leptin is present and increased in obese subjects (*Sections 1.2.4.1* and *1.2.5.1*).

1.2.4 Adipokines and the role of AT in physiology

The majority of research into endocrine factors released from AT has focused on those derived from WAT, as this is the largest store of AT in the body. A diverse range of factors have been identified, collectively termed "adipokines" to encompass factors produced and released from WAT. Adipokines can act locally within AT in an autocrine and/or paracrine fashion, and also distally in the central nervous system and systemic circulation in an endocrine manner. Consequently, adipokines play important roles in a range of physiological functions.

Mice carrying a genetic mutation that prevents the actions of C/EBP transcription factors (**Figure 1.1.2**) leaves them devoid of WAT. These mice also display stunted development, infertility, an enlarged liver, diabetes, elevated levels of circulating glucose and lipids and eventually premature death (315). This provides a stark illustration of the importance of WAT not only in the regulation of lipid metabolism and deposition, but also in normal growth and development.

1.2.4.1 Regulation of lipid metabolism and appetite

The major endocrine factor produced by adipocytes for energy homeostasis is leptin. Leptin is produced by adipocytes and the circulating levels of leptin relate to the level of energy storage, i.e. leptin tends to be elevated in fed states and reduced during fasted states (316). The effects of leptin are mediated through the leptin receptor (LR), of which there are several isoforms. LR-b is highly expressed in hypothalamic regions of the brain, where leptin mediates the majority of its metabolic effects. Binding of leptin to hypothalamic receptors induces the expression of anorectic peptides (e.g. α-melanocyte stimulating hormone) and also stems the secretion of orexigenic hormones (e.g. neuropeptide Y (316)). The combined effect leads to release of appetite-suppressing hormones such as oxytocin. Release of these hormones also increases fatty acid oxidation and decreases circulating glucose levels to restore energy balance following feeding.

Adiponectin also plays a role in regulating lipid metabolism and is produced exclusively by mature adipocytes. Adiponectin displays a multimeric conformation and can exist in high, middle and low molecular weight forms (317). Two main

isoforms of the adiponectin receptor have been described, adipoR1 which is highly expressed in muscle, and adipoR2 which shows high prevalence in the liver, though both receptors are also expressed in other peripheral tissues and the brain (318). Adiponectin confers its metabolic effects via phosphorylation of adenosine monophosphate-activated protein kinase (AMPK) leading to increased fatty acid oxidation and an inhibition of hepatic gluconeogenesis. The latter gives rise to the insulin-sensitising properties of adiponectin by reducing circulating glucose levels (319). The importance of adiponectin and AT in the regulation of insulin sensitivity is highlighted by pharmacological insulin-sensitising agents such as thiazolidinediones (TDZs) which increase circulating adiponectin levels (317). The actions of adiponectin in peripheral areas such as skeletal muscle help to induce energy expenditure, thereby reducing the risk of ectopic lipid deposition (318).

The transcription factor PPARγ is highly expressed in adipocytes, particularly the PPARγ2 isoform. In addition to controlling adipocyte differentiation, PPARγ regulates transcription of genes central to metabolism (301,320) such as lipoprotein lipase (involved in the storage, release and transport of lipids (321)). PPARγ also has an insulin-sensitising effect by directly inducing insulin-mediated uptake of glucose thus decreasing levels of FFAs and promoting lipid storage (321). PPARγ also reduces ectopic lipid deposition in the liver and muscles by mobilising lipids from these sites and promoting adipocyte storage. Furthermore, activation of PPARγ signalling leads to a redistribution of lipids from visceral to SC depots (321), thereby reducing the risks associated with visceral AT storage. TDZs such as Pioglitazone are pharmacological PPARγ agonists used to improve insulin sensitivity in T2D (322). Interestingly, as indicated above, treatment with TDZs can also increase adiponectin levels (317,322) suggesting PPARγ also regulates adiponectin secretion.

FABP4 is a cytosolic and secretory fatty acid trafficking protein highly expressed in adipocytes, accounting for ~1% of the total protein (323). FABP4$^{-/-}$ mice display increased circulating levels of triglycerides and FFA, and up to a 40% reduction in cellular lipolysis (324). This suggests FABP4 is involved in the cellular uptake and trafficking of lipids into adipocytes and their subsequent metabolism.

Resistin is a hormone that is preferentially secreted by adipocytes. Similarly to FABP4, the role of resistin was elucidated using knockout or gene silencing models

(325). Silencing RNA targeting resistin was shown to reduce the activity of transcription factors controlling lipogenic gene expression. Furthermore, lipid droplet size was reduced in resistin knockout adipocytes. Therefore, resistin seems to play a role in controlling lipid accumulation in the early stages of adipogenesis.

Visfatin is a relatively newly identified adipokine that was initially thought to be specific to visceral AT (326) though it has now been identified in SC AT. Visfatin is able to both control the secretion of insulin from pancreatic β-cells (327) and mimic the signalling effects of insulin (326).

1.2.4.2 Role in vascular function

As discussed in *Section 1.2.2.3*, perivascular AT is able to control local vascular function through the secretion of adipokines. Adipocytes in SC and visceral depots also secrete adipokines that can regulate haemostasis, angiogenesis and blood pressure that help AT to meet metabolic and physical demands. Circulating adiponectin induces NO production and reduces reactive oxygen species (ROS) generation in endothelial cells (328) thereby promoting vasodilation and protecting against ROS-induced vascular damage. Plasminogen activator inhibitor (PAI)-1 is a small protein secreted from a number of cells including adipocytes (329). As its name suggests, PAI-1 inhibits plasminogen which is involved in fibrinolysis. PAI-1 is produced by mature adipocytes and its expression is controlled by both resistin and PPARγ (330). The precise role of adipocyte-derived PAI-1 is unclear, though it may play both local and systemic roles in haemostasis. TF expression and release has also been observed in AT though similarly to PAI-1, the reason behind the presence of TF in AT is unknown (331). TF is a well-known initiator of coagulation and therefore may represent a mechanism for AT to control local haemostasis. TF is also vital for vascular development and may therefore play a role in formation of the AT microcirculation. Visfatin has also been shown to induce relaxation of aortic rings and stimulate endothelial proliferation and angiogenesis, the latter effect being through the generation of VEGF (332).

Adipocytes grow in close proximity to endothelial cells within AT in order to efficiently exchange nutrients and waste (333). As part of their adipokine repertoire,

adipocytes secrete factors that promote endothelial cell growth and angiogenesis. In fact, the growth of AT in *ob/ob* mice was inhibited by anti-angiogenic factors (334), indicating AT expansion is dependent upon local angiogenesis. Adipocytes express and secrete VEGF to promote local angiogenesis, but also leptin (335). Leptin was shown to induce angiogenesis of endothelial cells *in vitro* and *in vivo* indicating a peripheral role for leptin in addition to its central role in energy homeostasis.

Adipocytes also contain several components of the renin-angiotensin system (RAS), allowing them to regulate blood pressure. Angiotensinogen produced by adipocytes can be converted into angiotensin II by angiotensin converting enzymes present in AT (336) which can go on to induce vasoconstriction.

1.2.4.3 Immune interaction of AT

AT is recognised as an immunological organ, due to a vast network of immune cells present within WAT. The most abundant of these cells are Mϕ which are polarised towards an M2, anti-inflammatory phenotype. M2 Mϕ secrete IL-10 that helps to maintain insulin sensitivity and regulate glucose homeostasis (337). Polarisation of Mϕ towards an M2 phenotype is regulated by: adipocyte PPARγ expression (338); AT-resident eosinophils which secrete IL-4 (339); and a specialised subset of NK cells and Treg cells that secrete IL-10. Additionally, Treg cells participate in important crosstalk with adipocytes by reducing adipocyte secretion of MCP-1 and enhancing adipocyte insulin sensitivity via PPARγ (338).

1.2.4.4 AT and ageing

Ageing is associated with phenotypic and functional changes in AT. AT mass declines with age, coinciding with an accumulation of lipid in ectopic sites such as the liver and bone (340). Therefore, although AT mass undergoes redistribution, the overall proportion of body fat remains unchanged. Increases in ectopic lipid deposition account for many age-associated conditions, for example, the deposition of lipid in bone decreases mineral density, leading to osteoporosis and insulin resistance (IR) (341). Furthermore, preferential SC AT tissue cachexia prior to

visceral AT increases the risk of metabolic syndrome (340). The precise mechanisms behind age-related changes in AT are unknown, though several important alterations have been identified. Expression of pre-adipogenic markers (such as C/EBP and PPARγ) is reduced in aged AT, therefore reducing the capacity of preadipocytes to undergo adipogenesis (342). Additionally, increased differentiation of other cells, such as Mϕ towards an adipocyte-like phenotype has been reported, which express FABP4 and drive the progression of atherosclerosis (343). AT PAI-1 expression is also elevated with ageing, suggesting an increased procoagulant propensity of AT (329), though this may be a consequence of an increased ratio of visceral to SC AT.

Through the secretion of adipokines, AT is able to play a role in a diverse range of physiological functions from establishing metabolic functioning before birth to operating as an immune organ (summarised in **Figure 1.2.4**). Clearly, AT plays an important role in a number of homeostatic mechanisms in addition to its basic roles in energy storage, structural support and insulation.
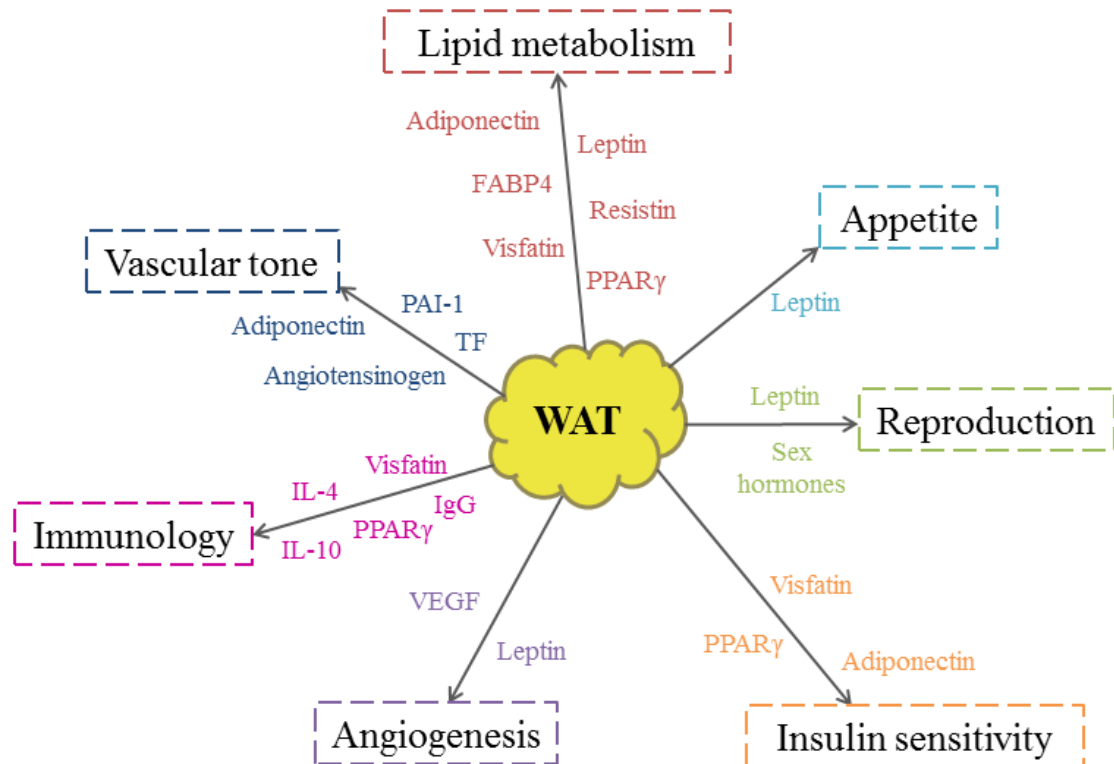
Figure 1.2.4: Physiological role of WAT. A summary of the physiological processes regulated by WAT and the adipokines involved.

1.2.5 Adipose tissue in disease

The ability of AT to serve as an endocrine organ facilitates its role in physiological processes. However, this endocrine signalling becomes detrimental in disease. The major cause of AT dysfunction is obesity. In 2014, just under 2 billion adults were overweight (39% of the world's adult population) (344). Dysregulation of AT in obesity leads to increased risks of CVD, diabetes and cancer; three of the leading causes of mortality. Obesity is caused by an imbalance between energy intake and expenditure, and is therefore, largely preventable.

1.2.5.1 Metabolic dysregulation in obese AT

A hallmark of AT disease and obesity is the dysregulated secretion of adipokines. Two major adipokines involved in the physiological regulation of lipid metabolism are dysregulated in obesity. Leptin deficient, *ob/ob* mice are severely obese, insulin resistant and hyperlipidaemic (312) highlighting the importance of leptin signalling in regulating lipid metabolism and appetite. Paradoxically, circulating levels of leptin are increased in diet-induced obesity. This may be a consequence of leptin resistance, perhaps due to decreased efficiency of leptin signalling in the hypothalamus (345). Contrastingly, circulating adiponectin levels are decreased in obese subjects (346). Plasma adiponectin levels directly correlate with insulin sensitivity and mutations in the adiponectin gene predisposes the carrier to IR (317,346). This draws attention to the insulin-sensitising role of adiponectin and suggests a causal role for reductions in adiponectin in the development of IR. Conversely, resistin which is increased in obesity induces IR by reducing the action of insulin (347).

$FABP4^{-/-}$ mice fed a high fat diet become obese but do not become insulin resistant. Additionally, these mice lacked TNF-α production in AT (associated with inflammation and IR). Together this suggests a direct link between FABP4 and the development of IR in obesity (324). In human studies, circulating levels and adipocyte expression of FABP4 are increased in subjects with obesity and metabolic syndrome (348,349). An inhibitor of FABP4 was also shown to prevent and treat T2D and atherosclerosis in an experimental model (350) indicating the inhibition of FABP4 may be an effective target for obesity-induced CVDs and co-morbidities.

1.2.5.2 Vascular dysfunction in obese AT

Dysregulated adipokine secretion in obesity can also lead to a hypertensive, hypercoagulable state (351,352). PAI-1 is increased in obesity, positively correlating with BMI, and has been suggested as a link between obesity and CVD (305,329). The main increase in PAI-1 in obesity is due to elevated adipocyte-derived PAI-1 production; expression was 5-fold higher in both SC and visceral AT of *ob*/*ob* mice compared to lean controls (353). Furthermore, PAI-1 expression is induced by TNF-α, insulin, TGF-β and FFAs, all of which are elevated in obesity. Visceral AT PAI-1 expression was also elevated compared to SC AT further emphasising the cardiovascular risk associated with android obesity (329). Moderate weight loss restored the haemostatic balance in obese subjects by reducing circulating levels of PAI-1 and hence reducing the risk of thrombosis (228). TF may also increase the hypercoagulable state in obesity. Several adipokines upregulated in obesity such as leptin, TNF-α and TGF-β induced TF expression in adipocytes (351). Expression of TF mRNA is increased in obese AT in response to TGF-β (331) perhaps highlighting TGF-β as a promoter of obesity-induced thrombosis. Furthermore, PPARγ and adiponectin modulate TF production, though their expression is decreased in obesity, relinquishing their inhibition of TF production (351). Leptin was also shown to induce platelet aggregation (354) suggesting increased leptin levels in obesity may contribute to a pro-thrombotic state and increase cardiovascular risk.

Imbalances in adipokine secretion may also increase local and systemic blood pressure. AT angiotensinogen expression is elevated in obesity, particularly in visceral AT (336) suggesting greater activation of the adipocyte-RAS. Additionally, increased adipocyte angiotensin II expression induces ROS generation from NO, thereby enhancing endothelial dysfunction and vasoconstriction (328). Elevated angiotensin II also enhances PAI-1 and endothelial integrin expression, promoting leukocyte adhesion and migration (328). Circulating levels of visfatin are increased in obesity (326,355), although the reason for this is unclear. Visfatin may promote leukocyte adhesion to endothelial cells (via increased integrin expression) (356) and increase the instability and rupture of atherosclerotic plaques (357).

AT VEGF expression may harbour a protective role in obesity. Mouse models have shown overexpression of VEGF in AT increases vascularisation and M2 Mϕ

recruitment (358). In response to a high fat diet, mice overexpressing VEGF displayed an increased insulin sensitivity, suggesting VEGF was able to protect against metabolic complications of diet-induced obesity. Furthermore, overexpression of VEGF in AT enhanced PPARγ expression and induced browning of white adipocytes by increasing UCP-1 expression (359). Conversely, ablation of VEGF within AT reduced the ability of AT to expand resulting an increase in ectopic lipid deposition (360). Therefore, AT VEGF may serve important functions not only in regulating angiogenesis and growth of AT, but in the maintenance of adipocyte lipid deposition and insulin sensitivity. VEGF has been proposed as a therapeutic target for improving adipocyte dysregulation in obesity (358,359). However, plasma VEGF is elevated in obese subjects and correlates with endothelial IL-8 expression which promotes atherogenesis (361). Therefore, further work is needed to elucidate whether targeting VEGF feasible for the treatment of obesity.

1.2.5.3 AT-derived inflammation

Dysfunctional AT in obesity has profound effects on the role of AT as an immunological organ by promoting a transition towards a proinflammatory state (**Figure 1.2.5**). Numbers of eosinophils, NK cells and Treg cells are all reduced in obese AT (337,339) thereby reducing the IL-4/IL-10-induced M2 phenotype of Mϕ. The loss of pro-M2 signals in combination with other obesity-driven factors promotes the transition of Mϕ towards a proinflammatory M1 phenotype (338). The proinflammatory, hypoxic environment of obese AT promotes adipocyte necrosis which leads to the classical arrangement of M1 Mϕ around necrotic adipocytes in so called "crown like structures" (CLSs). This further enhances AT inflammation through FFA release from ruptured adipocytes and enhanced TNF-α and IL-6 secretion from M1 Mϕ. The overriding effect is vicious cycle of excessive local inflammation within AT which leads to systemic inflammation and IR.

Sustained elevations in plasma leptin levels stimulates the release of proinflammatory cytokines from Mϕ (328) thereby adding to the systemic inflammation observed in obesity. Circulating and AT levels of TNF-α are elevated in obesity, showing a positive correlation with IR (259). TNF-α inhibits phosphorylation of the insulin receptor in AT and muscles thereby reducing insulin

sensitivity. Weight loss directly reduces levels of TNF-α and improves insulin sensitivity, suggesting the involvement of a network of obesity-related factors in the development of IR. For example, IL-6 has also been reported to affect hepatic insulin signalling and levels correlate strongly with adiposity (259). Furthermore, IL-6 has been shown to enhance hepatic C-reactive protein (CRP) release (259), an inflammatory cytokine used to predict cardiovascular risk (352). Levels of other proinflammatory cytokines such as IL-8, IL-1β and TGF-β are also elevated in obese AT, suggesting dysfunctional AT is a prime source of proinflammatory cytokines which may give rise to the systemic inflammation that is closely associated with obesity. In addition to the proinflammatory transition of AT Mϕ, the number of AT Mϕ also increases, suggesting an increased infiltration of Mϕ into AT. Resistin was shown to induce pro-inflammatory cytokine production and enhanced endothelial adhesion molecule expression, thereby promoting leukocyte adhesion (327). Furthermore, TNF-α induces adipocyte MCP-1 production to enhance Mϕ chemotaxis and infiltration in AT, further promoting AT inflammation. Visceral AT was shown to contain a higher number of M1 Mϕ, again supporting the notion that visceral AT plays a greater role in IR and metabolic syndrome in obesity (338,352).
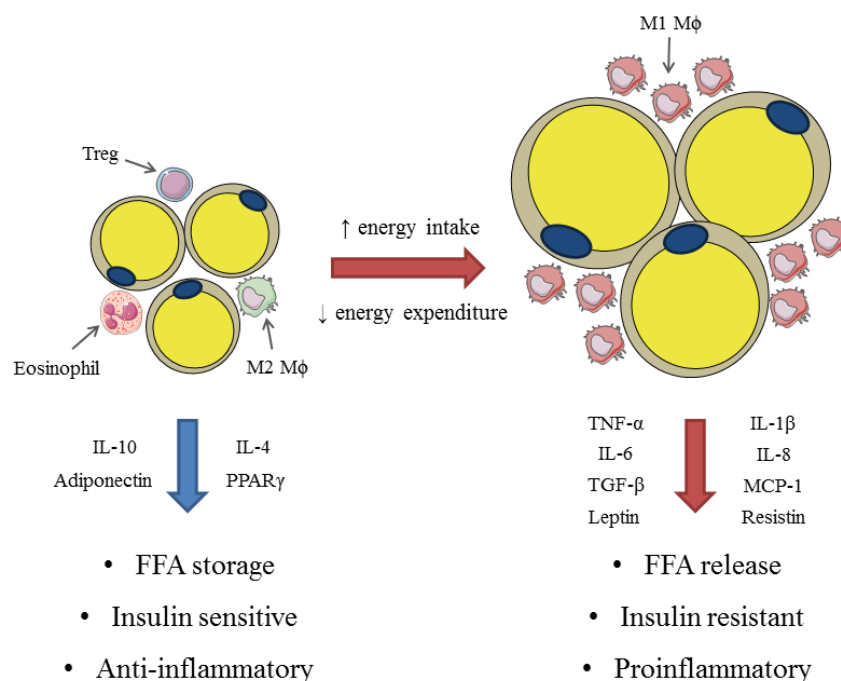
Figure 1.2.5: Obese AT inflammation. A simplified schematic summarising the transition of lean AT with an anti-inflammatory phenotype to obese AT with a proinflammatory phenotype.

1.2.6 Adipose tissue hypoxia

Section 1.2.2.1 alluded to the presence of a "metabolically healthy" obese phenotype, where obesity is not accompanied by obesity-related metabolic co-morbidities such as T2D, IR and dyslipidaemia. A study of overweight and obese individuals reported ~30% of the study population were metabolically healthy and were not at an increased risk of future cardiovascular events (282). Conversely, obese individuals with associated metabolic syndrome were at a greater risk of future cardiovascular events. As described in the previous section, AT tissue dysfunction is the initiator of the pathophysiological roles of AT in disease, suggesting dysfunctional AT is the root cause of co-morbidities in obesity with metabolic syndrome. The mechanism behind the development of AT dysfunction is not fully understood, though a number of theories have been proposed. One theory is that AT has a limited capacity to expand safely, which may vary on an individual basis (362). Therefore, controlled accommodation and storage of increases in energy influx into AT may retain metabolic health. Conversely, surpassing the limit of AT expandability may enhance ectopic lipid deposition and dysregulated adipokine secretion from maximally filled adipocytes. Deficiency of O_2 (hypoxia) of AT has also been proposed to initiate and exacerbate AT dysfunction and inflammation in obesity (259).

1.2.6.1 Rationale for AT hypoxia

It has been suggested that progressive obesity is associated with localised regions of hypoxia and that AT dysfunction and inflammation may stem from a local response of adipocytes to hypoxia (259). Adipocyte hypertrophy in obese AT can result in adipocytes spanning between 100-200 μm in diameter (265,266) which may surpass the limit of the adipocyte for safe lipid accumulation. Additionally, large diameter adipocytes may single-handedly exceed the maximal diffusion distance of O_2 from blood vessels, which is reported to be 100 μm (363). In general, WAT is considered to be poorly perfused (364), and this perfusion is further reduced in obese WAT (365,366). An abundance of large adipocytes in combination with poor vascular support is highly suggestive of a hypoxic environment. Unfortunately, the measurement of O_2 tension (partial pressure, pO_2) of AT *in vivo* or *in situ* is

challenging (*Section 1.2.6.2*), making it hard to concretely confirm the presence of hypoxia within AT.

1.2.6.2 Measurement of AT hypoxia

The presence of hypoxia in AT can be ascertained by monitoring the expression of molecular markers known to be associated with hypoxia, directly measuring AT O_2 tension, or by measuring the AT blood flow/perfusion (AT-BF).

Molecular approaches to measuring hypoxia usually involve the measurement of HIF-1α expression. HIFs are a group of transcription factors that regulate the cellular response to O_2 with HIF-1α being the most studied of the molecular O_2 sensors. HIF-1α is constitutively expressed but is immediately ubiquinated and targeted for degradation under normoxic conditions (364). In hypoxia, this inhibition is relinquished enabling HIF-1α to modulate gene expression. Elevated HIF-1α mRNA and protein expression has been detected in SC WAT of obese mice (367–369) and humans (370). The probe pimonidazole has also been used to report AT hypoxia at a molecular level in obese mice (367,369,371). Pimonidazole was originally used to detect hypoxic regions of tumours as the probe is activated in an O_2-dependent manner (372).

Alternatively, a number of studies have used electrodes and sensors to measure the pO_2 of AT and thus gauge the level of oxygenation (**Table 1.2.2**). Though this approach allows direct *in vivo* measurement of AT pO_2, results between studies show great variation both in lean and obese subjects. This may be because different of types of electrodes or sensors were used. Additionally, a caveat of electrode-based measurement is the limited area of sample measurement as only the region immediately surrounding the electrode or sensor will be measured (single point measure). AT hypoxia is more likely to exist in "pockets" of hypoxic tissue due to variations in adipocyte size and vascularisation throughout AT. Therefore, pO_2 measurements may not provide an accurate measure of the hypoxic state of AT. A number of studies have found decreases in AT pO_2 in obese subjects, though others have found no difference or even increases compared to lean controls (**Table 1.2.2**).

Species (Reference)	Technique	Location	Population	PO$_2$	Equivalent O$_2$
Human (373)	Polarographic electrode tonometer	SC, upper arm	Lean (BMI 24)	57 mmHg	7.5%
			Obese (BMI 51)	36 mmHg	4.7%
Human (374)	Clark electrode	SC, upper arm	Lean (BMI 24)	57 mmHg	7.5%
			Obese (BMI 46)	41 mmHg	5.3%
Mouse (369)	Fibre-optic sensor	Visceral, epididymal fat pad	Lean controls	47.9 mmHg	6.2%
			ob/ob	15.2 mmHg	2.0%
Human (375)	Polygraphic micro-oxygen sensor	SC, deltoid	Lean (BMI 22)	52 mmHg	6.8%
			Obese (BMI 46)	58 mmHg	7.6%
Mouse (368)	Fibre-optic sensor	Visceral, epididymal fat pad	Lean controls	60.4 mmHg	7.9%
			ob/ob	20.1 mmHg	2.6%
Human (376)	Clark electrode	SC, abdominal	Lean (BMI 22)	55 mmHg	7.2%
			Obese (BMI 32)	47 mmHg	6.1%
Mouse (377)	Fibre-optic sensor	Visceral, epididymal fat par	Young (6 months)	36 mmHg	4.7%
			Old (23 months)	21.7 mmHg	2.8%
		SC, Inguinal fat pad	Young (6 months)	33 mmHg	4.3%
			Old (23 months)	37 mmHg	4.8%
Human (365)	Optochemical sensor with microdialysis	SC, abdominal	Lean (BMI 23)	47.7 mmHg	6.2%
			Obese (BMI 34)	67.4 mmHg	8.8%

Table 1.2.2: A summary of studies measuring the partial pressure (PO$_2$) in adipose tissue (AT). BMI = body mass index; SC = subcutaneous.

AT-BF has been used to indicate the oxygenation state of AT. Though the physiological growth of AT is dependent upon increases in vasculature (334), obese AT expansion is not accompanied by increases in blood flow (374). Lean AT-BF is highly responsive to changes in circulating nutrient levels, showing large postprandial increases. Therefore, AT-BF plays a major role in regulating AT lipid metabolism and clearance of lipids from the circulation (378). AT-BF is reduced in obese subjects (365) and hence may lead to a dysregulation of lipid metabolism. AT-BF can be measured by monitoring removal of injected labels such as ^{133}Xe and ethanol, or by imaging techniques such as PET scanning (277). Blood oxygen level-dependent magnetic resonance imaging (BOLD-MRI) has recently been used to evaluate AT-BF and AT oxygenation of multiple fat depots simultaneously (379). Therefore BOLD-MRI may provide a promising alternative to assessing AT oxygenation that enables measurement of the tissue as a whole.

1.2.6.3 Impact of hypoxia on AT function

Hypoxia is known to induce functional changes in adipocytes which drive the dysfunction and inflammation of AT. Adipocyte hypoxia results in a metabolic switch from oxidative phosphorylation to anaerobic glycolysis (364). Consequently, reduced generation of ATP results in an increased requirement for glucose, thereby increasing the expression of glucose transporters (GLUTs) (380). GLUT-1 is particularly upregulated and is often used as a marker of adipocyte hypoxia (364). Increased anaerobic respiration also increases the lactate production, which again is used to indicate adipocyte hypoxia. Activation of HIF-1α downregulates PPARγ production in adipocytes and preadipocytes (381), thereby attenuating further adipocyte differentiation. This may favour expansion of AT by adipocyte hypertrophy rather than hyperplasia, hence exacerbating adipocyte hypoxia. Preadipocytes within hypoxic AT were also shown to secrete leptin (largely restricted to mature adipocytes) which may drive leptin resistance (364).

In addition to metabolic alterations, hypoxia also induces changes in adipokine levels, reducing secretion of adiponectin and increasing expression of leptin, IL-6 and IL-1β (380,382). Increases in these proinflammatory cytokines are associated with development of local and systemic IR (259,380,382) suggesting hypoxia-

induced release of these adipokines may initiate and drive the progression of IR. Hypoxic AT displays increased numbers of Mϕ which are associated with the development of AT inflammation (367). Hypoxia may induce apoptosis and necrosis of adipocytes, driving subsequent Mϕ infiltration to neutralise the necrotic cell. The hypoxic and inflammatory environment may then induce Mϕ towards an M1 phenotype forming CLSs around the necrotic adipocyte. Furthermore, MCP-1 expression is increased in hypoxic adipocytes (380) suggesting hypoxia may initiate the infiltration of additional Mϕ into AT which are phenotypically modified by the local environment to an M1 phenotype, therefore aiding the progression of AT inflammation.

Local hypoxia in obese AT may drive the dysregulation of adipokine secretion and adipocyte metabolism thereby stimulating local inflammation and Mϕ infiltration. Hypoxia may therefore be the initiator of AT dysfunction that leads to a metabolically unhealthy obese phenotype (**Figure 1.2.6**).
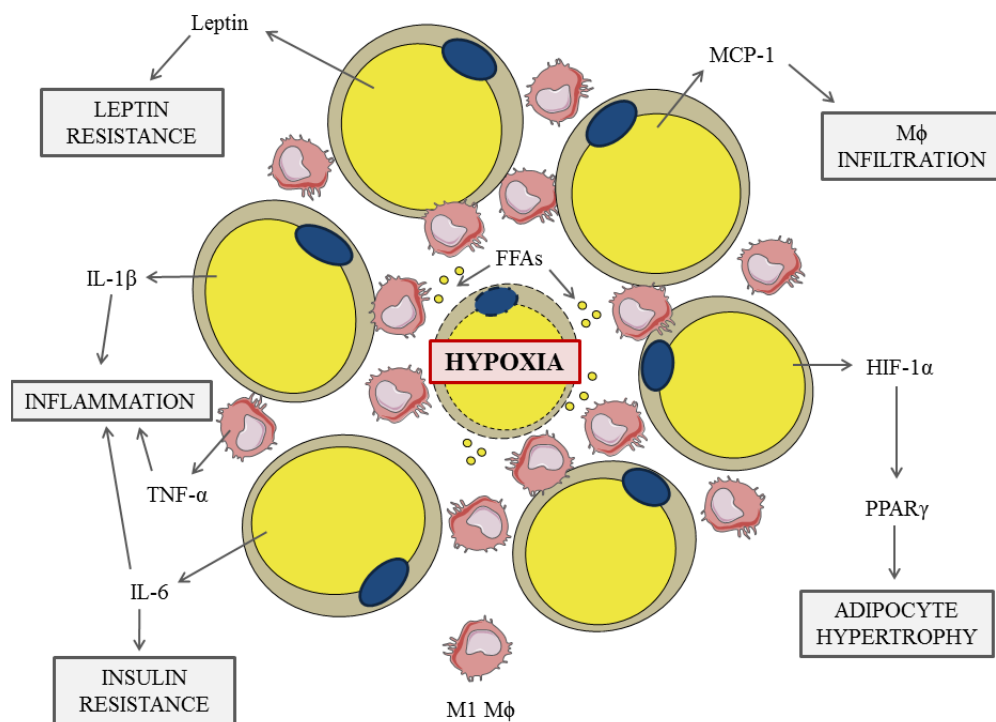
Figure 1.2.6: The role of hypoxia in AT inflammation and dysfunction. Adipocyte hypoxia increases release of HIF-1α, IL-6, IL-1β, leptin and MCP-1 which together lead to metabolic dysfunction of adipocytes, IR, Mϕ infiltration and further AT inflammation. Hypoxia also induces adipocyte necrosis releasing free fatty acids (FFAs) and further enhancing Mϕ infiltration which surround necrotic adipocytes, forming CLSs.

1.2.7 EVs as novel adipocyte communicators

In comparison with the wealth of data for both the adipocyte field and the EV field, studies into adipocyte-derived EVs are scarce. Some characteristics and functional aspects of adipocyte-derived EVs have been established using 3T3-L1 cells, primary adipocyte cultures, and AT explants.

1.2.7.1 Characteristics of adipocyte-derived EVs

Evidence for adipocyte-derived EVs was first published in 2007 where 3T3-L1 EVs were shown to contain the exosomal protein, MFG-E8 and adiponectin (66). EV release was also responsive to obese-mimicking conditions (high glucose, insulin and TNF-α), suggesting a role for EVs in adipocyte dysfunction. Studies using 3T3-L1 cells have since shown the presence of adiponectin and FABP4 in EVs (383–385). The majority (~99%) of EVs derived from visceral and SC AT explants were also shown to be positive for FABP4 (386), perhaps indicating this protein as a useful marker for adipocyte-derived EVs. However, little is known about the specific EV populations released from adipocytes and no data exist detailing the lipid composition of adipocyte-derived EVs.

1.2.7.2 Effects of adipocyte-derived EVs on metabolism

Adipocyte derived EVs may induce several metabolic effects on a variety of recipient cells. Large diameter rat primary adipocytes were shown to release EVs containing lipid droplet-associated factors such as perilipin, CD73 and specific mIRs which were able to induce lipogenesis in smaller adipocytes (387–389). Therefore, adipocytes may utilise EVs to shift the burden of lipid synthesis from large to small adipocytes thereby ensuring safe adipocyte hypertrophy. Conversely, adipocytes may utilise EVs to mediate pathological signals, for example, EVs derived from hypoxic 3T3-L1 cells were enriched in enzymes for *de novo* lipogenesis (390). As outlined in *Section 1.2.6*, hypoxic AT may drive AT dysfunction and inflammation. Therefore, hypoxic EVs harbouring a pro-lipogenic cargo may promote ectopic lipid deposition. EVs derived from visceral and SC AT explants were also shown to impair insulin

and TGF-β signalling in hepatocytes, suggesting adipocyte-derived EVs may contribute to hepatic IR and dysfunction *in vivo* (307,391).

1.2.7.3 Immunomodulatory properties of adipocyte-derived EVs

A number of interactions of adipocyte-derived EVs with AT-resident immune cells have been reported. Both primary adipocytes and visceral and SC AT explant-derived EVs induced differentiation of monocytes to Mϕ with a phenotype akin to AT Mϕ (306). Furthermore, EVs derived from visceral AT explants were enriched in IL-6 and MCP-1 compared to SC AT (307), were capable of inducing monocyte-to-Mϕ differentiation, and contained elevated levels of FABP4 which induced proinflammatory cytokine release from Mϕ (392). A recent study also demonstrated the ability of EVs derived from lipotoxic 3T3-L1 cells to enhance Mϕ migration both *in vitro* and *in vivo* (48). Together, these data suggest adipocyte-derived EVs may help to mediate the detrimental effects of visceral AT by enhancing local and systemic inflammation.

1.2.7.4 Other effects of adipocyte-derived EVs

EVs derived from mature 3T3-L1 cells contained pro-angiogenic factors including leptin and fibroblast growth factor-α, and were able to stimulate *in vitro* migration of HUVECs and *in vivo* angiogenesis (393). Adipocytes derived from MSCs also released EVs containing adipogenic mRNAs (such as PPARγ) which could be transferred and expressed in osteoblasts derived from MSCs (394), suggesting a role for EVs in modulating MSC lineage.

Though the majority of research into adipocyte-derived EVs has focused on mature adipocytes, interesting effects of preadipocyte-derived EVs have also been documented. For example, 3T3-L1 cells were shown to shed the adipogenic repressor, Src3 using EVs (akin to reticulocytes shedding the transferrin receptor (395)), to allow adipogenesis to occur (396). Conversely, 3T3-L1 preadipocyte EVs promoted tumour growth *in vivo* (397) suggesting preadipocyte-derived EVs can exert both physiological and pathophysiological functions.

1.3 Thesis aims and objectives

1.3.1 Rationale

EVs are emerging as novel cell-cell communicators that may have potential functions in a wide range of diseases, and hence could be a new avenue for therapeutics. However, the EV field is currently hampered by a lack of standardisation of isolation and measurement protocols. Our current knowledge of adipocyte-derived EVs is limited, despite the known homeostatic role of adipocytes and their known role in disease progression. Therefore, adipocyte-derived EVs may provide an additional facet to the endocrine functions of adipocytes in both health and disease.

1.3.2 Hypothesis

Adipocytes release EVs that reflect the functional characteristics of adipocytes and may help to aid physiological processes such as adipocyte differentiation. In conditions mimicking metabolic stress (hypoxia), adipocytes release EVs with altered characteristics that may then enhance metabolic risk and obesity-related disease progression. As such, adipocyte-derived EVs may provide a novel circulating biomarker of adipocytes *in vivo*.

1.3.3 Global thesis aim

The overarching aim of this thesis was to explore extracellular vesicles as a novel mechanism of signalling for adipocytes *in vitro* and *in vivo* whilst learning about the current limitations of the field.

1.3.4 Specific aims

1. To understand the practical limitations of EV methodologies in order to provide a firm background on which to base the experimental protocols for EV work in this thesis.

2. To characterise the homeostatic release of EVs from 3T3-L1 adipocytes, using the transition from pre- to mature adipocytes as a model of physiological adipocyte function.

3. To assess the effect of O_2 concentration on the characteristics of mature 3T3-L1 adipocyte EV release to determine whether the pathological stimulus of hypoxia could induce a change in the composition and release of EVs from adipocytes.

4. To monitor the effect of hypoxic 3T3-L1 adipocyte EVs on THP-1 Mϕ function by assessing their ability to alter the phenotype and migratory potential of Mϕ.

5. To apply the knowledge acquired from previous chapters to determine the existence of adipocyte-derived EVs in the human circulation.

6. To apply knowledge acquired from *Results Chapter 1* to a clinical cohort of patients with familial hypercholesterolaemia to assess the practicalities of EV measurements in the clinic and to determine whether apheresis treatment could impact upon circulating EV concentrations.

2. General Methods

2.1 Reagent list

Reagent/Chemical	Supplier
Annexin V binding buffer	BD Biosciences, UK
Ammonium persulphate (APS)	Fisher Scientific, UK
Formaldehyde	
Glycine	
Isopropanol	
Methanol	
10X Phosphate buffer saline (PBS)	
Sodium chloride (NaCl)	
Sodium dodecyl sulphate (SDS)	
Tris(hydroxymethyl)aminomethane	
Tween 20	
Sterile water	Fresenius Kabi, UK
DMEM (high glucose 4.5 g/L)	Gibco (Life Technologies), UK
FCS	
Ham's F12 nutrient mix	
30% (w/v) acrylamide	National Diagnostics, UK
DELFIA® buffers	PerkinElmer, UK
Radioimmunoprecipitation assay (RIPA) lysis buffer	Santa Cruz, CA
Chloroform	Sigma Aldrich, UK
Developer	
Dexamthasone	
Fixer	
Indomethacin	
Insulin solution from bovine pancreas (10 mg/mL)	
β-mercaptoethanol	
Oil Red O	
Pyronin Y	
TEMED	
Trypan blue	

2.2 3T3-L1 cells

2.2.1 3T3-L1 culture

3T3-L1 cells were kindly provided by Dr Mohd Shazli Draman (previously obtained from the American Type Culture Collection, ATCC). Cells were grown in specific media depending on their stage of differentiation (**Table 2.1**).

Component	CM	DM	MM
DMEM (high glucose 4.5 g/L)	45%	45%	45%
Ham's F12 nutrient mix	45%	45%	45%
FCS	10%	10%	10%
Penicillin/Streptomycin	1%	1%	1%
Insulin	-	10 µg/mL	10 µg/mL
Indomethacin	-	50 µM	-
Dexamethasone	-	1 µM	-

Table 2.1: Media used to culture 3T3-L1 cells. Compositions of media used throughout 3T3-L1 experiments. All % given are (v/v). CM = control medium; DM = differentiation medium; DMEM = Dulbecco's Modified Eagle Medium; FCS = foetal calf serum; MM = maintenance medium.

Preadipocytes were maintained at no more than 70% confluence between passages to retain a preadipocyte phenotype. **Figure 2.1** summarises the basic protocol used to culture 3T3-L1 cells for experiments in this thesis.

2.2.2 Cell counting and viability

Cells were gently removed from flasks using a cell scraper and pelleted by centrifugation at 1000 x g for 5 minutes. Cells were then resuspended in medium, diluted 1:1 (v/v) with trypan blue solution and counted using a Cellometer Auto T4 (Nexcelom Biosciences, USA).
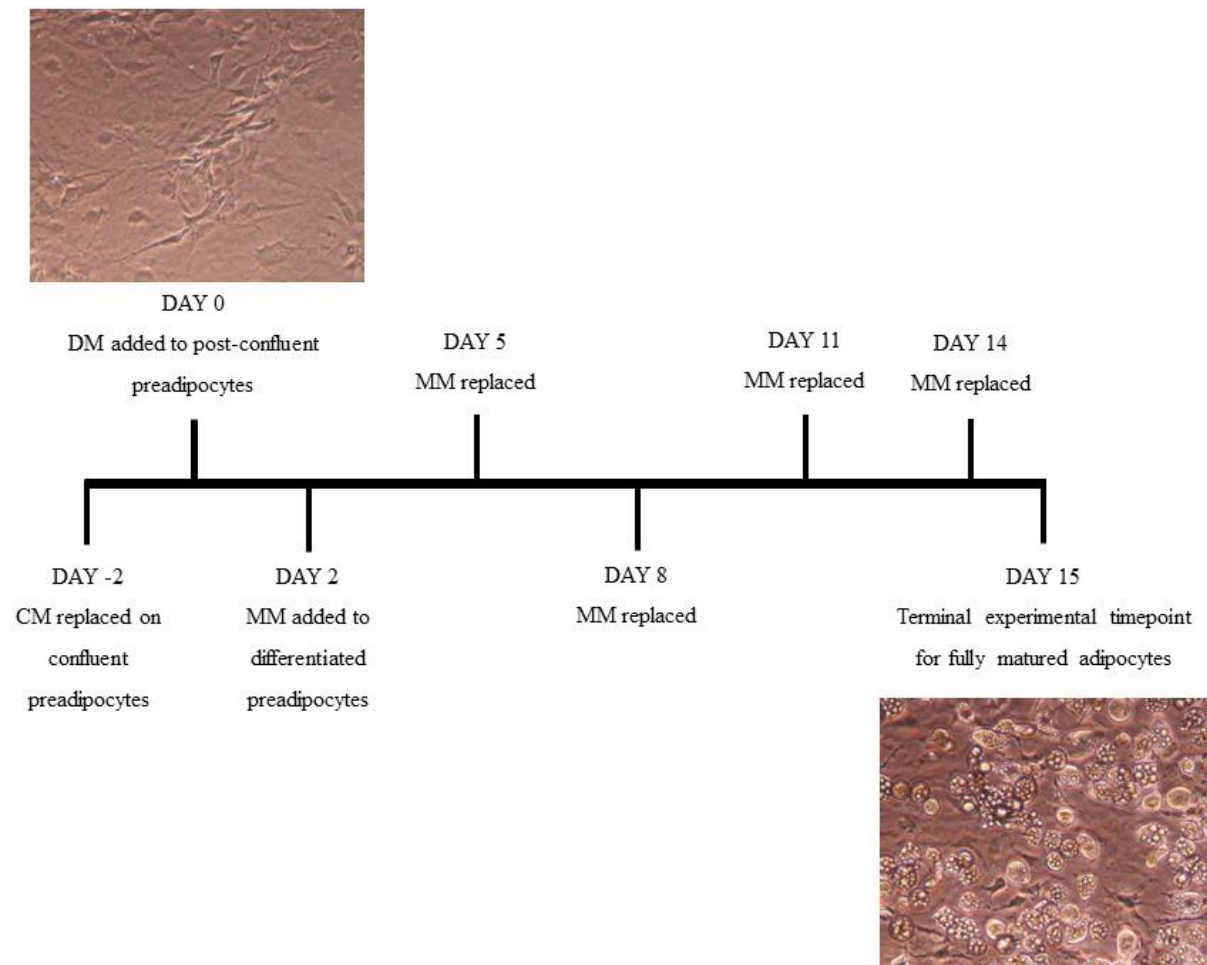
Figure 2.1: Timeline of 3T3-L1 culture. Details of 3T3-L1 growth for experimentation with accompanying images of confluent preadipocytes at day 0 (left) and mature adipocytes at day 15 (right). CM = control medium, DM = differentiation medium, MM = maintenance medium.

2.2.3 Oil Red O staining

3T3-L1 cells were cultured in 12 well plates and washed in sterile PBS prior to staining. Cells were then fixed in 10% formaldehyde (v/v in PBS) for 15 minutes at room temperature and subsequently washed with distilled water (dH$_2$O). Oil red O working solution was freshly prepared from 0.5% oil red O stock solution (w/v in isopropanol) which was diluted 3:2 (v/v) with dH$_2$O and left to stand for 15 minutes before being filtered through Whatman filter paper to remove precipitates. Cells were then stained with working solution for 15 minutes at room temperature. Excess stain was removed with 60% isopropanol (v/v in PBS) and washed twice with PBS before cells were photographed (Nikon Diaphot microscope, Nikon) at 10X magnification using ViewFinder™ software (version 3.0.1., Better Light Inc., USA). Cells were then washed a further two times with PBS, the intracellular stain was extracted using 100% isopropanol, and the optical density measured at 490 nm (Multiskan EX, MTX Lab Systems, Inc., USA).

2.3 Extracellular vesicle processing

2.3.1 Isolation of cell-derived extracellular vesicles

We (159) and others (113,398,399) have previously shown FCS-containing media harbours EVs that are co-pelleted with cell-derived EVs and could potentially overestimate EV concentration. 3T3-L1 cells were incubated in serum-free media for 24 hours before EV isolation. Conditioned culture medium was then removed from cells and subjected to differential ultracentrifugation as described previously (400). Firstly, medium was centrifuged at 1000 x *g* for 5 minutes to remove any cells in suspension. Supernatants were then centrifuged at 15,000 x *g* for 15 minutes at 4°C to eliminate any cell debris and larger vesicles (e.g. apoptotic bodies). Finally, supernatants were ultracentrifuged at 100,000 x *g* for 1 hour at 4°C to pellet EVs. Vesicle preparations were then resuspended in 1X PBS, filtered using a 0.22 µm Millex® filter unit (Merck Millipore, Ireland) unless otherwise stated. EVs were resuspended in a 40-fold concentrate, i.e. EVs were resuspended in 25 µL PBS per 1 mL conditioned medium centrifuged.

2.3.2 Isolation of plasma-derived extracellular vesicles

Blood from healthy volunteers was drawn gently into a syringe using a 21G butterfly needle (Hospira, UK) and divided between 3.2% (v/v) sodium citrate vacutainers (BD, UK). As recommendations are continually updated in the EV field, two different isolation protocols were used in this thesis. The first method, used in *Chapters 3* and *8*, obtained platelet-poor plasma (PPP) by immediately centrifuging blood at 1058 x *g* for 10 minutes at 4°C. PPP was then ultracentrifuged and resuspended as in *Section 2.3.1*, using a 4-fold concentrate.

The second method was used in *Chapter 7* and follows more recent recommendations. Blood samples were centrifuged twice at 2500 x *g* for 15 minutes at 21°C to isolate PPP and subsequently platelet-free plasma (PFP). PFP was then ultracentrifuged and resuspended as in *Section 2.3.1*, using a 10-fold concentrate.

2.3.3 Storage of extracellular vesicles

Wherever possible, EVs were analysed within 1 day of isolation. For short-term storage (1-3 days) EVs were stored at 4°C and for longer term storage (3-14 days), EVs were aliquoted and frozen at 1°C/minute using a Mr Frosty™ (ThermoScientific, UK) to -80°C.

2.4 Nanoparticle tracking analysis

2.4.1 Theory of operation

As discussed in *Chapter 1.1.7.3*, NTA is one of the most popular methods used by researchers in the EV field to determine the size and concentration of EV samples. NTA utilises the laser-scattering properties of vesicles in suspension over time to give a visual representation of EV distributions. A laser beam is refracted into a diluted sample of EVs through a glass prism, resulting in a fine beam of laser-illuminated particles in suspension. These EVs are then visualised real-time by a conventional light microscope (x20 magnification) with a high sensitivity digital camera attachment to allow the movement of EVs in suspension over time (Brownian motion) to be recorded (**Figure 2.2**).
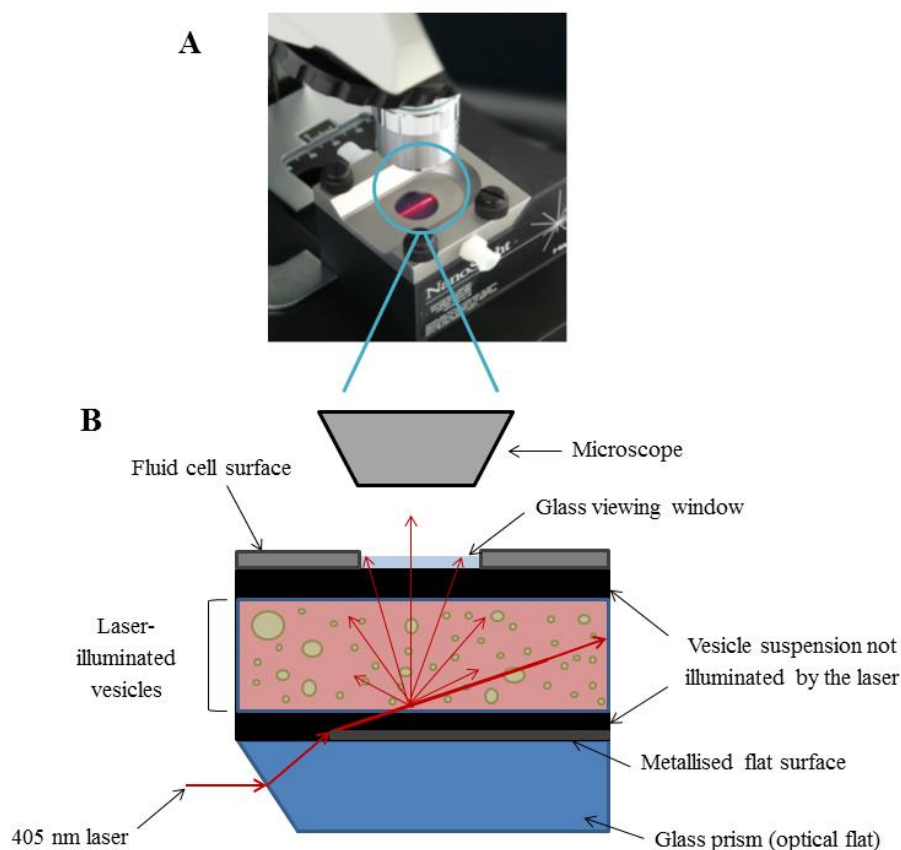
Figure 2.2: NTA operation. A 405 nm laser is refracted into the fluid suspension by a glass prism causing particles to scatter the laser light. This is then visualised by a microscope with a video camera attachment which traces the Brownian motion of illuminated particles over a set time period to calculate the size and concentration of EV samples. Image (**A**) ©Malvern Instruments Ltd.

The velocity and distance of individual EVs is tracked frame-by-frame so that the diffusion coefficient (Dt) of each vesicle can be determined from the Brownian motion over time. This can then be used with constant parameters such as temperature (T) and diluent viscosity (η) to calculate the particle size using a modified Stokes-Einstein equation (161) (**Figure 2.3**).

$$(x,y)^2 \; = Dt \; = \; \frac{K_B \mathrm{Tts}}{3\pi\eta d}$$

Figure 2.3: Stokes-Einstein equation used by NTA software. NTA software inputs data from individually tracked vesicles into a modified Stokes-Einstein equation which calculates the particle size from the particle motion in two dimensions. $(x,y)^2 =$ the squared average distance moved in the two dimensions; Dt = diffusion coefficient; K_B = Boltzmann's constant; T = temperature of the diluent (K); ts = sampling time (ms); η = viscosity of the diluent; d = sphere-equivalent hydrodynamic diameter (particle size).

2.4.2 Experimental methodology

All NTA analyses were undertaken using a NanoSight LM10 configured with a 405 nm laser and using software version 2.3 (Malvern Instruments Ltd, UK). Polystyrene beads (100 nm diameter) were measured prior to analysis of samples to ensure the machine was functioning properly and that the sample preparation was clear of contamination. Pre- and post-analytical settings were kept consistent to allow for intra- and inter-study comparison (**Table 2.2**).

Samples were diluted in particle-free sterile water (Fresenius Kabi, UK) to achieve a concentration between 2×10^8 and 1×10^9 particles/mL. Videos of 60 seconds were recorded in replicates of 5 per sample. EV size is presented as the mode of the population (nm). The concentration of plasma EV samples is presented as EVs/mL of plasma whilst the concentration of cell-derived EVs is presented as EVs/viable cell. Size distribution graphs were generated by totalling the concentration of EVs/mL plasma or EVs/viable cell in each 50 nm range (bin width) for plasma and cell-derived EVs respectively.

	Setting	Beads	EVs
Pre-analytical	Camera shutter	450	450
	Camera gain	250	250
	High threshold	3025	2275
	Low threshold	0	0
Post-analytical	Temperature	22 to 26 °C	22 to 26 °C
	Screen gain	9-10	13-15
	Detection threshold	6	4-6

Table 2.2: Pre- and post-analytical settings used for NTA experiments. Details of all pre- and post-analytical settings used when analysing bead and EV samples using NTA.

2.5 Tunable resistive pulse sensing

2.5.1 Theory of operation

As previously discussed (*Chapter 1.1.7.3*), tunable resistive pulse sensing (TRPS) is a method also used for EV quantification and sizing. TRPS is based on the "Coulter Principle" which measures the electrical impedance (usually of cells) passing through an aperture to determine the size and concentration (401). TRPS uses tunable thermoplastic polyurethane nanopores which are suspended between two fluid cells both containing silver/silver chloride electrodes. The pore is mounted on an adjustable stage ensuring the pore is fixed in place, but also allowing the stretch of the pore to be adjusted. Fluid cells are filled with electrolyte buffer so that when a voltage is applied, a current passes through the pore between the wells (**Figure 2.4**).

Electrolyte in the upper fluid cell can be replaced with a sample (diluted in electrolyte buffer) and voltage applied so that suspended vesicles pass through the pore with the current. Passage of vesicles through the pore causes a displacement of the electrolyte within the pore, temporarily increasing the resistance and hence decreasing the current. This is represented digitally by a "blockade event" (**Figure 2.4 D**). The magnitude of the blockade event is directly proportional to the volume of the vesicle. Therefore, calibration beads of known diameter and concentration can be analysed using TRPS to give uniform blockade parameters. The accompanying software can then use the calculated blockade parameters of individual calibration particles in an extraction algorithm to determine the size and concentration distributions of unknown spherical vesicles.
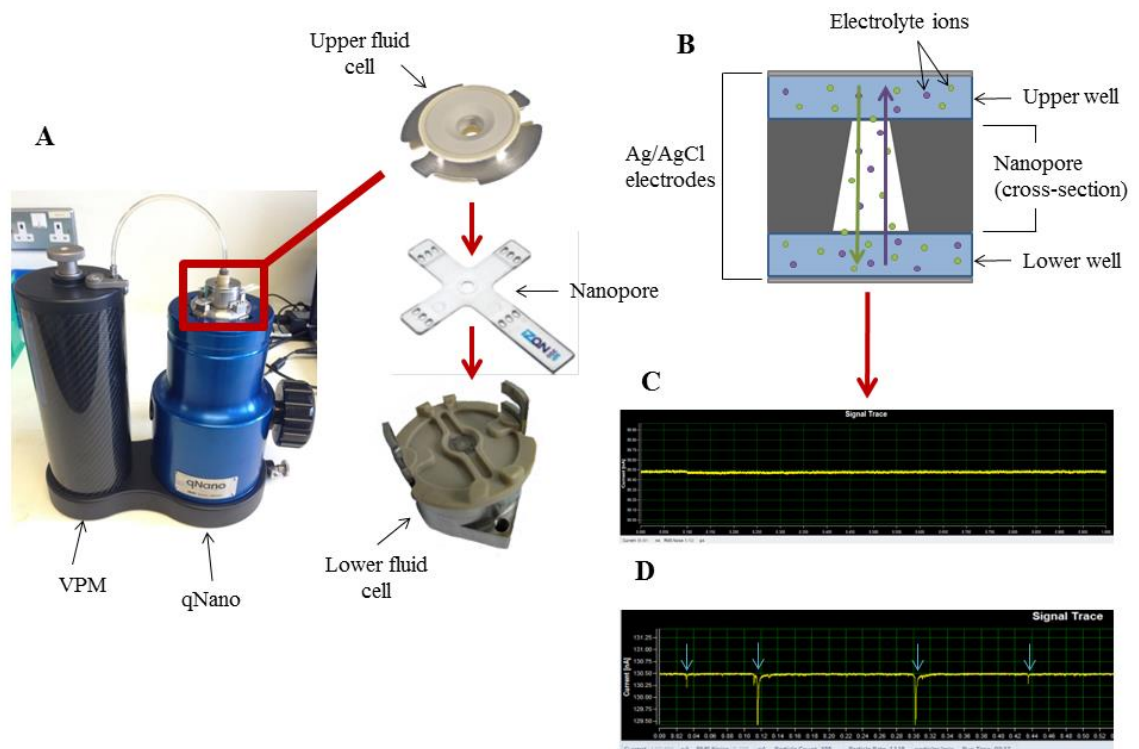
Figure 2.4: TRPS assembly and theory. (**A**) The assembled IZON qNano machine and variable pressure module (VPM) (left) and a schematic of the core individual components. A nanopore is fixed across the lower fluid cell and stretched to a specific width. The upper fluid cell is clipped onto the lower fluid cell on top of the nanopore to form a central seal between the 3 layers. (**B**) Electrolyte is added to the fluid cells and a voltage is applied creating a current two across the silver/silver chloride electrodes in each fluid cell caused by the movement of ions across the pore. (**C**) The electrolyte current is represented digitally by a flat baseline. (**D**) Particles passing through the pore displace the electrolyte and decrease the current resulting in individual "blockade events" - indicated by blue arrows. Images adapted from IZON training modules.

A fluid cell cap is secured upon the upper fluid cell acting as a Faraday cage (reducing the background noise of the system) but also serving as a point of attachment for the variable pressure module (VPM). The VPM applies pressure to the system which replaces electrophoretic mobility as the dominant force for vesicle movement through the pore. This enables equal transition of charged and uncharged vesicles across the pore and allows for determination of EV concentration.

2.5.2 Experimental methodology

TRPS experiments were performed using the qNano, CPC (carboxylated polystyrene particles) calibration beads, tunable nanopores and software version 2.2 (all IZON Science, NZ)). Prior to EV analysis, calibration beads (**Table 2.3**) were used to adjust the stretch of the nanopore and the voltage applied to achieve a blockade magnitude of 0.3 nA. This not only ensured that a range of EVs smaller and larger than the calibration beads could be analysed, but also that this same range could be analysed between different experiments. Fresh 1X PBS (prepared as in *Section 2.3.1*) was used as the electrolyte buffer and as a medium for calibration bead/sample dilution. A bandwidth filter of 5 kHz was applied and recordings were stopped if background noise exceeded 10 pA. Applied pressure was kept at 7 mbar and the minimum recordable blockade magnitude was set to 0.05 nA.

EV concentration data are presented as particles/mL plasma and the mode particle size (nm).

CPC	Mode size (nm)	Stock concentration (particles/mL)	Recommended pore
100	115	1.0×10^{13}	np100
200	203	1.3×10^{12}	np200
400	335	5.5×10^{11}	np400
500	475	3.6×10^{11}	np400
800	766	5.0×10^{10}	np800
1000	900	5.5×10^{10}	np800/1000

Table 2.3: IZON CPC calibration beads. Calibration beads and recommended nanopores supplied for use with the qNano. The mode size and stock concentration of each calibration bead is given.

2.6 Flow cytometry

Flow cytometry (FC) is often used to analyse phenotypic surface makers of cells and EVs (*Chapter 1.1.7.2*). **Figure 1.1.9** outlines the basic mechanism of FC. Here, FC was used to analyse the annexin V positivity (PS exposure) of 3T3-L1 cells and EVs (obtained from T75 cm^2 flasks), the presence of adipocyte markers in plasma EVs, and the cellular origin of plasma derived EVs in a patient cohort. Specific methods are given in *Chapters 7* and *8* for the measurement of plasma-derived EVs. Analyses were performed using a FACS Canto and FACS Diva™ software version 6 (both BD Biosciences, CA). Data were exported and subsequently analysed using FlowJo software version 10 (Tree Star Inc., OR).

2.6.1 Annexin V positivity of 3T3-L1 cells

Cells were gated based on their linear forward and side scatter properties with the assistance of Dr Kirsty Richardson. 3T3-L1 cells in PBS at a concentration of 1 x 10^6 cells/mL were analysed as a negative control. Cells were then pelleted at 1000 x *g* for 5 minutes and resuspended in 1X 0.22 µm-filtered annexin V binding buffer (BD Biosciences). Annexin V-FITC (Biolegend, CA) was added and cells were left to incubate in the dark for 15 minutes. Cells were then pelleted as before and resuspended in PBS for analysis, where 10,000 events per sample were recorded.

2.6.2 Annexin V positivity of EVs

The EV gate used was determined by Dr Gareth Willis using the logarithmic scatter of CPC beads (200 nm, 500 nm and 1µm, IZON Science). 3T3-L1 EVs were resuspended in annexin V binding buffer following ultracentrifugation as described in *Section 2.3.1* and ran as an unstained control. EVs were then stained and analysed as in *Section 2.6.1*.

2.7 Gas Chromatography

Lipid and phospholipid analysis of cells and EVs was performed with Dr Irina Guschina using gas chromatography with flame ionisation detection (GC-FID). In order to obtain enough EVs to perform phospholipid analysis, 7 x T175 cm^2 flasks were grown in parallel and pooled. GC experiments used repeats of EVs from 1 x T175 cm^2 flasks. An index of fatty acids is provided on Page VIII.

2.7.1 Lipid extraction

A 2:1 (v/v) solution of chloroform:methanol was added to the resuspension of cells and EVs in PBS. Further chloroform was added with Garbus solution (2 M KCl, 500 µM KPO$_4$, pH 7.4) and samples were vortexed and centrifuged at 250 x g for ~ 5 minutes to separate the inorganic and organic phases (402). The lower organic (chloroform) phase was carefully transferred to fresh tubes and completely dried down under a steady stream of N$_2$ gas at room temperature before being resuspended in chloroform. Lipids in chloroform were directly methylated for GC or prepared for phospholipid separation.

2.7.2 Fatty acid methylation and gas chromatography

A 2.5% sulphuric acid solution (v/v) in methanol:toluene (2:1, v/v) was used to methylate fatty acids for 2 hours at 70°C. Fatty acid methyl esters (FAME) were then extracted thrice with hexane for GC analysis. A known amount of C17:0 (margaric acid; Nu-Chek Prep, Inc,. Elysian, MN) was added as an internal standard so that subsequent quantification of peaks (and consequently lipids) could be performed. GC was undertaken using a Clarus 500 gas chromatograph (Perkin-Elmer, CT) fitted with a 30 m x 0.25 mm, i.d., 0.25 µm film thickness capillary column (Elite 225, Perkin-Elmer). The column temperature was held at 170°C for 3 minutes before being temperature-programmed to reach 220°C at 4°C/minute. Nitrogen was used as the carrier gas at a flow rate of 2 mL/minute. Data were acquired using Total Chrom Navigator (Perkin-Elmer) and the retention times of external standards (Supelco 37 Component FAME Mix, Sigma Aldrich) were used to identify FAME. An example

of a chromatogram is shown in **Figure 2.5**. Fatty acid concentration is expressed in mg/mL plasma, mg/10^6 cells or ng/10^6 EVs. Compositions of individual fatty acids were calculated as a percentage of total fatty acid concentration.
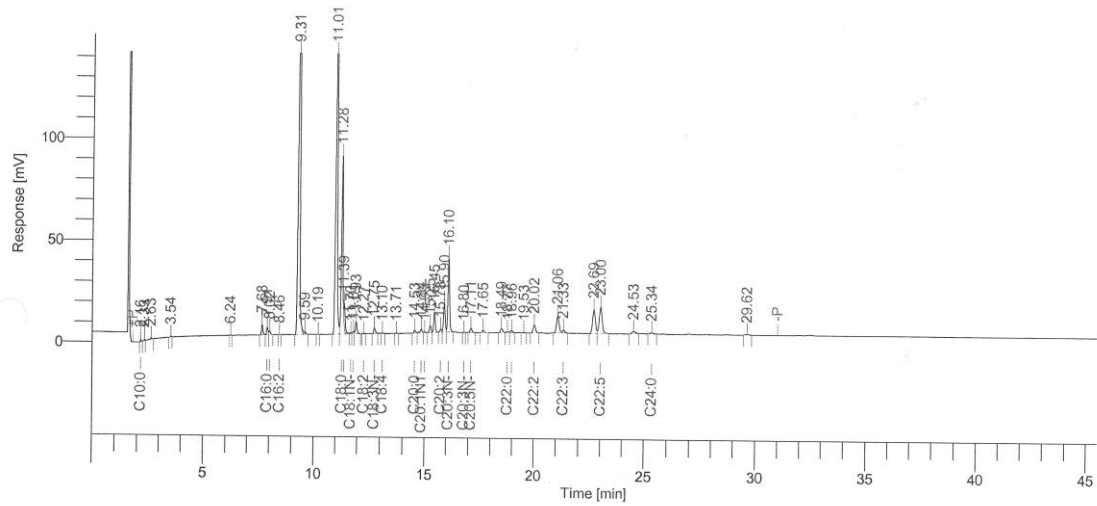
Figure 2.5: GC chromatogram. Example GC chromatogram data; long chain fatty acids have greater retention times and therefore take longer to elute.

2.7.3 Phospholipid separation

Lipids in chloroform were separated by two-dimensional thin layer chromatography (TLC) using silica gel 60 plates (10 x 10 cm, Sigma Aldrich) impregnated with boric acid (1.2% in ethanol/water; 1:1, v/v). Lipids were separated in the first dimension using a solution of chloroform:methanol:ammonium hydroxide (65:35:10, v/v/v) and using N-butanol:acetic acid: water (90:20:20, v/v/v) in the second. Plates were then completely dried and sprayed with a 0.05% solution of 8-anilino-4-napthosulphonic acid in dry methanol (v/v) and visualised under UV light to enable identification of lipid classes (**Figure 2.6**). Individual lipids were then scraped from the plates and methylated for GC as in *Section 2.7.2*. Phospholipids are presented as a proportion of the total lipid. Individual fatty acids of each phospholipid group are presented as a percentage of the total fatty acid concentration of the phospholipid.
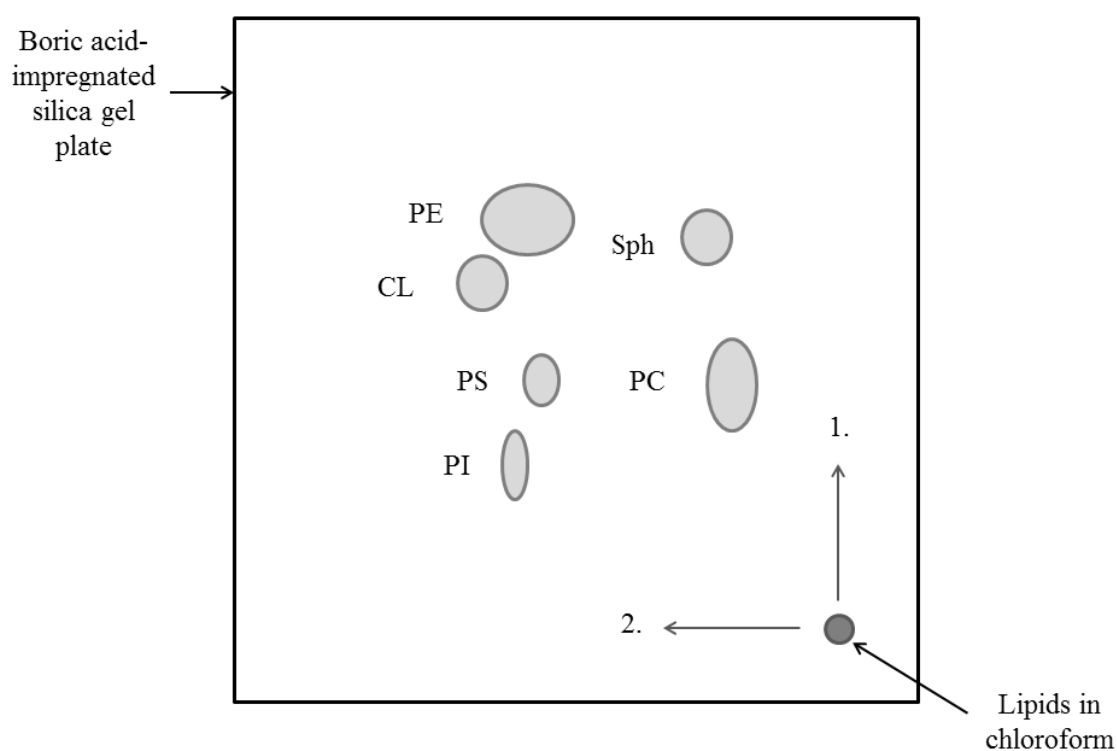
Figure 2.6: TLC separation of lipids. Extracted lipids in chloroform were spotted onto the corner of a silica gel plate impregnated with boric acid. Lipid classes were then separated in two dimensions (directions indicated by numbered arrows) and visualised under UV light. CL = cardiolipin; PC = phosphatidylcholine; PE = phosphatidylethanolamine; PI = phosphatidylinositol; PS = phosphatidylserine; and Sph = sphingomyelin.

2.8 BCA protein assay

2.8.1 Background

The bicinchoninic acid (BCA) protein assay measures a colourimetric change in the oxidation state of copper caused by the presence of protein. The assay initially utilises the principles of the biuret reaction where cupric ions (Cu^{2+}) present in the alkaline working solution are reduced by chelation with protein to form cuprous ions (Cu^{1+}). BCA then reacts with free Cu^{1+} causing a colour change from blue to purple which can be measured colourimetrically. The BCA assay was used to calculate protein concentrations of cells and EVs for EV immunophenotyping and Western blotting experiments.

2.8.2 Experimental procedure

The Pierce™ BCA protein assay kit (Thermo Scientific, UK) was used to determine protein concentration. Cell and EV samples were compared against serially diluted bonvine serum albumin (BSA) standards. Standards and samples were diluted in PBS and 25 μL of each was added to 200 μL of working reagent in a 96 well plate (Greiner Bio-One, Germany) in triplicate. The plate was mixed for 30 seconds, wrapped in foil and left to incubate for 30 minutes at 37°C according to the manufacturer's protocol. The absorbance was read at 562 nm and concentrations determined from the standard curve in μg/mL (**Figure 2.7**, r^2 value >0.99 for each assay).
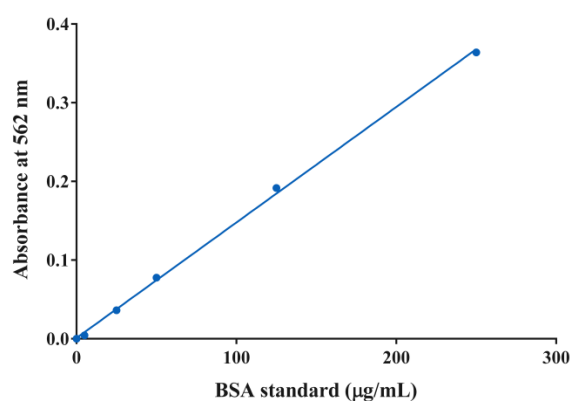
Figure 2.7: BCA assay standard curve. A typical 6-point standard curve obtained from a BCA assay. BSA standards diluted to 250, 125, 50, 25, 5 and 0 μg/mL.

2.9 Extracellular vesicle immunophenotyping

An immunophenotyping assay developed in the lab of Dr Aled Clayton (158) was used to determine the protein content of 3T3-L1 EV samples. The assay entails isolated vesicles being adhered to "sticky" ELISA plates then probing for antibodies of interest (**Figure 1.1.10**). The use of europium ensures a highly fluorescent signal enabling detection of less abundant antigens.

2.9.1 Immunostaining of EVs

EVs were immobilised on high protein binding ELISA plates (Greiner Bio-One) at a concentration of 1 µg (determined as in *Section 2.8.2*) per well and allowed to settle overnight at 4°C. RIPA (radioimmunoprecipitation assay) buffer (Santa Cruz, CA) was added for 1 hour at room temperature to permeabilise EVs for staining of antigens within the vesicles. EVs were then probed with primary antibodies diluted to 1µg/mL (**Table 2.4**) for 2 hours at room temperature on a plate shaker. Antigens were detected using specific biotin-labelled secondary antibodies and a streptavidin-europium conjugate (all Perkin-Elmer). Three washes were performed between each addition (6 washes following addition of streptavidin-europium) using DELFIA® wash buffer (Perkin-Elmer). Plates were analysed using time resolved fluorescence using both a Wallac Victor^2 plate reader (Perkin-Elmer) and a FLUOstar OPTIMA (BMG Labtech, UK). The focal height was set to 7.8 mm and the gain to 2048 a.u.. Each well received 200 flashes and the detection measurement started at 400 µs after the last flash and was recorded for 400 µs (integration "start" and "time" respectively). Data are presented in arbitrary TRF units which have been adjusted for background fluorescence by deducting negative control (EVs with no primary antibody) TRF values.

Antibody	Manufacturer and product code	Source	Dilution
Adiponectin (anti-mouse)	CST: #2789	Rabbit	1:10
Adiponectin (anti-human)	Abcam ab18065	Rabbit	1:15
Alix	CST: #2171	Mouse	1:450
CD9	Santa Cruz: sc-9148	Rabbit	1:200
CD63	Santa Cruz: sc-15363	Rabbit	1:200
FABP4	CST: #3544	Rabbit	1:1000
HIF-1α	Abcam: ab179483	Rabbit	1:117
IL-6	CST: #12912	Rabbit	1:101
IL-10	CST: #12163	Rabbit	1:101
MCP-1	CST: #2029	Rabbit	1:16
PPARγ	CST: #2443	Rabbit	1:50
PREF-1	CST: #2069	Rabbit	1:50
TNFα	CST: #11948	Rabbit	1:101
TSG101	Santa Cruz: sc-227	Rabbit	1:200

Table 2.4 Antibodies used for EV immunophenotyping. Details of primary antibodies used for EV immunophenotyping experiments. One μg/mL of each antibody was added to each well, accounting for the differences in dilution. CD = cluster of differentiation; FABP4 = fatty acid binding protein-4; HIF-1α = hypoxia inducible factor-1α; IL = interleukin; MCP-1 = monocyte chemoattractant protein-1; PPARγ = peroxisome proliferator-activated receptor γ; PREF-1 = preadipocyte factor-1; TNF-α = tumour necrosis factor-α; TSG101 = tumour susceptibility gene -101.

2.10 Western Blotting

2.10.1 Lysis of cells

Cells were washed with 1X PBS on ice, before the addition of cold lysis buffer (50 mM Trizma® base, 150 mM NaCl, 5 mM EGTA, 1% (v/v) Triton X100 in dH$_2$O, pH 7.6) supplemented with protease inhibitor cocktail (PIC, cOmplete tablets, Roche, UK). Cells were gently removed from flasks using a scraper. Samples were then centrifuged twice (13,000 x g, 4°C, 20 minutes) to pellet cell and vesicle debris. Supernatants were then analysed for their protein concentration as in *Section 2.8.2* and stored in sterile Eppendorf tubes at -20°C until required.

2.10.2 Separation of proteins by SDS-PAGE

Ten to twenty μg of protein was denatured by diluting 1:1 with loading buffer (**Table 2.5**), boiling for 5 minutes at 100 °C and centrifugation at 13,000 x g for 5 minutes.

Component	Volume (mL)
10% SDS	2
Glycerol	1
0.5 M Tris (pH 6.8)	1
Water	0.8
0.2% Pyronin Y	0.1
β-mercaptoethanol	0.1
10X PIC	0.5

Table 2.5: Loading buffer. Constituents and volumes used to make loading buffer; Percentages are given in w/v. SDS = sodium dodecyl sulphate; PIC = protease inhibitor cocktail.

Proteins were then loaded onto freshly prepared polyacrylamide gels (**Table 2.6**) and separated by sodium dodecyl sulphate polyacrylamide gel electrophoresis (SDS-PAGE). A pre-stained broad range colour ladder (11-245 kDa, Cell Signaling

Technologies, New England BioLabs, UK) was also loaded and samples were resolved at 200 V in 1X running buffer (**Table 2.7**) until bands reached the bottom of the running gel.

Component	Running gel (mL)				4% Stacking gel (mL)
30% Acrylamide	*8%*	*10%*	*12%*	*15%*	1.3
	2.64	3.30	3.96	4.95	
Water	3.58	2.92	2.26	1.27	6.1
1 M Tris (pH 8.8)	3.75				-
0.5 M Tris (pH 6.8)	-				2.5
10% SDS	0.1				0.1
10% APS	0.1				0.1
TEMED	0.005				0.01

Table 2.6: Polyacrylamide gels. Components and volumes of running and stacking gels used for SDS-PAGE. Running gels of differing acrylamide percentages were used depending on the size of the protein of interest. Gels and APS were freshly made on the day of experimentation. SDS = sodium dodecyl sulphate; APS = ammonium persulphate; TEMED = tetramethylethylenediamine. Percentages are given in w/v.

Component	Weight (g)
Tris	15
Glycine	72
SDS	5

Table 2.7: 5X Running buffer. Components of the running buffer made up to 1 L with distilled water and diluted 1:5 for running gels.

2.10.3 Electroblotting

Wet electroblotting was used to transfer proteins from the gel to a PVDF (polyvinylidene fluoride) transfer membrane (Amersham™ Hybond™-P 0.45, GE Healthcare, UK). Membranes were pre-wet briefly in methanol before transfer.

Proteins were transferred for 1 hour at 350 mA in blotting buffer (**Table 2.8**, cooled at -20°C for >1 hour prior to use) with a magnetic stirrer and ice pack.

Component	Amount
Tris	3.025 g
Glycine	13.66 g
Water	800 mL
Methanol	200 mL

Table 2.8: Blotting buffer. Components and volumes used to make blotting buffer, stored at -20°C for >1 hour before use.

2.10.4 Incubation of antibodies

Following transfer of proteins, membranes were washed in tris-buffered saline with Tween 20 (TBS-T, **Table 2.9**). All subsequent washes were performed 3 times for 5 minutes on an orbital shaker using TBS-T.

Component	Volume (mL)
10X TBS*	100
Water	900
Tween 20	1

Table 2.9: TBS-T wash buffer. Components and volumes of TBS-T wash buffer. *10X TBS was made from 24.2 g Tris, 80 g NaCl made up to 1 L with distilled water and adjusted to pH 7.6 with 10 M hydrochloric acid.

Membranes were then blocked for 1 hour at room temperature on an orbital shaker in blocking buffer (5% (w/v) skimmed milk powder (Marvel, UK) in TBS-T). Membranes were incubated with rabbit anti-mouse monoclonal primary antibody (specific details given in each chapter) overnight at room temperature. Membranes were washed before adding ECL™ peroxidase labelled donkey anti-rabbit secondary antibody (GE healthcare) diluted 1:5000 in blocking buffer for 1 hour at room

temperature. Finally, membranes were washed thoroughly (2 x 30 seconds, 1 x 15 minutes, and 3 x 5 minutes in TBS-T) to prepare for developing.

2.10.5 Developing of blots

Membranes were incubated in ECL Prime Western blotting detection reagent (GE Healthcare) for 5 minutes at room temperature before being exposed to photographic film (Amersham™ Hyperfilm ECL, GE Healthcare) in a dark room. Time of exposure varied with each antibody (see **Table 2.10**). Films were then developed using Kodak™ -D19 developer and fixer (Sigma Aldrich).

2.10.6 Densitometry

Densitometry analysis was conducted using ImageJ software (version 1.49, National Institutes of Health, USA). Raw densitometry values were then normalised to a control unless otherwise stated.

2.11 Statistical analysis

Data in this thesis were analysed using GraphPad Prism (version 6.0, GraphPad sortware Inc., USA). Details of specific statistical analyses are given in the Methods section of each Results chapter. Data are presented as mean ± SD unless otherwise stated and a *p* value of <0.05 was considered statistically significant.

3. Results I:

Developments in methodology

3. Perspective

The work detailed in this chapter was conducted at the beginning of my PhD as I was learning about the practicalities of working with EVs and the field-wide lack of standardisation. Our lab was fortunate to have regular access to two EV measurement techniques; NTA and TRPS, the latter being an emerging/less-widely used technique. This therefore presented a good opportunity to compare the two techniques whilst learning about their relative benefits and weaknesses. Furthermore, our interests prior to beginning work with EVs were in clinical measurements and so we were first interested in studying EVs derived from plasma. Consequently, I decided to begin establishing the effects of different pre-analytical processes on EV measurements. This was conducted using TRPS with the support of IZON Science and in parallel with *Chapter 8*.

Due to the novelty and ever increasing popularity of the EV field, much of the work in this chapter has since been conducted and published by others. Nevertheless, this chapter provides interesting and in-depth insights into methodological aspects and sample processing of EVs.

3.1 Introduction

In addition to discussing the potential of EVs as disease biomarkers and therapeutic targets, *Chapter 1.1* also introduced the inconsistencies and lack of standardisation that exist within the EV field which make inter-study comparison difficult. This disparity has perhaps been exacerbated by the rapid growth in interest in EVs in recent years. Though attempts are being made to standardise EV isolation, analysis and storage (16), there are currently no gold standard protocols or techniques.

At the outset of data collection for this chapter (2012-2013), many techniques were available to measure EV size and concentration including: TEM; DLS; FC; NTA (149,161,403) and the emerging TRPS. Each technique has its own advantages and disadvantages (149) and the use of a particular technique is often dependent on the desired outcome or variable to be measured (404). NTA, one of the most widely used of the techniques to measure EV size and concentration, video records the light scattering and Brownian motion of particles in suspension. NTA has been shown to give a better detection of polydispersity compared to DLS (405) which is often biased by the presence of larger vesicles, as scattered light from all EVs is pooled by a single detector (160,161). NTA is more user-friendly than TEM, requiring less sample preparation and hence reduces adverse effects on EV morphology (108). Finally, NTA provides superior sensitivity for EVs <300 nm compared with FC (161) where the lower detection limit and swarm detection of EVs may result in an underestimation of concentration (154). However, little was known about TRPS, which unlike other techniques, measures EVs on a particle-by-particle basis as they disrupt the current passing through a tuneable nanopore (406).

As with EV measurement, there are no established protocols for the isolation and storage of EVs used prior to analysis. This is partly due to the diversity of EV sources (e.g. plasma, saliva, urine and conditioned culture media) that require different pre-analytical processing. This, combined with the use of different measurement techniques, results in significant inconsistencies in reported EV concentrations (407). Investigations into varying the time before processing, the anticoagulant, the number and speed of centrifugation steps, and freeze-thawing are all reported effect EV concentration (59,107,108,408,409). Increases in EVs were observed when blood was not processed immediately after isolation and following

storage at -80°C for 1 month (107). Additionally, chelating anticoagulants (citrate, ACD and EDTA) yielded fewer EVs compared with protease inhibitor anticoagulants (sodium heparin, hirudin) (59). Storage of platelet-poor plasma (PPP) at -80°C for 1 week also increased the detection of certain EV subtypes (409). However, freezing was also shown to decrease subsets of EVs (60,409) particularly with long-term storage (107). These conflicting effects of pre-analytical processing were measured directly using FC, which as discussed in *Chapter 1*, may be inaccurate due to the low refractive index and "swarming" of EVs (154). Therefore, the effects of pre-analytical processing on EV size and concentration (particularly EVs below the detection limit for FC) may have not been fully characterised.

3.1.1 Aims

This chapter sought to explore TRPS as an EV measurement technique and to utilise TRPS to measure changes in EVs prepared using different pre-analytical processes.

The specific aims were:

1. Using calibration beads, to test the technical aspects of TRPS in terms of;
    a. Linearity compared with NTA
    b. Limits of detection compared with NTA
    c. Detection of polydispersity compared with NTA, DLS and FC
2. To use TRPS to assess the changes in plasma EV size and concentration following pre-analytical processing with:
    a. Citrate and EDTA vacutainers
    b. Filtering EV samples
    c. Method and length of storage of EVs

3.1.2 Hypotheses

TRPS may be an alternative technique for measuring EV size and concentration that overcomes the negatives of measuring EVs using light scattering-based techniques. Pre-analytical processing of EVs may change detected size and concentration of EVs detected by TRPS.

3.2 Methods

3.2.1 Nanoparticle tracking analysis

NTA analyses were carried out as described in *Chapter 2.4.2* using the analytical settings for beads (**Table 2.2**). Calibration beads (50, 100, 300 and 1000 nm; Malvern, UK) were used for NTA experiments. To create a standard curve, six dilutions of 100 nm beads were prepared in sterile water over a 16-fold dilution range (1.5 x 10^8 – 2.5 x 10^9 particles/mL). To test the limits of detection, 50, 100, 300 and 1000 nm beads were individually analysed and plotted together on one graph in particles/mL. Finally to test how NTA dealt with polydispersity, 50, 100 and 300 nm beads were prepared at a 1:1:1 ratio and analysed in triplicate.

3.2.2 Tuneable resistive pulse sensing

TRPS analyses were conducted as indicated in *Chapter 2.5.2* using CPC calibration beads (IZON Science, NZ) (**Table 2.3**). For the standard curve, an np200 pore was used with six dilutions of CPC200 beads in 1x PBS (filtered through a 0.22 μm pore prior to dilutions) over a 16-fold dilution range (5.5 x 10^8 – 8.8 x 10^9 particles/mL). For the limits of detection, CPC100, 200, 400, 500, 800 and 1000 nm beads were analysed using np100, np200, np400 and np800 pores. Nanopores were tested with each CPC bead until beads fell below the detection limit of the pore or the pore became blocked (which occurred frequently). Results were expressed as a percentage of the total count due to significant variations in concentrations between beads (see **Table 3.3.1**). Finally, to test the ability of TRPS to detect polydispersity, an np100 pore was used to analyse a mix of CPC100, 200 and 400 beads prepared at a 1:1:1 ratio.

3.2.3 Dynamic light scattering

A Zetasizer Helix (Malvern, UK) was assessed for its ability to detect individual populations of 50, 100 and 300 nm beads in a 1:1:1 mixture.

3.2.4 Flow cytometry

A custom-built BD FACSAria II was used to analyse a mix of 200, 500 and 800 nm fluorescent beads (Submicron bead calibration kit, Bangs Laboratories Inc., USA) prepared at a 1:1:1 ratio. Experiments and analyses were performed with the help of Dr Kristin Ladell (Cardiff University).

3.2.5 Isolation of plasma-derived extracellular vesicles

Blood was collected from healthy volunteers as described in *Chapter 2.3.2* using the first isolation method. Blood in this chapter was collected into both citrate and EDTA vacutainers for comparison of EV concentration.

3.2.6 Filtering of extracellular vesicles

Isolated plasma-derived EVs were further diluted in PBS (750 µL PBS for every 250µL EVs) and 4 aliquots were prepared as depicted in **Figure 3.2.1**. Briefly, half of the EV aliquot was passed through a 1 µm filter and the filtrate was either analysed immediately (**1**) or frozen at -20°C overnight before being analysed (**3**). The remaining unfiltered aliquot was analysed immediately (**2**) and one aliquot was frozen at -20°C before being analysed (**4**). All EV samples were analysed using TRPS with np200, 400 and 1000 pores.
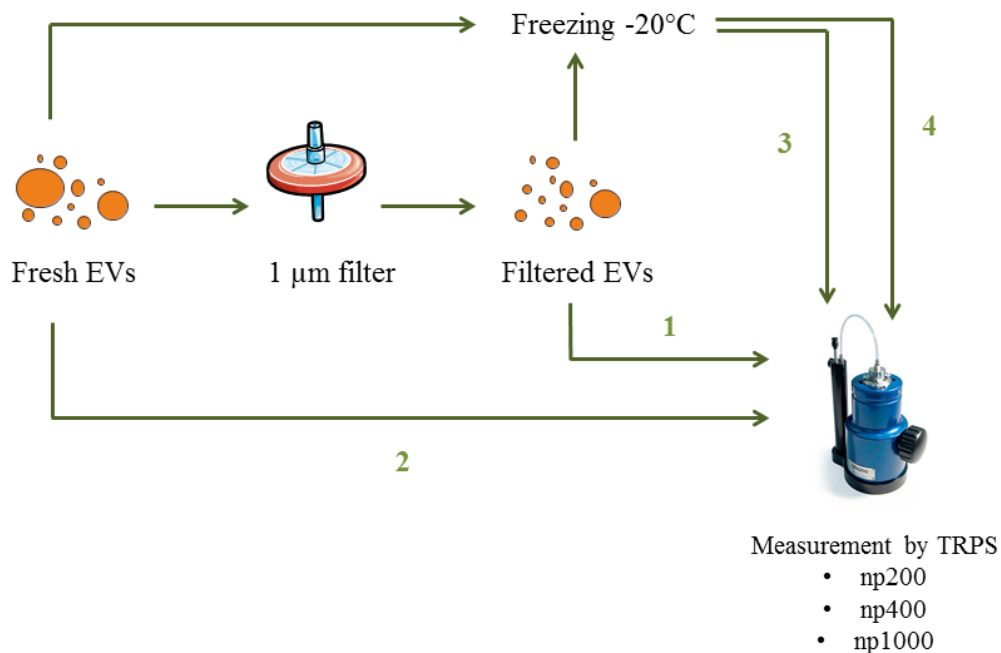
Figure 3.2.1: Filtering of EVs. Filtered and non-filtered plasma-derived EVs were analysed by TRPS. Freshly isolated EVs were filtered through a 1 μm pore (**1**) and analysed immediately by TRPS. Freshly isolated EVs were left unfiltered and analysed by TRPS (**2**). Filtered EVs were stored at -20°C overnight and analysed by TRPS (**3**) and finally unfiltered EVs were stored at -20°C overnight and analysed by TRPS (**4**). All samples were analysed using np200, np400 and np1000 pores where possible.

3.2.7 Method and length of storage of extracellular vesicles

Filtered (as above) plasma-derived EVs collected from 4 healthy volunteers were aliquoted and stored (**Figure 3.2.2**). Briefly, 6 different methods of storage and 4 lengths of time in storage were analysed for their effect on EV size and concentration. Fresh samples were analysed immediately following collection using TRPS with an np200 pore. Methods of storage tested included fresh EV samples: put directly into the fridge; stored at -20°C; snap frozen in liquid nitrogen; slow frozen to -80°C in a Mr Frosty™ (Thermo Scientific, UK); mixed with 5% (v/v) glycerol (Fisher Scientific, UK) and slow frozen at -80°C in a Mr Frosty™; and mixed with 0.05% (v/v) Tween 20 (Sigma Aldrich, UK) and slow frozen at -80°C in a Mr Frosty™. Aliquots were then stored for 1 day, 1 week, 1 month or 3 months and analysed by TRPS using an np200 pore.
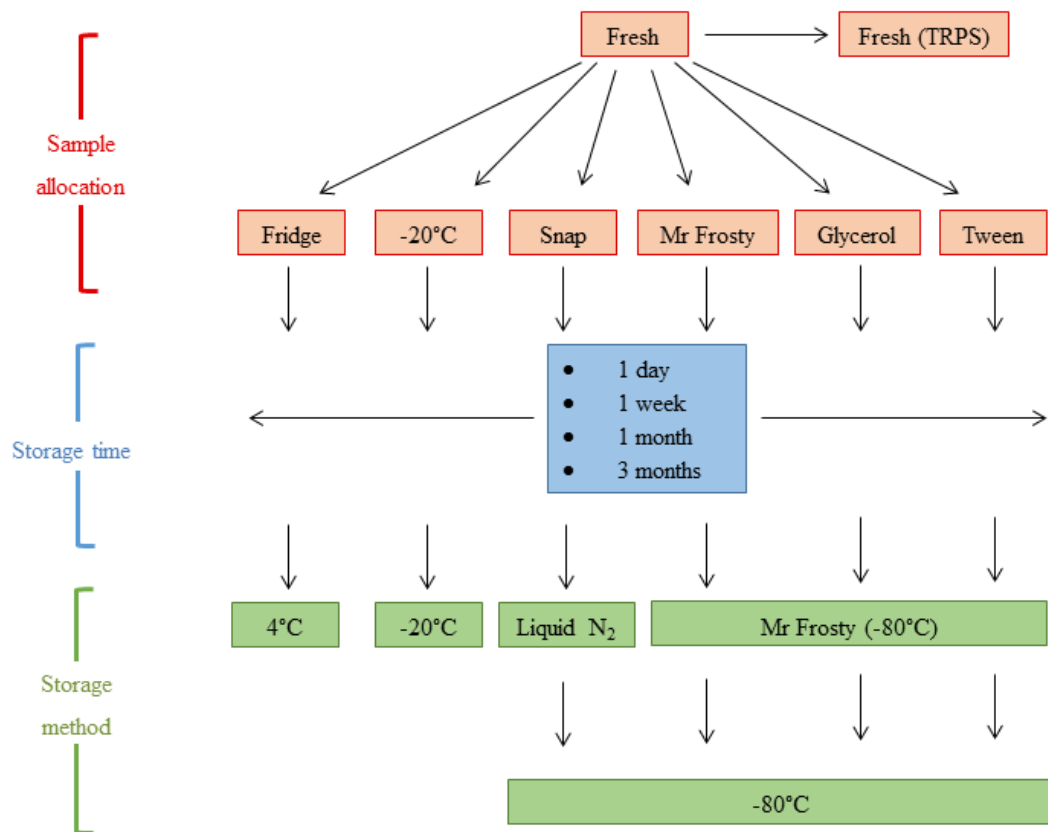
Figure 3.2.2: Method and length of EV storage. Plasma EVs filtered through a 1 μm filter were analysed for the effect of storage on size and concentration using TRPS. Fresh EVs were analysed on the day of isolation and were used to compare other samples to. EVs were stored by 6 different methods for 1 day, 1 week, 1 month and 3 months. "Snap" refers to samples snap frozen in liquid nitrogen and then stored at -80°C. "Glycerol" and "Tween" refer to samples mixed with either 5% Glycerol (v/v) or 0.05% Tween 20 (v/v), slow frozen in a Mr Frosty and then stored at -80°C.

3.2.8 Statistical analysis

Data were analysed using GraphPad Prism version 6 (GraphPad software, USA). Samples were tested for normality using D'Agostino and Pearson omnibus normality test to determine the need for a parametric or non-parametric statistical test. Data are presented as mean ± SD unless otherwise stated. An unpaired *t-test* or a Kruskal-Wallis test (with a Dunn's multiple comparisons post-hoc test) were used to compare means whilst a general linear model was used to assess the difference in mean concentration of EVs over time of storage. A *p* value of <0.05 was considered statistically significant.

3.3 Results

3.3 Part I: Comparison of EV methodologies

Upon beginning this chapter of work and my research in the EV field (2012-2013), there was an evident lack of clarity across all EV research. This was recognised by a number of companies at the time leading to competition in supplying key instrumentation to researchers. However, little was known about the reliability of such instrumentation to measure EV size and concentration. Therefore, to learn about the practicalities and pitfalls, a comparison was undertaken between NTA (widely used at the time) and TRPS (an emerging technique at the time).

3.3.1 Reliability of NTA and TRPS

Calibration beads were measured using NTA and TRPS over a range of six dilutions. Both NTA and TRPS show good linearity between the actual and measured concentrations of calibration beads over a range of dilutions ($r^2 = 0.988$ and 0.993 for NTA and TRPS respectively; **Figure 3.3.1 A/B**). Mode size of beads detected was relatively uniform with varying concentrations of beads for both NTA and TRPS (**Figure 3.3.1 C**; dilutions are labelled 1-6 as different concentration ranges are covered by NTA and TRPS). NTA showed a slightly higher mode size for all dilutions which gradually increased with the concentration whereas TRPS showed more deviation from the manufacturer-provided mode (203 nm).
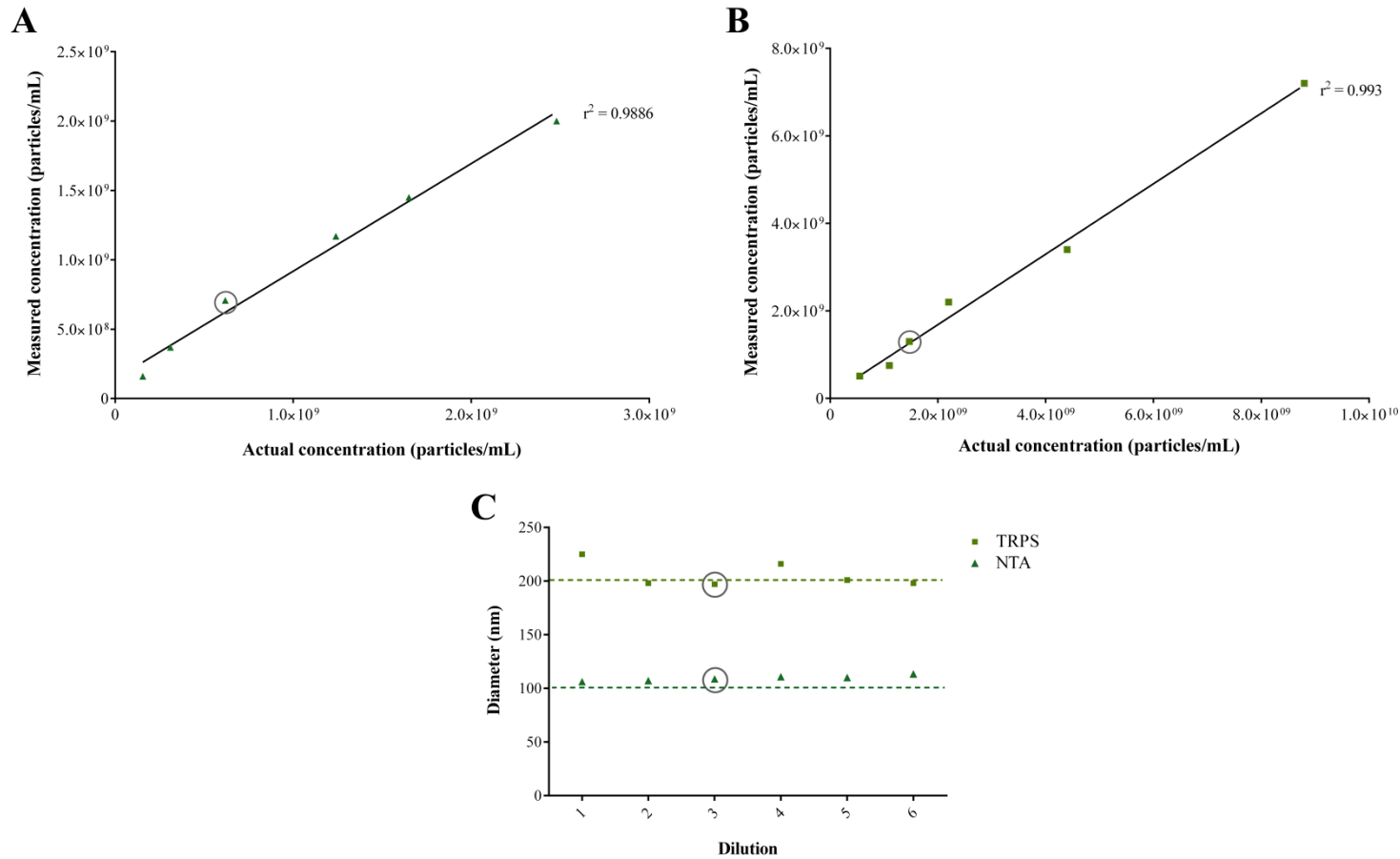
Figure 3.3.1: Calibration bead standard curves. Calibration beads were analysed over a range of dilutions using NTA with 100 nm beads (**A**) and TRPS with 200 nm beads and an np200 (**B**) respectively. The measured concentrations were then plotted against the diluted concentrations and fitted with linear regression. The effect of increasing bead concentration on mode size (**C**); circled points indicate the manufacturer recommended dilution.

3.3.2 Limits of detection

Manufacturer-provided calibration beads of varying sizes were analysed using NTA and TRPS to assess detectability across the EV range. NTA was able to detect each size of bead as an individual population when a single bead size was analysed (50 nm beads = 48 ± 6 nm, 100 nm beads = 97 ± 2 nm and 300 nm beads = 285 ±17 nm) though the size of 1000 nm beads was underestimated (703 ± 102 nm; **Figure 3.3.2 A**). In order to view the beads detected with each nanopore on one graph, TRPS data are presented as a percentage of the population by count (**Figure 3.3.2 B**). TRPS detected individual bead sizes across the EV range when using different pores. However, the detected concentration and mode size of beads varied between nanopores, particularly at the upper and lower limits of each nanopore (**Table 3.3.1**).

3.3.3 Detection of polydispersity

EV samples often contain a range of vesicle sizes. Therefore it is important that the technique used to measure EVs is able to distinguish between sizes in polydispersed samples. Fortunately, at the time of undertaking this experiment, 4 techniques commonly used to measure EV samples were available to analyse polydispersed mixtures of beads (**Figure 3.3.3**). DLS detected beads from around 50 – 300 nm, however, this was represented by a single peak with a mode size of around 150 nm (**A**). NTA was able to clearly distinguish between 100 and 300 nm beads, however, 50 nm beads were detected as a small shoulder on the 100 nm bead peak (**B**). The measured size of 300 nm beads was also underestimated in the polydispersed mix analysed with NTA. TRPS was able to identify each bead in the mixture as an individual population; however the measured mode size for each bead was under- or overestimated for CPC100/200 and CPC400 respectively (**C**). Finally, FC was able to distinguish between the 3 bead sizes (200, 500 and 800 nm); however, this was based on the fluorescence and side scatter of each bead (**D**).
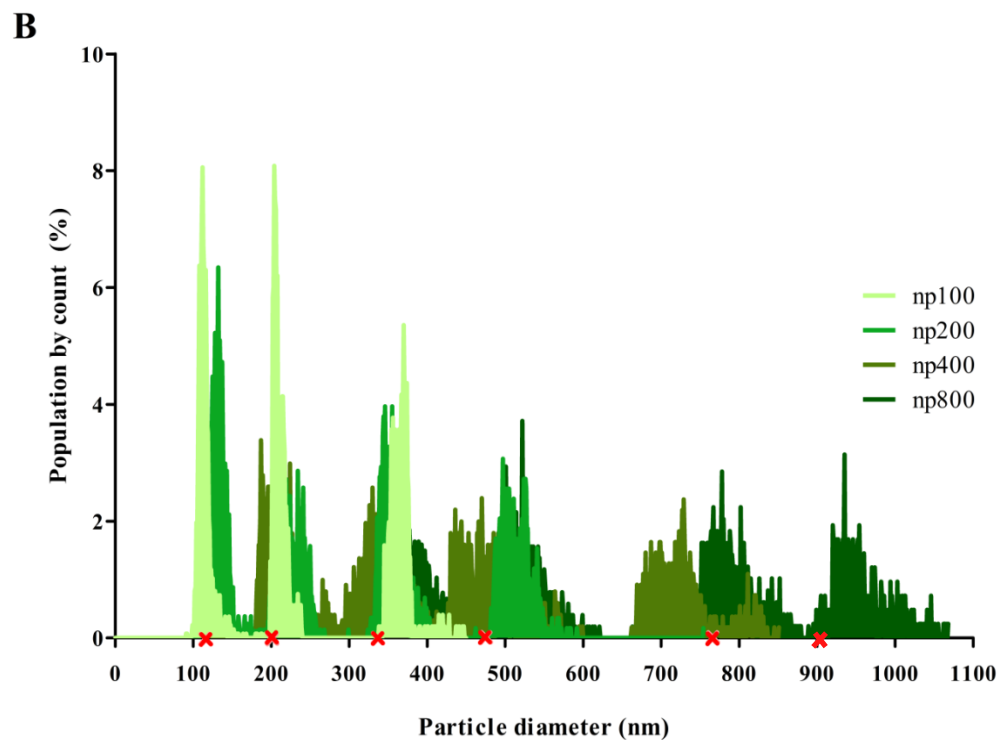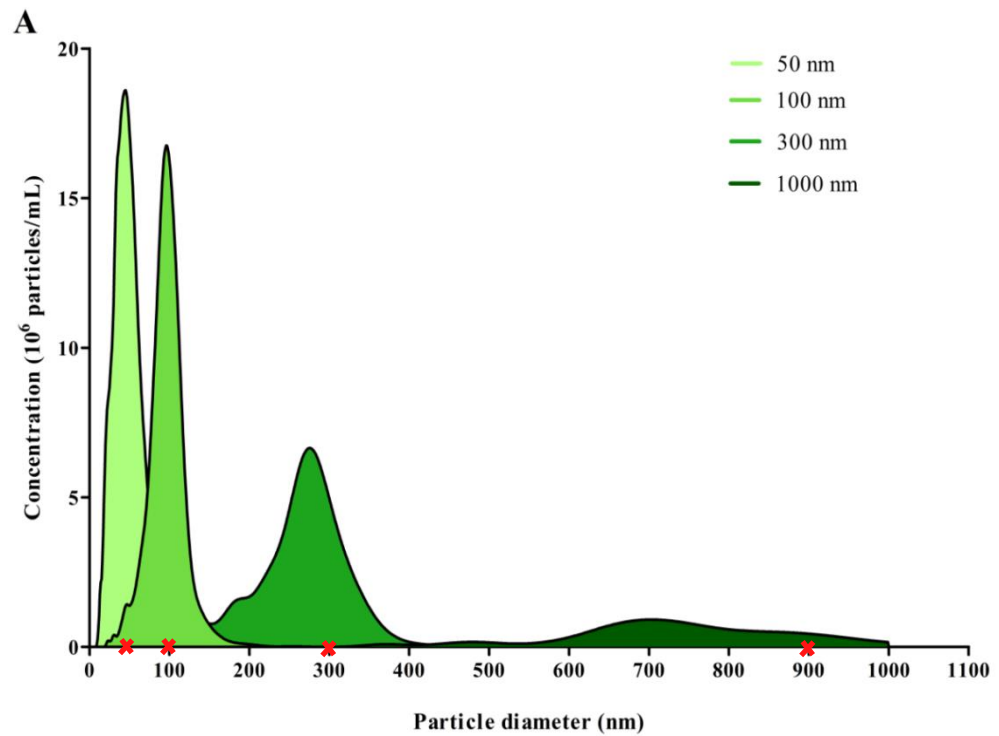
Figure 3.3.2: Ranges of detectability. The ability of both NTA and TRPS to detect beads across the EV range was measured. (**A**) NTA; Individual bead preparations of 50, 100, 300 and 1000 nm beads were analysed using NTA. (**B**) TRPS; CPC100, 200, 400, 500, 800 and 1000 were analysed using np100, 200, 400 and 800. The expected mode size of each bead (as denoted by the manufacturer) is marked with a red cross.

	np100	np200	np400	np800
CPC100	✔	✔		
Concentration	1.6×10^{13}	2.8×10^{12}		
Mode size	**115**	134		
CPC200	✔	✔	✔	
Concentration	2.5×10^{12}	1.1×10^{12}	1.4×10^{12}	
Mode size	203	**215**	194	
CPC400	✔	✔	✔	✔
Concentration	1.6×10^{12}	1.2×10^{12}	5.7×10^{11}	3.7×10^{10}
Mode size	376	350	**353**	360
CPC500		✔	✔	✔
Concentration		3.7×10^{11}	4.3×10^{11}	7.9×10^{10}
Mode size		524	**466**	513
CPC800			✔	✔
Concentration			1.3×10^{11}	5.2×10^{10}
Mode size			723	**771**
CPC1000				✔
Concentration				1.6×10^{10}
Mode size				947

Table 3.3.1: Variation between TRPS nanopores. Beads detected by each TRPS nanopore varied in both concentration and mode size. Mean concentration and mode size of beads are given in particles/mL and nm respectively. Designated calibration beads for each pore are highlighted in bold. Stock concentrations were: CPC100; 1.0×10^{13} particles/mL; CPC200; 1.2×10^{12} particles/mL; CPC400; 5.5×10^{11} particles/mL; CPC500; 3.6×10^{11} particles/mL; CPC800; 5.0×10^{10} particles/mL and CPC1000; 5.5×10^{10} particles/mL.
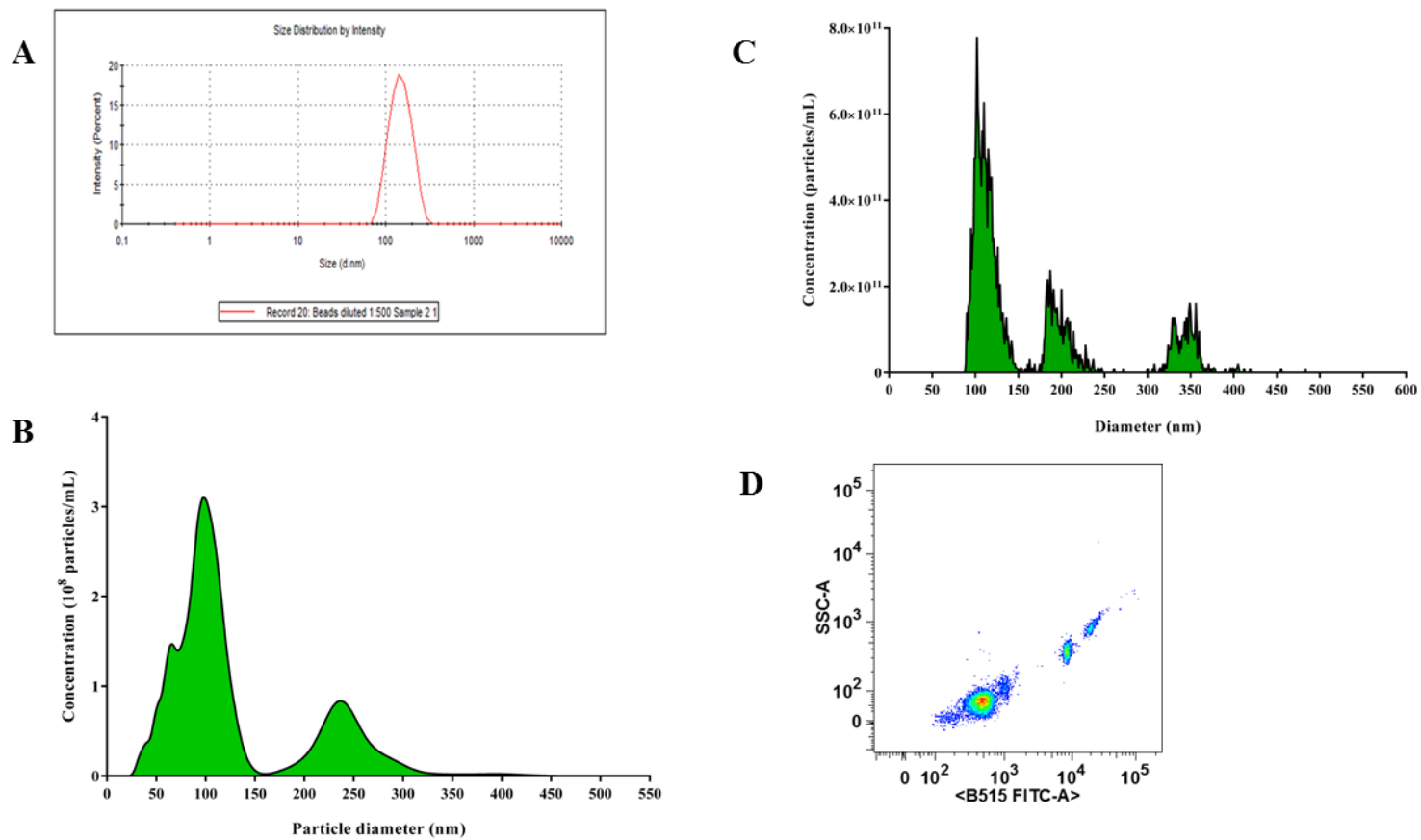
Figure 3.3.3: Detection of polydispersity. Four techniques widely used in the field to analyse EVs were compared for their ability to separate individual populations in a polydispersed mixture of beads. DLS (**A**) and NTA (**B**) were tested with 50, 100 and 300 nm beads. TRPS (**C**) using an np100 pore was tested with 100, 200 and 400 nm beads and FC (**D**) was tested with fluorescent 200, 500 and 800 nm beads.

3.3 Part II: Effects of pre-sample processing

Pre-sample processing of EVs - i.e. the steps taken to isolate EVs from the original source for analysis - is an area of great contention in the EV field. Again, a lack of standardisation makes comparisons between studies difficult. Therefore, the following experiments aimed to tackle some of the issues encountered with sample preparation and storage in relation to EV size and concentration.

3.3.4 Choice of vacutainer

Blood taken for subsequent EV isolation is usually treated with an anticoagulant. Here, EV concentration was compared in blood taken using citrate and EDTA vacutainers. TRPS analysis showed an increased number of EVs from blood taken into EDTA compared to citrate vacutainers (2.3 x 10^9 ± 1.2 x 10^8 vs. 7.2 x 10^8 ± 4.1 x 10^8 particles/mL respectively; **Figure 3.3.4**).
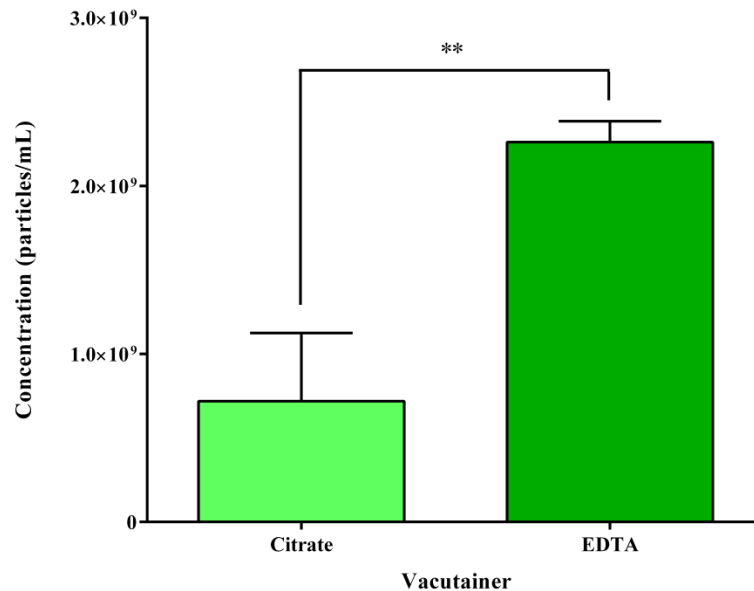
Figure 3.3.4: Choice of vacutainer. Citrate and EDTA vacutainers were used to collect blood from healthy volunteers. Isolated EVs from each vacutainer were then analysed by TRPS for their concentration. **$p = 0.003$ (n=3). EDTA = ethylenediaminetetraacetic acid.

3.3.5 Filtering of extracellular vesicles

As EVs are classified as being submicron, a 1 µm filter was used to remove any potential contaminants from plasma-derived EVs before and after freezing (**Figure 3.3.5**). Data from the np1000 showed a large reduction from unfiltered fresh to filtered fresh EVs (4.9 x 10^7 to 1.7 x 10^6 particles/mL; **Figure 3.3.5 A/B**). Frozen samples could not be detected with the np1000. The np400 also showed filtering fresh EVs reduced the concentration (7.6 x 10^8 vs. 3.8 x 10^8 particles/mL for fresh unfiltered and freshly filtered respectively; **Figure 3.3.5 C/E**). Filtering and then freezing EVs caused a slight increase in concentration (4.5 x 10^8 particles/mL), but when EVs were frozen and then filtered, there was a large decrease in concentration (1.3 x 10^8 particles/mL; **Figure 3.3.5 D/E** respectively). Finally, the np200 showed a large decrease in EVs that were filtered then frozen but a large increase in EVs that were frozen then filtered compared to fresh filtered EVs (**Figure 3.3.5 F/G**). Unfiltered fresh EVs could not be detected by the np200 due to frequent pore blocking.

Page | 122
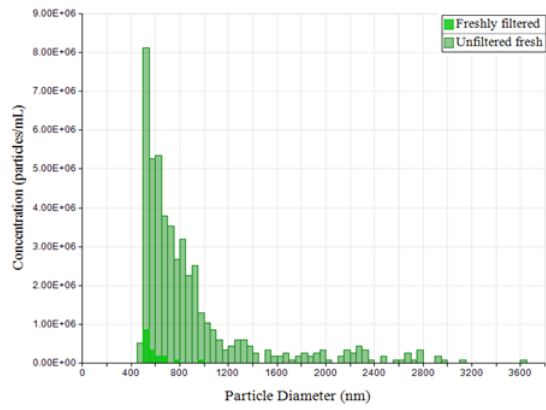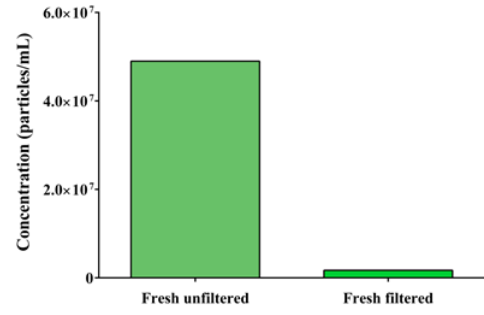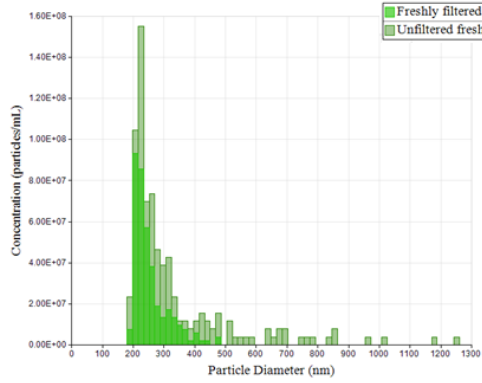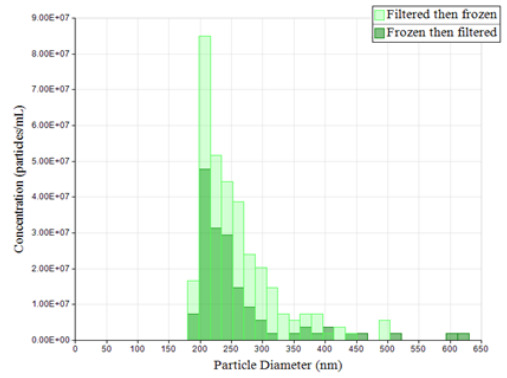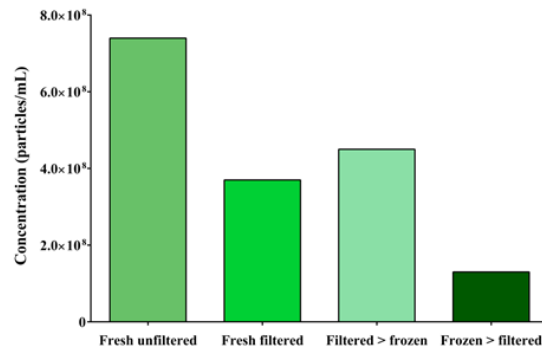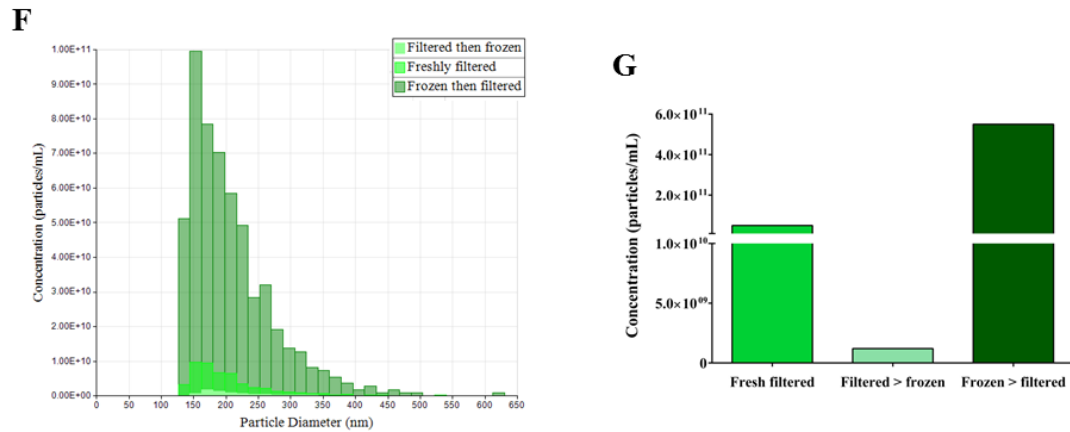
Figure 3.3.5: The effects of filtering and freezing EVs. EVs isolated from plasma were analysed using TRPS after either being filtered through a 1 μm filter (fresh filtered), or left unfiltered. Both filtered and unfiltered EVs were then frozen at -20°C. Filtered EVs were then thawed and re-analysed using TRPS (filtered then (>) frozen). Unfiltered EVs were thawed and filtered through a 1 μm filter and analysed using TRPS as before (frozen then (>) filtered). Samples were analysed using np1000 (**A/B**), np400 (**C-E**) and np200 (**F/G**) nanopores (n=1). Concentration distributions generated with the Izon software are shown for the np1000 for unfiltered fresh and filtered fresh (**A**); for the np400 for unfiltered fresh and filtered fresh (**C**) and filtered then frozen and frozen then filtered (**D**); and the np200 for fresh filtered, filtered then frozen and frozen then filtered (**F**). Mean concentrations were then plotted in GraphPad Prism for np1000 (**B**), np400 (**E**) and np200 (**G**).

3.3.6 Method and length of extracellular vesicle storage

Effective storage of EVs is vital to overcome the impracticalities of analysing samples on the same day as isolation. Therefore, it is important to know to what extent different methods and length of storage influence EV size and concentration. Five of the six methods of storage tested appeared to increase EV concentration compared to fresh EVs (analysed on the day of isolation) though this was not significant (**Figure 3.3.6 A**). Only EVs kept in the fridge seemed to retain the closest concentration to that of fresh EVs. Again, excluding EVs kept in the fridge, the method of freezing reduced the mode size of EVs, though this was not significant (**Figure 3.3.6 B**). Interestingly, the length of time for which EVs were stored caused an increase in EV concentration ($p = 0.002$, **Figure 3.3.6 C**). Past 1 week of storage, regardless of the initial method used to store EVs, measured concentration of EVs was increased, particularly by 3 months of storage compared with fresh samples ($p<0.05$). The mode size of EVs also decreased gradually with time in storage, however, this was not significant (**Figure 3.3.6 D**). Subsequent analysis using a general linear model indicated that length of storage was a significant factor in increasing EV concentration ($p = 0.009$).
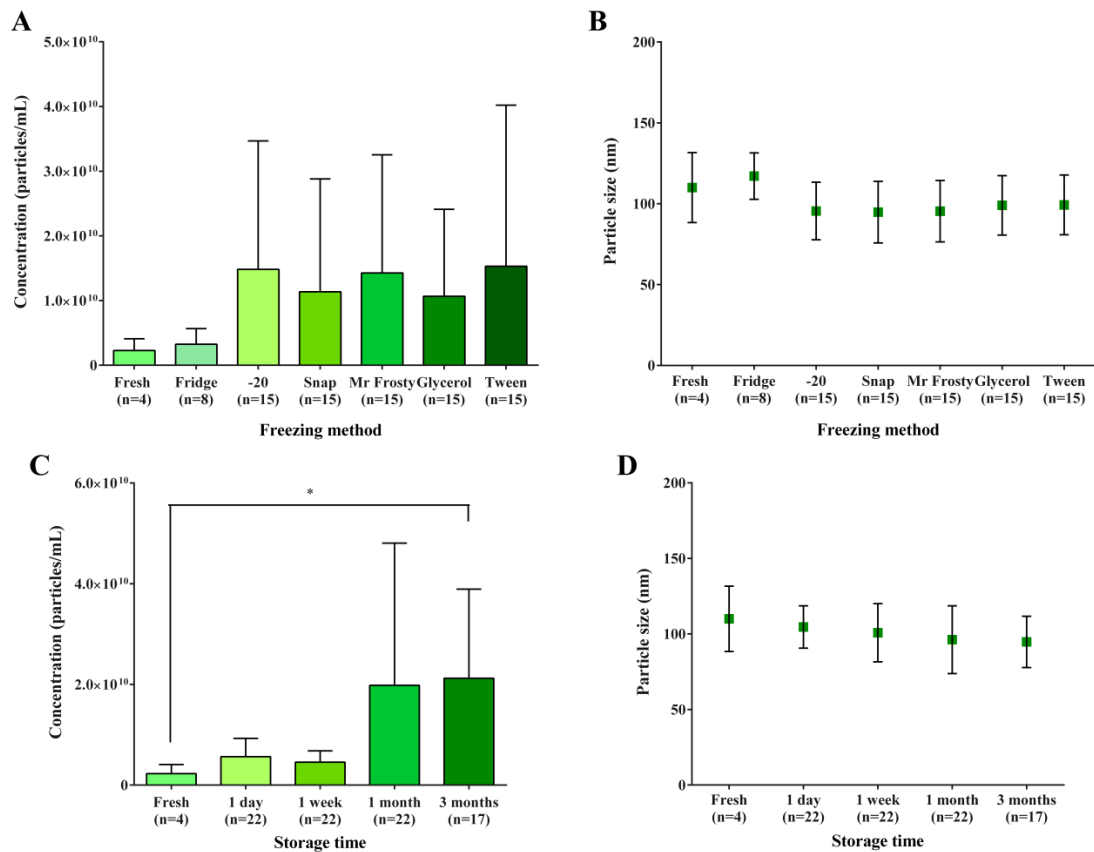
Figure 3.3.6: The effect of storage on EV concentration and size. Plasma-derived EVs were analysed on the day of collection (fresh) by TRPS using an np200 pore. EVs were then aliquoted and stored by 6 different methods for 4 lengths of time. At each time point EVs were thawed and analysed as with fresh samples. Methods of freezing were then compared to EVs analysed fresh in terms of concentration (**A**) and mode size (**B**). The effect of storage time on EV concentration (**C**) and mode size (**D**) was also compared to fresh EVs. $*p<0.05$, Sample n numbers are provided; the 3 month time point has a lower n number due to insufficient EV sample.

3.4 Discussion

3.4.1 Key findings

Methodological comparisons:

1. NTA and TRPS both show good linearity over a range of bead concentrations.
2. TRPS accurately measures beads over a wider range than NTA, however this requires the use of multiple nanopores.
3. Measured concentration between TRPS nanopores differs greatly, making it difficult to compare actual concentrations between nanopores.
4. Techniques used to measure EVs differ vastly in their ability to detect individual populations in polydispersed samples.

Pre-analytical processing:

5. Blood collected in EDTA vacutainers yields a greater concentration of EVs than blood collected in citrate vacutainers.
6. Filtering EVs (before or after freezing) reduces overall EV concentration.
7. Length of storage, regardless of method, increases EV concentration.

3.4.2 Main discussion

One of the biggest challenges facing the EV field is the attainment of standardised methods for the isolation, storage and measurement of EV samples. Evidently, this is complicated by the heterogeneity of EV sources, user experience and available instrumentation. Complete clarity of methods used and fulfilment of ISEV "minimal requirements" (16) are currently the best available options for regulation of published EV data. Data presented in this chapter are from experiments conducted at the beginning of my PhD that helped me to learn about the methodological limitations faced in the field but also helped to make an informed decision on how to approach analysis of EVs in cell-based and clinical studies.

The measurement of EV size and concentration is often the first and most important step in EV analysis. Sizing of EVs confirms isolation of a submicron EV population or of singular populations such as exosomes. Determining EV concentration is important in identifying differences between groups, or if a set numbers of EVs is required in further experiments. Therefore the initial technique used to determine EV size and concentration should be reliable and relatively fast (if many samples need to be analysed or further experiments need to be undertaken). Despite there being a number of techniques available for measurement of EV size and concentration, there is no gold standard and each technique has accepted advantages and limitations. Here TRPS, a new technique in the EV field at the time, was assessed to compare the detection over a range of concentrations and sizes of calibration beads with NTA. Both NTA and TRPS showed good linearity over a range of concentrations of calibration beads with little deviation from the expected mode size. This is useful when dealing with biological samples which can show great inter-sample variability in size and concentration. Dilutions were chosen for each standard curve based around the recommended dilutions of the manufacturer and have since been presented by others for NTA (161,405,410) and for TRPS (411).

It is essential for the measurement techniques to be able to accurately detect EVs over the whole EV range. Therefore the range of detection of both NTA and TRPS was measured using calibration beads of varying sizes. NTA accurately identified 50, 100, and 300 nm beads; however the mode size of 1000 nm beads was underestimated. Others have measured beads at the upper end of the EV range (≥500 nm) using NTA with greater accuracy (405,407,410). However, in these cases pre- and post-analytical settings were altered for each bead whereas in this chapter, they were kept the same. This means that here, although the settings may not be completely optimal for each bead size, the consistency of analysis was maintained between samples and the software was not then biased towards detecting a particular size. TRPS was able to detect six different bead sizes as distinct populations from 100 – 1000 nm, though to achieve this, multiple nanopores were required. This was time consuming and often frustrating due to frequent pore blocking. Although nanopores are tuneable, they are limited to a particular size range and are typically best suited (as demonstrated here) to measure their namesake diameter, for example the np200 and CPC200 beads. Each pore was able to detect 3 or more different sizes

of beads; however the accuracy in the reported mode size was lost at either extreme of the pore. The reported concentration of the same beads seemed to differ greatly between pores, for example, the concentration of CPC400 beads differed by almost 10 fold between np100 and np800 pore measurements. Generally, smaller nanopores reported higher concentrations of beads. This has been shown previously, though not directly alluded to (407) and little explanation has been offered (411).The most likely reason is that smaller nanopores are superior for the detection of small particles (which are able to have a higher concentration per unit volume than larger particles). Therefore larger pores report lower overall concentrations as smaller beads are below the detection limit or are indistinguishable from the noise of the pore. TRPS concentration is determined by comparing the particle rate and pressure of the sample to that of the calibration bead (164,411,412) used for the pore with a known stock concentration and mode size (**Table 2.3**). Here, the pores tended to overestimate the concentration of beads considered large for that pore and underestimate the concentration of beads considered small for that pore. For example, the concentration of CPC400 beads was overestimated 3-fold by the np100 and underestimated 15-fold by the np800. Therefore the increased concentration of beads with smaller pores and decreased concentrations with larger pores cannot entirely be explained by the difference in sensitivity between pores. Perhaps because the stock concentration of beads used to calibrate smaller nanopores is higher (e.g. 1 x 10^{13} particles/mL for CPC100 for np100), the pore is then predisposed to detect a higher overall concentration, particularly at the upper extremity of the pore. This could be tested by calibrating an np100 pore with CPC400 beads and seeing whether the concentrations of CPC100/200 beads are then underestimated.

EV samples are almost always heterogeneous regardless of the biological source. When characterising a population of EVs it is important for the technique to be able to detect EVs across a range of diameters. Therefore, 4 techniques commonly used for EV detection were tested for their ability to separate beads of different sizes in a polydispersed mix. As outlined in *Chapter 1.1.7.3*, DLS calculates particle size and concentration from the scattered light of particles in suspension. The Brownian motion of particles causes a Doppler Shift (fluctuation in scattered light). These fluctuations in scattered light are measured by a photon detector and the data are

used in the Stokes-Einstein equation (**Figure 2.3**) to derive particle size and concentration. DLS has been shown to be highly accurate for sizing monodispersed suspensions, particularly those < 200 nm (413), though this accuracy is lost on heterogeneous samples. The scattered light is collected simultaneously (161) meaning the resulting size of particles is biased by a small number of large particles scattering more light (414). Here, DLS (using a mix of 50, 100 and 300 nm beads) showed a single peak from 50-300 nm with no distinction of bead populations, indicating the result was biased by the scattering of 300 nm beads. Others have shown that DLS gives more detailed size distributions and also detects differences in EV samples when the angles of detection for light scattering are increased and improved calculation algorithms are used (149,160). DLS is also simple to operate and requires minimal amounts of sample (415). However, until detection is improved, DLS is impractical and inaccurate for the measurement of polydispersed samples.

NTA is technically similar to DLS though particles are visualised and video-tracked over time allowing measurement of individual particles (161). Here, NTA was able to distinguish 100 and 300 nm beads (as demonstrated by others (161)); however, 50 nm beads were measured as a shoulder of the 100 nm peak. Though NTA gives superior detection compared to DLS, large particles can still influence measurements in polydispersed samples. With NTA, larger particles tend to scatter more light creating a "halo" effect around the particles (161) (**Figure 3.4.1**) which is sometimes measured as smaller particles leading to a decreased overall mode size. Alterations in pre- and post-analytical settings can also give rise to differences in size and concentration (411). However, despite the potential subjectivity, with a prior appreciation of the limitations and a small amount of training, NTA is a simple and rapid technique to measure EV size and concentration. A recent recommendation for measuring polydispersed EV samples is to use at least two dilutions of the sample and optimise pre- and post-analytical settings for each sample (149,161,162,407).
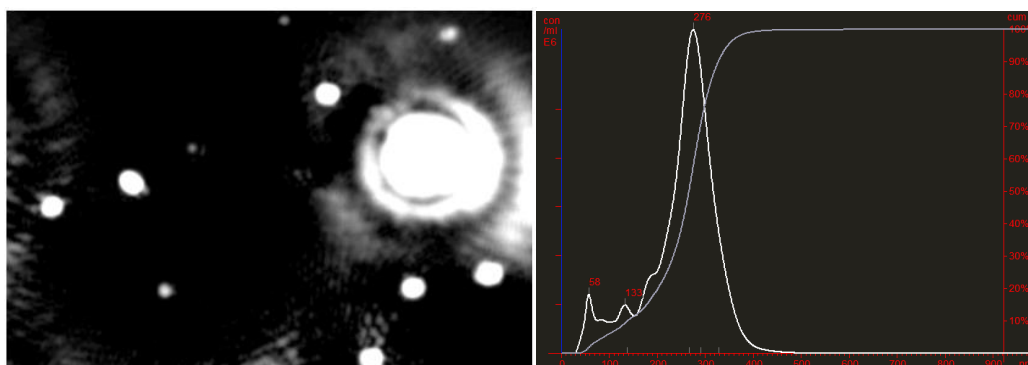
Figure 3.4.1: Measuring large particles with NTA. Still of a NTA video (left) measuring polydispersed beads. Larger beads scatter more light creating rings of light around the particle which are counted as smaller particles (right) causing an underestimation of mode size for larger particles.

TRPS is a non-optical technique for measuring EV size and concentration that analyses samples on a particle-by-particle basis (416). Using an np100 pore, a mix of 100, 200 and 400 nm beads were clearly visualised as individual populations. The mode size of each bead showed a slight deviation from the expected size though each was still within 15 nm of the actual size. Though TRPS (as illustrated here) is potentially more accurate in detecting individual sizes in polydispersed samples, the adoption of the qNano for measuring EV samples has been less successful than that for NTA. This may perhaps boil down to the usability of TRPS compared with NTA. Possibly the greatest limitation of TRPS is the frequent pore blocking due to a polydispersity range greater than that of the nanopore resulting in inconsistent data and time-consuming and frustrating measurements (411,412). Consequently TPRS requires at least one nanopore to measure an EV sample (containing vesicles ranging from 50 – 1000 nm) which has been referred to by others as "high and low sensitivity measurement" (407,411). Though in principle this is similar to measuring samples twice with NTA with different dilutions and settings, in reality the use of two pores requires more time and effort in changing and recalibrating new pores. Additionally, as discussed above the variation in measured concentration between pores may not entirely be due to differences in sensitivity. Therefore merging of data between pores (at the point of crossover of concentration) may lead to an overestimation of concentration. Finally, I and others have observed variation between different batches of the same nanopore, and also with the longevity of the

nanopore (411,417). This may be due to differences in the nanopore geometry (411,417,418) which result from inconsistencies in pore manufacturing.

FC is one of the most widely-used applications to analyse EV populations (419), possibly because it is one of the most accessible of the four techniques and it has the potential to assess multiple functional markers. A flow cytometer measures the light scattered by samples as they pass through a laser beam. The use of different lasers allows for excitation of a variety of fluorophores, enabling measurement of surface markers as well as scatter profiles. Here, beads could be identified as separate populations when based on fluorescence but not when plotted by scatter. The forward and side scatter profiles give important information about the refractive index of particles. Unfortunately, the low refractive index of EVs (420) means that most flow cytometers are incapable of detecting EVs < 300 nm (149,155,421,422) which is the size range in which the vast majority of EVs fall (120,149). Furthermore, the refractive index of polystyrene beads (such as the ones used here) is much higher than that of EVs (423,424) causing incorrect assumptions of particle sizing and inaccurate gating strategies to be used for EVs (420). The current opinion is that FC is a useful tool to analyse surface markers (155) rather than size and concentration of EVs if it is employed correctly. Recent developments such as high resolution flow cytometers to detect EVs ~100 nm (155,425) and binding of EVs to micrometre beads (117) are helping to overcome the shortfalls of EV detection with FC.

Every step taken from sample collection to the isolation of EVs introduces potential variation in final EV concentration. This is due to a lack of standardisation for pre-analytical processing of EVs and results in great variations in reported EV concentrations. Therefore, the following work sought to identify and characterise sources where variation may be introduced in order to optimise our own protocols.

When analysing blood-derived EVs, the anticoagulant used to collect the blood has been shown to affect EV concentration. Flow cytometric studies have found that chelating anticoagulants produce fewer EVs than protease inhibitor anticoagulants (59). Interestingly, administering heparin to thrombophilic women throughout pregnancy reduced *in vivo* EV concentration and reduced pregnancy loss (frequently

associated with thrombophilia) (426). Citrate has previously been shown to minimise changes in platelet morphology compared to EDTA (427), despite EDTA being a stronger chelator of Ca^{2+} (428). However, no study has compared the effects of anticoagulants on EV concentration using a more accurate technique than FC. Here, TRPS data showed that plasma-derived EVs from blood collected into EDTA vacutainers contained significantly higher concentrations of EVs than plasma EVs from citrated blood. Others have attributed the effects of different anticoagulants on EV counts to *ex vivo* microvesiculation from platelets (60,429) though György et al., observed a reduction in non-platelet as well as platelet-derived EVs in ACD vacutainers (429). This indicates that varying quiescence of platelets with differing anticoagulants does not entirely account for differences in EV counts. Jayachandran et al., concluded that differences in EV counts were due to a loss of EVs from calcium chelation rather than an *ex vivo* generation with protease inhibitors (59) no explanation is given as to how calcium chelation reduces EV production *ex vivo*. Furthermore, EV counts and origin were assessed using FC meaning the majority of EVs may not have been detected. In order for the effects of different anticoagulants on EV concentration and origin to be assessed completely, a direct comparison of the most commonly used anticoagulants (EDTA, citrate, ACD and heparin) needs to be undertaken using an accurate technique to enumerate and phenotype EVs.

Differential ultracentrifugation is one of the most popular ways to isolate EVs from complex fluids. However, as well as requiring specialist equipment, pellets may also be contaminated with soluble components (125), protein aggregates and lipoproteins (118) which may contribute to the final EV concentration. Microfiltration has successfully been employed to enhance the isolation of exosomes from cell culture models (125,430). However, this has not been applied to the EV population as a whole. Here, the effect of passing plasma-derived EVs isolated with ultracentrifugation through a 1 μm filter was analysed across the EV range using TRPS with np1000, np400 and np200 nanopores. Initial analysis with the np1000 confirmed removal of the majority of material above 1μm but also a great deal < 1 μm with over a 96% reduction in EV concentration post-filtration. The same trend was observed when these samples were analysed with the np400 pore, though to a lesser extent with a 50% reduction in concentration. This difference in reduction may be because the np400 cannot measure larger particles present in the unfiltered fresh

sample but also because many smaller particles present in the filtered fresh sample are below the detection limit of the np1000. This is also illustrated by the np200 which could not record the unfiltered sample due to frequent pore blocking from large particles. Unfortunately, as TRPS used in this context could only determine the size and concentration of samples, the identity of the material caught in the filter is unknown. Therefore though a reduction was seen using a 1 µm filter, we cannot be sure EVs were not also removed. The point at which EV samples were filtered was also analysed by filtering EV samples both before and after freezing (-20°C). Frozen EV samples could not be detected using the np1000, however the np400 showed that filtering before freezing had less of an effect on EV concentration than filtering after freezing, which decreased EV concentration. Interestingly, when the same samples were analysed with the np200, samples that were filtered before freezing showed a reduced concentration compared to freshly filtered EVs whilst EVs frozen and then filtered showed a large increase in concentration. One possible reason for this is that freeze-thawing of samples may cause damage and degradation of EVs. Therefore EVs filtered after freezing may appear to have a reduced concentration with an np400 but increased concentration with an np200 because larger particles present at the time of freezing disintegrated into smaller particles measured by the np200 but not the np400. Though filtering may well reduce the presence of large particulate contaminants, using TRPS alone we cannot be sure that EVs are not also removed by filtration. Future studies could assess this by monitoring changes in EV markers such as CD9 with filtration and visually check sample preparations with TEM.

As EVs have the potential to be biomarkers for a number of diseases, it may become important for EV samples to be analysed in large scale studies where it would be impractical to analyse samples fresh. Previous studies have analysed the effects of storage on EV counts using FC with conflicting results (60,107,108,146,409,431). Therefore EV samples were stored using a variety of different methods and varying lengths of time to assess the effects on EV size and concentration. The method of storage used was not shown to have a significant effect on EV concentration or size, though all methods (apart from storing EVs in the fridge) seemed to increase EV concentration and decrease EV size compared with fresh EVs. Biological variation was high among volunteers so greater numbers may be required to further analyse the method of storage. However, others have also shown that the method of

cryopreservation had no effect on EV counts (432) or morphology (148). EV concentration was increased with the length of storage, independently of the method of storage used. After 3 months of storage, EVs were significantly increased compared to their original fresh samples. These effects may have been apparent after 1 month of storage though this did not reach significance. There was also a decline in mode size, however this was not significant. Freezing by any method may cause an increase in EV concentration which becomes a significant problem the longer the sample is stored for. This increase may arise from fragmentation of EVs by the freeze-thaw process which is then measured as an overall rise in concentration. Others observing a rise in EV concentration with freezing have also attributed this to vesiculation from larger EVs and contaminants (146,409). Indeed, this may explain why some studies using FC observed a decrease in EV concentration with freezing (60,107,409) as larger EVs (>300 nm) normally detected by flow fragment and pass below the detection limit of the machine. Despite the reduced sensitivity of FC for particles <300 nm, reduced forward and side scatter profiles have been observed following freezing which was attributed to an increase in smaller EVs (409,431). Furthermore, flow cytometric studies (despite conflicting results of overall EV concentration), show increases in annexin V positivity and specific surface markers with freezing (59,60,107,409) with one study showing platelet-derived EVs to be more procoagulant following freezing (145). Effects on other EV components with freezing are not well characterised, though mRNA was reduced in EVs following freezing (148). Until the full effects of storage method and length are characterised for all aspects of EVs, measurements of EVs should be carried out fresh wherever possible or stored in the fridge and analysed within 1 week. It is important to keep methods the same between samples to allow for accurate comparison.

3.4.3 Limitations

Comparisons of DLS and FC with NTA and TRPS were only undertaken once for polydispersity measurements. Though our group have access to NTA and TRPS, we did not at the time have liberal access to DLS or FC. Therefore we were not able to make a complete methodological comparison of all 4 techniques here and relied on published data for comparisons of DLS and FC for reliability and limits of detection.

The effects of filtering EVs were only measured once using TRPS with 3 different pores. Therefore without repeating the study, the interpretations presented here are only speculations and require confirmation with repeated numbers. Finally, concentration measurements using TRPS were made using a one-point calibration (as advised by IZON at the time) where calibration beads were analysed once at one pressure (which was then maintained for samples). IZON have since updated their recommendations for concentration measurements to include a 3-point calibration where the calibration bead and subsequent samples are analysed at 3 different pressures (**Figure 3.4.2**). Particle concentration is now defined as being "proportional to the gradient of the fitted line" (IZON training module, version 3.2) as opposed to "calibration allows the particle rate to be used to determine the particle concentration of the sample" (IZON training module, version 2.0). This may help to account for differences observed in concentration of beads between pores if the incorrect gradient was applied.

Particle concentration is proportional to the **gradient** of the fitted lines in Figure 2c.

$$Sample\ Conc = \frac{Sample\ Gradient}{Cal\ Gradient} \times Cal\ Conc$$

If concentration is calculated at a single pressure the software will calculate a gradient based on the fitted line passing through the origin. This can introduce significant errors, especially with smaller nanopores (NP200 and below) where a large proportion of particles are driven through the nanopore due to applied voltage V.

Page | 17

Figure 3.4.2: Revision of TRPS concentration analysis. Screenshots from the latest Izon training manual that explain how calibration beads are used to calculate sample concentration. The graph shows the importance of the relationship between applied pressure and particle rate between calibration beads and samples. The manual also indicates the negatives of using single-point calibration.

3.4.4 Conclusions

The EV field as a whole is undergoing continuous development with a wide array of measurement, isolation and storage protocols being used. It may be impossible to completely standardise procedures due to the great variety of biological sources from which EVs can be derived. Here, TRPS and NTA were shown to be reliable techniques for measuring size and concentration of EV samples. However, knowledge of the theory of operation and training is required for each technique to avoid misuse and false reporting of EV size and concentration. FC is not suitable for determining EV size and concentration; however it is currently the simplest method for phenotyping surface antigens of EVs. Pre-analytical variables such as the choice of vacutainer, filtering and storage all affected EV concentration. Until some level of standardisation is introduced, it is imperative for researchers to understand the limitations and to report results of their chosen methodologies with complete clarity.

4. Results II:

Characterisation of adipocyte-derived EVs

4. Perspective

Having learnt about the variety of potential pitfalls with EV analysis from work presented in *Chapter 3*, I was able to implement this knowledge in work conducted in Chapter 4. For example, when EVs could not be analysed on the same day as isolation, they were slow frozen to -80°C in a Mr Frosty and stored for a maximum of 1 week to minimise the damaging effects of freezing. Also, NTA was chosen to size and quantitate EVs primarily because of its ease of use compared to TRPS. Multiple samples can quickly and easily be analysed in replicates with NTA, often meaning analysis can be performed on the same day as isolation of EVs.

Parts of this chapter have been published in:

Connolly KD, Guschina IA, Yeung V et al. Characterisation of adipocyte-derived extracellular vesicles pre- and post-adipogenesis. *Journal of Extracellular Vesicles*. 2015 Nov 24; 4: 29159.

4.1 Introduction

As discussed in Chapter 1, many different cell types secrete EVs into their extracellular space. The release of EVs from adipocytes is an emerging area in the EV field. The traditional view of AT as an inert storage organ has changed dramatically over recent years with the discovery of adipokines, revealing an endocrine role for adipocytes (433,434). Therefore, adipocyte EVs may provide a new dimension to adipocytes as endocrine communicators.

The unipotent preadipocyte cell line 3T3-L1 is widely used to study adipocyte biology both at the pre- and mature adipocyte stage (294). The differentiation process of 3T3-L1 cells undergoes well defined stages of confluency and mitosis of preadipocytes followed by a growth arrest and commitment to a mature adipocyte phenotype (435). During this period, activation of various transcription factors trigger a variety of signalling pathways, inducing multiple changes in mRNA and protein expression (274). This tightly orchestrated process controls the transition of a fibroblast-like preadipocyte to a fully mature, rounded adipocyte capable of accumulating lipid (**Figure 1.1.2**). Previous research has focused on the intracellular role of transcription factors in adipocyte differentiation though there is evidence for external mediators in assisting the differentiation process (301). Adipocytes, including 3T3-L1 cells, have been shown to produce EVs *in vitro* (48,66,306,307,383,392,393). 3T3-L1 EVs contain both adipokines (66,383) and factors that promote angiogenesis *in vivo* (393). EVs derived from rat primary adipocytes act in an autocrine fashion to promote lipid esterification in neighbouring adipocytes (387). Human AT explants also produce EVs that modulate monocyte differentiation and alter insulin signalling in adipocytes (306) and hepatocytes (307). However, these studies have focused on potential functional aspects of adipocyte-derived EVs without having first established the baseline characteristics of these EVs and how these characteristics may dictate EV function. Furthermore, these studies did not quantify adipocyte EVs by any means, or used sub-optimal techniques such as FC.

Despite the growing evidence for roles of adipocyte EVs in autocrine and endocrine functions, little is known about the physiological characteristics of adipocyte EVs and whether these change (as the cell does) following adipogenesis.

4.1.1 Aims

The aims of this chapter were to characterise adipocyte-derived EVs in terms of:

- Morphology
- Size and concentration
- Annexin V positivity
- Fatty acid concentration and composition
- Phospholipid composition (and fatty acid composition)
- Protein content

This chapter aims to establish these parameters of the 3T3-L1 EVs, comparing them to their cell of origin and assessing the effect of adipogenesis on EV characteristics.

4.1.2 Hypotheses

EV release and character differs depending on the stage of differentiation. EVs share some characteristics of their cell of origin but may possess their own unique fatty acids and proteins.

4.2 Methods

4.2.1 Cell culture

3T3-L1 cells were cultured as outlined in *Chapter 2.2*. Post-confluence, serum-free CM was added to cells for 24 hours for subsequent EV isolation (day 0). Cells to be analysed at day 15 were differentiated (as outlined in **Figure 2.1**) and were placed in serum-free MM for 24 hours for EV isolation at day 15. Oil Red O staining was used to confirm the stage of adipogenesis of cells (methods detailed in *Chapter 2.2.3*).

4.2.2 Western blotting

Cell and EV lysates were prepared for Western blotting as described in *Chapter 2.10*. Ten micrograms of protein was loaded for each sample, separated on running gels and probed for antigens of interest (**Table 4.2.1**). Loading controls were not used for cell lysates; however, FABP4 and PREF-1 blots of EV samples were washed in TBS-T overnight, blocked and re-probed with CD63. Densitometry was conducted as described in *Chapter 2.10.6*.

Protein	Polyacrylamide running gel	Antibody dilution	Typical exposure
Adiponectin (CST #2789)	12%	1:500 (5% BSA/TBS-T)	15 minutes
CD63	n/a	1:200 (5% milk/TBS-T)	1 minute
FABP4	15%	1:100 (5% BSA/TBS-T)	15 seconds
PREF-1	10%	1:100 (5% BSA/TBS-T)	1 minute

Table 4.2.1: Western blotting. Details of the proteins analysed by Western blotting and the acrylamide gels used to separate them. CD63 was used a control for EV proteins so an acrylamide percentage is not provided. BSA = bovine serum albumin; CD = cluster of differentiation; CST = Cell Signaling Technologies; FABP4 = fatty acid binding protein-4; PREF-1 = preadipocyte factor-1; TBS-T = tris-buffered saline – tween 20 (1% v/v).

4.2.3 Extracellular vesicle isolation

After 24 hours in serum-free media, conditioned supernatants were immediately centrifuged and stored as described in *Chapter 2.3.1* and *2.3.3* respectively.

4.2.4 Scanning electron microscopy

EM was performed with Dr Christopher Von Ruhland (Central Biotechnology Services, Cardiff University). Scanning EM (SEM) was used to visualise cells at day 0 and day 15. Cells were cultured in 35 mm glass-bottomed dishes (Cellvis, USA). At day 0 and day 15, cells were washed in PBS and fixed in 1% gluteraldehyde (v/v in PBS) at room temperature for 1 hour. Fixed cells were kept in PBS at 4ºC until processing for SEM. Samples were then dehydrated through graded propan-1-ol (50, 70, 90% and 2x100%) for 10 minutes at each grade followed by three exchanges in hexamethyldisilazane (5 minutes per exchange). Samples were air dried and splutter coated with gold and viewed at 5 kV in a JOEL 840 SEM (JEOL, Japan). Images were acquired with analysis software (Munster, Germany) and processed with Photoshop CS2 (Adobe, USA).

4.2.5 Transmission electron microscopy

TEM was used to visualise EVs at day 0 and day 15. EVs were isolated from cells grown in T175 cm^2 flasks to ensure enough EV material for the TEM process and stored at 4ºC in PBS until analysis. EVs (50 µL droplets) were adsorbed onto formvar/carbon-coated grids for 20 minutes before fixation with 1% gluteraldehyde (v/v) for 10 minutes at room temperature. Grids were then washed (3 x 1 minute in PBS and 6 x 1 minute in water) before negative staining with 2% (w/v) uranyl acetate for 10 minutes. Surplus stain was shaken off and grids were allowed to air dry before being examined in a Philips CM12 TEM (FEI Ltd, UK) at 80 kV. Images were acquired with a Megaview III camera and processed using Photoshop CS2.

4.2.6 Optiprep™ separation of EVs

Optiprep™ (60% w/v solution of Iodixanol in water, Sigma) was used to prepare 10 fractions in 5% increments from 5-50% in PBS (v/v). Fractions (1 mL) were then carefully layered in ultracentrifuge tubes in a discontinuous gradient and EV samples from day 0 or day 15 (100 μL) were added to the top-most fraction (**Figure 4.2.1**). Centrifugation was then performed at 100,000 x *g* for 3 hours at 4ºC and 1 mL fractions were carefully removed and analysed using NTA (*Chapter 2.4.2*).
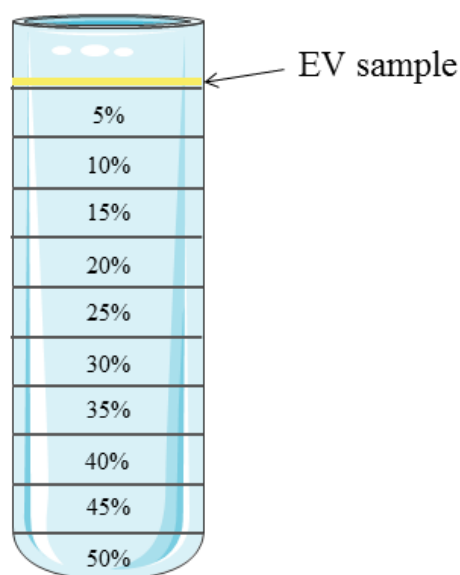
Figure 4.2.1: Optiprep™ separation of EVs. Ten fractions (1 mL) of prepared Optiprep™ solution were layered into ultracentrifuge tubes as shown above. EV samples (100 μL) from day 0 or day 15 were gently floated on the top fraction before ultracentrifugation.

4.2.7 Extracellular vesicle size and concentration analysis

EV size, mean concentration and distributions were determined using NTA as detailed in *Chapter 2.4.2*. Cells to yield EVs were cultured using T175 cm^2 flasks (Cellstar®, Greiner Bio-One, Germany).

4.2.8 Annexin V positivity

Annexin V positivity of cells and their corresponding EVs at both day 0 and day 15 was measured by FC (*Chapter 2.6*). Results are displayed as the percentage of annexin V positive events from the total population of cells or EVs.

4.2.9 Fatty acid analysis

GC-FID was used to determine fatty acid concentration and composition of cells and EVs at day 0 and day 15 (*Chapter 2.7.1/2*). Cells and EVs were isolated from T175 cm^2 flasks. Individual fatty acid data are presented as the change in composition from day 0 to day 15.

4.2.10 Phospholipid analysis

Proportions and fatty acid compositions of phospholipid groups of cells and EVs at day 0 and day 15 were determined by 2D-TLC followed by GC-FID (*Chapter 2.7.3*).

4.2.11 Extracellular vesicle immunophenotyping

EVs at day 0 and day 15 were probed for exosomal and adipocyte markers using an immunophenotyping assay described in *Chapter 2.9*. Details of EV (lightly shaded) and adipocyte (darker shaded) primary antibodies used are provided in **Table 4.2.2**. EV markers were chosen based on the ISEV minimal requirements for an EV population (**Table 1.1.2**) and adipocyte markers were selected to cover proteins expressed during different stages of adipogenesis (**Figure 1.2.2**).

Antibody	Dilution
Alix	1:450
CD9	1:200
CD63	1:200
TSG101	1:200
PREF-1	1:50
PPARγ	1:49
Adiponectin (CST #2789)	1:10
FABP4	1:25

Table 4.2.2 Antibodies used for EV immunophenotyping. Details of primary antibodies used for EV immunophenotyping experiments. One µg/mL of each antibody was added to each well, accounting for the differences in dilution. CD = cluster of differentiation; CST = Cell Signaling Technologies; FABP4 = fatty acid binding protein-4; PPARγ = peroxisome proliferator-activated receptor γ; PREF-1 = preadipocyte factor-1; TSG101 = tumour susceptibility gene -101.

4.2.12 Statistical analysis

Data were analysed using GraphPad Prism (version 6.0). Normality was tested using D'Agostino and Pearson omnibus normality test before subjection to statistical analysis. An unpaired student's *t-test* or a one- or two-way ANOVA were used to analyse the differences between means. Data are presented as mean $\pm$ SD and p values <0.05 were considered statistically significant.

4.3 Results

4.3.1 Confirmation of adipogenesis

Oil red O staining was used for semi-quantitative analysis of lipid accumulation in cells at day 0 and day 15 (**Figure 4.3.1**). Lipid accumulation was greatly increased with differentiation, as illustrated by microscopy (**Figure 4.3.1 A/B**) and by absorbance (**Figure 4.3.1 C**).
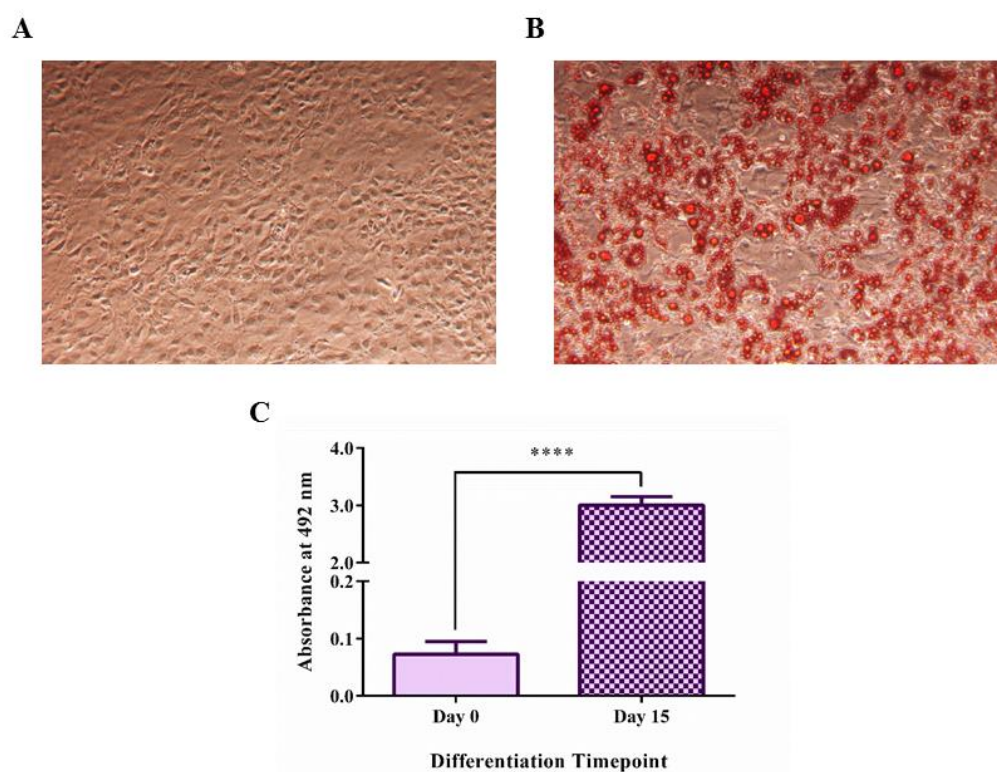
Figure 4.3.1 Confirmation of adipogenesis. 3T3-L1 cells at day 0 and day 15 were stained with oil red O to confirm the stage of adipogenesis. Degree of staining was analysed visually by microscopy: (**A**) day 0 cells and (**B**) day 15 cells; and by measuring the absorbance at 492 nm (**C**). ****$p<0.0001$, (n=4).

Adipogenesis was further confirmed by Western blot analysis of cell lysates from both timepoints (**Figure 4.3.2**). PREF-1 was significantly higher in day 0 cell lysates compared with day 15 (day 0: $57,801 \pm 6,743$; day 15: 572 ± 784 raw densitometry units, $p = 0.0054$; **Figure 4.3.2 A**). Both adiponectin and FABP4 were higher in day 15 cell lysates compared to day 0 (adiponectin: day 0; 729 ± 824, day 15; $14,371 \pm$

2,849 raw densitometry units, $p = 0.0076$, **Figure 4.3.2 B**; FABP4: day 0; 1,547 ± 2,629, day 15; 88,112 ± 6,688 raw densitometry units, $p = 0.0014$, **Figure 4.3.2 C**).
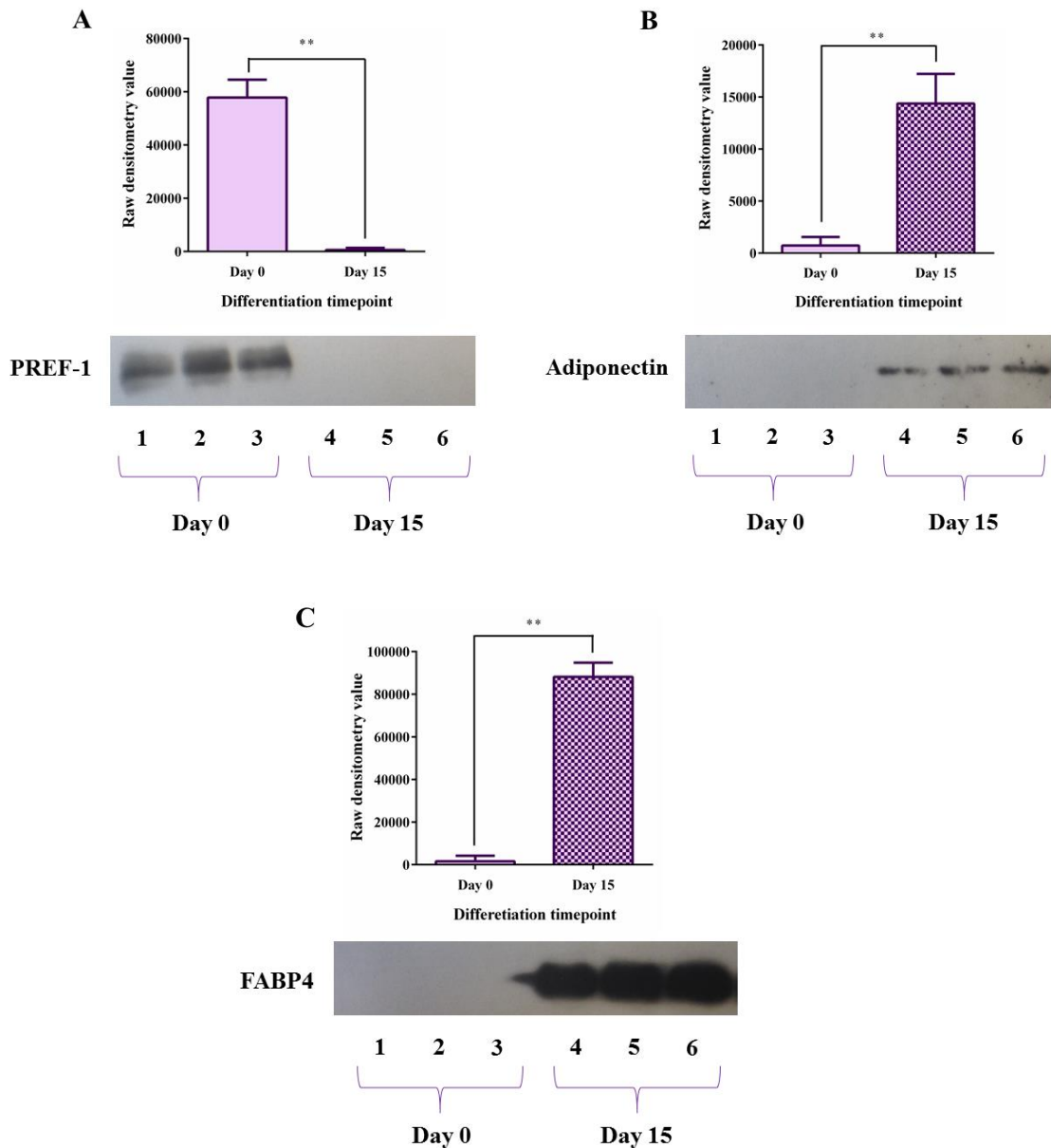
Figure 4.3.2: Western blot analysis of cell lysates. Western blots of day 0 and day 15 cell lysates were probed for the preadipocyte marker, PREF-1 (**A**), and mature adipocyte markers adiponectin (**B**) and FABP4 (**C**). Raw differences in densitometry are shown for each protein. **$p<0.01$, (n=3). Western blots were performed without loading controls; therefore conclusions should not be drawn between differences in band density between markers.

4.3.2 Electron microscopy

EM was used to visualise 3T3-L1 cells and EVs at both time points. SEM images show cells at day 0 are connected by long projecting networks that connect multiple cells (**Figure 4.3.3 A**). Preadipocytes also seem to be quite flat with little evidence of lipid accumulation. Cells at day 15 however, have a rounder morphology and are much larger in diameter (**Figure 4.3.3 B**). Mature adipocytes appear more individualised and spherical with large vacuole-like structures.

TEM images show that EVs at both time points are polydispersed in nature and display a classic "cup-like" morphology (**Figure 4.3.3 C/D**).
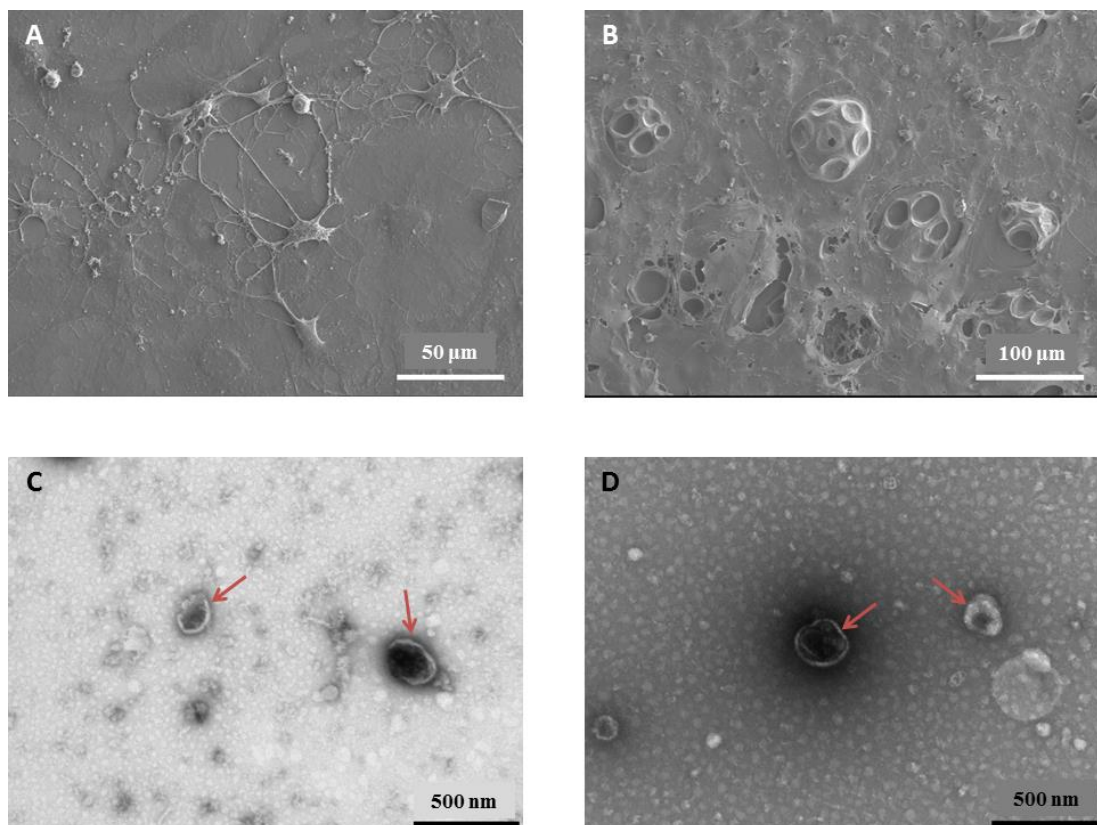
Figure 4.3.3: 3T3-L1 cells and EVs viewed by EM at day 0 and day 15. Cells pre- (**A** - day 0) and post-adipogenesis (**B** - day 15) were visualised using SEM. Isolated 3T3-L1 EVs at day 0 (**C**) and day 15 (**D**) indicated by red arrows were imaged using TEM. Note the differences in scale bars between preadipocytes and mature adipocytes and between cells and EVs.

4.3.3 Optiprep™ separation of extracellular vesicles

Optiprep™ was used to examine any differences in buoyancy of EV isolates from day 0 and day 15. EVs from both day 0 and day 15 have a range of buoyant densities, however a greater proportion of EVs from day 15 were present in the lower density fractions compared to EVs from day 0 (**Figure 4.3.4**).
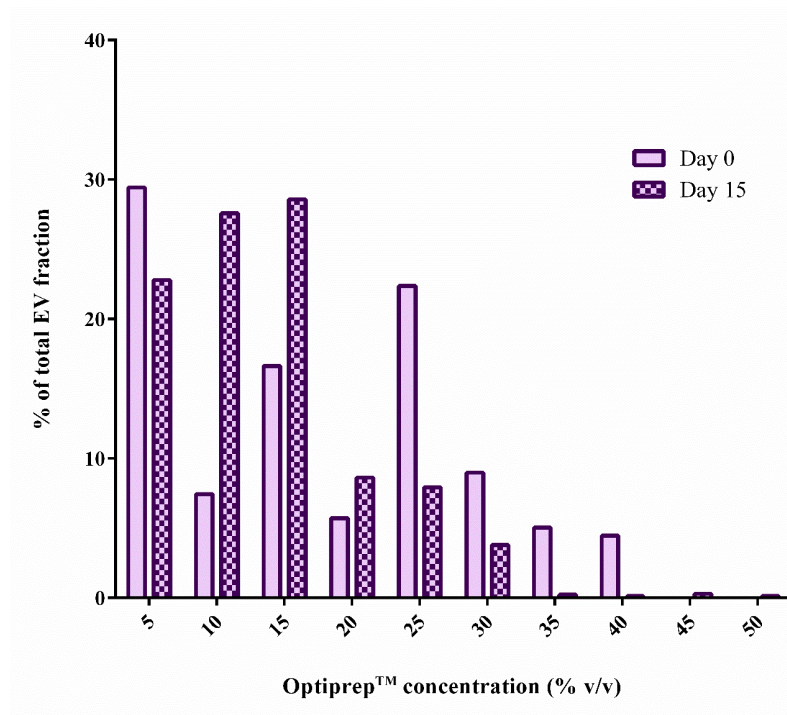
Figure 4.3.4: Optiprep™ separation of EVs. EVs from both day 0 and day 15 were added to a discontinuous gradient of Optiprep™ solution. Each fraction was then analysed using NTA. Data are expressed as the percentage of the total EV sample present in each fraction at each time point (n=1).

4.3.4 Extracellular vesicle size and concentration

The number of viable cells was measured using trypan blue exclusion and showed an increase of ~3 fold from day 0 to day 15 ($1.7 \times 10^6 \pm 5.1 \times 10^5$ to $5.2 \times 10^6 \pm 8.4 \times 10^5$ cells/mL, $p<0.0001$, **Figure 4.3.5 A**). NTA was used for size and concentration analysis of EVs. EV production was higher per cell at day 0 compared with day 15 (992.7 ± 226.2 to 276.5 ± 104.8 EVs/viable cell, $p<0.0001$, **Figure 4.3.5 B**). Mode size of EVs did not change between the two time points (135.4 ± 8.9 to 137.1 ± 7.6 nm, $p = 0.6$,). When the concentration was split into 50 nm bin-widths, the decrease in EVs at day 15 was observed across the EV spectrum, particularly in EVs <300 nm (**Figure 4.3.5 C**).
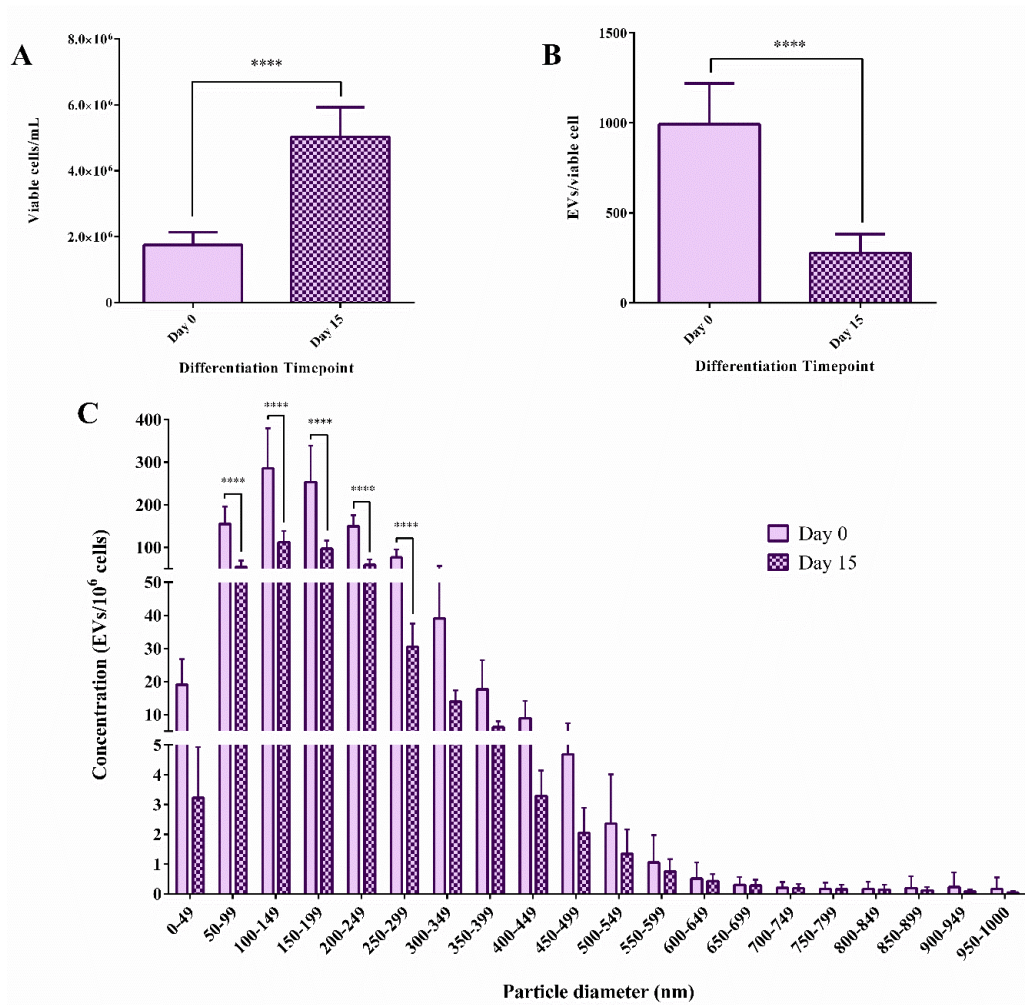
Figure 4.3.5: 3T3-L1 EV size and concentration. The effect of differentiation of 3T3-L1 cells on: (**A**) viable cells/mL; (**B**) EV production per viable cell; and (**C**) EV size and concentration distribution. **** $p<0.0001$, *** $p<0.001$, *** $p<0.01$, day 0 (n=6) and day 15 (n=5).

4.3.5 Annexin V positivity

PS exposure of cells and EVs was determined by annexin V binding measured by FC. Annexin V positivity of cells fell from day 0 to day 15 (2.1 ± 1.7 to $0.4 \pm 0.2\%$, $p=0.04$, **Figure 4.3.6 A**). The same trend was observed with EVs however this was non-significant (6.3 ± 6.6 to $2.9 \pm 2.2\%$, $p = 0.3$, **Figure 4.3.6 B**). Generally, EVs possessed a higher annexin V positivity than that of cells.
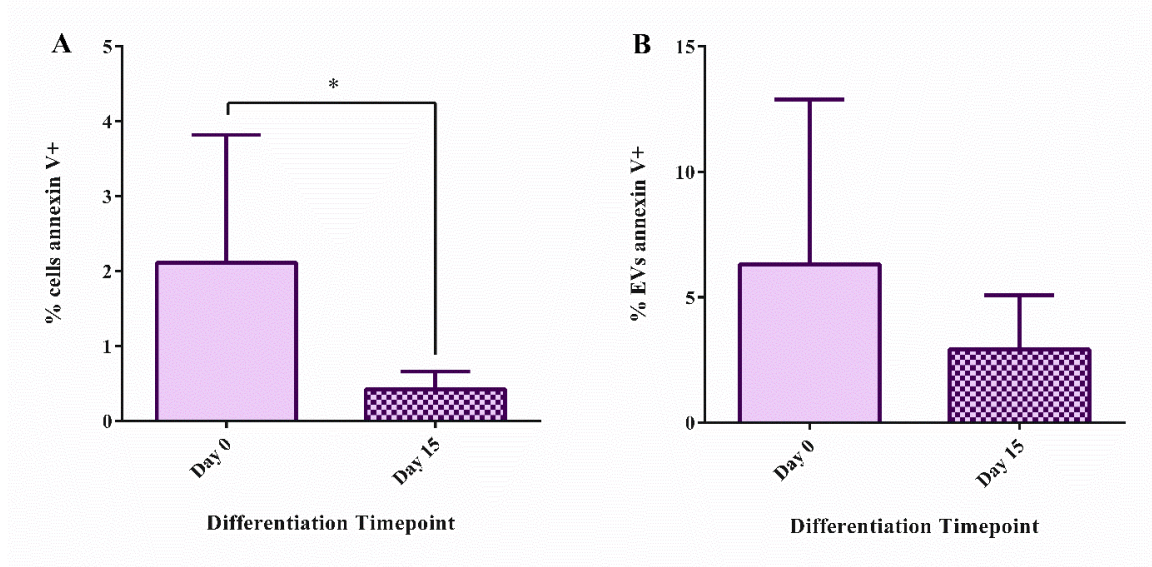
Figure 4.3.6: Annexin V positivity of 3T3-L1 cells and EVs. Changes in phosphatidylserine exposure of 3T3-L1 cells (**A**) and EVs (**B**) with differentiation were measured by annexin V binding. *$p<0.05$, (n=6).

4.3.6 Fatty acid concentration and composition

GC-FID was used to determine the concentration and composition of fatty acids of cells and EVs. Total concentration of fatty acids in both cells and EVs was increased from day 0 to day 15 (Cells: 0.1 ± 0.04 to 0.7 ± 0.2 mg/10^6 cells, $p<0.0001$, **Figure 4.3.7 A** and EVs: 12.2 ± 1.7 to 27.3 ± 10.1 ng/10^6 EVs, $p=0.005$, **Figure 4.3.7 C**). The fatty acid compositions of both cells and EVs were greatly altered by differentiation. Out of 25 fatty acids detected, the compositions of 18 in cells and 17 in EVs changed significantly from day 0 to day 15 (**Figure 4.3.7 B** and **D** respectively).
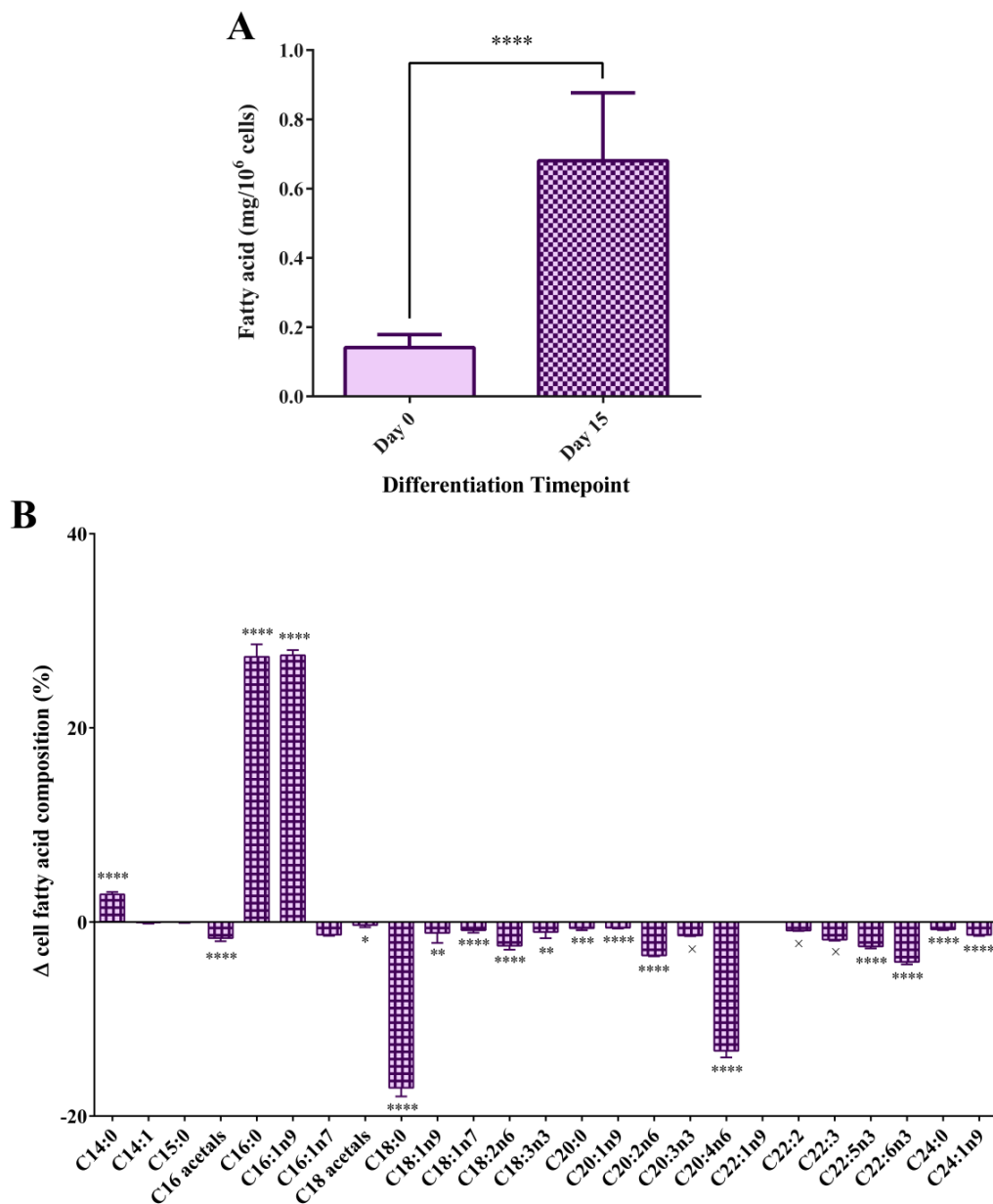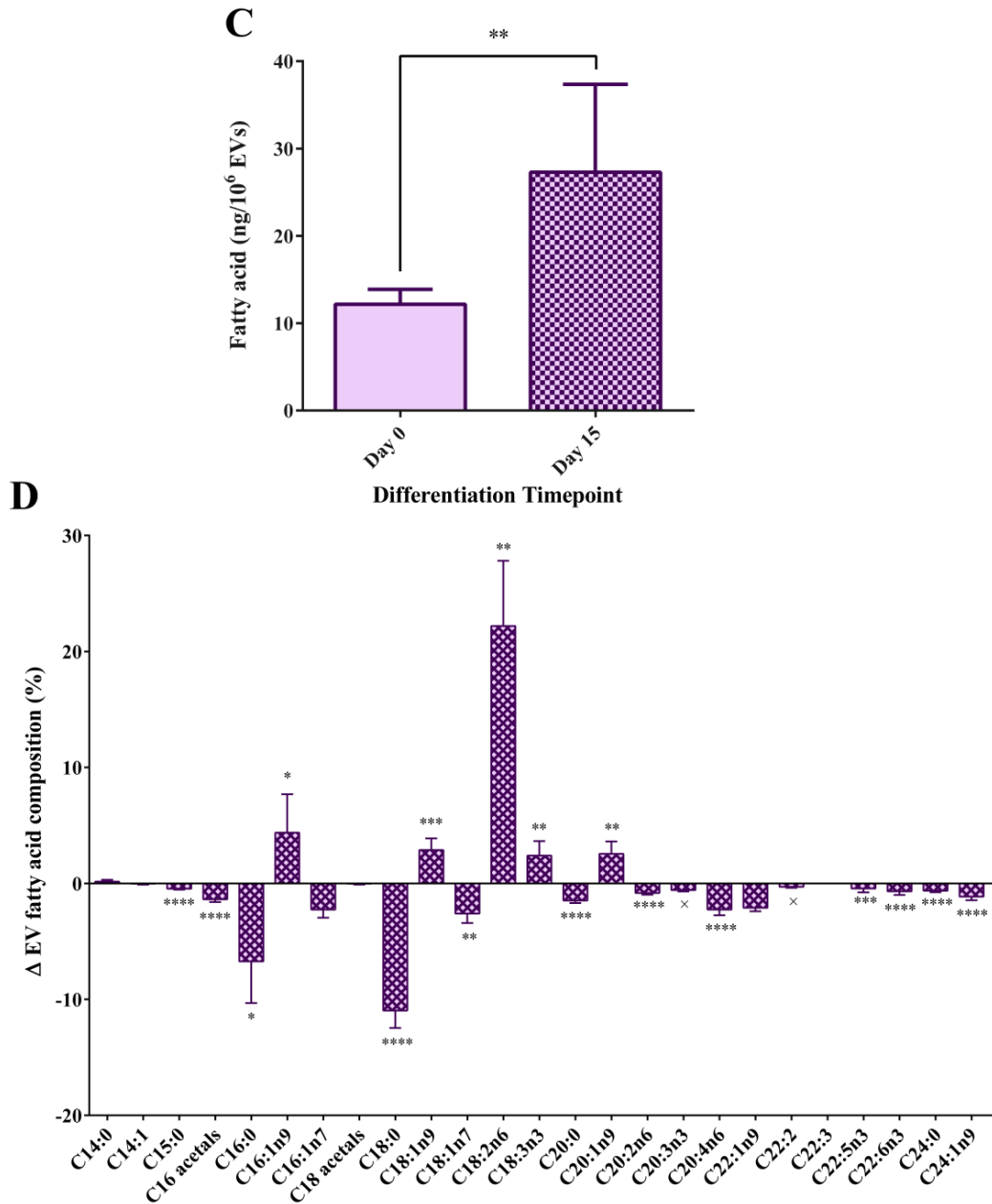
Figure 4.3.7: Fatty acid analysis of 3T3-L1 cells and EVs. (**A**) Total fatty acid concentration of 3T3-L1 cells and (**C**) EVs at day 0 and day 15 of differentiation. (**B**) Proportional changes of individual fatty acids in cells and (**D**) EVs between day 0 and day 15 of differentiation. **** $p<0.0001$, ***$p<0.001$, **$p<0.01$, *$p<0.05$, [x] indicates a fatty acid present at only one time point, day 0 (n=6) and day 15 (n=5).

The majority of fatty acids were reduced (in proportion to the total) with differentiation in cells and EVs, for example, arachidonic acid (C20:4n6). Generally, differentiation caused the same trends in proportional changes of fatty acids; however the effect was sometimes unique to the cell or EV. For example, oleic acid (C18:1n9) was decreased in cells but increased in EVs from day 0 to day 15. Certain fatty acids were also unique to the stage of differentiation, for example, eicosatrienoic acid (C20:3n3) was only present in cells and EVs at day 0.

The composition of lipid classes was also altered with adipogenesis, and when comparing the EV to its corresponding cell (**Figure 4.3.8**). EVs in particular seemed to contain a higher proportion of polyunsaturated fatty acids (PUFAs) compared to cells. Individual changes in fatty acids within each class are provided in **Appendix: Table I**.
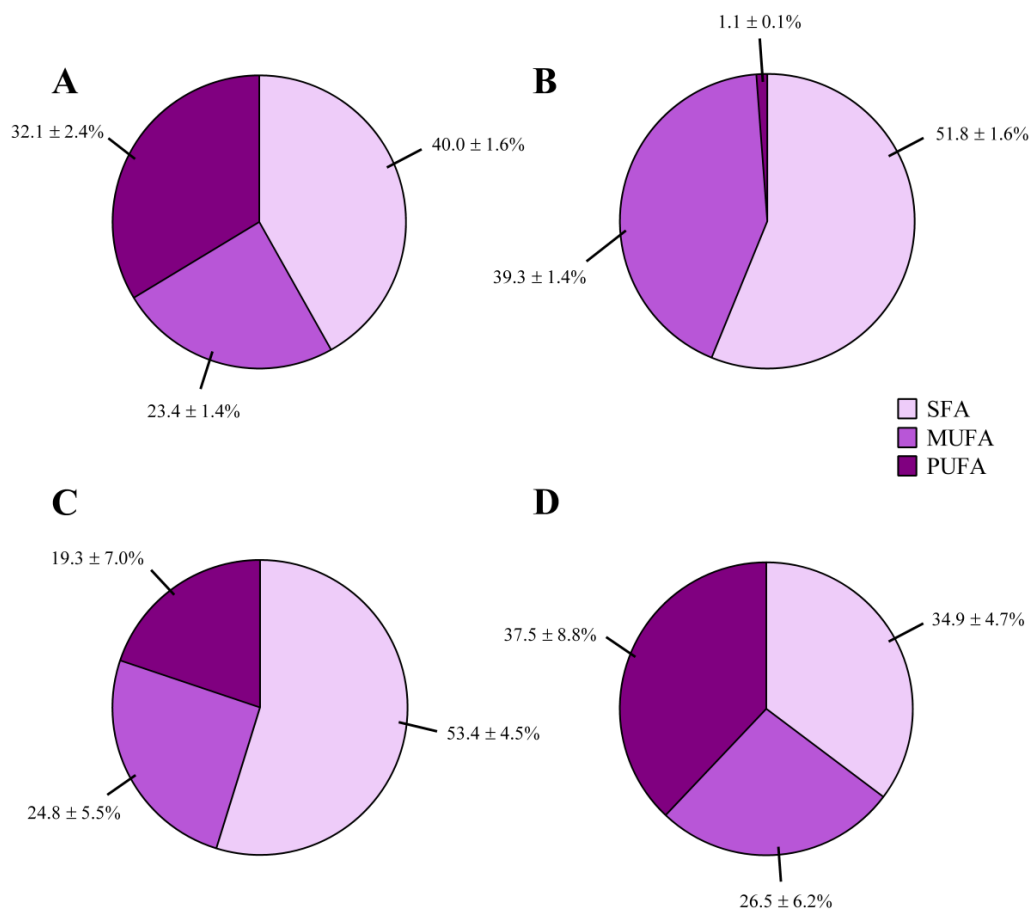
Figure 4.3.8: Changes in lipid classes. Alterations in lipid classes between (**A**) day 0 cells, (**B**) day 15 cells, (**C**) day 0 EVs and (**D**) day 15 EVs. SFA = saturated fatty acids, MUFA = monounsaturated fatty acids; PUFA = polyunsaturated fatty acids, day 0 (n=6) and day 15 (n=5).

4.3.7 Phospholipid analysis

Phospholipids were separated from lipid extracts using 2D-TLC. The proportions (percentage of total) of each phospholipid class present in cells and EVs pre- and post-adipogenesis are presented in **Figure 4.3.9**. Between day 0 and day 15, the proportion of phosphatidylethanolamine (PE) increased in cells and EVs whereas the proportions of phosphatidylinositol (PI) and sphingomyelin decreased in cells but increased in EVs. Phosphatidylcholine (PC) was the most abundant phospholipid present in all samples (45.0 – 62.3%), slightly increasing in cells following adipogenesis but decreasing in EVs over the same time. Cells and EVs had higher proportions of PS at day 0. Cardiolipin was detectable only in cells, increasing with adipogenesis.
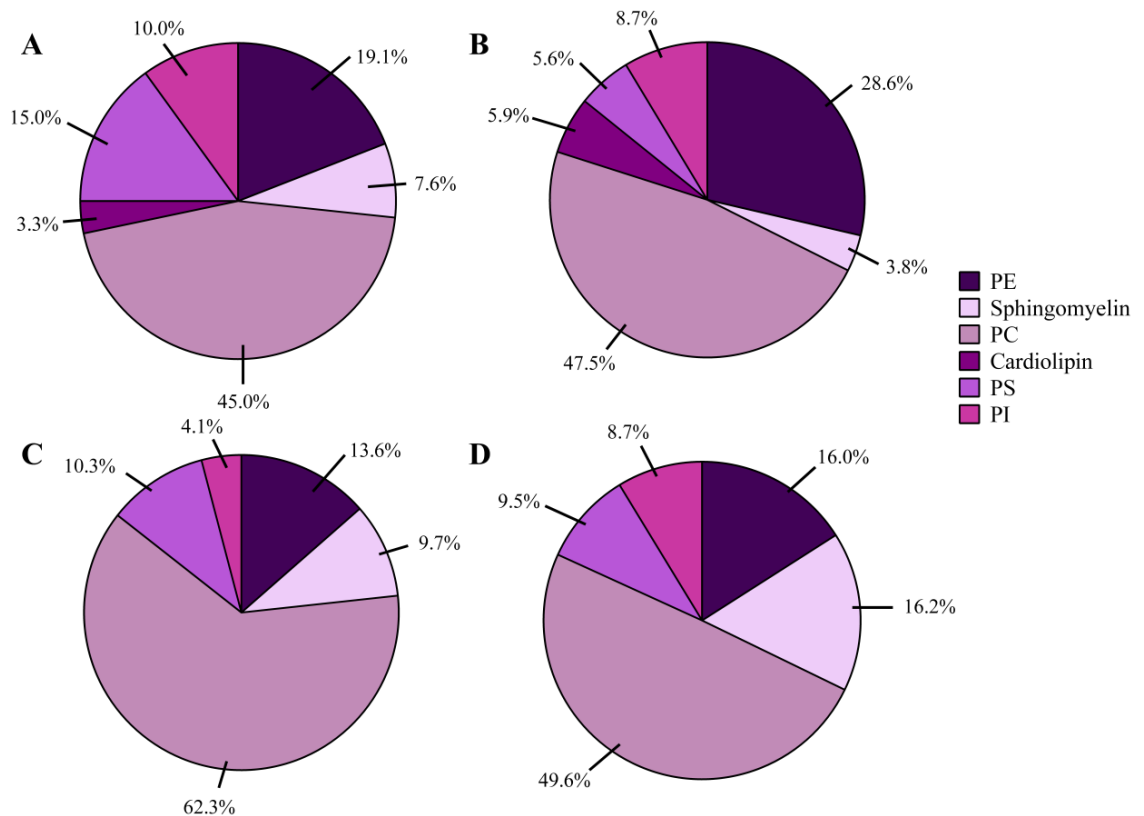
Figure 4.3.9: Phospholipid composition pre- and post-adipogenesis. Proportions of individual phospholipids present in cells and EVs pre- and post-adipogenesis. Proportions were calculated as a percentage of the summed total of all phospholipids. (**A**) day 0 cells; (**B**) day 15 cells; (**C**) day 0 EVs; (**D**) day 15 EVs (n=1). PE = phosphatidylethanolamine; PC = phosphatidylcholine; PS = phosphatidylserine; PI = phosphatidylinositol.

Phospholipid extracts were also analysed by GC to give individual fatty acid compositions of each phospholipid (**Appendix: Table II**). Phospholipids contained a range of saturated fatty acids (SFAs), mono unsaturated fatty acids (MUFAs) and PUFAs in cells and EVs at both time points, and these seemed to differ both with differentiation and between cells and EVs. In particular, phospholipids from day 0 cells and EVs were highly enriched in PUFAs, specifically arachidonic acid which decreased following adipogenesis.

4.3.8 Immunophenotyping of extracellular vesicles

An immunophenotyping assay was used to measure the content of vesicular and adipocyte proteins within EVs at each time point (**Figure 4.3.10**). No differences were observed in exosomal markers pre- and post adipogenesis. Of the adipocyte markers, PPARγ showed no change. However, adiponectin showed an increase pre- to post-adipogenesis ($76,242 \pm 11,501$ to $161,886 \pm 30,371$ arbitrary TRF units, $p<0.0001$). Both FABP4 and PREF-1 were shown to decrease in EVs following adipogenesis ($108,256 \pm 7,640$ to $93,088 \pm 4,804$, $p = 0.002$ for FABP4 and $86,958 \pm 18,164$ to $58,918 \pm 7,485$ arbitrary TRF units, $p = 0.006$ for PREF-1 respectively).
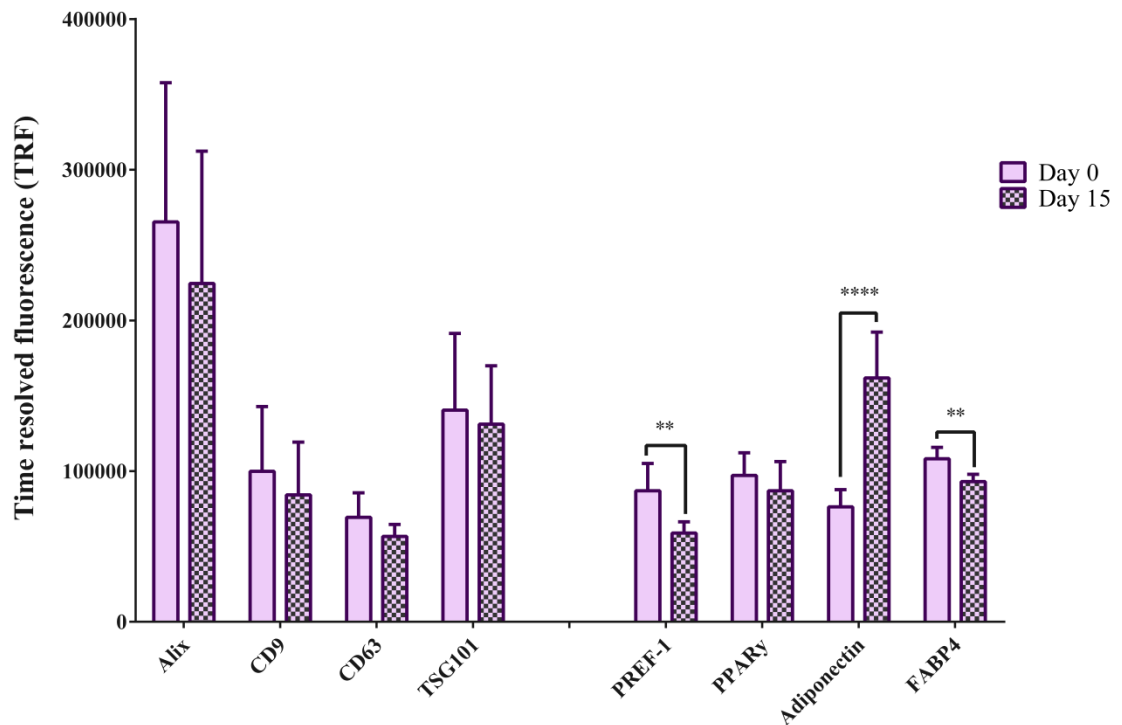
Figure 4.3.10: Protein content of EVs pre- and post-adipogenesis. Exosomal (CD9, CD63, TSG101 and alix) and adipocyte (FABP4, PREF-1, adiponectin and PPARγ) proteins in EVs from day 0 and day15 cells were analysed by an immunophenotyping assay. Proteins were detected using a streptavidin-europium conjugate and measured using TRF (given in arbitrary units). **$p<0.01$, ****$p<0.0001$, (n=3).

4.3.9 Retrospective Western blot analysis

Following analysis of data from the immunophenotyping of EVs using EV immunophenotyping, Western blots were performed for day 0 and day 15 EVs probing for PREF-1 and FABP4 (**Figure 4.3.11**). Western blots showed that in fact, PREF-1 was barely detectable at day 15 and FABP4 was highly abundant at day 15. This contradicts data from **Figure 4.3.10** which shows a modest, but significant decrease in PREF-1 and FABP4 from day 0 to day 15.
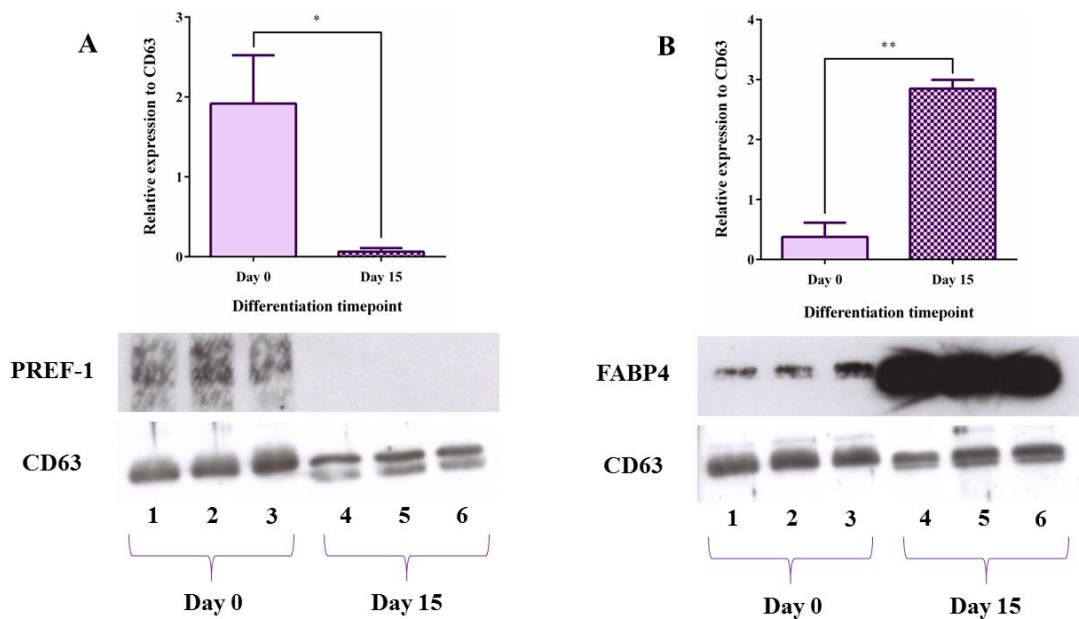
Figure 4.3.11: Western blot analysis of EV lysates. Lysed EVs were analysed for expression of the preadipocyte marker, PREF-1, the mature adipocyte marker, FABP4 and the exosomal protein, CD63. Densitometry was then performed and PREF-1 (**A**) and FABP4 (**B**) are presented as relative expression to CD63. *$p<0.05$, **$p<0.01$ (n=3).

4.4 Discussion

4.4.1 Key findings

1. EVs from 3T3-L1 adipocytes display a classic EV morphology.
2. EV release is higher prior to adipogenesis, particularly vesicles <300 nm.
3. Cellular and EV fatty acid composition is altered following adipogenesis.
4. EVs display a different fatty acid composition to that of their cells of origin.
5. Adipogenesis seems to alter phospholipid (and associated fatty acid) composition in EVs and cells.
6. EVs contain exosomal and adipocyte proteins, some of which are altered following adipogenesis.

4.4.2 Main discussion

From *Chapter 3*, it is clear that the EV field is still developing, requiring further clarity and standardisation. As such, a fundamental protocol was developed when our group began to study adipocyte-derived EVs. This method has been used throughout the thesis to ensure consistency, but these methods also addresses key elements outlined in the ISEV position paper (16). With the growing popularity of EV research, more and more cell types are being reported to release EVs, yet often little information is given concerning the characteristics of these vesicles. In this chapter, I sought to characterise EVs from pre- and mature adipocytes using the well-established 3T3-L1 adipocyte cell line.

Until relatively recently, AT was regarded as little more than a passive store of excess energy. It is now recognised as an endocrine organ that plays an influential role in many important physiological processes both within AT itself and systemically with other organs and tissues. These interactions are primarily orchestrated through the secretion of adipokines released directly from adipocytes (316). More recently, adipocytes have been shown to shed EVs *in vitro*, perhaps providing an additional method of adipocyte communication (66,306,307,383,387,393). However, little is known about the characteristics of these EVs.

Transition from a preadipocyte to a mature adipocyte phenotype is a complex process involving a chronological pattern of gene expression and changes in cell cycle status (294). At day 0, the cell-cell contact between preadipocytes is crucial in initiating differentiation (436) and intercellular communication is known to peak in preadipocytes at confluency then rapidly decline during differentiation (437). Consistent with this, SEM images of 3T3-L1 cells at day 0 show long projections suggesting networks of intercommunication between cells. Additionally, EV production per cell was greater at day 0, particularly in exosomes and smaller microvesicles (<300 nm) despite there being no change in the overall mode size of EVs. This may be a consequence (or perhaps a cause) of the differentiation process such that EVs act as intercellular communicators to aid initiation of the transition to a mature adipocyte. Conversely, cells at day 15 are much larger and rounder with multiple lipid vacuoles. Taken together with the lower EV production per cell, this suggests that cells at this time point may be less communicative.

Many studies support the principle that the release of EVs is preceded by a disruption of the normal phospholipid asymmetry of the plasma membrane, subsequently exposing PS. However, it is debated whether this externalised PS is retained on the EV (63,67). Therefore PS exposure of EVs and their original cells was characterised using annexin V binding. Cells and EVs at both time points showed a relatively low annexin V positivity (<10%); lower than the reported 50-90% reported for plasma-derived EVs (55,56,76). However, it is hypothesised that the majority of plasma-derived EVs are of platelet origin and that their high annexin V positivity - and hence high density PS exposure - can aid promotion of coagulation (438). It is unlikely that adipocyte-derived EVs would promote coagulation perhaps partially explaining their lower annexin V positivity.

Much of the research within the EV field is focused towards how changes in the quantity or genetic content of EVs may potentially affect their function. Little has been reported about the potential effects of lipid composition on EV function, despite the known role of lipids as precursors to many signalling pathways and their importance as signalling molecules in their own right. Therefore GC-FID was used

to comprehensively characterise the fatty acid composition of 3T3-L1 cells and EVs pre- and post-adipogenesis. As expected, the total lipid content of cells increased with adipogenesis and interestingly, this was also reflected in the EVs. Perhaps as the cells at day 15 are so lipid laden, the resulting EV incorporates some of this lipid during its formation. EVs at day 15 certainly seemed to have a lower overall density as shown by their Optiprep™ separation where the majority of EVs at this time point were found in the upper fractions containing the least Optiprep™ solution. This suggests these EVs are less dense, perhaps because they contain more lipid per volume.

The fatty acid composition of cells and EVs was clearly affected by differentiation, likely reflecting the transition in function from a preadipocyte to mature adipocyte. For instance, palmitic acid, the most abundant storage fatty acid in animals (439) showed a large increase with adipogenesis as cells accumulated lipid. The transition in function was also represented by the presence or lack of some fatty acids at each time point. For example, the PUFA eicosatrienoic acid is generally detected in tissues where levels of FFAs are low. Here, eicostrienoic acid was present at day 0 but not at day 15. Cells at day 15 are likely to be abundant in FFAs perhaps ameliorating the need for eicosatrienoic acid at this time point. Additionally it has been reported that PUFAs, particularly n-3 PUFAs, are better activators of PPARγ (upon which adipocyte differentiation is dependent) than other fatty acids (440). Here, cells at day 0 contained a greater proportion of PUFAs than cells at day 15 suggesting that preadipocytes are equipped with a greater reserve of PUFAs to aid PPARγ activation. Cells and EVs at day 0 also had a greater proportion of arachidonic acid - a major precursor for many signalling pathways - than those at day 15. Taken together with the increased concentration of EVs at day 0, this supports the notion that EVs may be enhancing intercellular communication in the initial stages of differentiation. In keeping with this, exosome isolates from human adipose-derived stem cells (hASCs) undergoing adipogenic differentiation were recently shown to assist the transition of undifferentiated hASCs towards a mature adipocyte phenotype (441).

As well as maintaining the structural integrity of cells, organelles and vesicles, phospholipids are also part of a variety of signalling pathways. The major phospholipid classes of 3T3-L1 cells and their corresponding EVs pre- and post-adipogenesis were separated by TLC before subsequent GC-FID to determine individual fatty acid composition of individual phospholipids. A common theme among the fatty acids within phospholipid groups was the high degree of saturation. The primary role of phospholipids is to form a bilayered membrane to support the structure of the cell and to enclose its contents. The predominance of SFA acid tails of phospholipids here likely provides enough rigidity to the cell membranes for structural support but the presence of MUFAs and PUFAs ensure enough fluidity remains for membrane components to remain dynamic.

PC and PE were the most abundant phospholipids in all samples, accounting for around half of all phospholipids measured. PC and PE have previously been shown to be the most abundant phospholipids in adipocytes (442) and in blood-derived microparticles (443); the data in this thesis suggests this is also the case for adipocyte-derived EVs. The proportion of PE in 3T3-L1 cells and EVs increased with differentiation, a concept previously reported in 3T3-L1 cells (444).

As observed with the total fatty acid composition of cells and EVs, arachidonic acid was more abundant in cells and EVs at day 0 within 4 of the 6 phospholipids analysed here. Arachidonic acid is a major precursor to many intracellular signalling molecules, principally eicosanoids (445). Therefore higher proportions of arachidonic acid at day 0 suggest both cells and EVs harbour a greater reserve of signalling fatty acids. The composition of PUFAs at day 0 was also much higher compared with day 15. PUFAs, as described before can act as ligands for PPARγ (445) which is essential to differentiation. Increased amounts of PUFAs at day 0 may help to initiate PPARγ activation to bring about differentiation and also illustrates the role of PE in cell signalling as well as membrane structure.

Sphingomyelin is often associated with brain tissues where this class of phospholipids coat axons to accelerate transmission of action potentials. However, sphingomyelin is also an important phospholipid in many eukaryotic plasma membranes providing structural support and sphingolipid signalling molecules such as ceramide which as described in *Chapter 1.1.3.1*, play a role in classical exosome

formation (25,446). Sphingomyelin has been shown to form a high content in EVs providing structural rigidity and resistance to physiochemical changes (169). Here, sphingomyelin was decreased in cells following adipogenesis, suggesting day 0 cells have a higher capacity for ceramide production and subsequent exosome formation. This is reflected in the EV concentration data, which shows a greater proportion of EVs in the exosomal range at day 0.

Cardiolipin was present in cells at both time points but was not detected in EVs. Cardiolipin is a major phospholipid of the mitochondrial membrane and is known to interact with and facilitate the actions of mitochondrial proteins such as cytochrome *c* (447). As well as mitochondrial proteins, cardiolipin is also known to interact with adipocyte cytosolic proteins such as FABP4, particularly when there is a greater degree of unsaturation (448). Here, the composition of cardiolipin was higher in day 15 cells and the level of unsaturation at this time point was also greater. Cellular FABP4 was increased at day 15 perhaps reflecting the increased need to interact with proteins such as FABP4 at this time point.

PS is an anionic phospholipid which resides predominantly on the inner membrane leaflet (under physiological conditions) and consequently has roles in many intracellular signalling pathways (449). The negative charge associated with PS allows interaction with key signalling molecules bearing positively charged moieties such as tyrosine kinases, Ras/Rho GTPases, protein kinase C and annexin V (450). The overall proportion of PS was higher in cells and EVs at day 0 as was the composition of arachidonic acid of PS at day 0. Taken together, this suggests that cells at day 0 have an increased intracellular signalling capacity which may also transferred to day 0 EVs. Therefore, EVs at day 0 are potentially equipped with a greater cargo of bioactive signalling fatty acids which could be used to enhance intercellular communication and initiate differentiation.

A subject of great interest in the EV field is how changes in EV protein expression can occur following stimulation or stress of the cell of origin (451). The most popular techniques for measuring changes in vesicular protein expression are currently FC and Western blotting. However, as discussed in *Chapter 3*, there are several disadvantages to these techniques, primarily the limits of detection and lack

of sensitivity for FC and the amount of EV sample required for Western blotting. Here, an immunophenotyping method (36,158)) was used to analyse surface and intravesicular EV proteins pre- and post-adipogenesis. Analysis of EV proteins by this method allows simultaneous analysis of multiple markers, using low amounts of sample (1 µg/well). The use of europium as the reporter probe allows detection of signal over a wide dynamic range ensuring a good sensitivity for lowly and highly expressed antigens. Results have been shown to be comparable with Western blot data (36,158) and the technique has been used by others in the EV field (119). Levels of transmembrane (CD9/CD63) and intravesicular (alix/TSG101) exosomal markers showed no change in EVs pre- vs. post-adipogenesis. This suggests that although the number of EVs (particularly exosomes) is higher at day 0, the relative expression of exosomal proteins within EVs does not change between time points. A range of adipocyte markers that are known to be present at different stages of adipogenesis (301,320) were selected for analysis within EVs. PREF-1 represses differentiation and promotes a preadipocyte phenotype (452). As confirmed by Western blot analysis of cell lysates (**Figure 4.3.2 A**), PREF-1 expression is higher at day 0. In keeping with this, EV PREF-1 decreased from day 0 to day 15, allowing progression to a mature adipocyte phenotype. However, at day 15 there is still PREF-1 present in EVs whereas expression within cells seems to be absent. The reasons for this could be a combination of factors. Firstly, the immunophenotyping detection is more sensitive than Western blotting and so PREF-1 may still be present in cells but the expression far less than that at day 0. Secondly, *in vitro* differentiation of adipocytes is never 100% efficient and therefore some preadipocytes are still present in the culture. Therefore these residual preadipocytes may be producing EVs containing PREF-1 that is detectable by immunophenotyping but not by Western blotting in the total day 15 cell lysate. PPARγ is a nuclear receptor required for both the induction (including the growth arrest of cells (301)) and the maintenance of adipogenesis (320). Here, EV PPARγ content was unchanged pre- vs. post-adipogenesis suggesting that PPARγ produced by cells to initiate growth arrest around day 0, and by cells at day 15 to maintain an adipocyte phenotype is transferred to corresponding EVs. Adiponectin is an adipocyte-specific adipokine produced by mature adipocytes (453) with roles in regulating insulin sensitivity and glucose metabolism (454). The content of adiponectin in cells was higher at day 15 compared with day 0 (**Figure 4.3.2 B**), which was again mirrored in the EVs at this time point. Finally, FABP4 is a

cytosolic fatty acid trafficking protein (455) that is highly expressed in mature adipocytes (confirmed in **Figure 4.3.2 C**) accounting for ~1% of the total protein of the cytosolic fraction (323). FABP4 within EVs decreased from day 0 to day 15 perhaps reflecting a role for EVs that is independent of their cell of origin or perhaps a specific packaging of FABP4 into EVs.

Retrospective Western blot data contradicted the results of EV immunophenotyping for PREF-1 and FABP4. Indeed, blots were conducted in hindsight for these two proteins after evaluating the immunophenotyping results, which were unexpected. It is not clear why these two techniques gave such differing results. One potential explanation is that the immunophenotyping may need validation for different types of EV and for different antibodies. Concentrations of EVs and antibodies used in this chapter were based on a protocol for prostate cancer-derived exosomes, which yielded similar results when analysed by Western blot (119,232). Additionally, the exosomes used for immunophenotyping in these studies had been washed following isolation and therefore may have a higher purity than the EVs in this chapter. Therefore, 1 µg (the amount of EVs loaded per well) may be very different between the two EV preparations. Furthermore, as the immunophenotyping is a novel technique, commercial antibodies that were used to probe for the antigens are not yet validated for this technique as they are for Western blotting. Hence, a different working concentration of antibody may be required for optimal detection.

4.4.3 Limitations

There are several potential limitations of this study. Firstly, 3T3-L1 cells were used throughout the chapter for characterisation. Others have successfully isolated EVs from primary adipocyte sources such as mouse AT (392), rat primary adipocytes (387,456) and human AT explants (306,307). Though 3T3-L1 cells are not a primary cell line, they are widely used as a reliable model to study adipocyte biology (294). Their use here also enabled more detailed analyses requiring large sample amounts such as TLC and GC-FID to yield novel data about lipid and phospholipid profiles of adipocyte EVs. The data presented here also tally with data from primary adipocyte EV sources in terms of the presence of adipocyte and exosomal protein within EVs.

There are currently a number of issues surrounding standardisation of protocols in the EV field, meaning preparatory techniques are constantly being updated. Here, differential centrifugation was used to isolate adipocyte EVs as described previously (393). Intermediary centrifugation steps of 10,000 – 20,000 x g have recently been reported to pellet larger microvesicles (17). Therefore the use of a 15,000 x g spin may pellet larger microvesicles as well as cell debris and apoptotic bodies, thus removing them from the final EV sample. However, NTA detected EVs up to 1 µm in diameter (**Figure 4.3.5 C**), indicating the presence of larger microvesicles.

A further practical limitation of this study was the use of FC to assess the annexin V positivity of EVs. As discussed in *Chapter 3*, many conventional flow cytometers have a practical lower limit of ~300 nm due to the low refractive index of EVs (420), meaning smaller microvesicles and exosomes may not be detected by this method. Therefore the annexin V positivity may have been underestimated here, particularly if a proportion of larger microvesicles (known to have a greater annexin V positivity) were removed by the 15,000 x g spin. Future studies could couple EVs to 1 µm latex beads before assessment with FC (117) or use a dedicated small particle high resolution flow cytometer (155) to ensure capture of the whole EV spectrum.

Immunophenotyping of EVs, whilst potentially less time- and sample-consuming than Western blotting, was not optimised for use with adipocyte-derived EVs in this chapter. Background fluorescence of day15 EVs alone (without primary antibody), was often significantly higher than day 0 EVs. Interestingly, when cells and EVs were analysed by FC for annexin V positivity, unstained day 15 cells (and EVs to a lesser extent) showed significant auto-fluorescence in the FITC channel. Perhaps because cells (and EVs) at day 15 contain more lipid, this may auto-fluoresce to cause higher levels of background noise compared to day 0 samples which contain significantly less lipid. My colleagues have since performed a validation of the immunophenotyping assay for the detection of EV proteins in plasma-derived EVs. Firstly, the concentration of EVs used per well was found to be extremely important. Lower concentrations of EVs per well gave higher background TRF readings (without the presence of primary antibody). This effect was eventually saturated for plasma EVs by using higher concentrations of around 5 x 10^{10} particles/mL of EVs in each well. Therefore, the number of EVs per well must be titrated for each source of EV. Here, 1 µg of EVs were added to each well which equated to around 2 x 10^8

particles at day 0 and 5 x 10^7 particles at day 15. Therefore, too few EVs may have been added per well (particularly for day 15 EVs) resulting in higher background signals. Secondly, the concentration of primary and secondary antibodies was shown to be important. Following titration, it was found that a concentration of 3 µg/mL of primary antibody was sufficient to detect maximal signal. Here, a concentration of 1 µg/mL was used, so some antibodies may not have been at an optimal concentration to detect the entirety of available antigen. Evidently, validation is needed to ensure agreement with Western blot analysis before this technique can replace Western blot for adipocyte EV protein analysis.

Finally, serum-free media was used for the 24 hour conditioning period prior to EV isolation to avoid contamination of FCS-derived EVs (159). The requirements of the cells at each time point are different and hence serum-free media was supplemented with insulin prior to EV isolation at day 15, whereas media at day 0 was not. This was to minimise changes to normal media components at each time point, however, it is possible that the addition of insulin may have affected EV release at day 15.

4.4.4 Conclusions

To summarise, the production of adipocyte EVs is shown to be significantly affected by the differentiation process. Prior to adipogenesis, EV concentration is higher and EVs are enriched in fatty acids and phospholipids with known involvement in cell signalling. This suggests that EVs released prior to adipogenesis may aid communication between preadipocytes to enhance the transition to mature adipocytes. EVs retained certain aspects of their cell of origin including annexin V positivity, fatty acid content and protein expression, but also possessed unique differences in fatty acid composition and protein content. These concurrent similarities and differences may allow EVs to represent their cell of origin but to also harbour unique qualities that potentially confer different functional properties. Future studies should explore the functional impact of EVs on the control of adipogenesis and their wider implications in the role of AT as an endocrine organ.

5. Results III:

Effects of hypoxia on adipocyte-derived EV production

5. Perspective

Having completed a comprehensive characterisation of adipocyte-derived EVs using 3T3-L1 cells in *Chapter 4*, I was able to apply these techniques to analyse EVs derived from adipocytes exposed to disease-like conditions (hypoxia). It should be noted that EV immunophenotyping used and described in *Chapter 4* was also used in this chapter to characterise vesicular protein content. However, a set number of EVs were added per well instead of a set amount of EV protein to attempt to address some of the issues experienced in *Chapter 4*. The number of EVs used (5×10^9 EVs) was based on pilot data from my colleague, Mr Nick Burnley-Hall, who had found this concentration of EVs to be sufficient for the detection of exosomal and other markers in EVs derived from an endothelial cell line.

5.1 Introduction

As discussed in *Chapter 1*, dysfunctional adipose tissue AT is a risk factor for obesity-related complications such as IR and T2D (378), though the root cause of dysfunction remains to be elucidated. AT hypoxia has been proposed as a potential instigator of impaired AT functioning and AT from obese subjects is known to have a reduced blood supply compared to that from lean subjects (366). Hypoxic conditions have also been shown to alter EV release and functionality in prostate cancer cells (457). Therefore, hypoxic adipocyte EVs may play a role in the development of AT dysfunction.

Growth and expansion of AT occurs through adipocyte hyperplasia and hypertrophy (458). In obese AT, hypertrophy of adipocytes can result in cells up to 200 μm in diameter (265,266) which is at the upper limit of the diffusion distance of oxygen (O_2) in a tissue (363). Despite the increase in AT mass, blood flow to AT is reduced in obesity (365,366), suggesting that blood vessel growth in AT is insufficient to maintain the same blood flow as provided to lean AT. It is likely therefore, that obese AT is littered with regions of hypoxia. Indeed, obese AT has been shown to have a reduced oxygen tension (partial pressure, pO_2) in both obese mice models (368,369,377) and human studies of obesity (373–376), though the reported pO_2 of AT varies greatly between studies (**Table 1.2.2**). *In vitro* studies of adipocytes in hypoxia shows the transition towards a pro-inflammatory state through the production of inflammatory adipokines such as TNF-α, IL-6 and PAI-1 (380). Upregulation of these adipokines is primarily attributed to the activation of HIF-1α during hypoxia (459). HIF-1α in hypoxia also targets the activation of genes controlling angiogenesis and metabolism such as VEGF and leptin to attempt to restore oxygenation (380). Unfortunately, the overarching effect is AT inflammation which leads to dysregulation of lipid metabolism, storage and adipokine secretion (352,460–462). Obesity is associated with low grade systemic inflammation (352), though whether this is the cause or consequence of AT inflammation is unknown.

Given that EV release is often increased in response to conditions of cellular stress, it is no surprise that hypoxia has been shown to increase EV generation in a number of cell types (241,463,464). HIF-1α is thought to play a central role in this response as data from our lab and others show that knockdown or silencing of HIF-1α reduces

hypoxia-induced EV formation (241,463). Studies into the hypoxic enhancement of EV release have largely focused on cancer cell lines, where the hypoxic EVs can promote angiogenesis to fulfil the demands of the growing tumour and to encourage metastasis (253,463,465,466). 3T3-L1-derived EVs from unstimulated cells have been shown to induce angiogenesis *in vivo* (393); an effect which may been enhanced in hypoxic conditions. Despite the potential similarities between the growth of obese AT to tumour progression (259), to date only one study exists detailing hypoxic adipocyte-derived EVs (390). This study focused on the metabolic enhancement of *de novo* lipogenesis by hypoxic 3T3-L1 exosomes; however, the authors did not quantitate the effects of hypoxia on EV characteristics such as EV size and concentration, lipids and protein content.

5.1.1 Aims

The aims of this chapter were to determine the effects of different ambient O_2 levels on:

1. Cell morphology, viability and lipid accumulation
2. EV size and concentration
3. Cell and EV annexin V positivity
4. Cell and EV fatty acid composition
5. Cell and EV phospholipid (and fatty acid) composition
6. Cell and EV adipocyte and inflammatory protein expression

5.1.2 Hypotheses

Hypoxia may elevate EV concentration but also alter the lipid/protein content of the EV compared to normoxic EVs, and perhaps compared to hypoxic cells.

5.2 Methods

5.2.1 Cell culture

3T3-L1 cells were cultured as outlined in *Chapter 2.2*. Serum-free media was added to cells at day 14 post-differentiation and cells were either kept in the incubator (95% air with 5% CO_2, "normoxic"), or transferred to an Invivo 2 hypoxic workstation 400 (Baker Ruskinn, UK) and maintained under set Oxygen conditions ("hypoxic") for 24 hours. Oxygen (O_2) conditions included: 1, 2, 5, 10 and 21% O_2 and were monitored using a i-CO_2N_2 gas mixing system (Baker Ruskinn, UK).

Cells were counted as described in *Chapter 2.2.2*; hypoxic cells were removed from flasks and added into cell counting slides in the hypoxic chamber. Morphological changes of cells were observed using a Nikon Diaphot microscope (Nikon) and images captured at 10X magnification using ViewFinder™ software (version 3.0.1, Better Light Inc., USA). Oil Red O staining was used to quantify changes in lipid droplets as described in *Chapter 2.2.3* in 1% O_2 experiments; fixing of 1% O_2 cells was carried out in the hypoxic chamber.

5.2.2 Isolation and measurement of extracellular vesicles

After 24 hours of incubation, serum-free media was removed from cells and processed as described in *Chapter 2.3.1*. Media from cells in hypoxia was collected in the hypoxic chamber. Isolated EVs were stored as described in *Chapter 2.3.3*. NTA was used to measure EV samples as outlined in *Chapter 2.4.2*.

5.2.3 Flow cytometry

Flow cytometric analyses were conducted to assess the annexin V positivity of cells and corresponding EVs isolated from 1, 2, 5 10 and 21% O_2, each with normoxic controls as described in *Chapter 2.6*. Due to variation between analyses, results are expressed as a delta change in percentage positivity from normoxic controls.

5.2.4 Gas chromatography

Fatty acid concentration and composition of normoxic and hypoxic cells was measured using GC-FID as outlined in *Chapter 2.7*. Due to variation in reported fatty acid concentration for normoxic controls between experiments, fatty acid concentration of cells and EVs is presented as a change from the respective normoxic control (delta change).

5.2.5 Thin layer chromatography

Two-dimensional TLC was used to determine proportions of phospholipids present in normoxic and 1% O_2 cells and EVs as described in *Chapter 2.7*.

5.2.6 Western blotting

Normoxic and 1% O_2 cells were lysed as described in *Chapter 2.10.1*. Twenty to fifty µg of protein was loaded per well and were separated using specific running gels (**Table 5.2.1**) and probed with primary antibodies (incubated at room temperature overnight). Membranes were washed thoroughly in TBS-T overnight before being blocked and subsequently re-probed for β-actin. Densitometry was conducted as described in *Chapter 2.10.6*.

Protein	Running gel	Antibody dilution	Typical exposure time
β-Actin	n/a	1:2000 (1% milk/TBS-T)	1 minute
Adiponectin (CST #2789)	12%	1:500 (5% BSA/TBS-T)	15 minutes
FABP4	15%	1:1000 (5% BSA/TBS-T)	15 seconds
HIF-1α	8%	1:500 (1% milk/TBS-T)	20 minutes
IL-6	12%	1:500 (5% BSA/TBS-T)	15 minutes
IL-10	15%	1:500 (5% BSA/TBS-T)	15 minutes
MCP-1	15%	1:500 (5% BSA/TBS-T)	15 minutes
PPARγ	10%	1:1000 (5% BSA/TBS-T)	2 minutes
TNF-α	15%	1:500 (5% BSA/TBS-T)	15 minutes

Table 5.2.1: Details of Western blotting. Details of the proteins analysed by Western blotting and the percentage of acrylamide gels used to separate them. Note, β-actin was used as a control for all proteins so a running gel acrylamide percentage is not provided. Dilutions and diluents for antibody preparation and exposure times for the development of membranes are given for each protein. BSA = bovine serum albumin; CD = cluster of differentiation; CST = Cell Signaling Technologies; FABP4 = fatty acid binding protein-4; HIF-1α = hypoxia inducible factor-1α; IL = interleukin; MCP-1 = monocyte chemoattractant protein-1; PPARγ = peroxisome proliferator-activated receptor γ; TBS-T = tris-buffered saline – tween 20 (1% v/v); TNF-α = tumour necrosis factor – α.

5.2.7 Extracellular vesicle immunophenotyping

EVs from 1% O_2 and normoxic cells were added to wells at a concentration of 5 x 10^9 EVs/well and analysed using TRF as described in *Chapter 2.9* for an array of markers (**Table 5.2.1**). A set concentration of EVs was added per well as opposed to a set amount of protein of EVs per well (1 μg) following validatory data collected by Mr Nick Burnley-Hall using an endothelial cell line. The data indicated a level of background fluorescence from the ELISA plate. This could be abrogated by using a

concentration of EVs to sufficiently cover the bottom of each well. This concentration was found to be 5 x 10^9 EVs per well for endothelial-derived EVs and so this concentration was applied to TRF in this chapter.

Antibody	Dilution
CD9	1:200
Adiponectin (CST #2789)	1:10
FABP4	1:25
PPARγ	1:49
IL-10	1:101
IL-6	1:101
TNFα	1:101
MCP-1	1:16
HIF-1α	1:117

Table 5.2.2: Primary antibodies used for EV immunophenotyping. Antibodies and dilutions used for EV immunophenotyping experiments. CD= cluster of differentiation; CST = Cell Signaling Technologies; FABP4 = fatty acid binding protein-4; HIF-1α = hypoxia inducible factor-1α; IL = interleukin; MCP-1 = monocyte chemoattractant protein-1; PPARγ = peroxisome proliferator-activated receptor γ; TNF-α = tumour necrosis factor – α.

5.2.8 Statistical analysis

Data were analysed using GraphPad Prism software (version 6.0). As hypoxic experiments were conducted at different times, each level of hypoxia required a normoxic control. Therefore, the variation between normoxic controls was compared using a one-way ANOVA with multiple comparisons for each parameter presented in this chapter. With the exception of flow cytometry and gas chromatography samples, normoxic control samples did not significantly vary between experiments, and so "normoxia" refers to normoxic data averaged from different hypoxic experiments.

5.3 Results

5.3.1 Effect of hypoxia on adipocyte morphology, number and viability

Following 24 hours incubation in normoxia or hypoxia, cells were imaged for potential morphological changes (**Figure 5.3.1**). Compared with normoxic cells (**Figure 5.3.1 A**), cells incubated from 2-21% O_2 (**Figure 5.3.1 C-F**) showed no significant changes in cell morphology with cells still appearing rounded and lipid laden. However, cells at 1% O_2 appeared less rounded with fewer lipid droplets (**Figure 5.3.1 B**). Cell number and viability showed no significant change with varying levels of hypoxia compared to normoxia (**Figure 5.3.1 G/H** respectively).
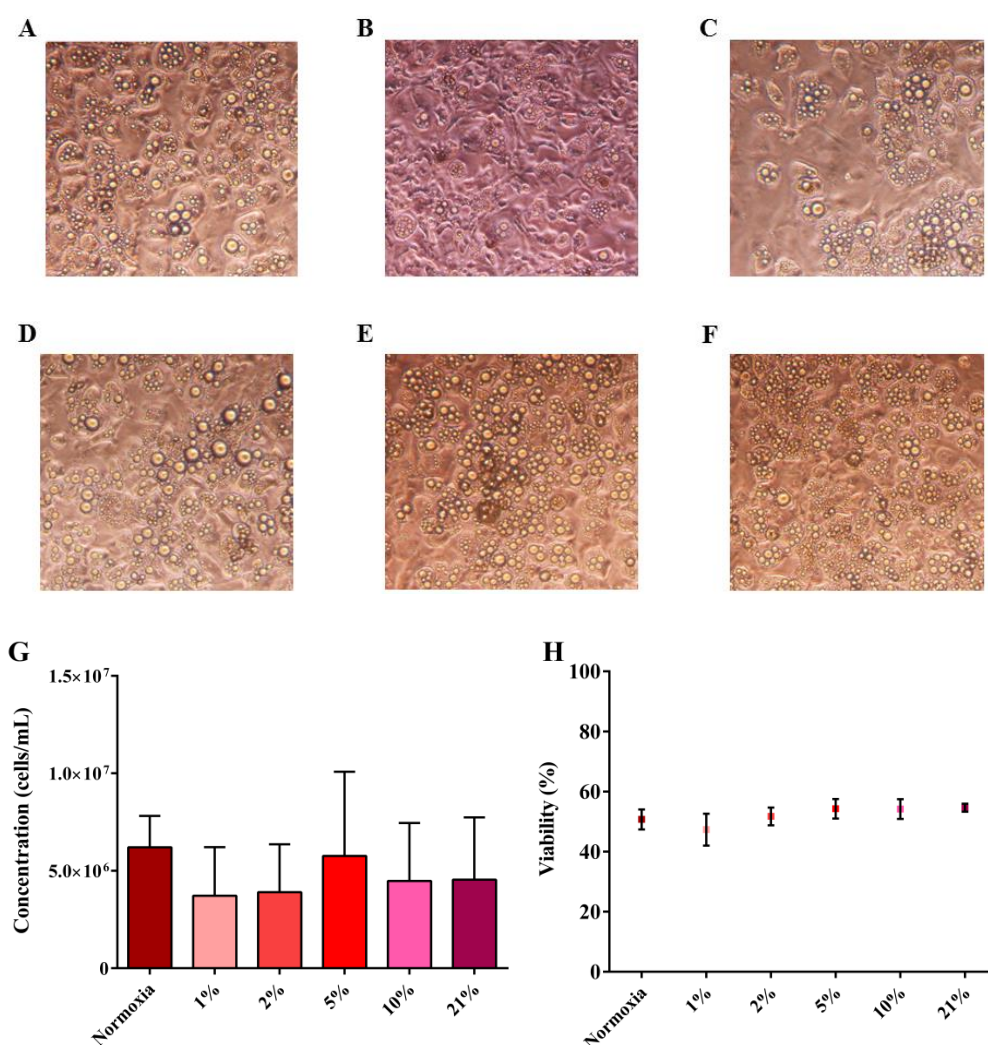
Figure 5.3.1: Effect of hypoxia on adipocyte characteristics. Representative images of adipocytes after incubation in normoxia (**A**) or hypoxia: (**B**) 1%; (**C**) 2%, (**D**) 5%, (**E**) 10% and (**F**) 21% O_2. Cell number (**G**) and viability (**H**) was measured from each condition using Trypan Blue exclusion, (n=3).

5.3.2 Oil Red O staining

When lipid accumulation was assessed by Oil Red O staining, there was no significant difference between 1% O_2 and normoxic cells (**Figure 5.3.2**).
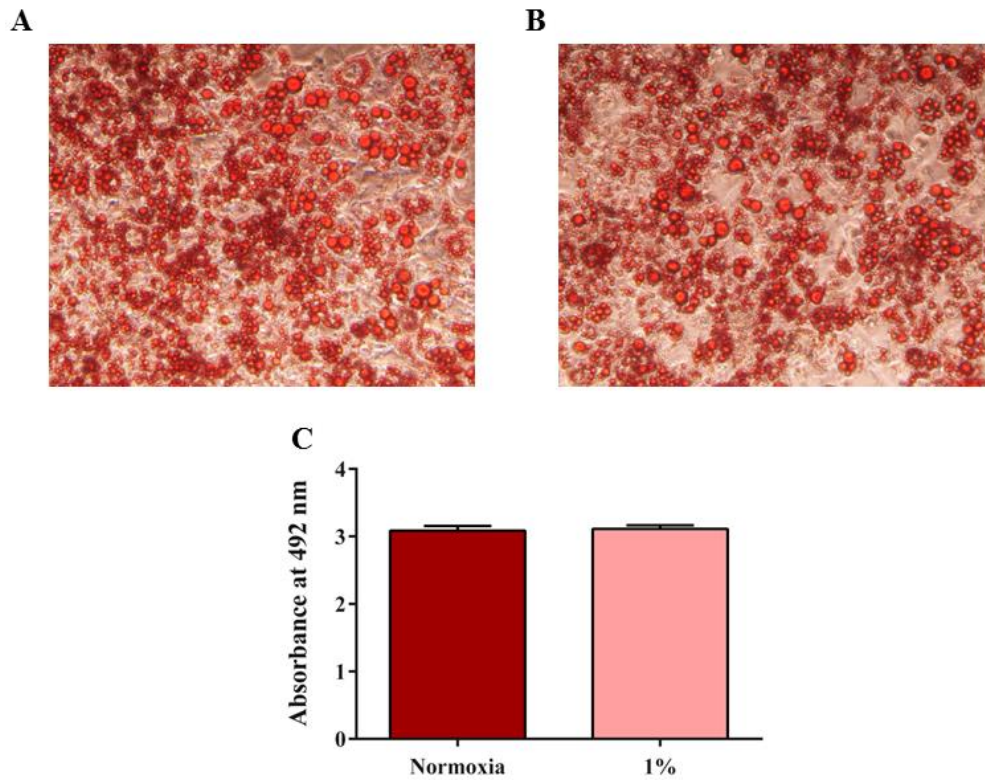
Figure 5.3.2: Oil Red O staining. Cells from normoxia (**A**) and 1% O_2 (**B**) were fixed and stained with Oil Red O to assess lipid accumulation. (**C**) The stain was then extracted and the absorbance measured at 492 nm (n=4).

5.3.3. Effect of hypoxia on extracellular vesicle size and concentration

EV concentration and size from 3T3-L1 cells incubated in normoxia and hypoxia were measured using NTA (**Figure 5.3.3**). EVs from 1% O_2 cells were significantly increased compared to normoxia (137.3 ± 42.4 to 391.1 ± 219.8 EVs/viable cell, $p = 0.003$; **Figure 5.3.3 A**). Other hypoxic conditions showed no effect on EV concentration compared to normoxia. The mode size of EVs showed no change with varying levels of hypoxia (**Figure 5.3.3 B**).
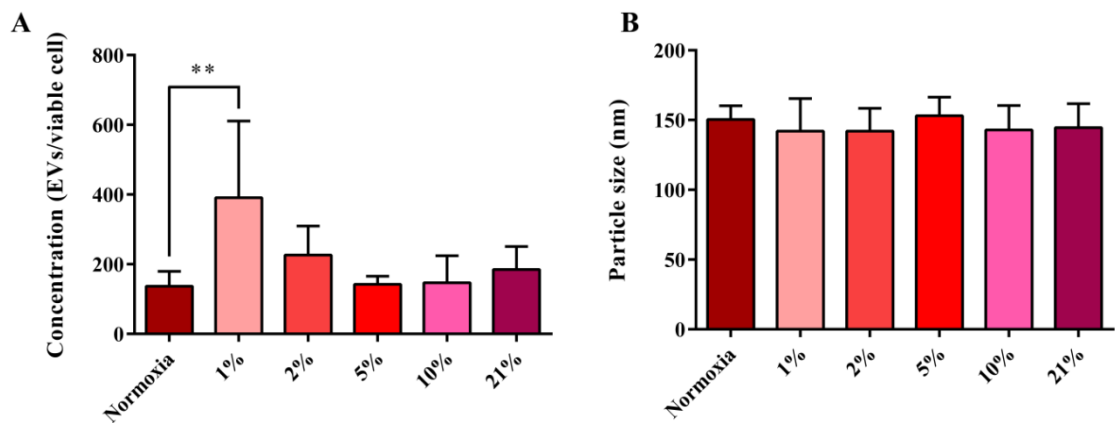
Figure 5.3.3: EV concentration and size following hypoxia. EVs collected from normoxic and hypoxic cells were measured using NTA and (**A**) expressed as concentration of EVs/viable cell and (**B**) mode particle size in nm **$p = 0.003$ (n=6).

When EV concentration was split into 50 nm bin-widths, the most significant changes were observed in 1% O_2 EVs which were increased between 50 and 200 nm compared to normoxic controls (**Figure 5.3.4**). EVs from 2% O_2 cells were also significantly elevated compared to normoxic controls between 100 and 200 nm. No significant changes were observed in other hypoxic conditions.
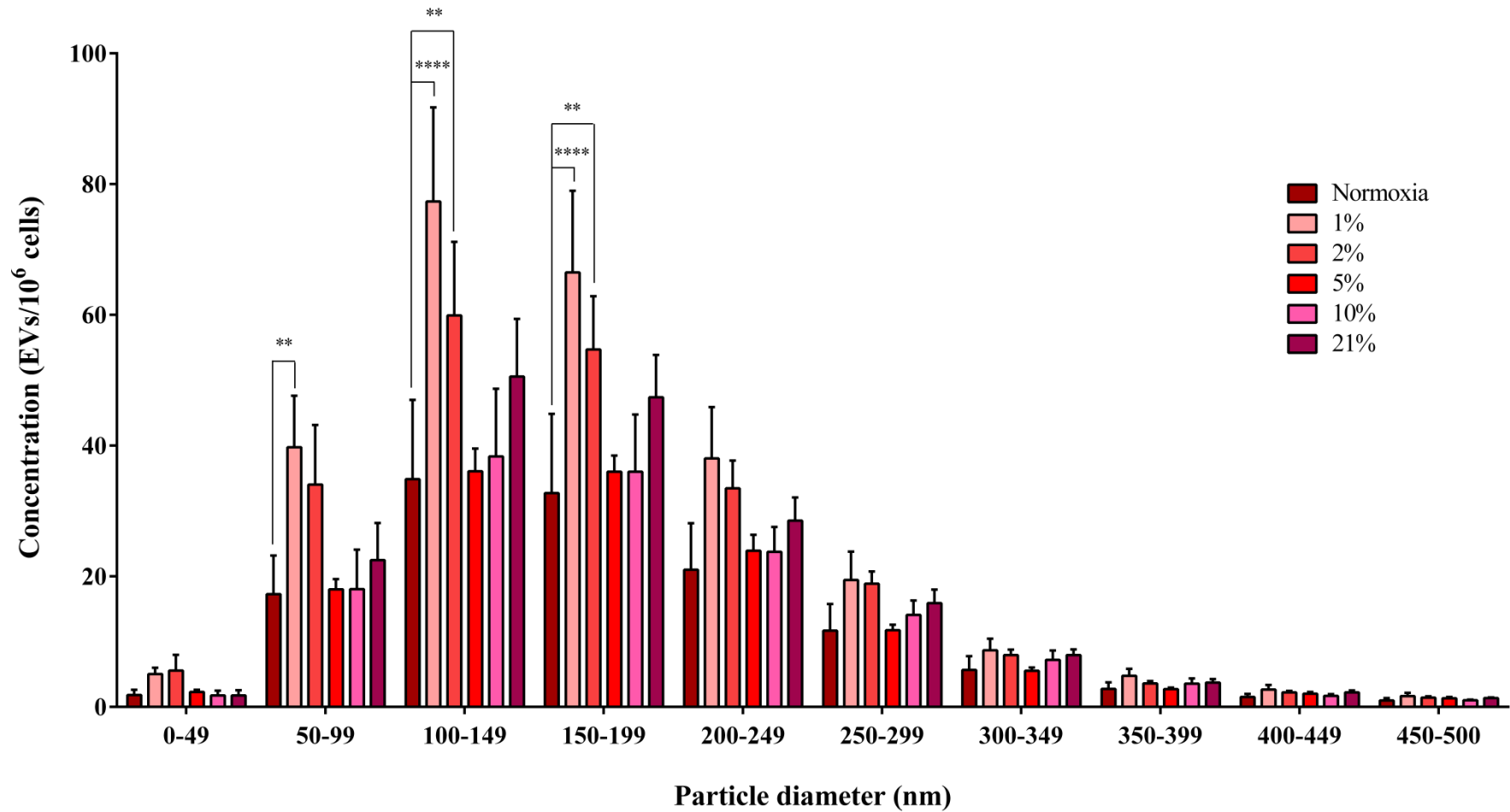
Figure 5.3.4: Size and concentration distribution. EV concentration was split into 50 nm bin-widths over the EV range for normoxic (n=5) and hypoxic (1, 2, 5, 10 and 21% O$_2$, n=6) EVs. ****$p<0.0001$, **$p<0.01$.

5.3.4 Effect of hypoxia on annexin V positivity

FC was used to assess the annexin V positivity of adipocytes and corresponding EVs in response to hypoxia. Unfortunately, measurements varied greatly between O_2 experiments, particularly within normoxic controls (**Figure 5.3.5/6 A**). However, when normalised to their respective normoxic control, 1% O_2 cells were significantly more annexin V positive (1.0 ± 0.0 to 1.3 ± 0.05 for normoxic and 1% O_2 cells respectively; $p = 0.0004$; **Figure 5.3.5 B**). Annexin V positivity of cells from 2-21% O_2 was not different from respective normoxic controls (**Figure 5.3.5 C-F**).
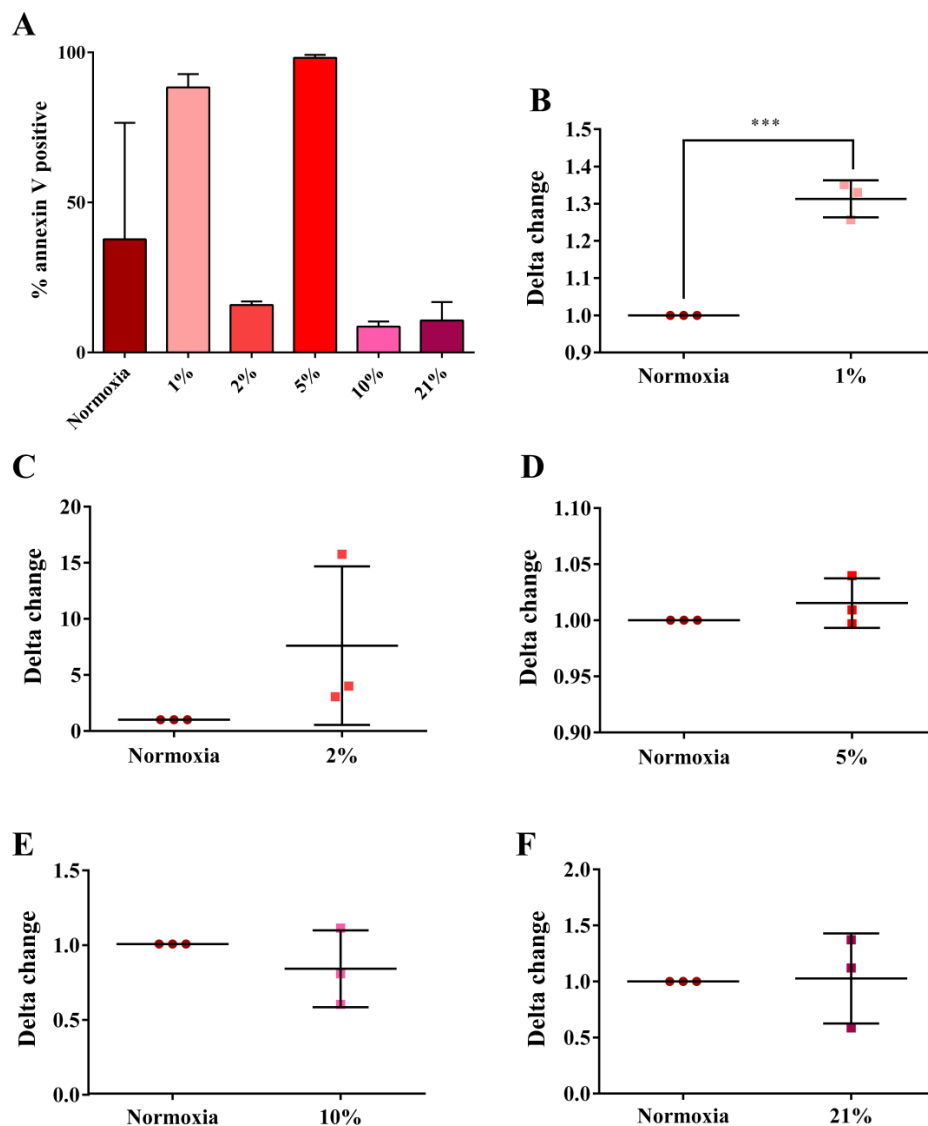
Figure 5.3.5: Cellular annexin V positivity. (**A**) Raw percentage of annexin V positivity. Delta change compared to normoxic controls was calculated for (**B**) 1%, (**C**) 2%, (**D**) 5%, (**E**) 10% and (**F**) 21% O_2 by normalising to respective normoxic values. ***$p = 0.0004$, (n=3).

EVs from 5% O_2 cells had a lower annexin V positivity than normoxic EVs (1.0 ± 0.0 to 0.4 ± 0.3 for normoxic and 5% O_2 EVs respectively, $p = 0.04$; **Figure 5.3.6 D**). EVs from other percentages of O_2 were not significantly different from normoxic controls.
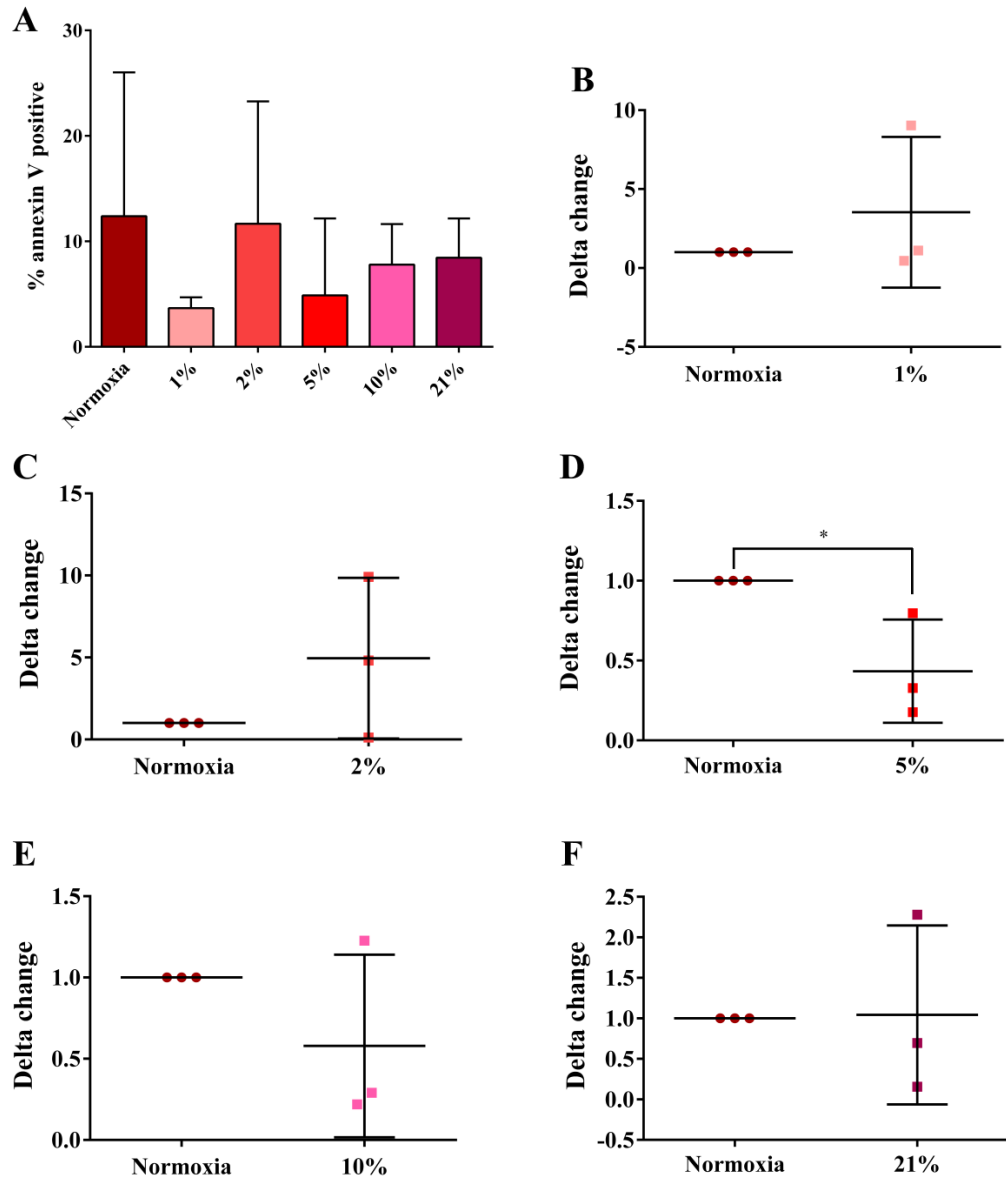
Figure 5.3.6: EV annexin V positivity. (**A**) Raw percentage of EV annexin V positivity. Delta change compared to normoxic controls was calculated for (**B**) 1%, (**C**) 2%, (**D**) 5%, (**E**) 10% and (**F**) 21% O_2 by normalising to respective normoxic values. *$p = 0.04$, (n=3).

5.3.5 Effect of hypoxia on fatty acid concentration and composition

Total fatty acid concentration and individual compositions of cells and EVs was determined by GC-FID. Due to variation in fatty acid concentrations of normoxic cells and EVs between hypoxic experiments, results are presented as delta change from respective normoxic controls. No changes were observed between cells or EVs in fatty acid concentration compared to normoxic controls (**Figure 5.3.7**).
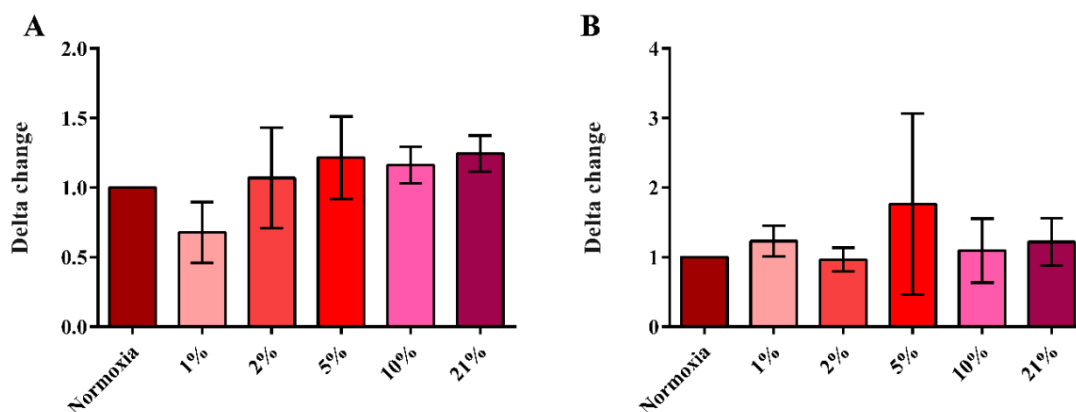
Figure 5.3.7: Fatty acid concentration of cells and EVs. Total fatty acid concentrations of (**A**) cells and (**B**) EVs at varying percentages of O_2 were determined by GC-FID. Due to inter-experiment variation between normoxic samples, data are presented as delta change (n=3).

Analysis of individual fatty acids by GC-FID revealed significant changes in 4 fatty acids between normoxic and hypoxic cells (**Figure 5.3.8**). Palmitic acid was increased in 1, 2 and 5% O_2 cells compared with normoxia (normoxia: $42.0 \pm 2.0\%$ to: 1% O_2; $45.2 \pm 1.0\%$, 2% O_2; $44.0 \pm 0.1\%$, 5% O_2; $45.4 \pm 2.0\%$, $p<0.0001$ for all) and was decreased in 21% O_2 cells compared with normoxia (normoxia: $42.0 \pm 2.0\%$, 21% O_2: $37.2 \pm 1.2\%$, $p<0.0001$). Palmitoleic acid was decreased in 1, 2 and 5% O_2 cells compared with normoxic controls (normoxia: $32.9 \pm 1.5\%$ to: 1% O_2; $27.8 \pm 0.9\%$, 2% O_2; $27.6 \pm 0.1\%$, 5% O_2; $29.4 \pm 1.2\%$, $p<0.0001$ for all) and was increased in 21% O_2 cells compared with normoxia (normoxia: $32.9 \pm 1.5\%$, 21% O_2: $35.5 \pm 0.9\%$, $p<0.0001$). Stearic acid was increased in 1 and 2% O_2 cells compared with normoxic controls (normoxia: $3.1 \pm 0.2\%$ to: 1% O_2; $4.3 \pm 0.05\%$, 2% O_2; $4.3 \pm 0.07\%$, $p<0.05$ for both).
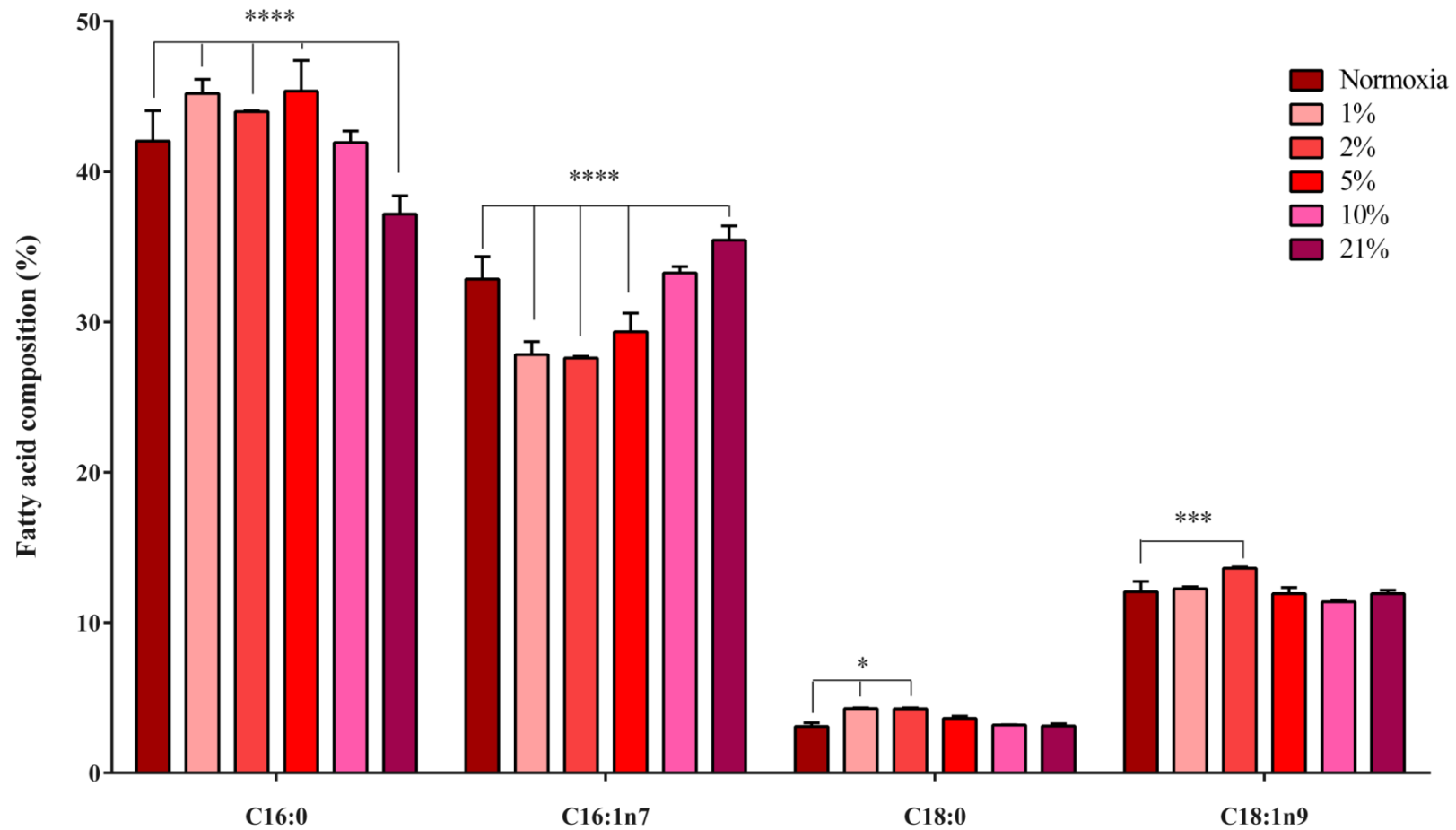
Figure 5.3.8: Cellular fatty acid composition. Significant changes in individual fatty acid compositions of normoxic and hypoxic cells. ****$p<0.0001$, **$p<0.01$, *$p<0.05$, normoxia (n=15) and 1, 2, 5, 10, 21% O_2 (n=3).

Finally, oleic acid was increased in 2% O_2 cells compared to normoxic controls (normoxia: $12.1 \pm 0.7\%$, 2% O_2: $13.6 \pm 0.08\%$, $p<0.001$). No changes were observed in the remaining detected fatty acids between normoxic and hypoxic cells (**Appendix: Table III**).

The same 4 fatty acids differed significantly between normoxic and hypoxic EVs (**Figure 5.3.9**). Palmitic acid was increased in 1 and 21% O_2 EVs compared to normoxic controls (normoxia: $36.2 \pm 2.6\%$ to: 1% O_2; $40.5 \pm 0.05\%$, $p<0.05$, 21% O_2; $45.1 \pm 3.0\%$, $p<0.0001$). Palmitoleic acid was decreased in 1% O_2 EVs and increased in 2 and 10% O_2 EVs compared to normoxia (normoxia: 19.2 ± 6.4 to: 1% O_2; $8.3 \pm 0.1\%$, 2% O_2; $26.2 \pm 0.01\%$, 10% O_2; $23.8 \pm 0.01\%$, $p<0.0001$ for all). Stearic acid was decreased in 2% O_2 EVs compared with normoxia (normoxia: $14.5 \pm 3.7\%$, 2% O_2: $10.3 \pm 0.0\%$, $p<0.05$). Finally, oleic was increased in 1% O_2 EVs compared with normoxic controls (normoxia: $13.1 \pm 2.4\%$, 1% O_2: $16.9 \pm 0.03\%$, $p<0.05$). No changes were detected in other fatty acids in EVs or fatty acids classes from normoxia to hypoxia (**Appendix: Table IV**).

Differences were observed in classes of fatty acids in cells with hypoxia, particularly with 1% O_2 (**Figure 5.3.10**). For example, SFA were higher in 1% O_2 cells compared with normoxic cells (normoxia: $48.1 \pm 2.6\%$ to: 1% O_2; $52.6 \pm 1.2\%$ $p<0.01$). MUFA were significantly lower in 1% O_2 cells compared with normoxic cells (normoxia: $49.2 \pm 2.9\%$ to: 1% O_2; $41.4 \pm 1.2\%$, $p<0.0001$). No differences were observed in cellular PUFA or EV lipid classes with hypoxia, however, similarly to Chapter 4, PUFAs were enriched in EVs compared with cells. The effects of the remaining hypoxic conditions on cellular lipid classes and individual fatty acids are given in **Appendix Table III**.
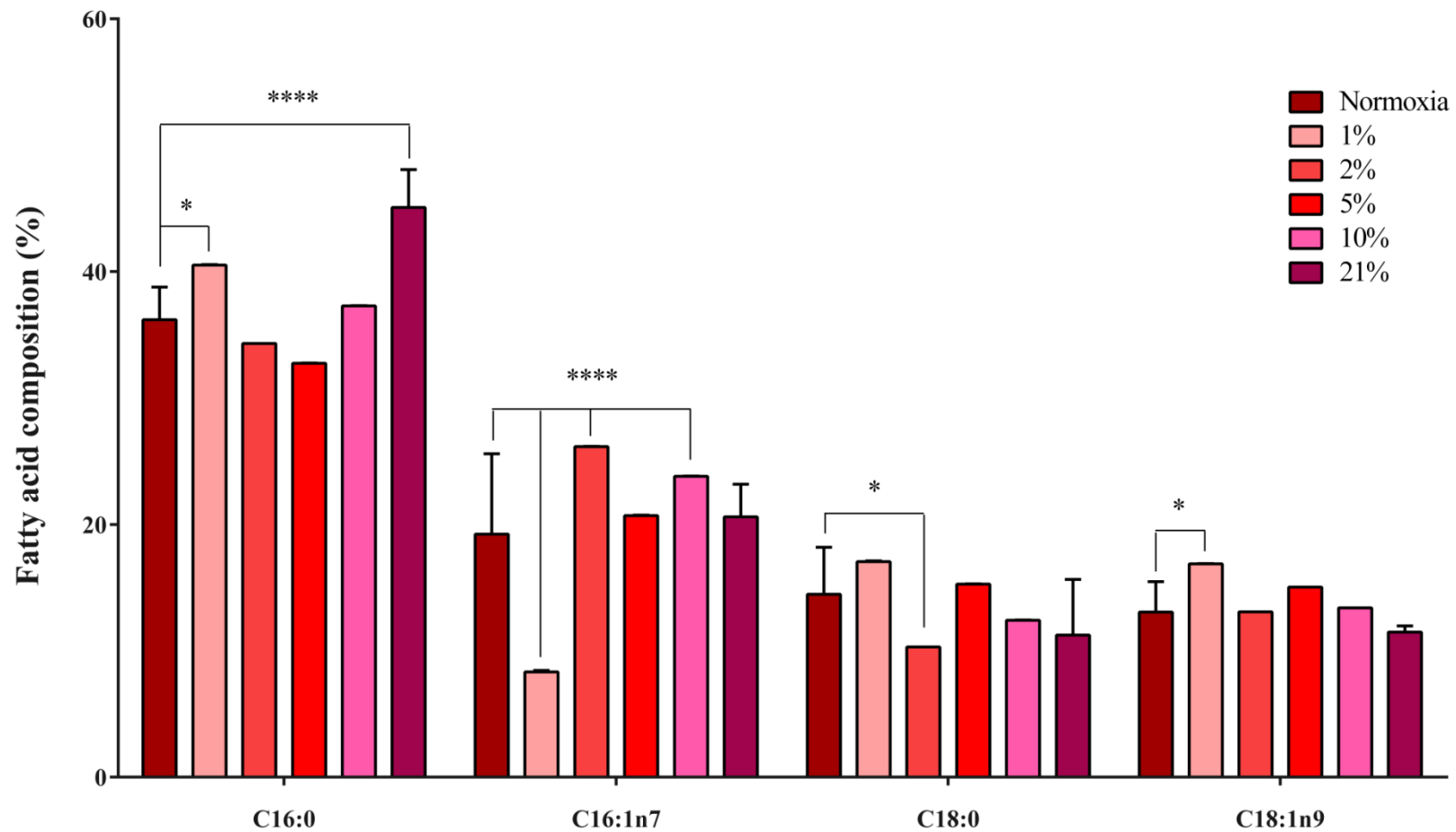
Figure 5.3.9: EV fatty acid composition. Significant changes in individual fatty acid composition between normoxic and hypoxic EVs. ****$p<0.0001$, **$p<0.01$, *$p<0.05$, normoxia (n=15) and 1, 2, 5, 10, 21% O_2 (n=3).
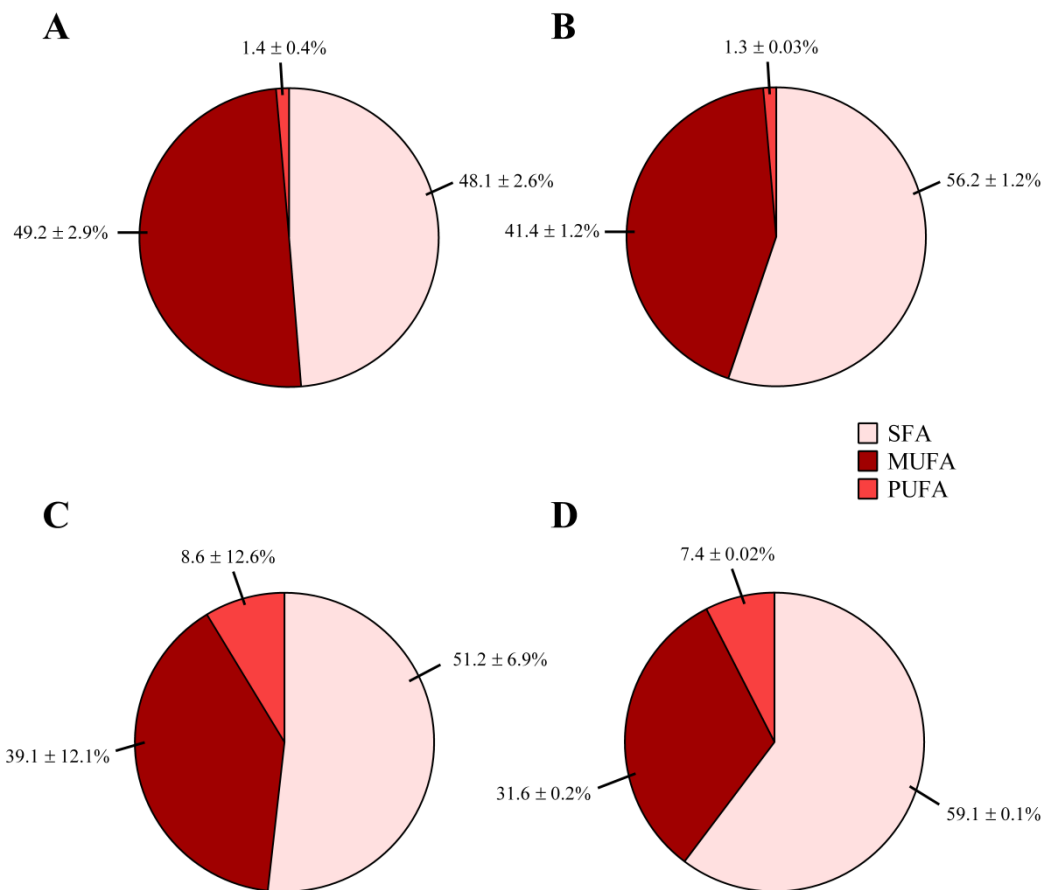
Figure 5.3.10: Changes in lipid classes with hypoxia. Alterations in major lipid classes between (**A**) normoxic cells, (**B**) 1% O_2 cells, (**C**) normoxic EVs, and (**D**) 1% O_2 EVs. SFA = saturated fatty acids, MUFA = monounsaturated fatty acids; PUFA = polyunsaturated fatty acids, (n=3).

When comparing the fatty acid composition of cells with their corresponding EVs, hypoxic EVs showed more differences compared to hypoxic cells than normoxic samples (**Appendix: Table V**). In particular, hypoxic EVs were enriched in PUFAs such as arachidonic acid and α-linolenic acid compared to hypoxic cells.

5.3.6 Effect of hypoxia on phospholipid composition

From here on in, 1% O_2 was chosen (and is referred to) as the hypoxic challenge. From the data presented above, 1% O_2 gave the most significant hypoxic challenge (without affecting the cell viability) and also the remaining experiments required a large amount of EV sample, so only one hypoxic challenge was practical.

Two-dimensional TLC was used to separate phospholipid groups in normoxic and hypoxic cell and EV samples. Proportions of each phospholipid were calculated as a percentage of the total concentration (**Figure 5.3.11**). Changes in phospholipids were marginal in normoxic and hypoxic cells. EVs showed increases in PC and PS and decreases in PE, sphingomyelin and cardiolipin in hypoxia compared with normoxia. PC and PE were the most abundant phospholipids present in all samples.
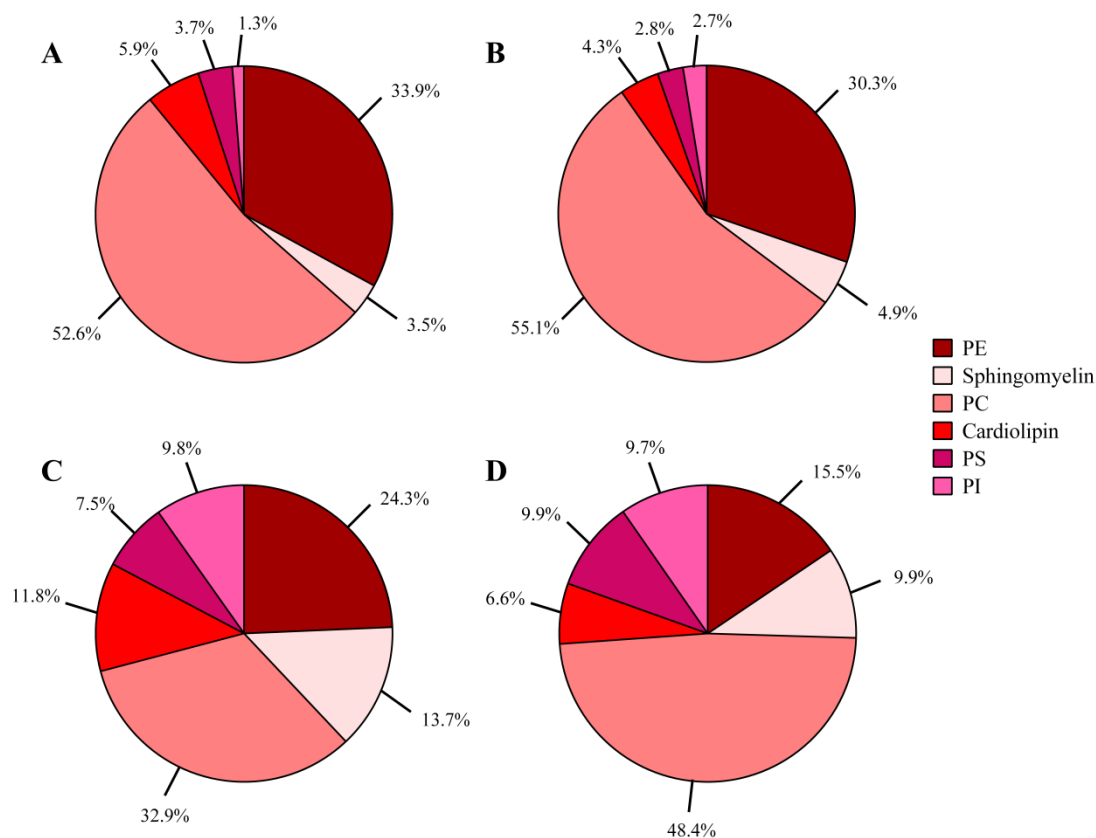
Figure 5.3.11: Phospholipid composition of cells and EVs. Phospholipids were separated using TLC in normoxic and hypoxic (1%) cells and EVs. Proportions of each phospholipid were calculated as a percentage of the total concentration of all phospholipids. (**A**) normoxic cells; (**B**) hypoxic cells; (**C**) normoxic EVs; (**D**) hypoxic EVs (n=1). PE = phosphatidylethanolamine; PC = phosphatidylcholine; PS = phosphatidylserine; PI = phosphatidylinositol.

Separated phospholipids were then further analysed by GC to identify individual fatty acids present within phospholipid fractions (**Appendix: Table VI**). Similarly to *Chapter 4,* EVs were enriched in PUFAs, particularly in hypoxic conditions where arachidonic acid was abundant. Interestingly, the PUFA, α-linolenic acid was reduced in hypoxic EV samples.

5.3.7 Effect of hypoxia on cellular protein content

Cell lysates from normoxic and hypoxic cells were analysed for their expression of adipocyte and inflammatory proteins by Western blotting (**Figure 5.3.12**). Of the adipocyte proteins, adiponectin appeared to be decreased in hypoxic cells, though this was not significant (**A**). Expression of FABP4, though not significant, increased in hypoxic cells (**B**). PPARγ expression was significantly reduced in hypoxic cells (normoxia: 2.37 ± 0.08; hypoxia: 0.85 ± 0.2 relative expression compared to β-actin, p = 0.0003; **C**). Inflammatory proteins (TNF-α and IL-10) showed no change between normoxia and hypoxia (**D/E**). IL-6 could not be detected by Western blotting despite maximisation of the amount of protein loaded, the concentration of antibody used and exposure time. No change was observed in MCP-1 (**F**), however hypoxic cells contained significantly more HIF-1α (normoxia: 0.2 ± 0.2; hypoxia: 1.7 ± 0.7 relative expression compared to β-actin, p = 0.02; **G**).
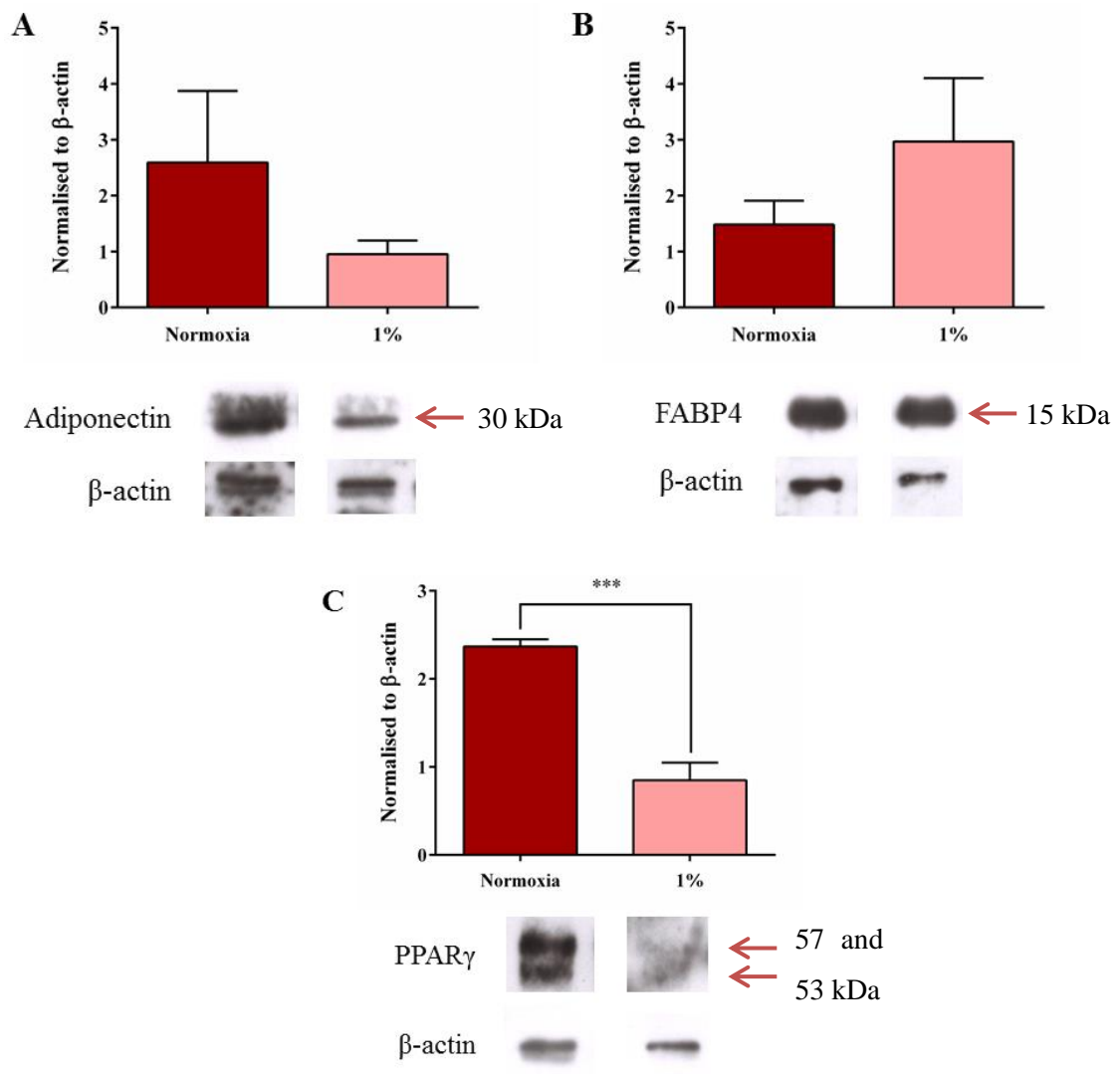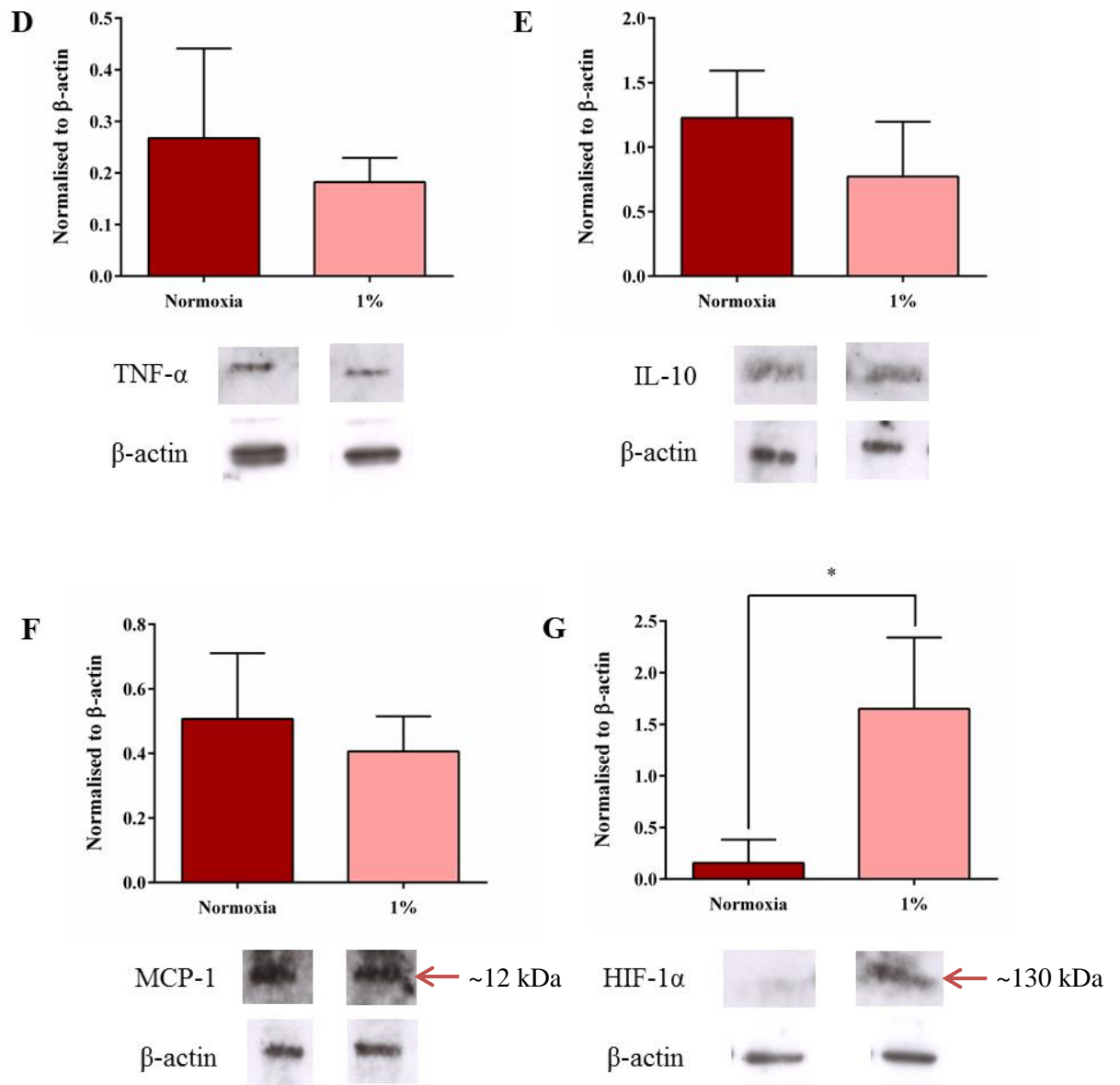
Figure 5.3.12: Western blot analysis. Western blots of cell lysates from normoxia and 1% O$_2$ cells probed for adipocyte markers: (**A**) adiponectin, (**B**) FABP4, (**C**) PPARγ and inflammatory markers: (**D**) TNF-α, (**E**) IL-10, (**F**) MCP-1 and (**G**) HIF-1α. Differences in densitometry values compared to β-actin are presented as well as representative bands of the protein of interest and β-actin control. Observed molecular weights are given for each protein (β-actin = 42 kDa)*$p<0.05$, ***$p<0.001$ (n=3).

5.3.8 Effect of hypoxia on EV protein content

EV protein content of normoxic and hypoxic EVs was measured using EV immunophenotyping (**Figure 5.3.13**). The exosomal protein CD9 and adipocyte proteins, adiponectin, FABP and PPARγ, showed no difference between normoxia and hypoxia. Levels of inflammatory proteins, IL-6, TNF-α and IL-10 were not changed with 1% O_2. MCP-1 was significantly increased in hypoxic EVs (17,615 ± 3,249 to 26,946 ± 6,928 arbitrary TRF units, $p = 0.01$). No change was observed in EV HIF-1α between normoxia and hypoxia.
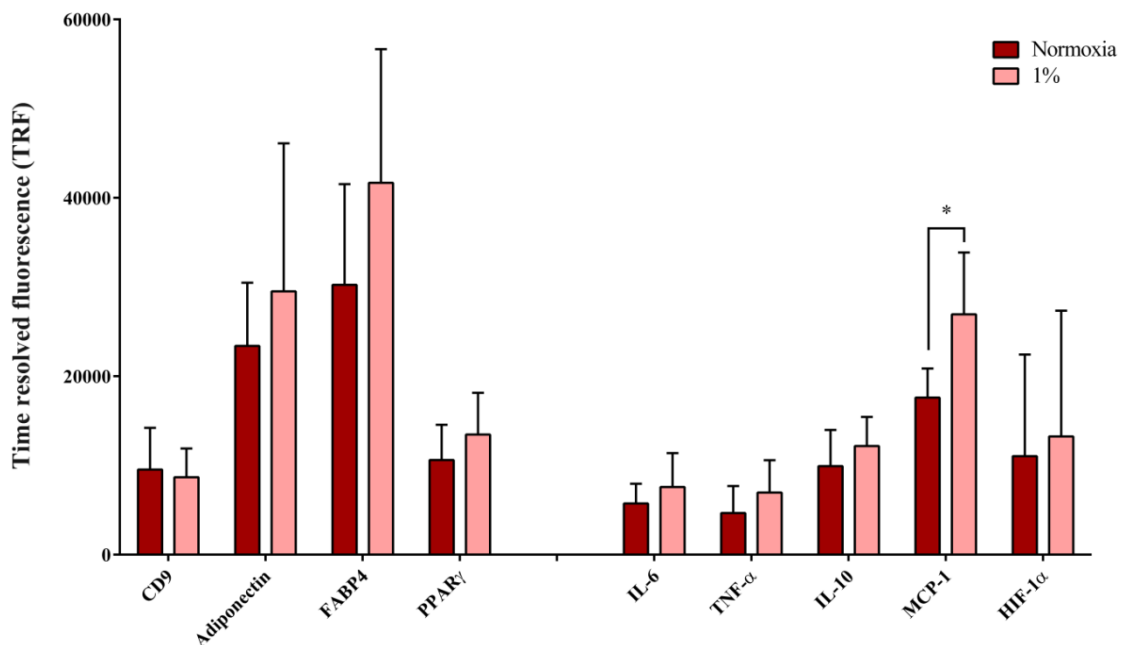
Figure 5.3.13: Protein content of normoxic and hypoxic EVs. The exosomal protein CD9, adipocyte proteins; adiponectin, FABP4 and PPARγ, inflammatory proteins; IL-6, TNF-α and IL-10, and MCP-1 and HIF-1α were analysed in normoxic and hypoxic EVs using EV immunophenotyping. Europium was used as the assay reporter and was measured using time resolved fluorescence (TRF). Data are presented in arbitrary TRF units, *$p<0.05$ (n=3).

5.4 Discussion

5.4.1 Key findings

1. Hypoxia (1-21% O_2) had no effect on adipocyte number or viability.
   a. Cells in 1% O_2 had an altered morphology but their lipid storage was unchanged.
2. EV production is increased in hypoxia (1% O_2), particularly EVs <200 nm.
3. Hypoxia (1% O_2) increased cellular annexin V positivity, EVs from 5% O_2 cells were less annexin V positive than controls.
4. Fatty acid composition was affected by hypoxia with similar compositional changes in cells and EVs.
5. Apportion and fatty acid composition of phospholipids was effected by hypoxia in cells and EVs.
6. Cellular expression of PPARγ and HIF-1α were altered by hypoxia.
7. MCP-1 was increased in hypoxic EVs.

5.4.2 Main discussion

Obesity is associated with local inflammation in AT and increases in circulating inflammatory makers, both of which increase the risk of cardiovascular co-morbidities (352). Obese AT is prone to hypoxic areas which leads to a functional reprogramming of endocrine and metabolic processes within AT and results in AT inflammation (**Figure 1.2.6**). EV release is also increased during hypoxic conditions and functional studies have shown hypoxic EVs may enhance disease pathology. Therefore, EVs released from hypoxic adipocytes may initiate or enhance the shift towards inflamed adipocytes which are associated with an increased cardiovascular risk. This chapter sought to characterise the effects of O_2 on adipocyte EV release.

The actual concentration of O_2 surrounding adipocytes *in vivo* is unknown, largely due to the complexity and diversity of AT between individuals. The most recent estimation of AT pO_2 is between 3 and 11% (365) though values vary greatly between studies. A major reason for the observed differences in reported pO_2 values

may be due to the use of different techniques to measure AT oxygenation (see *Chapter 1.2.6*). Furthermore, the majority of techniques used to measure AT pO_2 are probe-based meaning O_2 is only measured in a specific part of the tissue so the reading may not represent that of the whole tissue. Therefore in this chapter, 3T3-L1 adipocytes were incubated at a range of different O_2 levels (1% to 21%) for 24 hours to compare differences in both the cells and the EVs following this period, but also to establish a pathologically relevant "hypoxic" condition for 3T3-L1 adipocytes. Morphology, cell number and viability were unchanged between different O_2 conditions, though 1% O_2 cells bore more of a resemblance to preadipocytes. Lipid droplet accumulation has been shown to be reduced in 3T3-L1 adipocytes incubated in 5% O_2 (for 1 week) due to increased lipolysis (467). Mobilisation of FFAs is increased in hypoxic adipocytes (368,467) and in obesity (468,469). Oil Red O staining of 1% O_2 cells showed no difference compared to normoxic cells, though this technique may not be sensitive enough to detect more subtle metabolic changes (470).

Previous studies have shown increased concentrations of EVs in hypoxia in: cancer cell lines (241,463,471); endothelial cells (472); and increased exosomal protein content of placental- (473) and adipocyte-derived EVs (390) from hypoxia. Data presented in this chapter are in agreement with these studies. A significant elevation in adipocyte-derived EV concentration was observed only in 1% O_2, with no difference in overall mode size compared to normoxic controls. Interestingly, when EV concentrations were plotted in 50 nm bin-widths, this increase in 1% O_2 samples was shown to be attributable to EVs in the range of 50 – 200 nm. Also EVs from 2% O_2 samples were increased in the range of 100 – 200 nm compared to normoxia. This suggests a propensity for hypoxia to induce secretion of exosomes and small microvesicles in adipocytes which has been previously attributed (in part) to HIF-1α. Silencing of HIF-1α abates the hypoxia-induced increase in EV production in breast cancer cells (463) though the exact mechanisms through which this occurs and whether other transcription factors are involved are unknown. Hypoxia may induce a stress response (perhaps via HIF-1α) causing alterations in plasma membrane lipids and receptors. Such alterations may lead to an endocytic remodelling of the plasma membrane which may in turn favour an increase in EV formation (474). Indeed,

induction of HIF-1α has been shown to activate reorganisation of the actin cytoskeleton (475); a key requirement for EV formation (476).

Plasma membrane remodelling during hypoxia may also lead to changes in phospholipid distribution across the plasma membrane. Reorganisation of the normal phospholipid asymmetry is thought to be a precursory event in EV generation, primarily though the externalisation of PS. To assess this, hypoxic (1-21% O_2) and normoxic cells and EVs were analysed for their annexin V positivity, a measure of PS exposure. Unfortunately, there was great variation in the reported baseline annexin V positivity of cells and EVs between hypoxic experiments, therefore hypoxic samples were expressed as a delta change from normoxic annexin V positivity for a given experiment. Cells from 1% O_2 were significantly more annexin V positive than normoxic cells. This is in keeping with hypoxia increasing exposure of PS on the outer leaflet of the plasma membrane as a precursor to increased EV generation. Interestingly, there was no change in the annexin V positivity of 1% O_2 EVs compared to normoxic controls. As discussed in *Chapter 4*, the PS exposure of EVs is often used as an indicator of the procoagulant potential of EVs which is unlikely to be an important feature of adipocyte-derived EVs. Furthermore, the increased PS positivity of 1% O_2 cells may serve as a reservoir for increased EV generation and therefore the concentration of EVs increases but the annexin V positivity of individual EVs remains the same. The annexin V positivity of 5% O_2 EV was significantly reduced compared to normoxic EVs indicating exposed PS was reduced in 5% O_2 EVs. However, the raw percentage of annexin V positivity (**Figure 5.3.6 A**) shows great deviation between 5% EV replicates, meaning the data are likely to be skewed by an outlier. Therefore, greater 'n' numbers may be required to ensure this reduction is real.

Lipids play fundamental roles in forming energy reserves and in maintaining cell and organelle structure, though they are often overlooked as potential signalling mediators. It is estimated that up to two-thirds of the EV volume is composed of lipids (78), indicating an important role for lipids in EV function. Here, the fatty acid composition of normoxic and hypoxic (1-21% O_2) cells and EVs was analysed to

evaluate potential functional changes. No changes were observed in overall fatty acid concentration between hypoxic and normoxic cells and EVs. Fatty acid concentration of 1% O_2 cells was reduced compared to normoxic cells though this was not significant. This is in agreement with morphological data of 1% O_2 cells which looked to have reduced lipid droplet accumulation, though no difference was observed in Oil Red O staining. GC-FID is a more sensitive assessment of the presence of lipids than Oil Red O staining which may account for difference between the two techniques.

Analysis of individual fatty acids revealed compositional differences in four fatty acids between normoxic and hypoxic EVs. Palmitic acid was increased in hypoxic cells compared to normoxic cells. Palmitic acid is a major storage fatty acid (439) however, lipid storage (as indicated by total fatty acid concentration and Oil Red O staining) was not different between normoxic and hypoxic cells. Diets enriched in SFAs promote ectopic lipid storage, increase mean adipocyte size, and promote adipose tissue inflammation (477). Here both stearic acid and SFAs overall were increased in lower O_2 conditions (<2% O_2) perhaps indicating a shift towards dysfunction compared to normoxic cells. Conversely, MUFAs as a whole, including palmitoleic acid were decreased in hypoxic cells. Palmitoleic acid has been shown to have beneficial effects on glucose metabolism in adipocytes compared to palmitic acid (478). Therefore glucose metabolism in lower O_2 conditions may be impaired due to a decreased abundance of palmitoleic acid. A simultaneous increase in SFAs and decrease in MUFAs in hypoxia may be due to reduced activity of stearoyl-CoA desaturase enzymes which require O_2 to desaturate SFAs to MUFAs (479). Interestingly, the MUFA oleic acid was upregulated in 2% O_2 cells. Oleic acid has been shown to improve IR and have anti-inflammatory effects (480) suggesting the negative effects of lower O_2 may be abrogated slightly in 2% O_2 cells.

The same four fatty acids were altered in EVs with hypoxia though the effects were not always the same as in the cell of origin. Palmitic acid was increased and palmitoleic acid was decreased in 1% O_2 EVs compared to normoxia, largely reflecting 1% O_2 cells. Oleic acid was increased in 1% O_2 EVs, however, suggesting EVs may reflect the fatty acid profile of the cell to some extent, but also possess unique differences. The enrichment of oleic acid in 1% O_2 EVs may help to

counteract the potential negative effects of palmitic acid in EVs. Intriguingly, when the fatty acid composition of 1% O_2 EVs was compared directly with 1% O_2 cells, a number of compositional differences were observed. Hypoxic EVs (1% O_2) were preferentially enriched in SFAs and less abundant in MUFAs than 1% O_2 cells. In tumour cells, increased SFAs in hypoxia were shown to promote stress of the endoplasmic reticulum (ER) (479), suggesting hypoxic EVs may be more potent at inducing ER stress. Furthermore, hypoxic EVs were richer in PUFAs compared to hypoxic cells, particularly arachidonic acid and α-linolenic acid. This suggests that hypoxic EVs harbour greater signalling potential compared to their corresponding cells as arachidonic acid and α-linolenic acid are precursors for eicosanoid signalling molecules (445,481). Additionally, α-linolenic acid can also induce PAI-1 expression, an adipokine with connotations in the development of inflammatory AT (482,483). However, α-linolenic acid is an ω-3 fatty acid, and is generally regarded as anti-inflammatory (484). Together, the results confirm that EVs are specifically packaged with a particular cargo and do not merely reflect uptake of the cellular milieu.

Phospholipids form the structural basis of cell membranes, providing a permeability barrier but also a source of bioactive fatty acids (485). Two-dimensional TLC was used to identify the major phospholipid groups followed by GC to characterise individual fatty acids within each phospholipid group in normoxic and hypoxic cells and EVs. No changes were observed in the proportions of phospholipids between normoxic and hypoxic cells. One may have expected an increased proportion of PS in hypoxic cells given their increased annexin V positivity. However, annexin V positivity is a measure of the external exposure of PS whereas TLC with GC-FID measures the total proportion of PS in the phospholipid membranes of the cell. Therefore, externalisation of PS may be higher in hypoxic cells but the overall proportion of cellular PS is not changed from normoxia. EVs showed a number of proportional changes in phospholipids between normoxia and hypoxia which are discussed below with respect to changes in individual fatty acids.

Across all phospholipid samples measured, the most abundant fatty acids were usually palmitic acid, palmitoleic acid and stearic acid and hence overall, SFAs and

MUFAs were the dominant classes of lipids. This is likely due to their roles in membrane structure as SFAs maintain structural rigidity of membranes (439) whilst MUFAs add flexibility to preserve membrane dynamics. Again, as noted in *Chapter 4*, EVs contained a higher composition of PUFAs compared to cells. PUFAs can be used to generate eicosanoids such as arachidonic acid that can go on to activate a number of signalling pathways. Indeed, arachidonic acid was also enriched in EVs, particularly hypoxic EVs, suggesting EVs may be equipped with a greater cargo of signalling fatty acids compared to cells and normoxic EVs.

PE and PC were the dominant phospholipids detected in both cells and EVs, as reported in *Chapter 4* and elsewhere (442,443). The proportion of PE was reduced in hypoxic EVs despite no change in cellular PE. PE and PS are known to be co-regulated (486) so perhaps the increase in PS in hypoxic EVs caused a concurrent decrease in PE.

Sphingomyelin, a major structural lipid and component of plasma membrane lipid rafts, was reduced in hypoxic EVs. Reduced sphingomyelin content has previously been shown to enhance insulin sensitivity in cells (487). Impaired insulin sensitivity is a hallmark of obesity and related disorders, therefore hypoxic EVs may have a reduced sphingomyelin content in an attempt to maintain insulin sensitivity in deteriorating AT. As in *Chapter 4*, sphingomyelin samples contained high proportions of SFAs which may contribute to the structural role of sphingomyelin. Sphingomyelin is also known to be required for exosome secretion by providing the required lipids for ceramide production (25). Unfortunately, ceramide content of EVs was not measured here, though the proportion of sphingomyelin was reduced in hypoxic EVs, perhaps indicating an increased conversion to ceramide in order to generate the increased concentration of EVs observed in hypoxia.

The mitochondrial phospholipid, cardiolipin, was found to be present in all samples, and was decreased in hypoxic EVs. A previous study found no change in the proportion of cardiolipin between normoxic and hypoxic prostate cancer cells (488). Though the proportion of cardiolipin was not changed between normoxic and hypoxic cells, the fatty acid composition was very different. Cardiolipin in normoxic cells was rich in MUFAs whilst hypoxia cells were rich in SFAs. A greater degree of unsaturated fatty acids is associated with an increased interaction with cytosolic

proteins such as FABP4 (448). Therefore, the increased saturation of fatty acids in hypoxic cells may impair their ability to interact with cytosolic proteins such as FABP4. Despite being a mitochondrial-associated phospholipid, cardiolipin was detected in both normoxic and hypoxic EVs. This may be due to experimental error when scraping TLC plates for GC as cardiolipin is close to PE after separation (**Figure 2.5**), perhaps resulting in PE contamination. However, the profiles of fatty acids of cardiolipin in EVs detected are very different to those detected in PE in EVs, arguing against significant PE contamination. Profiles of fatty acids in EVs were also similar to those of cells, suggesting EVs contain cardiolipin in a similar composition to that of the cell.

As discussed before, PS is predominantly distributed on the inner leaflet of the plasma membrane. The anionic nature of PS allows it to serve as a point of initiation for intracellular signalling cascades for second messengers such as protein kinase C (449,450). PS was increased in hypoxic EVs, again suggesting that hypoxic EVs have an increased signalling capacity compared to normoxic EVs. Normoxic EVs had a higher composition of α-linolenic acid compared to hypoxic EVs in PS, but also in the majority of other phospholipids. α-linolenic acid has been shown to be important in normal adipocyte functioning (440) and may have anti-inflammatory effects (484), suggesting that a reduced amount (as in hypoxic EVs) may be detrimental to the recipient adipocytes.

Adipocytes are known to synthesise and secrete an array of adipokines, many of which are dysregulated in obese AT. Here, a selection of adipocyte, hypoxia-associated, and inflammatory proteins were analysed in cells and EVs to determine differences between normoxia and hypoxia. Cell lysates were analysed using Western blotting and compared using optical density of bands relative to that of β-actin. EVs were analysed using an immunophenotyping method, described in *Chapter 4*.

Of the three adipocyte proteins analysed, cellular levels of FABP4 appeared to be increased by hypoxia whilst adiponectin showed a slight reduction and PPARγ was significantly reduced. No changes were observed in EV adipocyte proteins between normoxia and hypoxia. FABP4 expression is abundant in AT due to its role in

shuttling fatty acids and lipid molecules around and between cells (455). However, FABP4 has been implicated in a number of obesity-related pathologies such as heart disease (489), metabolic syndrome (349) and atherosclerosis (490). Indeed, mouse models have illustrated that silencing FABP4 prevents mice from developing IR (324) and can ameliorate the symptoms of type 2 diabetes and atherosclerosis (350). Here, hypoxia looked to increase cellular protein expression of FABP4 despite previous studies indicating a reduction in FABP4 expression in hypoxic adipocytes (491,492). However, these studies measured the mRNA levels of FABP4 which were not monitored here. The apparent increase in cellular FABP4 here is likely due to decreased β-actin content in hypoxic cells probed for FABP4. β-actin was not shown to be different in other Western blots, suggesting a slight discrepancy in the β-actin result of the FABP4 blot. Vesicular FABP4 content was not changed between normoxic and hypoxic cells, indicating no effect of hypoxia on EV FABP4 content.

The nuclear receptor PPARγ is required for both the induction and maintenance of adipogenesis (320). Previous studies have shown that hypoxia blunts preadipocyte differentiation through inhibition of PPARγ gene expression, and levels of PPARγ mRNA are lower in hypoxic adipocytes (371,381). Here, PPARγ protein expression was significantly reduced in hypoxic adipocytes, suggesting hypoxia effects PPARγ expression at both the gene and protein level. PPARγ content of hypoxic EVs, however, was not different to normoxic EVs suggesting this change in PPARγ expression was not passed on to the EV.

Adiponectin is an adipokine that can be detected in the circulation with metabolic and anti-inflammatory properties (371). Circulating adiponectin levels of obese subjects have been shown to be lower than those of healthy subjects (493) suggesting a role for adiponectin in physiological AT function. Cellular adiponectin expression was decreased in hypoxic cells though this was not significant. Previous studies have found that hypoxia reduces adiponectin mRNA expression through negative regulation of the adiponectin promoter (371). Adiponectin content of EVs was not different between normoxia and hypoxic EVs again suggesting this change in adipocyte protein expression was exclusive to the cell.

Of the inflammatory markers measured in cell lysates, no changes were observed in TNF-α or IL-10 between normoxia and hypoxia, and IL-6 could not be detected. No

changes were observed in the EV protein content of TNF-α, IL-6 or IL-10 between normoxia and hypoxia. The systemic inflammation in obesity is characterised by elevated circulating levels of IL-6 and TNF-α (364) and levels of IL-6 and TNF-α mRNA have been shown to be elevated in hypoxic adipocytes (380). The latter study also conducted a time-course of expression of inflammatory genes showing that upregulation of TNF-α mRNA is transitory, peaking at 2 hours incubation in hypoxia then returning to normoxic levels by 4 hours. Therefore, the hypoxia-induced increase in TNF-α may have been missed in the experiments conducted as part of this thesis due to the 24 hour incubation time. Wang et al., also showed that IL-6 mRNA expression reached a peak at 24 hours in hypoxia (380) though here cellular IL-6 protein expression could not be detected after 24 hours in hypoxia. IL-6 is often secreted into the supernatant or extracellular space, so if the protein expression did indeed change, this protein may have been secreted from the cell without changing the intracellular levels. Indeed, hypoxia has previously been shown to induce IL-6 and TNF-α secretion into 3T3-L1 supernatants (494). Perhaps the same is also true for IL-10, an anti-inflammatory adipokine, which showed no change in cellular protein expression following hypoxia. IL-10 has previously been detected in 3T3-L1 supernatants (495), suggesting the majority of these cytokines may be secreted. IL-6, TNF-α and IL-10 were detected in EVs but no changes were observed between normoxia and hypoxia suggesting that hypoxic EVs do not have an altered inflammatory protein profile to normoxic EVs.

Hypoxia in any cell type is usually characterised by an elevated expression of HIF-1α, a transcription factor which regulates the cellular response to hypoxia. In fact, HIF-1α is thought to inhibit the gene expression of PPARγ and adiponectin (369) which may explain the reduced level of PPARγ and the non-significant reduction in adiponectin here in hypoxic adipocytes. Cellular levels of HIF-1α were significantly increased in hypoxic cells, confirming hypoxia at the molecular level and in keeping with previous *in vitro* hypoxia studies. Furthermore, HIF-1α expression is increased in obese mouse (369) and human AT (370), confirming both a role for HIF-1α in the adipocyte response to hypoxia, and also the presence of hypoxia in AT. No change was observed in HIF-1α content of EVs; however, recent data from our lab suggests that increased EV release from endothelial cells in hypoxia may, in part, be mediated by HIF-1α.

Adipocyte hypoxia is thought to stimulate the activation and migration of tissue-resident and distal Mϕ towards the site of hypoxia where they become proinflammatory and create AT dysfunction (**Figure 1.2.6**). MCP-1 is a protein secreted from a number of cell types (including adipocytes) to stimulate recruitment of monocytes and T cells. Cellular MCP-1 mRNA and secretory protein has previously been shown to be elevated in hypoxic adipocytes and was subsequently shown to be responsible for Mϕ recruitment to hypoxic adipocytes (494). Here, cellular MCP-1 protein showed no change between normoxia and hypoxia, though again, this may be because the majority of MCP-1 is secreted from the cell into the surrounding milieu. Interestingly, levels of MCP-1 were increased in hypoxic EVs, suggesting that hypoxic vesicles have an increased capacity to drive Mϕ migration.

5.4.3 Limitations

Many of the same limitations outlined in *Chapter 4.4.3* apply to this chapter including the use of 3T3-L1 cells to study adipocyte EVs, the differential ultracentrifugation protocol to isolate EVs, the use of FC to assess the annexin V positivity of EVs, and the use of serum-free media for EV isolation.

A hypoxic chamber was used to control O_2 levels, meaning only one hypoxic condition could be analysed at a time. Therefore different O_2 conditions were conducted as individual experiments with their own normoxic controls so that comparisons could be made between experiments. Variation was observed between different hypoxic experiments meaning some data had to be expressed as a change from the respective control. However, great care was taken to ensure consistency was maintained between experiments to minimise potential variation.

The duration of the hypoxic challenge used in this study was 24 hours in serum-free media. Proteins such as TNF- α have a rapid response to hypoxia (<2 hours) (380) meaning peaks in protein expression may have returned to baseline by 24 hours. However, 24 hour incubation was required to ensure adequate EV generation for subsequent analyses. Future experiments could look to analyse changes in cellular and EV protein over a series of time points in order to capture the full spectrum of changes. Other studies have also observed changes in mRNA expression with hypoxia. These could also be analysed in EVs to see whether functional changes in mRNA in hypoxic adipocytes are incorporated into hypoxic vesicles. Immunophenotyping in this chapter was conducted slightly differently to that described in *Chapter 4* in an attempt to reduce the previous limitations. However, the concentration of EVs used per well was based on pilot data from endothelial EVs, which may possess different characteristics to adipocyte-derived EVs; therefore EV immunophenotyping data should be validated using Western blotting.

The increased exposure of PS measured in 1% O_2 cells could be inferred as hypoxia-induced is induced apoptosis in these cells. Apoptosis also causes PS externalisation and release of apoptotic bodies (which are included in by many in the EV field as EVs, though they often form vesicles > 1μm) (17). However, the overall viability of 1% O_2 cells was not affected and the hypoxia-induced increase in EV concentration was observed in the exosomal and smaller microvesicle range. This suggests that 1%

O_2 presented a genuine hypoxic challenge that did not induce apoptosis, and release of apoptotic bodies was not responsible for the observed increase in EV release. To completely confirm this however, propidium iodide could be used in combination with annexin V to fully assess the apoptotic state of adipocytes using FC.

Finally, "normoxia" in this thesis refers to a standard cell culture incubator which provides cells with a gas mixture of 95% air and 5% CO_2. As previously described, the actual pO_2 of adipocytes and AT is unknown, but is estimated to be 3-11% O_2 (365). Therefore a "normoxic" condition of 95% air (containing 21% O_2) may provide slightly hyperoxic conditions to adipocytes. However, AT pO_2 measurement is extremely difficult and is often representative of the area surrounding the oxygen probe, meaning measurements are only reflective of small sections of tissue. Until more accurate measurements of adipocyte and AT pO_2 are published, the most sensible option for normoxic conditions seems to be cell culture incubators.

5.4.4 Conclusions

In summary, hypoxia significantly affected the production of adipocyte-derived EVs, particularly at 1% O_2. Hypoxic cells released a greater overall concentration of EVs (predominantly exosomes and small microvesicles). These hypoxic EVs were equipped with fatty acids associated with negative effects on adipocyte function, and a change in phospholipid fatty acids that is suggestive of an increased signalling potential. Hypoxia seemed to interfere with specific aspects of adipocyte functioning such as regulation of adipokine production and lipid droplet storage. Hypoxic EVs were also enriched with MCP-1 suggesting these EVs may facilitate the recruitment of Mϕ to hypoxic adipocytes thereby promoting a proinflammatory, hypoxic environment. Therefore, hypoxic EVs may assist the progression of adipocyte dysfunction in hypoxia. Future studies should look to further characterise these EVs for functional changes in mRNA and microRNA expression and determine whether these EVs can have a detrimental effect on adipocytes and other cells resident in AT such as Mϕ and endothelial cells.

6. Results IV:

The effects of hypoxic adipocyte-derived extracellular vesicles on macrophage function

6. Perspective

Having shown that hypoxia could increase the concentration and change the characteristics of EVs released from adipocytes in *Chapter 5*, I wanted to test whether this translated into differential functionality. Therefore, this chapter examines the potential effects of hypoxic EVs on Mφ phenotype and migration. Unfortunately due to logistical problems and practical issues with establishing the model system at the laboratory of a collaborator, experimental repetitions could not be completed in time and thus data presented in this chapter present beginnings of work that is on-going.

6.1 Introduction

As discussed in *Chapters 1 & 5*, obesity is complex condition associated with a variety of comorbidities and diseases such as CVD, T2D, metabolic syndrome, cancer and many others (496–498). Obesity is also characterised by a low grade of systemic inflammation and inflamed AT (352) though the sequence of events leading to obesity-associated inflammation are unknown. Hypoxia, caused by expanding AT, is one possible initiator of the production of localised and circulating proinflammatory factors by adipocytes and AT-resident Mϕ (352,371,460,461). *Chapter 5* illustrated how hypoxic conditions can enhance EV release, suggesting hypoxic adipocyte-derived EVs could have a part to play in the initiation of inflammation induced by hypoxia.

Tissue resident Mϕ are highly heterogeneous (499) and are found in a variety of tissues including the liver, kidneys, bone, the central nervous system and AT (500). As well as tissue specific functions, tissue-resident Mϕ are important regulators of innate immunity as they are able to phagocytose foreign and necrotic material and initiate the recruitment of additional Mϕ and leukocytes (501). However, a specific role for Mϕ in AT has not been identified. The heterogeneity of Mϕ allows their phenotype to be influenced by the tissue microenvironment. Changes in Mϕ phenotype generally follow two lines of polarisation: M1 and M2 (499). Proinflammatory mediators such as lipopolysaccharide and interferon-γ induce polarisation towards a classically activated (M1) phenotype which further promotes a proinflammatory environment through the production of cytokines such as TNFα, IL-1β and IL-6 (338,502). Alternatively activated (M2) Mϕ are produced in response to anti-inflammatory stimuli such as IL-4, and promote an anti-inflammatory phenotype through increased generation of IL-10, IL-1 receptor antagonist (IL-1Ra) and dectin-1 (338,503,504). Mϕ in lean AT are predominantly of an M2 phenotype, whereas Mϕ in obese AT are of an M1 phenotype (**Figure 1.2.5**) (338,502). High-fat feeding of mice has been shown to induce a phenotypic shift in polarisation of AT Mϕ from an anti-inflammatory M2 state to a pro-inflammatory M1 phenotype (338). Furthermore, the production of proinflammatory cytokines such as TNFα and IL-6 by M1 Mϕ in obese AT can inhibit insulin signalling within adipocytes, contributing to the emergence of IR (460).

In addition to an altered phenotype of tissue-resident Mϕ, obese AT is also infiltrated by increased numbers of Mϕ (460,500,505), though the mechanism by which this occurs is unknown. Mϕ within obese AT often form crown-like structures (CLSs), surrounding necrotic and apoptotic adipocytes (506). CLSs in obese AT have also been found in association with hypoxia (507), suggesting a link between hypoxia and the infiltration of Mϕ (**Figure 1.2.6**). Hypoxia is likely to induce activation of adipocytes and eventually apoptosis and necrosis if the hypoxia persists or remains unresolved (e.g. by new blood vessel growth). *Chapter 5* illustrated how hypoxia (1% O_2) induced the release of EVs from adipocytes that were enriched in MCP-1 and pro-signalling fatty acids. Recently, Eguchi et al., demonstrated how adipocytes activated by palmitic acid produced microparticles that actively cause Mϕ migration *in vitro* and *in vivo* (48) highlighting the potential functional interactions of adipocyte EVs with Mϕ. Therefore, hypoxic adipocyte-EV release may cause recruitment of Mϕ to hypoxic AT which may further exacerbate the hypoxic/inflammatory environment and contribute to the development of obesity-associated inflammation.

6.1.1 Aims

This chapter aimed to compare the effects of normoxic and hypoxic adipocyte-derived EVs on:

- M1 Mϕ cytokine release
- M2 Mϕ gene expression markers
- Mϕ migration

6.1.2 Hypotheses

Hypoxic adipocyte-derived EVs may promote a proinflammatory phenotype in Mϕ by increasing M1 cytokine production, decreasing M2 gene expression and enhancing Mϕ migration. The release of EVs from hypoxic adipocytes may therefore contribute to the initiation of inflammation in obese AT.

6.2 Methods

6.2.1 3T3-L1 culture and extracellular vesicle isolation

3T3-L1 cells were cultured using T175 cm^2 flasks to a mature phenotype (14 days post-differentiation) as described in *Chapter 2.2*. Cells were then exposed to normoxic or hypoxic conditions as outlined in *Chapter 5.2.1*. Conditioned serum-free media for EV isolation was collected and processed as before (*Chapter 5.2.1*). The concentration of EV isolates was measured by NTA on the day of isolation and EVs were then stored as described in *Chapter 2.3.3*.

6.2.2 THP-1 phenotype assay

Human promyelocytic cells (THP-1) were cultured by Mr Nurudeen Hassan (Cardiff Metropolitan University) in RPMI 1640 (Gibco, UK) supplemented with 10% heat-inactivated FCS (Labtech International), 1% sodium pyruvate, 1% non-essential amino acids and 1% penicillin (100 IU/mL)/streptomycin (100 µg/mL, all given (v/v), Gibco). THP-1 were differentiated into Mϕ *in vitro* using 6 x 10^5 cells/mL treated with 8 nM phorbol-myristate-acetate (PMA; Sigma) for 48 hours. Differentiation was maintained using serum-free media without PMA for a further 48 hours. Normoxic or hypoxic EVs (100µL) were then added to cells in 6 well plates. Following a 24 hour incubation with EVs, cell supernatants were collected for assessment of classical M1 cytokine secretion by ELISA. Cells were then processed for RNA isolation and qPCR of classical M2 markers.

6.2.3 ELISA

Human TNF-α and IL-1β DuoSet® ELISA kits (R&D systems, UK) were used to quantify the release of M1 cytokines into cell supernatants following incubation with normoxic or hypoxic EVs. M1 cytokines were analysed by ELISA as they are more readily secreted compared to M2 cytokines. Assays were completed according the standard manufacturers protocol.

6.2.4 Quantitative reverse transcription PCR

RNA was isolated from Mϕ following incubation with EVs using TRI Reagent (Life Technologies, ThermoFisher, UK) according to the manufacturer's instructions. Isolated RNA was converted to cDNA using a High Capacity cDNA Reverse Transcription kit (Applied Biosystems, UK). M2 marker gene expression was then analysed using reverse transcription (RT)-PCR with Fast SYBR® Green and a Fast 7500 Real-Time PCR System (Applied Biosystems). Relative gene expression was compared to GAPDH and calculated using the comparative CT method ($2^{-\Delta\Delta CT}$). Primer sequences are given in **Appendix**: **Table VII**.

6.2.5 THP-1 migration assay

THP-1 cells for migration assays were cultured by Miss Parbata Chauhan (Aston University). A sterile glass coverslip (22 x 22 mm) was carefully added to each well of a 6 well plate and coated with poly-D-lysine hydrobromide solution (0.1 mg/mL in sterile water). THP-1 culture medium consisted of RPMI 1640 (Sigma, UK) supplemented with 10% (v/v) FCS, 2 mM L-glutamine, 100 µg/mL streptomycin and 100 IU/mL penicillin (all Gibco, UK). THP-1 cells (at a density of 4 x 10^5 cells) were stimulated with 100 nM 1,25-dihydroxvitamin 3 and added to each well containing a coverslip. Mϕ were then incubated for up to 3 days at 37°C and 5% CO_2.

Once the Mϕ had sufficiently adhered to the glass coverslips, the Dunn chamber (DCC100, Hawksley, UK) was prepared for the migration assay (**Figure 6.2.1 A**). Both inner and outer wells were filled with chemically defined Mϕ medium (Gibco, UK) and the glass coverslip was placed atop the Dunn chamber with the adhered Mϕ on the underside. The coverslip was then gently positioned to expose a small slit of the outer well and was fixed into place using candle wax. The outer well was drained of Mϕ medium using Whatman filter paper, and 100 µL of normoxic or hypoxic EVs was slowly introduced, avoiding any air bubbles. The outer well and edges of the coverslip were then completely sealed with candle wax and coated with Vaseline® petroleum jelly (Unilever, UK) to prevent air bubbles being introduced and drying out of the chamber.

The Dunn chamber was then placed under a Zeiss Axiovert 200 M fluorescent microscope (Carl Zeiss Ltd., UK) in a humidity-controlled sealed chamber that was preheated to 37°C. The microscope was focused over the bridge between wells (**Figure 6.2.1 B**) at 10X magnification for 2 hours, with an image being captured by a Hamamatsu Orca camera driven by Volocity™ (version 6.3, Perkin-Elmer, UK) every 10 minutes (eventually creating 13 frames).
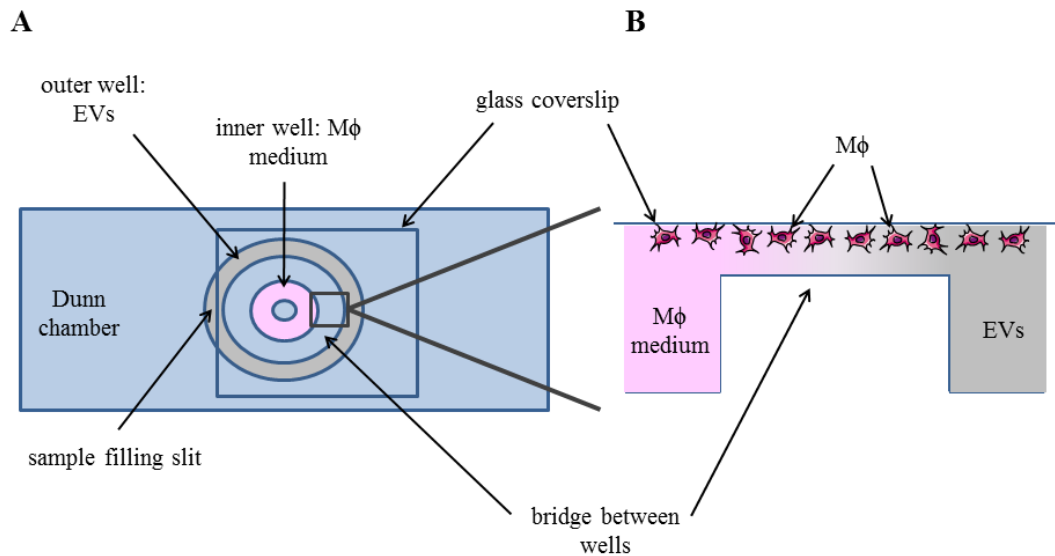
Figure 6.2.1: Mφ migration assay using a Dunn chamber. Schematic summarising the experimental theory of using a Dunn chamber to monitor Mφ migration. (**A**) Set-up of the Dunn chamber. A glass coverslip with Mφ adhered to the underside was positioned so that a small slit of the outer well was exposed allowing for draining and filling. The coverslip was secured in place using wax and the outer well was filled with 100 µL of normoxic or hypoxic EVs. The filling slit and the edges of the coverslip were then completely sealed with wax. (**B**) A cross-section of the Dunn chamber illustrates how Mφ adhered to the coverslip can migrate across the bridge between inner and outer wells, which is 20 µm in diameter.

Images collected over the course of the assay were then exported as stacked tagged image file format files, and imported into ImageJ software (version 1.49, National Institutes of Health, USA). Forty cells were individually tracked per sample using the "Manual Tracking" plugin (**Figure 6.2.2 A**). Tracks were then saved and imported into the Chemotaxis and Migration Tool plugin (Ibidi GmbH, Germany). Mφ migration was then plotted as illustrated in **Figure 6.2.2 B** (with Mφ beginning at the intersect and the hypothesised chemoattractant at the northern point). Mφ were then assessed for:

- Angle of migration
- Accumulated distance (cumulative distance migrated, µm)
- Euclidean distance (as the crow flies, µm)

- Directionality (Euclidean distance/accumulated distance): 0 (indirect) → 1 (direct)

- yFMI (forward migration index along the y axis/accumulated distance)

- Velocity (speed of migration, μm/sec).

A

B
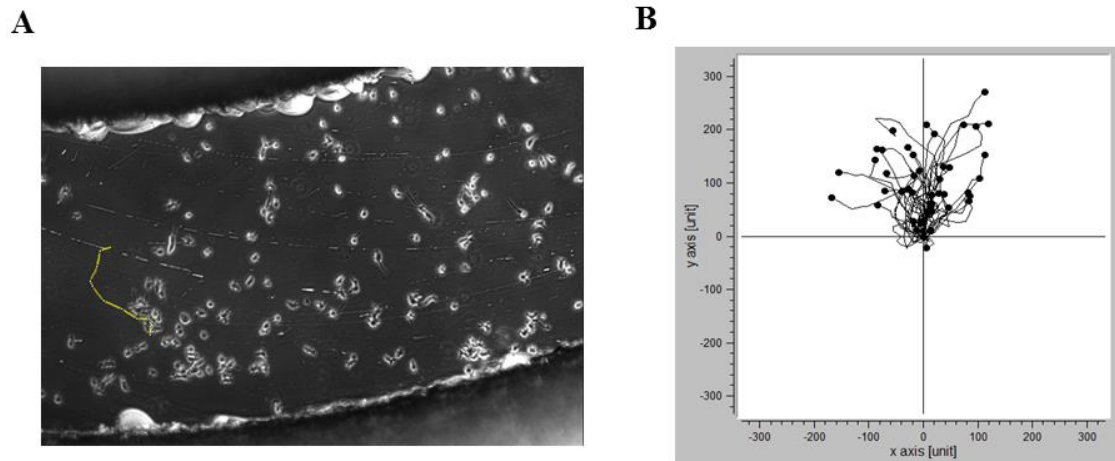
Figure 6.2.2: Tracking and analysis of Mϕ. Stacked images of Mϕ were manually tracked using ImageJ software and analysed using a chemotaxis and migration tool. (**A**) An example of the manual tracking of an individual Mϕ over 13 frames creating a path of migration (yellow). (**B**) An example plot of forty individual Mϕ tracks from which the overall migration of the sample is analysed by a series of parameters. The intersect marks the starting position of the cells and the northern point indicates the position of the hypothesised chemoattractant.

6.2.6 Statistical analysis

Data were analysed using GraphPad Prism software (version 6.0). Normoxic and hypoxic data were compared using an unpaired Students *t-test*, data are presented as mean ± SD (unless otherwise stated) and a *p* values of <0.05 was considered statistically significant.

6.3 Results

6.3.1 M1 cytokine secretion

The effect of normoxic and hypoxic adipocyte EVs on M1 cytokine secretion was measured by ELISA. No difference was observed in the secretion of IL-8 and TNF-α with incubation of normoxic or hypoxic EVs (IL-8: normoxia; 55.6 ± 14.8 pg/mL vs. hypoxia; 65.2 ± 8.7 pg/mL, **Figure 6.3.1 A**, TNF-α: normoxia; 9.5 ± 1.2 pg/mL vs. hypoxia; 10.7 ± 0.2 pg/mL, **Figure 6.3.1 B**). Mϕ secretion of IL-1β was reduced following incubation with hypoxic adipocyte EVs (normoxia; 2.4 ± 0.06 pg/mL vs. hypoxia; 1.0 ± 1.2 pg/mL, **Figure 6.3.1 C**).

6.3.2 M2 mRNA expression

The effect of normoxic and hypoxic EVs on M2 gene expression was measured using qRT-PCR. Mϕ expression of IL-10 and IL-1Ra were unchanged between incubations of normoxic or hypoxic EVs (IL-10: normoxia; 1.2 ± 0.3 fold change vs. hypoxia; 1.2 ± 0.1 fold change, **Figure 6.3.1 D**, IL-1Ra: normoxia; 1.4 ± 0.3 fold change vs. hypoxia; 1.3 ± 0.2 fold change, **Figure 6.3.1 E**). Expression of dectin-1 showed a slight increase following incubation with hypoxic EVs (normoxia; 0.9 ± 0.1 fold change vs. hypoxia; 1.3 ± 0.2 fold change, **Figure 6.3.1 F**).
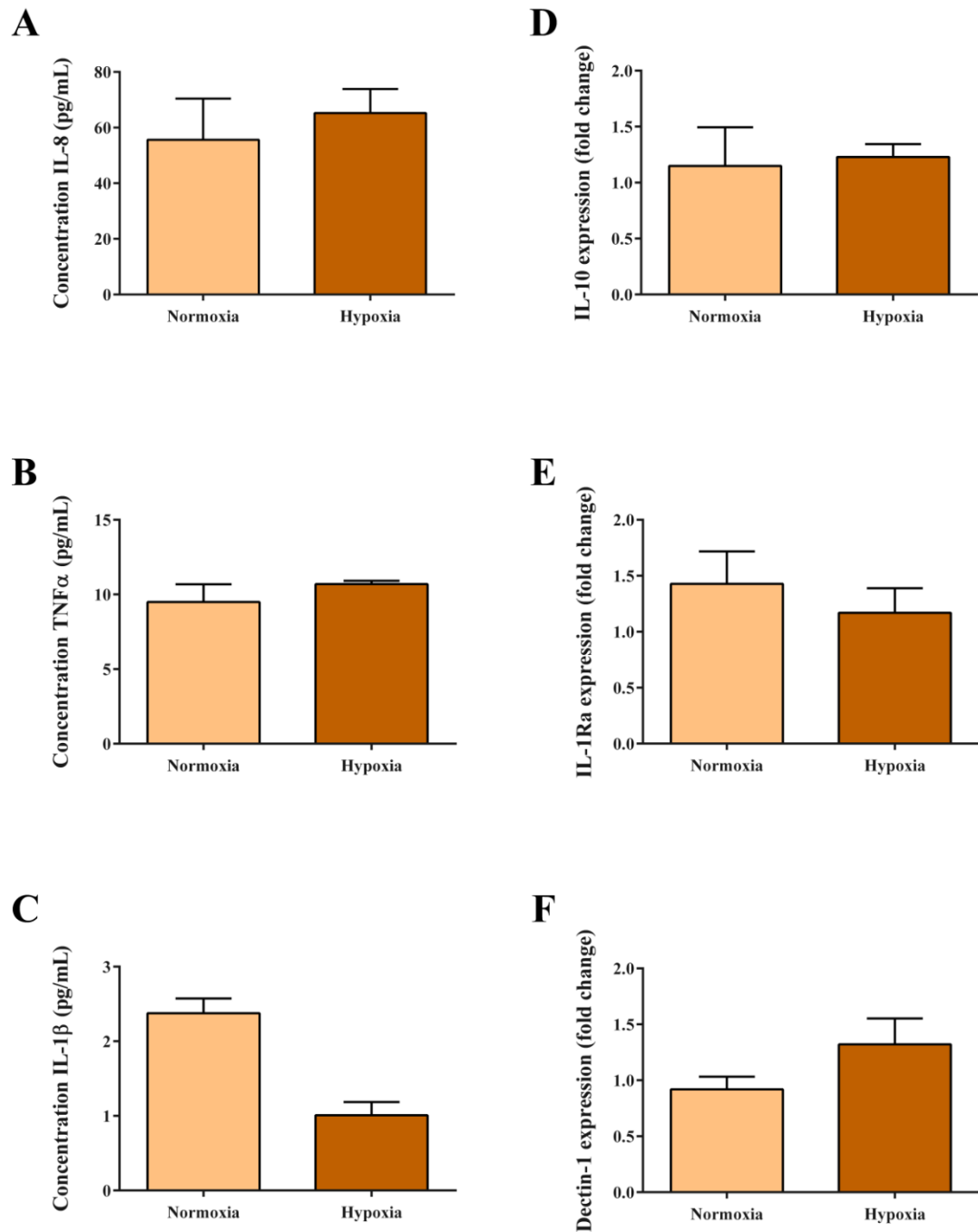
Figure 6.3.1: Effects of hypoxic adipocyte EVs on Mϕ phenotype. Alterations in the phenotypic characteristics of THP-1 Mϕ following incubation with normoxic or hypoxic 3T3-L1 adipocyte-derived EVs. Release of M1 cytokines including (**A**) IL-8, (**B**) TNF-α and (**C**) IL-1β (pg/mL) were measured by ELISA. Gene expression of M2 markers including (**D**) IL-10, (**E**) IL-1Ra and (**F**) Dectin-1 (fold change compared to GAPDH) were measured by qRT-PCR. Technical repeats (n=3), experimental repeats (n=1).

6.3.3 Mɸ migration

The migration of Mɸ towards normoxic and hypoxic vesicles was measured using a Dunn chamber. Of the parameters measured (**Figure 6.3.2**), the distance migrated (both accumulated and Euclidean) and the velocity of migration showed no difference between normoxic and hypoxic EVs (accumulated distance: normoxia; 189 ± 13.9 μm vs. hypoxia; 183.7 ± 19.8 μm, **Figure 6.3.2 B**, euclidean distance: normoxia; 105.6 ± 15.9 μm vs. hypoxia; 112.8 ± 23.9 μm, **Figure 6.3.2 C**, velocity: normoxia; 4.3 ± 0.9 μm/min vs. hypoxia; 4.5 ± 0.5 μm/min, **Figure 6.3.2 F**). There was a trend towards a decreased angle of migration (normoxia; 109.5 ± 20.2° vs. hypoxia; 91.2 ± 11.6°, **Figure 6.3.2 A**) and an increased directionality and yFMI (directionality: normoxia; 0.4 ± 0.1 a.u. vs. hypoxia; 0.6 ± 0.9 a.u., **Figure 6.3.2 D**, yFMI: normoxia; 0.3 ± 0.1 a.u. vs. hypoxia; 0.5 ± 0.1 a.u., **Figure 6.3.2 E**) towards hypoxic EVs compared to normoxic EVs.
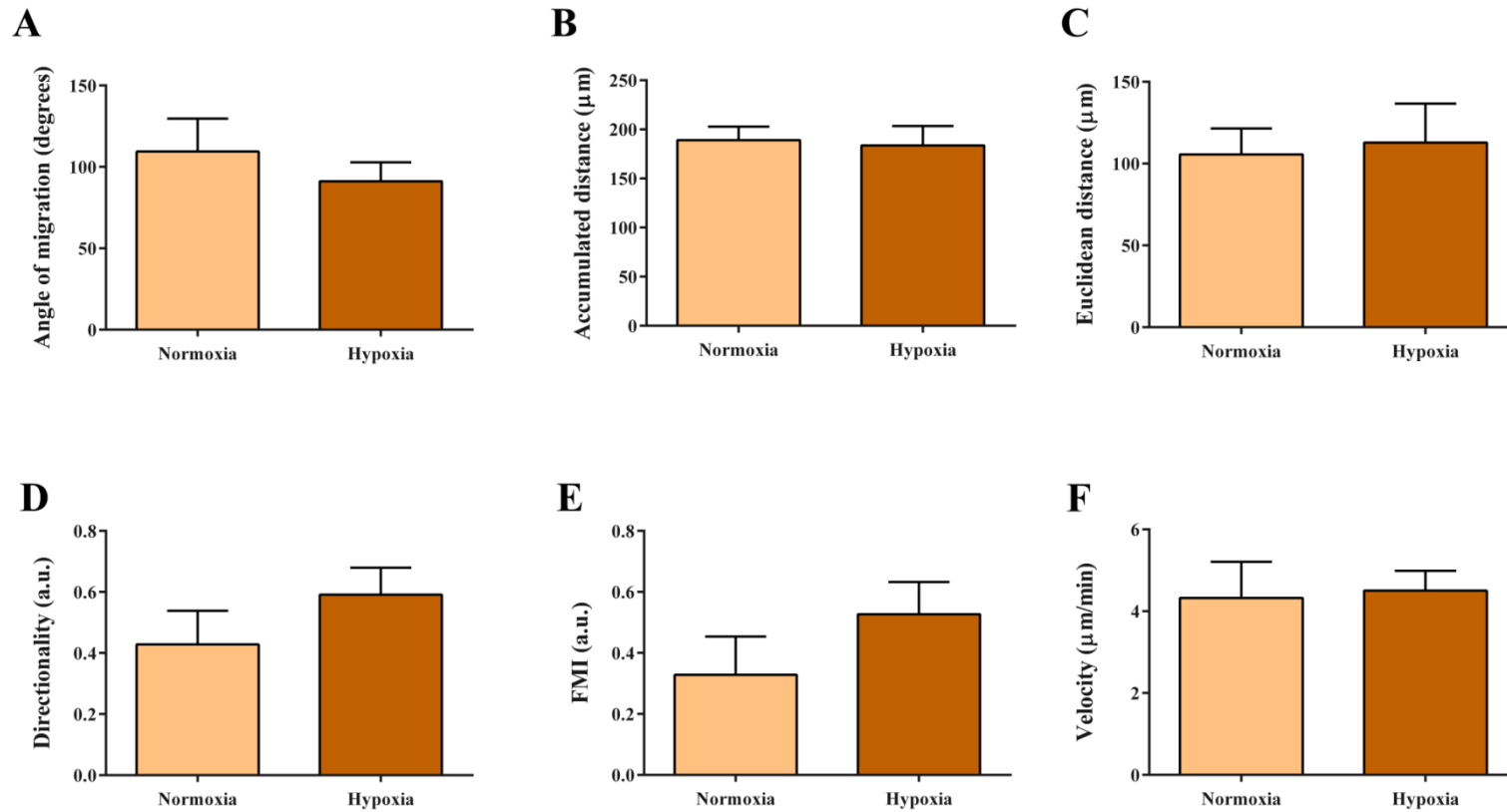
Figure 6.3.2: Mϕ migration towards adipocyte-derived EVs. The migration of THP-1 Mϕ towards normoxic and hypoxic adipocyte-derived EVs was measured using a Dunn chamber setup. Migration was assessed by (**A**) the angle of movement (degrees), (**B**) the accumulated distance (μm), (**C**) the Euclidean distance (μm), (**D**) directionality (a.u.), (**E**) the FMI (a.u.) and (**F**) velocity (μm/min). Technical repeats (n=3), experimental repeats (n=1).

6.4 Discussion

6.4.1 Key observations

The key observations of this chapter were:

1. Hypoxic EVs may reduce the secretion of the inflammatory M1 marker, IL-1β.
2. Hypoxic EVs may enhance the gene expression of the anti-inflammatory M2 marker, dectin-1.
3. Mφ may tend to migrate more efficiently towards hypoxic EVs.

6.4.2 Main discussion

Hypertrophy of adipocytes combined with a lack of supporting vascular growth in obesity highly increases the risk of localised hypoxia within AT (259,365). Alterations in adipocyte gene expression in response to hypoxia results in the release of an altered adipokine profile that promotes local inflammation, IR and Mφ infiltration (**Figure 1.2.6**). *Chapter 5* showed that hypoxic adipocytes also release an increased concentration of EVs that are enriched in MCP-1. Therefore, hypoxia may provide a mechanism for the onset of AT dysfunction that ultimately leads to local and systemic inflammation that is characteristic of obesity. This chapter sought to investigate whether hypoxic adipocyte-derived EVs may exacerbate this process by promoting the migration and phenotypic transition of Mφ.

Circulating monocytes and tissue-resident Mφ are highly plastic cells, capable of responding rapidly to changes in the microenvironment by altering their phenotype and thus their function (508). AT contains a variety of immune cells, the majority of which are M2 Mφ that help to maintain insulin sensitivity, glucose homeostasis and limit inflammation (337,508). An M2 phenotype is promoted in lean AT through the actions of IL-10 and PPARγ (338). However, expression of M2 polarising agents are reduced in obese AT and secretion of proinflammatory cytokines (such as IL-6 and TNF-α) from dysfunctional adipocytes is elevated, resulting in a phenotypic shift of AT-resident Mφ towards an M1 phenotype (338). As hypoxia may initiate dysregulated adipokine secretion and alter EV production from adipocytes, M1 and

M2 markers were measured using THP-1 Mϕ following incubation with normoxic and hypoxic 3T3-L1 adipocyte-derived EVs. The M1 Mϕ phenotype is very well defined and M1 cytokines are readily secreted. Therefore, M1 phenotype was measured using ELISA to assess the release of M1 cytokines into THP-1 supernatants. The pilot data presented here indicated that the secretion of M1 cytokines IL-8 and TNF-α is no different between normoxic and hypoxic adipocyte EV incubation. The secretion of IL-1β however is reduced following incubation of Mϕ with hypoxic EVs. Levels of IL-1β are increased in obese AT, most likely due to the predominance of M1 Mϕ, and levels of IL-1β correlate with IR (502). Therefore, a decrease in IL-1β secretion following incubation with hypoxic EVs suggests that these EVs may aim to attenuate the proinflammatory response and improve insulin signalling. TNF-α also plays an important role in regulating insulin sensitivity in obesity (259) and secretion of TNF-α was not reduced by hypoxic EVs, indicating the anti-inflammatory properties of hypoxic adipocyte EVs may act in a TNF-α-independent manner. In contrast to M1 Mϕ, the M2 Mϕ phenotype seems less well defined and may follow more of a continuum of multiple phenotypes with subtle changes in cytokine expression. Furthermore, markers of an M2 phenotype are not as widely secreted as M1 cytokines, therefore qRT-PCR was used to identify potential alterations in gene expression of classical M2 markers. Gene expression of IL-10 and IL-1Ra did not differ between normoxic and hypoxic adipocyte EV incubation. Previous studies have found IL-1Ra to be elevated in obese AT (509). As IL-1Ra is an endogenous antagonist of the proinflammatory cytokine, IL-1, this increase in obesity may be an attempt to combat the proinflammatory environment by blocking IL-1. Conversely, IL-10 expression is reduced in obese AT though expression of the IL-10 receptor is unchanged between lean and obese AT (338). Together, this suggests that obese AT attempts to maintain an anti-inflammatory environment but is eventually overwhelmed by proinflammatory cytokine expression. Dectin-1, a pattern recognition receptor expressed on the Mϕ cell surface, was slightly increased with hypoxic EV incubation compared to normoxic EVs. Previous studies have shown dectin-1 activation to lead to IL-10 mRNA expression (503) again suggesting the initial interaction of hypoxic adipocyte EVs with Mϕ may stimulate anti-inflammatory pathways.

In addition to a transition of AT-resident Mϕ towards a proinflammatory M1 phenotype in obese AT, the number of Mϕ present within AT is also increased (460,500,505), suggesting a higher rate of infiltration. Adipocyte-derived MCP-1 seems to play a critical role in the recruitment of Mϕ to obese AT and is also elevated in circulating plasma and AT of obese subjects (510). Interestingly, a recent study found that MCP-1 expression was partially controlled by specific microRNAs which are dysregulated in obese subjects leading to elevated Mϕ infiltration and AT inflammation (511). MCP-1 mRNA and secretory protein have previously been found to be elevated in hypoxic adipocytes (494), and analysis of the protein content of EVs in *Chapter 5* showed increases in MCP-1 protein in hypoxic EVs. Therefore, in addition to secreted MCP-1 protein, hypoxic adipocyte-derived EVs may also be capable of inducing Mϕ migration. Therefore, the ability of normoxic and hypoxic adipocyte EVs to stimulate THP-1 Mϕ migration was assessed using a Dunn chamber. No difference was observed in the distance (accumulated or euclidean) or the velocity of Mϕ movement between normoxic and hypoxic adipocyte EV. The angle of Mϕ movement was slightly reduced and the index of directionality was slightly increased with hypoxic EVs. Furthermore, the y fmi, which provides an indication of the efficiency of forward migration of cells along the y axis (**Figure 6.2.2 B**) showed a slight increase with hypoxic EVs. Together this suggests Mϕ may migrate more directly towards hypoxic EVs than towards normoxic EVs. Mϕ migration was recently shown to be enhanced by EVs derived from adipocytes stimulated with palmitic acid (48). FFAs such as palmitic acid are often released from apoptotic and necrotic adipocytes and are able to stimulate Mϕ migration in order to resolve the resultant lipotoxicity. Interestingly, palmitic acid content was increased in hypoxic cells and EVs (**Figure 5.3.8/9**), suggesting hypoxia may act upstream of adipocyte apoptosis and necrosis by altering fatty acid metabolism to increase reservoirs of chemotactic lipids. Therefore, hypoxic EVs may aid the progression of initial Mϕ migration into hypoxic AT, perhaps due to their increased cargo of MCP-1 and chemotactic fatty acids.

6.4.3 Limitations

The major limitation of this chapter is the lack of experimental repeats. Due to unforeseen circumstances, the remaining repeats could not be analysed in time for the submission of this thesis. It is however, anticipated that these data will be completed to form part of a paper on the effects of hypoxia on adipocyte-derived EVs and the potential influence on Mϕ migration and phenotype. The delay in sample processing has given me an opportunity to evaluate the experimental methodology and therefore, 2 alterations will be made to future experiments. Firstly, EVs will be added to Mϕ at set concentrations (5 x 10^9 and 1 x 10^{10} EVs and a 1:10 dilution of the EV resuspension) to determine whether the effects are concentration-dependent and/or whether any observed effects are due to changes in EV composition between normoxia and hypoxia. Secondly, chemotaxis experiments will be undertaken with a pre-incubation of EVs with Mϕ, and the migration towards a standard chemoattractant (such as MCP-1) monitored. The EVs themselves may not be strong chemoattractants, however, *in vivo*, these EVs may be able to enhance Mϕ migration into hypoxic AT.

Though MCP-1 was found to be increased in hypoxic EVs and is suspected to play a role in the potential chemotactic ability of hypoxic adipocyte-derived EVs, the role of MCP-1 was not assessed in these experiments. Future experiments could look to downregulate MCP-1 expression of adipocytes to see if phenotypic alterations and migratory ability of Mϕ are changed. However, it is also important to highlight that Mϕ infiltration of AT may not be solely due to increases in MCP-1 and that other factors may play a role. A recent study indicated that knockdown of MCP-1 only partially inhibited Mϕ infiltration into AT of mice fed a high fat diet (512), indicating a role for other adipocyte-derived chemoattractants.

A further limitation of this study may be the time point used for Mϕ supernatant collection for ELISA experiments. As outlined in *Chapter 5*, some cytokines such as TNF-α may have a more rapid response time, and therefore may have peaked and returned to baseline by the 24 hour measurement point. Therefore, future experiments may seek to analyse a range of time points in order to capture the spectrum of response.

Additionally, these pilot experiments have used 3T3-L1 adipocytes and THP-1 Mϕ which are well-established cell lines of adipocytes and monocytes/Mϕ respectively. In addition to these sources being cell-lines, they are also of differing origin, with 3T3-L1 cells being of murine origin and THP-1 cells being of human origin. Therefore there is a potential for sub-optimal interactions between these two cell lines due to species differences. However, it is hoped that these studies will provide important pilot data for our group that will be used to examine the interaction between human adipocytes and leukocytes in obesity.

6.4.4 Conclusions

To summarise, hypoxic adipocyte-derived EVs may enhance an M2 Mϕ phenotype by reducing IL-1β secretion and increasing dectin-1 expression. Furthermore, these hypoxic EVs may increase the directionality of Mϕ migration. Taken together, EVs derived from hypoxic adipocytes may initially intend to recruit Mϕ into hypoxic AT to resolve the consequences of adipocyte hypoxia (including adipocyte necrosis and lipotoxicity) by promoting an M2 phenotype. However, upon entering the hypoxic AT, the recruited Mϕ may be forced towards an M1 phenotype by the proinflammatory milieu generated by hypoxic adipocytes. Infiltrated Mϕ may then exacerbate AT inflammation by forming CLSs and adding to local secretion of proinflammatory cytokines which increase systemic inflammation and IR. Future studies should assess the ability of hypoxic adipocyte-derived EVs to stimulate Mϕ migration into AT *in vivo* and examine mechanisms to reduce this, such as inhibitors of EV biogenesis.

7. Results V:

Evidence for adipocyte-derived extracellular vesicles *in vivo*

7. Perspective

The overarching focus of this thesis was to characterise the release of EVs from adipocytes; thus, I sought to confirm their existence *in vivo*. The work in this chapter presents pilot data to show the presence of adipocyte markers in plasma-derived EVs using the variety of methods used to characterise adipocyte EVs in this thesis. Data in this chapter also formed the basis for a successful project grant application that is currently on-going and continuing on from this work.

7.1 Introduction

Chapter 1.2 details the importance of the autocrine, paracrine and endocrine actions of adipocytes and AT both in health and disease. As illustrated in *Chapters 4, 5 and 6* and by other researchers, adipocytes produce EVs *in vitro* (66,383,387,393). These EVs may facilitate differentiation of adipocytes (*Chapter* 4); are able to respond to conditions of hypoxia (*Chapter 5*) through interaction with Mϕ (*Chapter 6* and (48,306)); are able to affect metabolism of neighbouring adipocytes (387) and promote angiogenesis *in vivo* (393). Despite growing evidence for autocrine and paracrine roles of adipocyte-derived EVs, their potential endocrine roles *in vivo* remain largely unexplored. This may be due to a number of reasons. Firstly, although "adipocyte-specific" proteins exist (e.g. adiponectin and PPARγ2), these adipokines are secretory making it difficult to identify a specific marker for adipocyte-derived EVs. Secondly, adipocytes *in vivo* exist within AT, therefore presenting a number of barriers between adipocyte-derived EVs and the systemic circulation.

The initial hypothesis when undertaking this work was that adipocyte EVs could be identified in the circulation using adipocyte markers such as FABP4, PPARγ and adiponectin. During the course of undertaking this project, preliminary evidence has emerged for the presence of these adipocyte markers in plasma-derived EV fractions. FABP4-containing microvesicles in human plasma have been detected using FC (54). However, the use of FC for EV measurement is sub-optimal as the lower limit of many conventional flow cytometers is ~300 nm. Though FABP4 is largely generated in adipocytes, it is also expressed in Mϕ (513) and therefore should not be used in isolation to determine an adipocyte-derived EV population. Circulating levels of FABP4 correlate with IR and the metabolic dysfunction associated with obesity (324,348,349). Therefore, adipocyte EV-associated FABP4 may provide an important indication of the metabolic status of AT. Adiponectin has also been shown to be associated with exosomes isolated from mouse serum using Western blotting (514), though this has not been confirmed in human plasma-derived EVs. Adiponectin is specifically generated in adipocytes and is involved in maintaining insulin sensitivity and vascular function (319,328). Therefore, the presence of adiponectin in adipocyte EVs may provide a reflection of the physiological functioning of AT. Proteomic profiling of plasma-derived EVs also revealed an association of PPARγ with human plasma-derived exosomes (515). PPARγ is a

transcription factor predominantly produced in adipocytes with a critical role adipogenesis and maintaining adipocyte function (321). Therefore, similarly to adiponectin, detection of PPARγ in plasma-derived EV fractions could provide an indication of the regular functioning of AT. None of the above studies detecting adipocyte markers in plasma EVs measured the size or concentration of EVs to confirm an EV population, with the exception of Looze et al., who used TEM to confirm an EV population (515). Recently, it has also been suggested that adipocyte-specific material packaged within exosomes may circulate *in vivo* following transfer into leukocytes (516).

There is evidently great potential for an endocrine role of adipocyte-derived EVs *in vivo*. However, lack of specific markers and use of sub-optimal techniques has so far prevented confirmation of their existence in circulating plasma-EV fractions. Therefore, there is a need for comprehensive evidence for the existence of adipocyte-derived EV *in vivo* in order to further explore their potential as novel circulating communicators of adipocytes and AT *in vivo.*

7.1.1 Aims

This chapter aimed to detect adipocyte-derived EVs within the population of circulating EVs of healthy volunteers, specifically by:

1. Isolating and measuring the size and concentration of plasma-derived EVs.
2. Assessing isolated plasma-derived EVs for the presence of FABP4, adiponectin and PPARγ using:
    a. Western blotting
    b. Flow cytometry
    c. Time resolved fluorescence
3. Testing isolated leukocytes for the presence of adipocyte makers.

7.1.2 Hypotheses

Adipocyte-derived EVs can be detected in a population of circulating plasma-derived EVs using multiple adipocyte-markers and measurement techniques.

7.2 Methods

7.2.1 Cell culture and extracellular vesicle isolation

3T3-L1 cells were cultured to a mature adipocyte phenotype (14 days post-differentiation) as described in *Chapter 2.2.1*. EVs were isolated as described in *Chapter 2.3.1* using a 24 hour incubation with serum-free media and differential ultracentrifugation. Cells and isolated EVs were then lysed and processed to isolate protein as outlined in *Chapter 2.10.1* and stored at -20°C until analysis.

7.2.2 Plasma extracellular vesicle isolation

Plasma-derived EVs were isolated from the blood of healthy volunteers using the second isolation method outlined in *Chapter 2.3*.2. Isolated EVs were resuspended in either 1 X PBS (0.22 µm-filtered) for NTA measurements, FC analyses and TRF measurements, or lysis buffer for Western blotting.

7.2.3 Nanoparticle tracking analysis

Cell and plasma-derived EVs were quantified using NTA as described in *Chapter 2.4.2*. To compare the distribution of EVs between 3T3-L1- and plasma-derived EVs, the raw NTA distributions were plotted without adjusting for NTA dilution and ignoring differences in reported concentrations.

7.2.3 Leukocyte isolation

Blood (10 mL, collected as above) was gently transferred to a universal container containing 100 µL heparin sodium solution (5000 I.U./mL; Wockhardt Ltd). To this, 2.5 mL 6% (w/v) Dextran (Sigma Aldrich) was added, mixed gently by inversion and transferred to a fresh universal container to settle for ~45 minutes at room temperature. The "buffy coat" layer was carefully transferred to a fresh universal container and centrifuged (258 x *g*, 1 minute) to pellet leukocytes. Leukocytes were briefly resuspended in 1 mL distilled water to lyse any contaminating erythrocytes,

and then osmolarity was restored by adding 20 mL balanced salt solution (130 mM NaCl, 2.65 mM KCl, 8 mM Na_2HPO_4 adjusted to pH 7.4). Leukocytes were centrifuged (258 x *g*, 2 minutes) and resuspended in lysis buffer, processed and stored as outlined in *Chapter 2.10.1*.

7.2.4 Western Blotting

Western blotting was undertaken using protocols described in *Chapter 2.10*. Ten µg of cell lysate and 20 µg of EV lysate were loaded per well using running gels and primary antibodies outlined in **Table 7.2.1**. Two antibodies were required to detect both human (leukocytes/ plasma EVs) and mouse (3T3-L1 cells and EVs) adiponectin. Loading controls were not used as only the presence/lack of markers was being observed. However, for this reason, no comparisons between band densities should be made.

Antibody	Polyacrylamide running gel	Antibody dilution	Typical exposure
Adiponectin (Abcam ab18065)	12%	1:2500 (5% milk/TBS-T)	15 minutes
Adiponectin (CST #2789)	12%	1:500 (5% BSA/TBS-T)	1 minute
FABP4	15%	1:1000 (5% BSA/TBS-T)	15 seconds
PPARγ	10%	1:1000 (5% BSA/TBS-T)	1 minute

Table 7.2.1: Details of Western blotting. Details of the antibodies and polyacrylamide gels used for Western blotting. Two antibodies were required for detection of human (Abcam) and mouse (CST) adiponectin in leukocyte/plasma EV samples and 3T3-L1 samples respectively. BSA = bovine serum albumin, CST = Cell Signalling Technologies, FABP4 = fatty acid binding protein-4, PPARγ = peroxisome proliferator-activated receptor γ, TBS-T = tris-buffered saline – Tween 20 (1% v/v).

7.2.5 Flow cytometry

Isolated plasma EVs in PBS were immediately placed on ice and fixed in cold formaldehyde (2% v/v) for 5 minutes. EVs were then pelleted by ultracentrifugation (as before) and resuspended in 1 X PBS tween (0.1%, v/v). EVs were blocked in rabbit serum for 1 hour at room temperature before being pelleted and resuspended as before. EVs were incubated with antibodies to adiponectin (Abcam ab18065), FABP4 and PPARγ or no antibody (negative control) overnight at room temperature. EVs were again pelleted and resuspended to allow for incubation with AlexaFluoro®488 goat anti-rabbit IgG (Life Technologies) for 1 hour at room temperature. EVs were pelleted for the final time and resuspended in 1X PBS (0.22 μm-filtered), gated and analysed with a BD FACSCanto as outlined in *Chapter 2.6*.

7.2.6 Extracellular vesicle immunophenotyping

Immunophenotyping of adipocyte markers in plasma EVs was conducted as described in *Chapter 2.9* using TRF by Dr Justyna Witczak as part of a larger clinical study. A concentration of 5×10^{10} EVs were laid down per well in duplicate and allowed to settle overnight. EVs were then probed with anti-human rabbit monoclonal antibodies to adiponectin (Abcam, ab18065), FABP4 (Abcam, ab92501), PPARγ (Abcam, ab191407), CD9 as a marker for EVs (Abcam ab92726) and a negative control (no primary antibody).

7.2.7 Statistical analysis

Graphical representation of data was generated using GraphPad Prism software (version 6.0). Where applicable, data are presented as mean ± SD. No statistical analyses were conducted in this chapter as data were not being compared and only the presence or lack of adipocyte markers was being assessed.

7.3 Results

7.3.1 Quantitation of adipocyte- and plasma-derived extracellular vesicles

The raw NTA distributions of EVs from 3T3-L1 adipocytes were compared to those of plasma derived-EVs (**Figure 7.3.1**). 3T3-L1-derived EVs (mode size ~140 nm) showed a greater distribution across the EV range compared to plasma EVs (mode size ~90 nm). Due to the 100 fold difference in reported concentrations of 3T3-L1 and plasma-derived EVs, distributions were not adjusted for NTA dilutions so that the range of EV sizes of both samples can be compared on the same graph.
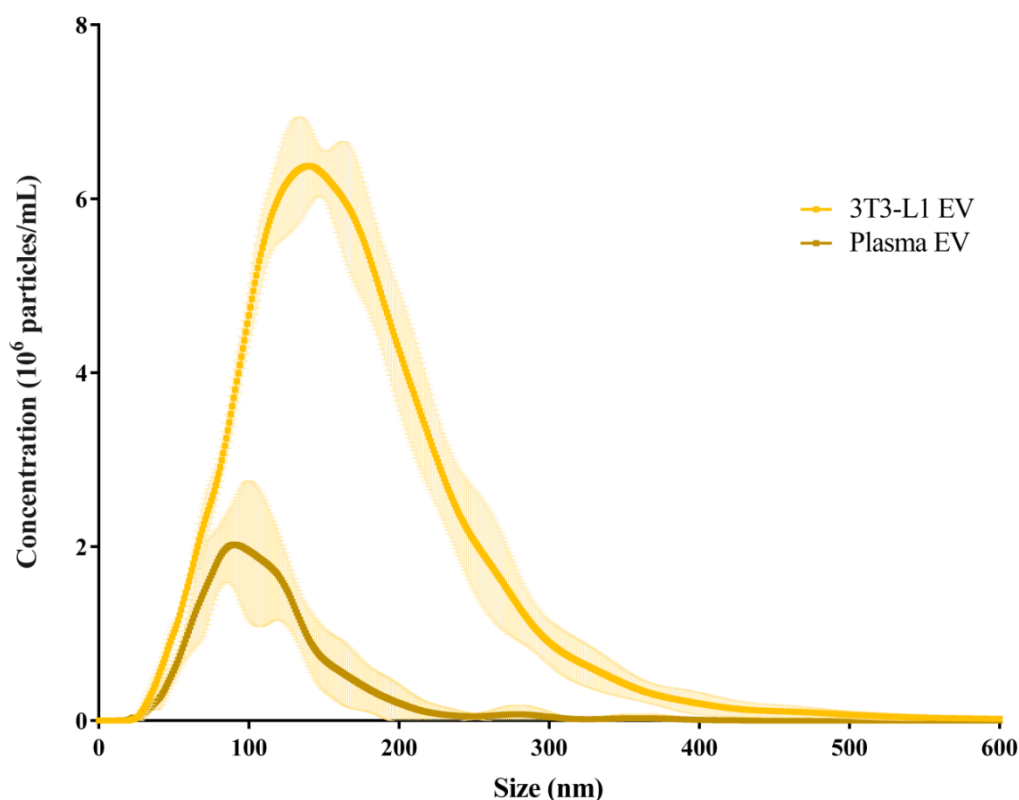
Figure 7.3.1: NTA distributions of 3T3-L1- and plasma-derived EVs. Raw size distributions (not adjusted for NTA dilutions) for 3T3-L1- and plasma-derived EVs. Data are presented as the mean (solid line) ± the SD (lighter shade), (n=5).

7.3.2 Western blot analysis of adipocyte markers

Western blotting was used to analyse samples for the presence of adipocyte markers (**Figure 7.3.2**). 3T3-L1 cells and corresponding EVs were used as controls (to illustrate characteristic expression). FABP4 and PPARγ were enriched in 3T3-L1 cells compared with corresponding EVs, however adiponectin seemed to be enriched in 3T3-L1 EVs. No adipocyte markers were detected in leukocyte samples whilst all adipocyte markers were present in plasma-derived EVs.
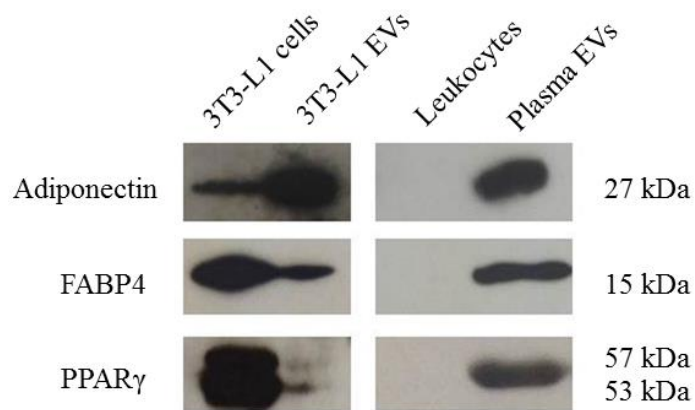
Figure 7.3.2: Western blot analysis of adipocyte markers. Adiponectin, FABP4 and PPARγ were analysed by Western blot in 3T3-L1 cells, 3T3-L1 EVs, leukocytes and plasma-derived EVs. Representative blots (n=3). As the presence/lack of markers was being observed, loading controls were not used.

7.3.3 Flow cytometric analysis of adipocyte markers

Plasma-derived EVs were probed for adiponectin, FABP4 and PPARγ and analysed using flow cytometry (**Figure 7.3.3**). EVs were positive for both adiponectin and FABP4; PPARγ could not be detected. Overall positivity of plasma-derived EVs for adipocyte markers was low (adiponectin: $0.4 \pm 0.7\%$; FABP4: $0.5 \pm 0.6\%$).
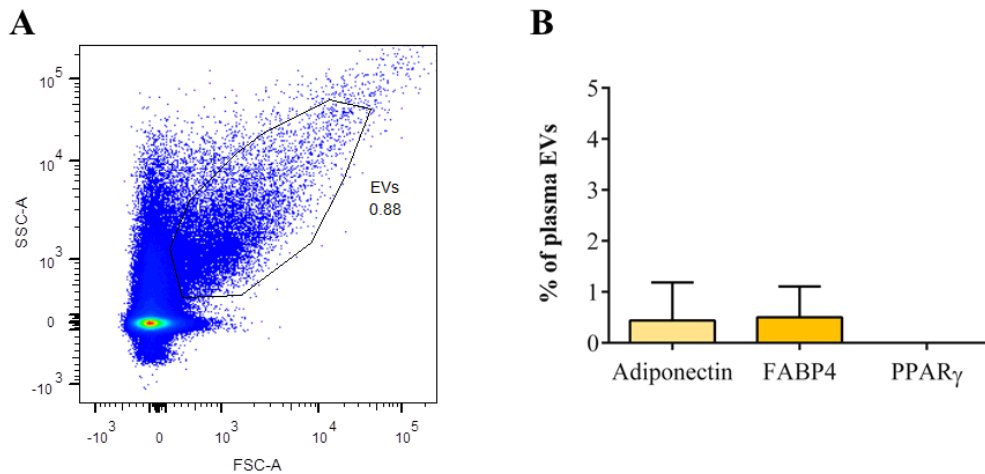
Figure 7.3.3: Flow cytometric analysis of adipocyte markers. Isolated plasma-derived EVs were fixed, blocked and stained with antibodies to adiponectin, FABP4 and PPARγ. EVs falling within the pre-defined gate (**A**) were then analysed for their fluoresence compared to a negative control and plotted as a percentage of the total plasma EVs (**B**). FSCA- = forward scatter area; SSC-A = side scatter area, (n=3).

7.3.4 Detection of adipocyte markers using immunophenotyping

Isolated plasma-derived EVs were probed for adipocyte markers using immunophenotyping (**Figure 7.3.4**). The exosomal marker, CD9, was detected in plasma-derived EVs (11,666 ± 2,716 arbitrary TRF units). Adiponectin, FABP4 and PPARγ could all be detected within plasma-derived EVs (adiponectin: 26,400 ± 2,339; FABP4: 3,850 ± 2,459; PPARγ: 3,144 ± 2,407 arbitrary TRF units). Negative control values (EVs with no primary antibody) were subtracted to give the raw TRF values presented below.
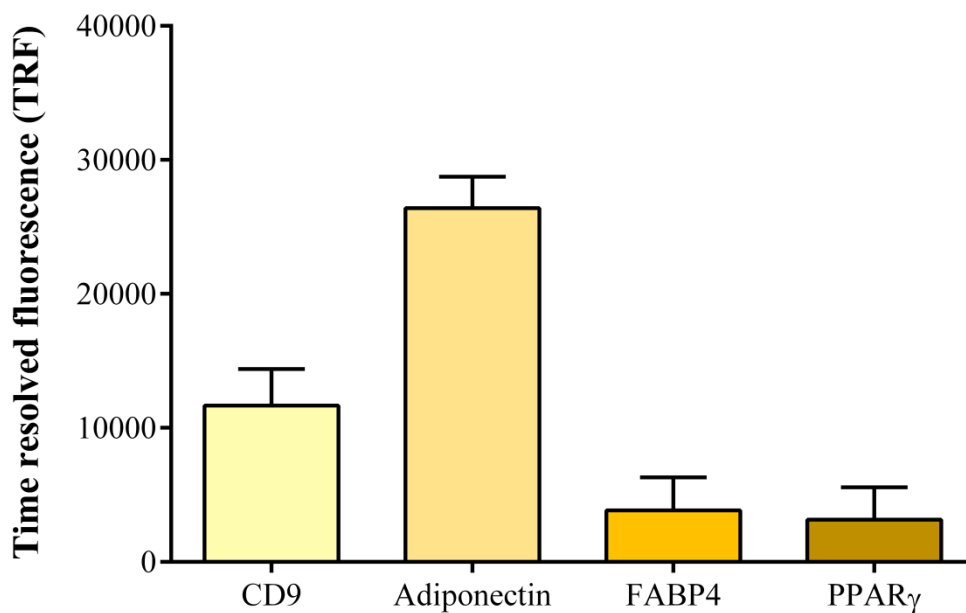
Figure 7.3.4: Immunophenotyping of adipocyte markers. Adipocyte markers were detected in plasma-derived EVs using TRF. Data are presented as raw TRF values (with negative IgG control values subtracted), (n=3).

7.4 Discussion

7.4.1 Key findings

The key findings of this chapter were:

1. The size distribution of plasma EVs are different to those of 3T3-L1 adipocyte-derived EVs.
2. Adiponectin, FABP4 and PPARγ can be detected in plasma-derived EVs by Western blotting. No adipocyte markers were detected in lysed leukocytes.
3. Adiponectin and FABP4 could be detected by flow cytometry in plasma-derived EVs; PPARγ was not detected.
4. Adiponectin, FABP4 and PPARγ were detected by TRF along with the exosomal marker, CD9.

7.4.2 Main discussion

The endocrine role of adipocytes and AT in both health and disease is becoming ever-more apparent. EVs released from adipocytes are being shown to play a novel part in crosstalk between adipocytes and other systems such as the vasculature, the immune system and the brain. However, the measurement of adipocyte-derived EVs in the circulation has not been concretely reported. This chapter therefore aimed to strengthen the evidence for the existence of adipocyte-derived EVs in plasma by using three markers of adipocytes and using three different measurement techniques.

The distribution of EV sizes was compared between 3T3-L1- and plasma-derived EVs. Though not shown here, the concentration of plasma-derived EVs was ~100 fold higher than that measured for 3T3-L1 derived EVs. This is unsurprising given they represent two very different model systems: the greater reservoir of EV sources in blood (such as platelets, endothelial cells, leukocytes and erythrocytes) compared to the singular source of adipocyte-derived EVs from 3T3-L1 cells. Furthermore, EVs in culture are collected from a limited amount of medium and a restricted number of cells in a flask, whereas plasma will come in contact with many more cells and will represent the circulating EV population. When the relative size distributions of EVs were compared by NTA, the majority of 3T3-L1 EVs detected

were between 50 – 400 nm, showing a greater range of EV sizes compared to plasma EVs which were mainly between 50 – 200 nm. This suggests that circulating plasma-derived EVs contain a higher proportion of exosomes compared to EVs from adipocyte culture.

Mature adipocytes can be characterised by the expression of hallmark proteins such as FABP4, adiponectin and PPARγ (320,323,453). Their secretion into the circulation, in combination with the lack of a distinct marker for adipocyte-derived EVs presents a challenge for their detection on EVs *in vivo*. Therefore, plasma EVs from healthy volunteers were probed for all three adipocyte markers using a range of techniques. Firstly, EVs were assessed for adipocyte markers using Western blotting, with 3T3-L1 cell and EV lysates as adipocyte and antibody controls. Adiponectin, FABP4 and PPARγ were all detected in plasma EV lysates, suggesting the presence of these adipocyte markers in the plasma EV fraction. Ogawa et al., have previously illustrated that adipocytes can transfer mRNA to Mϕ via EVs and that this may in part account for the presence of adipocyte-specific mRNA in the circulation (516). However, in our studies none of the adipocyte markers could be detected in leukocytes isolated from the same blood sample as plasma-derived EVs, suggesting that the presence of these markers in plasma-derived EVs is due to direct adipocyte origin. The expression looked to be fairly consistent between adipocyte markers in plasma EVs, though a loading control was not used to confirm this.

As previously discussed in this thesis, the use of FC to analyse EVs often results in inaccuracies as the majority of EVs pass below the detectability of conventional cytometers, as evidenced by NTA data presented above. However, it remains widely used as a technique to phenotype the origin of EVs due to its potential for dual (or multiple) staining of markers. Therefore, plasma-derived EVs were assessed for adipocyte markers using FC. As all three adipocyte markers are likely to be contained within EVs (as opposed to surface-bound - adiponectin and FABP4 are cytoplasmic and secreted, and PPARγ is nuclear-localised), EVs were first fixed and permeabilised to allow antibody access. Both adiponectin and FABP4 could be detected by FC though the percentage of total plasma-derived EVs exhibiting these markers was very low (<0.5%). FABP4 has previously been reported to be present in adipocyte-derived microvesicles at ~0.5% of the total population (54). PPARγ could not be detected in plasma-derived EVs using FC. The low detection of adiponectin

and FABP4 and lack of PPARγ may represent the low relative population of adipocyte-derived EVs in comparison to the total plasma EV pool. Alternatively, adipocyte markers may be more closely associated with smaller microvesicles and exosomes which are below the detection limit of FC. Indeed, previous data has found both adiponectin and PPARγ to be associated with plasma exosomes (514,515). As illustrated by the size distribution of plasma-derived EVs, the majority of EVs are <300 nm and so are unlikely to have been detected by the cytometer.

Adipocyte markers in plasma-derived EVs were also assessed using TRF immunophenotyping. All three adipocyte markers could be detected in EVs, with adiponectin giving the highest fluorescent signal. This again supports the presence of adipocyte-derived material in the circulating plasma EV fraction. Furthermore, CD9 was also detected in this fraction, a marker commonly associated with EVs (16) indicating a "true" EV fraction. Indeed, data recently amassed by our group indicate a strong positive correlation (r=0.54, $p<0.001$) of CD9 with FABP4 in a population of forty healthy individuals across a range of BMIs, indicating FABP4 is likely associated with EVs (**Figure 7.4.1**). No correlations were observed between adiponectin and PPARγ with CD9 though, as suggested above, these markers may be specifically associated with exosomes (514,515). As CD9 may now emerging as a more generic EV marker (53), the correlations with adiponectin and PPARγ may have been lost. Therefore, future work should look to compare these markers with exosomal markers such as CD63, alix or TSG101.
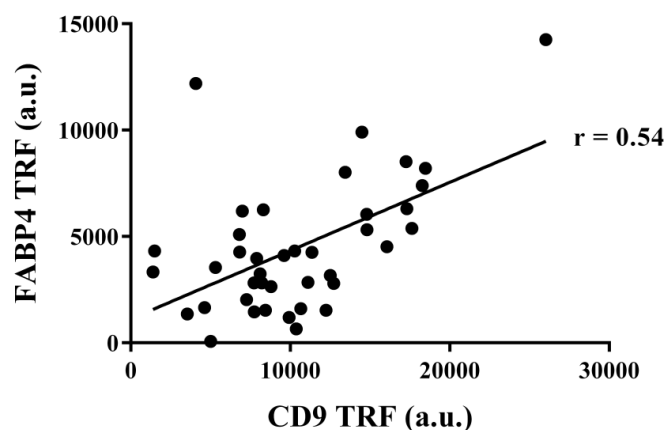
Figure 7.4.1: Relationship between CD9 and FABP4. Correlation between CD9 and FABP4 TRF values of healthy individuals over a range of BMIs (n=40). Data are courtesy of Dr Justyna Witczak, a.u. = arbitrary units.

Evidence presented in this chapter is highly suggestive of the presence of adipocyte-derived EVs amongst the plasma EV population. However, adipocytes are located within AT, which presents a physiological barrier between adipocyte-derived EVs and access to the circulation. Hence, an obvious question is how do adipocyte-derived EVs make it into the systemic circulation? Lean AT is relatively well vascularised by capillary networks and evidence is emerging for the intracellular trafficking of EVs in a number of different cell types (*Chapter 1.1.5*). Therefore, adipocyte-derived EVs in the AT extracellular matrix could traverse single endothelial cells of capillaries and be transported intact into the AT microcirculation. As outlined in *Chapter 1.2*, obese AT is often poorly vascularised, which may reduce the likelihood of this route of exit for adipocyte EVs from AT. Local and systemic inflammation result in an increased vascular permeability due to a loss of endothelial tight junction barriers (517). Therefore, the inflammation associated with obesity may increase the permeability of AT microvasculature, thereby providing a route for adipocyte-derived EVs exit from AT in between "leaky" endothelial cells into the circulation. These hypotheses will be tested by our group as part of the newly awarded grant, using endothelial cell transwell experiments and monitoring adipocyte-derived EVs in upper and lower wells. Different conditions will also be tested including inflammatory endothelial cells, and also adipocyte-derived EVs will be generated under hypoxic and inflammatory conditions.

7.4.3 Limitations

The data presented in this chapter harbours some potential limitations. Western blotting experiments were performed without the use of a housekeeping gene such as β-actin for cells and CD9 or CD63 for EVs. This therefore prevented semi-quantitative analysis to compare the levels of the three markers. However, as the aim of the present chapter was to simply illustrate the detectability of adipocyte-derived EVs *in vivo*, future studies could quantify the proportions of these markers in plasma-derived EVs.

Leukocytes were isolated and lysed from the buffy coat without further separation of leukocyte subsets, such as Mϕ. Therefore adipocyte protein may have been present within Mϕ, but diluted by the total protein in the leukocyte fraction. Further

experiments could specifically isolate Mφ to lyse and analyse for adipocyte markers to ensure the detection in plasma EV fractions is not due to Mφ EV contamination. Additionally, the leukocyte fraction would have ideally been probed for a typical leukocyte maker such as CD45, to confirm the successful isolation of the leukocyte population.

As EVs were isolated by differential ultracentrifugation, the co-pelleting of soluble proteins with EVs cannot be eliminated. Therefore, our group are currently trialling SEC columns, density gradient ultracentrifugation and immuno-affinity magnetic bead methods to determine the extent of soluble protein contamination of EV samples following ultracentrifugation.

7.4.4 Conclusions

To summarise, adipocyte-derived EVs can be reliably detected in plasma-derived EV fractions. Adipocyte markers within plasma EVs were clearly visible by Western blot and TRF. Flow cytometry could barely detect adiponectin and FABP4 and was unable to detect PPARγ within plasma EVs, most likely due to the majority of EVs being <300 nm. Future studies could use the markers presented in this chapter to specifically isolate adipocyte-derived EVs from plasma and compare the properties of these EVs between lean and obese and healthy and diseased individuals. Adipocyte-derived EVs *in vivo* could eventually be novel circulating markers for the functional status of AT and hence act as important indicators of future cardiovascular risk. As stated above, this work is currently being pursued in a newly awarded grant based on the data presented in this chapter.

8. Results VI:

Lipoprotein apheresis reduces circulating EVs in individuals with familial hypercholesterolaemia

8. Perspective

At the time of starting my PhD, our group was beginning a clinical study to evaluate EVs in individuals with familial hypercholesterolaemia with an interest in the potential cardiovascular applications of EV concentrations in a patient cohort. This work was carried out in parallel with *Chapter 3* and therefore it was also a good opportunity to compare two of the most widely-used techniques to measure EVs (TRPS and NTA) in a clinical setting. The study represented an *in vivo* model that allowed us a unique opportunity to study the influence of a method that could selectively remove certain EV populations.

At the time, FC was the most established technique for the detection of cellular epitopes on the surface of EVs. It is important to highlight that during the course of this PhD study and in line with the fast moving development in the EV field, *Chapters 3 – 7* show how technical and methodological aspects have been further developed and/or superseded. Nevertheless, techniques used in this chapter were optimised at the time of study.

Parts of this chapter have been published in:

Connolly KD*, Willis GR*, Datta DB, Ellins EA, Ladell K, Price DA, Guschina IA, Rees DA, James PE (2014). Lipoprotein-apheresis reduces circulating microparticles in individuals with familial hypercholesterolemia. *Journal of Lipid Research*. 55 (10): 2064-72.

8.1 Introduction

High cholesterol, particularly low-density lipoprotein (LDL) cholesterol is a risk factor for CVD. Familial hypercholesterolaemia (FH) is a common genetic disorder that causes elevated levels of atherogenic lipoproteins in the plasma, particularly LDL. The LDL receptor is mutated in more than 85% of cases of FH, rendering these receptors unable to bind or internalise LDL and leading to an accumulation of LDL in the plasma (518). FH is an autosomal dominant disorder, resulting in heterozygote, or more serious homozygote forms (519). Severe FH is typically difficult to treat by alterations in diet or lipid lowering medications alone as these interventions are insufficient to adequately lower LDL levels to completely abate atherosclerotic plaque formation (520). These patients therefore require frequent lipoprotein-apheresis (hereafter termed "apheresis") treatments in combination with dietary and pharmacological intervention to regulate LDL levels (521).

Apheresis involves the blood being drawn from one arm and passed through a column to remove atherogenic lipoproteins before being returned to the body via the other arm. Different types of apheresis columns and procedures may be utilised, though all show equal efficacy, with approximately 70% of circulating LDL removed immediately following treatment (522–525). However, LDL levels are known to rebound to 50% of pre-treatment values within 2-4 days of apheresis treatment (526). Despite this transiency, apheresis is associated with superior long-term cardiovascular benefits compared with alternative therapies (527–531).

Increased concentrations of EVs in the circulation, particularly platelet-derived EVs, have been previously reported in CVD (*Chapter 1.1.9.1*, (532,533)). Platelet EVs are thought to amplify the physiological and pathophysiological roles of platelets, for example helping to regulate haemostasis but also promoting coagulation and thrombus formation. The surface of platelet EVs is reportedly up to 100-fold more procoagulant than that of the surface of activated platelets (438), highlighting platelet EVs as important biomarkers for risk of CVD. Furthermore, EVs contain a bioactive cargo of lipid and genetic signalling mediators that can be transferred to target cells, though the mechanism of interaction is still unclear and may be cell-specific (*Chapter 1.1.5*). To date, little is known about the lipid composition and profile of

plasma-derived EVs, though platelet EVs have been shown to transfer proinflammatory lipids to platelets leading to activation (534).

Individuals with FH have previously been shown to have increased circulating levels of endothelial- and leukocyte-derived EVs compared to individuals with non-FH hypercholesterolaemia (535,536). However, quantification of EVs in these studies was achieved using FC, and therefore may be suboptimal, due to the techniques lack of sensitivity for vesicles <300 nm. To date, no data exist detailing the effects of apheresis treatment on EVs in individuals with FH, though other extracorporeal methods have been previously shown to remove EVs (537,538).

8.1.1 Aims

The aims of this chapter were to characterise the effect of apheresis on individuals with FH in terms of:

1. EV size and concentration
2. EV origin
3. Plasma and EV fatty acids
4. EV thrombin generation

This chapter also aimed to compare the profile of EVs from individuals with FH to those of healthy volunteers. Finally, this chapter sought to compare the results of two well-established techniques for EV measurement in a clinical cohort.

8.1.2 Hypotheses

Routine apheresis treatment may alter the profile of circulating EVs in individuals with FH. The concentration of EVs may be elevated in individuals with FH compared to healthy volunteers.

8.2 Methods

8.2.1 Apheresis and sample collection

Twelve patients undergoing fortnightly apheresis consented to take part in the study. The individuals were previously characterised by Dr Dev Datta as having clinically significant dyslipidaemia and were attending the Lipid Unit at University Hospital Llandough, Cardiff for apheresis treatment as part of their routine clinical care. For clinical reasons, three different apheresis techniques (described previously (539)) were used: polyacrylate whole blood adsorption (DALI®; n=8), whole blood dextran sulphate adsorption (n=1) and plasma dextran sulphate adsorption (n=3). Individuals had fasted for at least 4 hours prior to apheresis treatment and had continued to take prescribed medications for at least 1 hour prior to the study. Individuals taking vasoactive medications were asked to refrain from taking these prior to the study. Routine anthropometric measurements were carried out prior to apheresis treatment.

Ethical approval for collecting blood samples was obtained by Miss Elizabeth Ellins (as part of a parallel study) and was provided by South East Wales Research Ethics Committee. Individuals were rested for 15 minutes before vascular access using 16 gauge 25 mm fistula needles into two anatomically distinct upper limb veins, or by arteriovenous fistula. Blood samples were then drawn prior to, and immediately following completion of apheresis (approximately 3 hours later). Seven healthy volunteers (free from CVD and medication) also consented to take part in the study for comparison of EV concentration, size distribution, cellular origin and fatty acids with FH individuals.

8.2.2 Biochemical measurements

Blood samples were collected as described above into EDTA or citrate vacutainers. Total serum cholesterol (TC), HDL and triglycerides were measured using an Architect automated analyser (Abbott Diagnostics, UK). LDL was then estimated using the Friedwald equation (**Figure 8.2.1**). Glucose levels were determined using the Architect chemistry system (Abbot Diagnostics) and high sensitivity C-reactive protein (hs-CRP) was measured using nephelometry (BN™ II system, Dade Behring, UK). Blood pressure (BP) measurements were taken by Miss Elizabeth Ellins with

individuals seated using the Vicorder system (Skidmore Medical, UK) as part of a separate study into vascular measurements following apheresis.

$$LDLc = (TC - HDLc) - \left(\frac{Triglycerides}{2.2}\right)$$

Figure 8.2.1: The Friedwald equation. Details of the Friedwald equation used to calculate LDL cholesterol (LDLc) from the levels of total cholesterol (TC), HDL cholesterol (HDLc) and triglycerides.

8.2.3 Isolation of extracellular vesicles

Blood samples were collected into both EDTA and citrate vacutainers and were processed by myself and Dr Gareth Willis using the first isolation method (*Chapter 2.3.2*). PPP from EDTA vacutainers was snap frozen in liquid nitrogen for GC analysis. PPP from citrate vacutainers used to pellet EVs. The EV pellet was then either resuspended in filtered PBS (as in *Chapter 2.3.1*) and snap frozen in liquid nitrogen (for GC analysis), or resuspended in 1X filtered PBS containing 0.05% (v/v) Tween 20 (for EV size and concentration analysis). The latter was then passed through a 1 μm filter (Supelco, Sigma, UK) and slow-frozen overnight at -80°C in a Mr Frosty (Nalgene, ThermoScientific, UK). Plasma and EVs were maintained at -80°C until analysis.

8.2.4 Nanoparticle tracking analysis

Size and concentration of EV samples was analysed using NTA as described in *Chapter 2.4.2* by Dr Gareth Willis.

8.2.5 Tunable resistive pulse sensing

Size and concentration of EV samples was also analysed using TRPS (undertaken by myself) as outlined in *Chapter 2.5.2* using np100 and np200 nanopores.

8.2.6 Flow cytometry

Cellular origin of EVs was analysed using FC and conducted by myself and Dr Kirstin Ladell (Cardiff University) using a custom-built BD FACSAria II (BD Biosciences, USA) in the laboratory of Dr David Price. Forward scatter area (FCS-A) and side scatter area (SSC-A) were set to log scale and EVs were gated based on their FSC-A/SSC-A profile and in relation to platelets in fresh plasma. EVs were resuspended in 1X 0.22 µm-filtered annexin V binding buffer (BD Biosciences) and 100 µL of this was used for staining. EVs were stained (in the dark for 15 minutes at room temperature) with annexin V-FITC, and antibodies against CD41-phycoerythrin (PE)- cyanine (Cy) 5, CD11b-PE-Cy7, CD144-allophycocyanin (APC) and CD235a-pacific blue (PB) as markers of EVs, platelets, monocytes, endothelial cells and erythrocytes respectively (BioLegend, USA). Data were exported and analysed as described in *Chapter 2.6*.

8.2.7 Gas chromatography

GC-FID was conducted by Dr Gareth Willis and Dr Irina Guschina to determine the fatty acid concentration and composition of plasma and EV fractions. Lipids were extracted as described in *Chapter 2.7.1* from 200 µL plasma or 250 µL isolated EVs.

8.2.8 Thrombin generation

The procoagulant potential of EVs was tested by their ability to stimulate thrombin generation and was conducted by myself and Dr Gareth Willis. To provide a working reservoir of plasma in which to test the thrombin generation of EVs, blood from healthy volunteers was taken into a syringe containing trisodium citrate (Sigma) and 20 µg/mL corn trypsin inhibitor (Cambridge BioScience, UK). Blood was

immediately centrifuged as in *Section 8.2.3* to isolate "vehicle" PPP which was stored at -80°C until analysis.

Calibrated automated thrombography (CAT) was used with minor modifications to a previously described protocol (540) to assess EV thrombin generation. Samples were measured in duplicate using 96-well plates (round-bottomed, Immulon 2HB, ThermoScientific). Eighty microliters of vehicle PPP (containing endogenous clotting factors) was added to each well with 20 µL of diluted HEPES/NaCl buffer (pH 7.4) tissue factor (TF) solution to yield a final concentration of 1 pM (Innovin, Sysmex UK Ltd., UK). FH EV samples were assayed for thrombin generation with and without exogenous TF addition. Therefore, EVs (20 µL) were added to sample wells with the addition of either saline (20 µL, 0.9 % (w/v) NaCl) or TF (20 µL, 1 pM final). Each sample was calibrated to a well containing 80 µL of PPP and 40 µL of thrombin calibrator (600 nM, Synapse BV, Netherlands). The plate was then warmed to 37°C for 5 minutes before addition of fluorogenic substrate (20 µL, benzyloxycarbonyl-Gly-Gly-Arg-7-amido-4-methylcoumarin, Bachem, UK). The fluorescent signal was then measured using a Fluoroskan Ascent plate reader (ThermoLabsystems, Finland) equipped with a 390/460 nm filter set (excitation/emission) at 15 second intervals until the thrombin generation reaction was complete. Data were analysed using Thrombinoscope™ software (Synapse BV) and correlated with EV concentration data.

8.2.9 Statistical analysis

Data were analysed by myself and Dr Gareth Willis using GraphPad Prism (version 6.0) and are presented as mean ± SEM. A paired *t-test* (two-tailed) or a Wilcoxon matched pairs test was used for parametric and non-parametric data respectively. A *p* value of <0.05 was considered statistically significant.

8.3 Results

8.3.1 Anthropometric and biochemical data

Of the 12 participants in the study, 9 were male and 3 were female with a mean age of 57.9 ± 10.3 years and a mean BMI of 30.0 ± 4.0 kg/m^2. The healthy volunteer comparison group were 7 males with a mean age of 34.0 ± 8 years and a mean BMI of 25.0 ± 3.0 kg/m^2. A summary of biochemical measurements is given in **Table 8.3.1**. TC, HDL, triglycerides, LDL, and hsCRP were reduced post-apheresis. Systolic BP was increased following apheresis. No changes were observed in glucose levels, diastolic BP or heart rate with apheresis.

Parameter	Pre-apheresis	Post-apheresis	*p*-value
TC (mmol/L)	6.1 ± 0.5	2.7 ± 0.2	*<0.0001*
HDL (mmol/L)	$1.1 (0.4 - 2.3)$	$0.9 (0.2 - 2.1)$	*0.003*
Triglycerides (mmol/L)	1.8 ± 0.2	0.9 ± 0.1	*<0.0001*
LDL (mmol/L)	4.1 ± 0.4	1.4 ± 0.2	*<0.0001*
TC/HDL	$5.8 (3.3 - 10.0)$	$3.1 (1.9 - 8.2)$	*0.0005*
Glucose (mmol/L)	5.7 ± 0.3	6.1 ± 0.3	0.07
hsCRP	$0.8 (0.2 - 16.9)$	$0.6 (0.2 - 13.8)$	*0.003*
Systolic BP (mmHg)	140 ± 5	148 ± 6	*0.02*
Diastolic BP (mmHg)	81.8 ± 2.8	82.8 ± 2.7	0.45
Heart rate (bpm)	55.8 ± 2.9	58.8 ± 3.4	0.09

Table 8.3.1: Biochemical and physiological measurements pre- and post-apheresis. Baseline and post-apheresis biochemical and physiological measurements with accompanying *p* values. Data are presented as mean ± SD for parametric data or as median (interquartile range) for non-parametric data. Significant *p* values are in italics, (n=12). TC = total cholesterol, HDL = high density lipoprotein, LDL = low density lipoprotein, hsCRP = high sensitivity C-reactive protein, BP = blood pressure, bpm = beats per minute.

8.3.2 *Effect of apheresis on extracellular vesicle size and concentration*

The concentration and size distribution of EVs from individuals with FH (pre-apheresis) were compared with those of healthy volunteers (**Figure 8.3.1**). No change was observed in the mean concentration of EVs, though there was a trend towards an increased concentration of EVs in FH (**A**). Comparison of the size distributions revealed an increase in EVs between $50 - 100$ nm in individuals with FH compared to healthy volunteers (**B**).
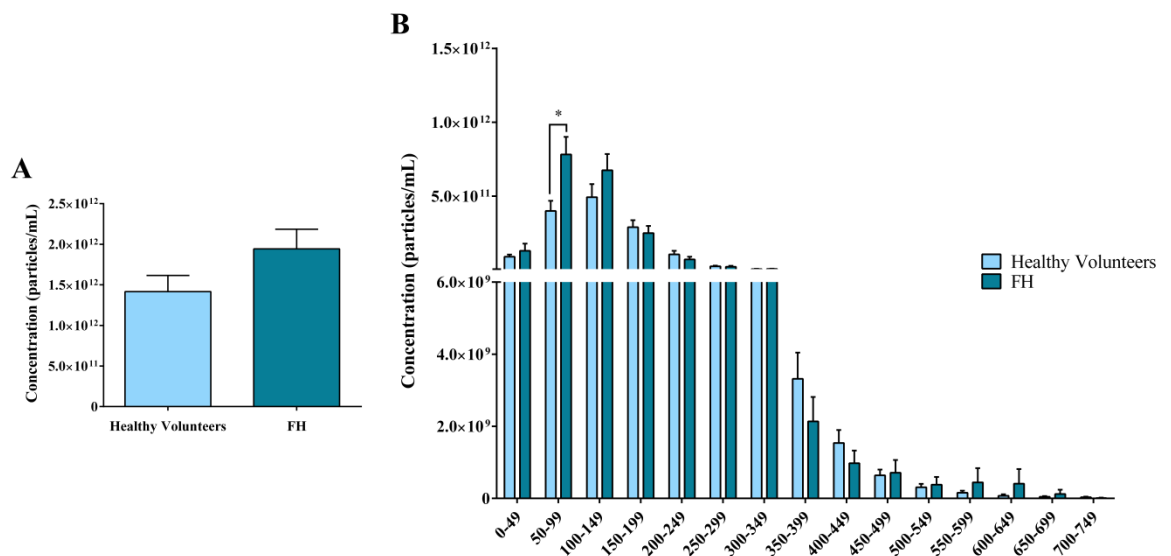
Figure 8.3.1: EVs of healthy volunteers vs. individuals with FH. Comparison of the mean EV concentration (**A**) and the size distribution of EVs (**B**) from healthy volunteers vs. individuals with FH, as measured by NTA. Healthy volunteers (n=7), FH (n=12), *$p<0.05$.

To assess the effect of apheresis on EV size and concentration, two techniques were used: TRPS (using np100 and np200 nanopores) and NTA (**Figure 8.3.2**). No difference in mode EV size was detected using TRPS np100 (81.1 ± 19.6 nm to 78.4 ± 16.7 nm, $p = 0.3$; **Figure 8.3.2 A**). No significant difference was observed in EV concentration pre-post apheresis with this technique (4.6 x 10^{11} ± 1.3 x 10^{11} particles/mL to 3.1 x 10^{11} ± 1.0 x 10^{11} particles/mL, $p = 0.2$; **Figure 8.3.2 B**). TRPS np100 showed no preferential reduction according to EV size (**Figure 8.3.2 C**).
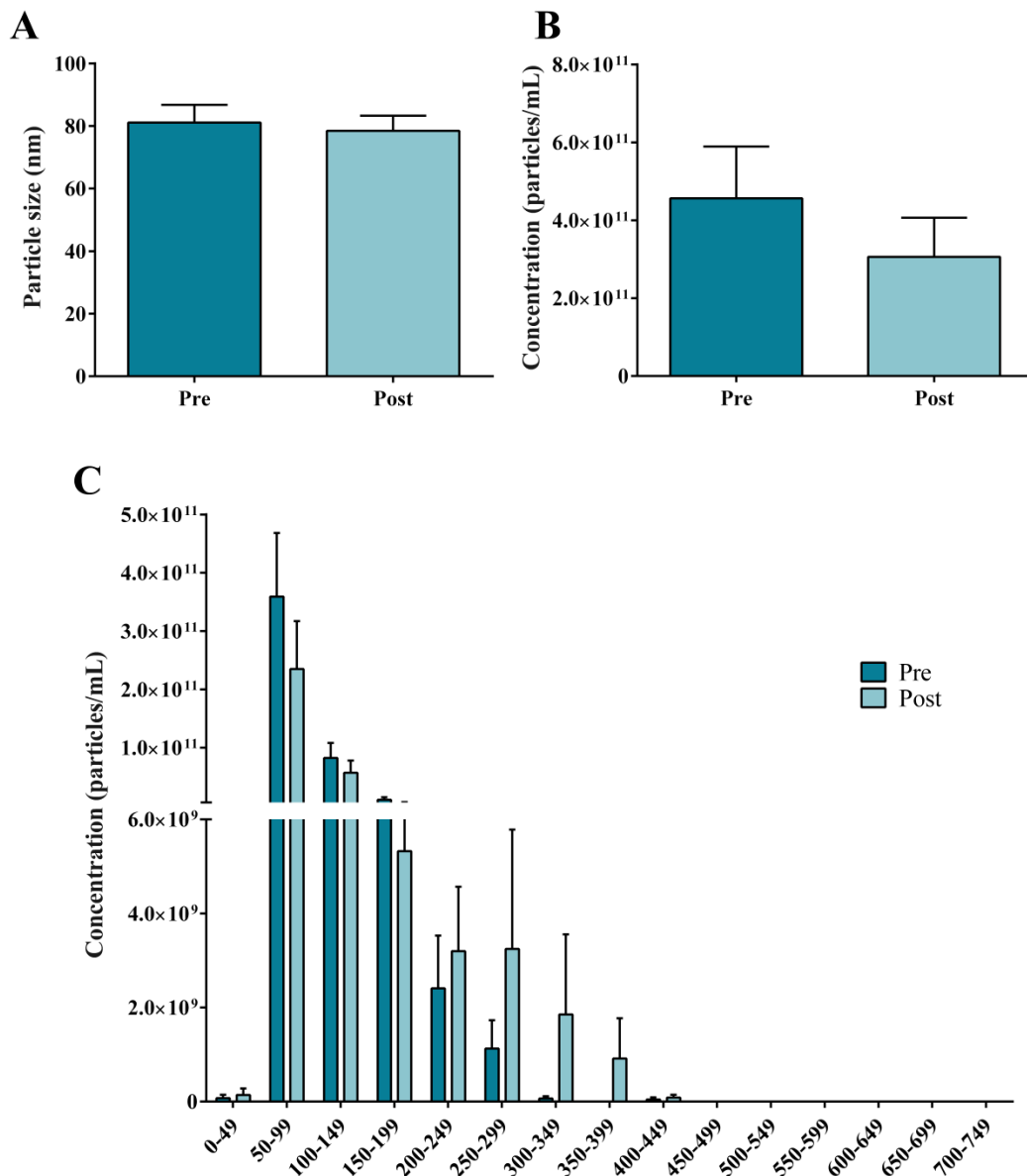
Figure 8.3.2 A-C: TRPS np100 EV size and concentration pre- and post-apheresis. EV samples pre- and post-apheresis were measured using TRPS with an np100 nanopore. (**A**) Mode size of EVs, (**B**) mean concentration of EVs and (**C**) size distribution of EV concentration (n=12).

No difference was found in mode size of EVs with TRPS np200 (170.3 $\pm$ 40.6 nm to 163.6 $\pm$ 29.2 nm, p = 0.18; **Figure 8.3.2 D**. Concentration of EVs measured by TRPS np200 was significantly reduced post-apheresis (4.7 x 10^{10} $\pm$ 8.8 x 10^{9} particles/mL to 3.1 x 10^{10} $\pm$ 5.6 x 10^{9} particles/mL, p = 0.01; **Figure 8.3.2 E**). TRPS np200 size distribution revealed this reduction predominantly to be in EVs between 200-249 nm (p = 0.01, **Figure 8.3.2 F**).
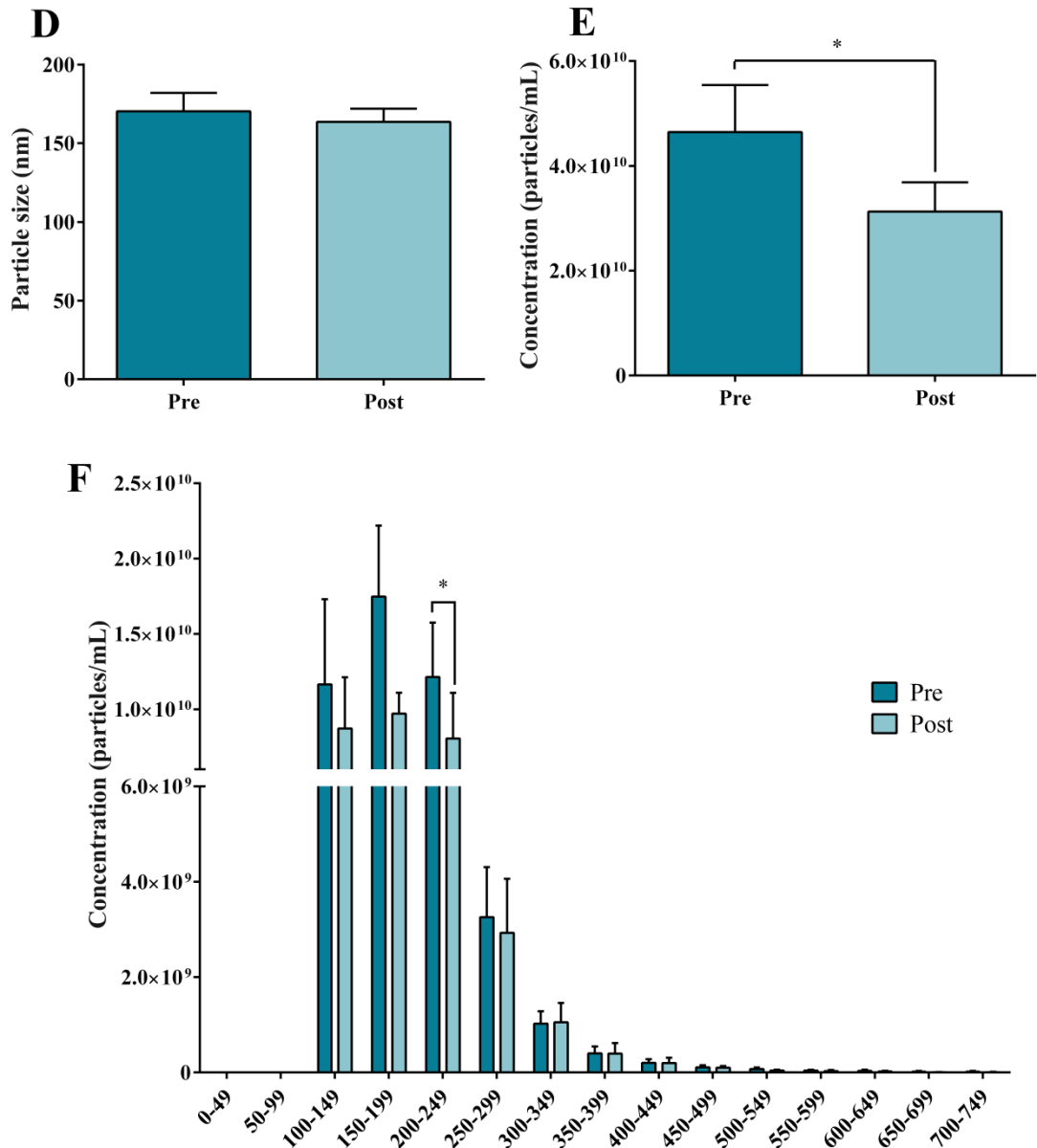
Figure 8.3.2 D-F: TRPS np200 EV size and concentration pre- and post-apheresis. EV samples pre- and post-apheresis were measured using TRPS with an np200 nanopore. (**D**) Mode size of EVs, (**E**) mean concentration of EVs and (**F**) size distribution of EV concentration. *p<0.05, (n=12).

As with TRPS, NTA detected no change in overall mode EV size following apheresis (93.3 ± 21.0 nm to 88.2 ± 14.7 nm, $p = 0.3$; **Figure 8.3.2 G**). Mean concentration as measured by NTA was reduced post-apheresis (1.9 x 10^{12} ± 2.4 x 10^{11} particles/mL to 1.5 x 10^{12} ± 2.4 x 10^{11} particles/mL, $p = 0.03$; **Figure 8.3.2 H**). However, no specific reduction in EV size distribution was observed with NTA (**Figure 8.3.2 I**).
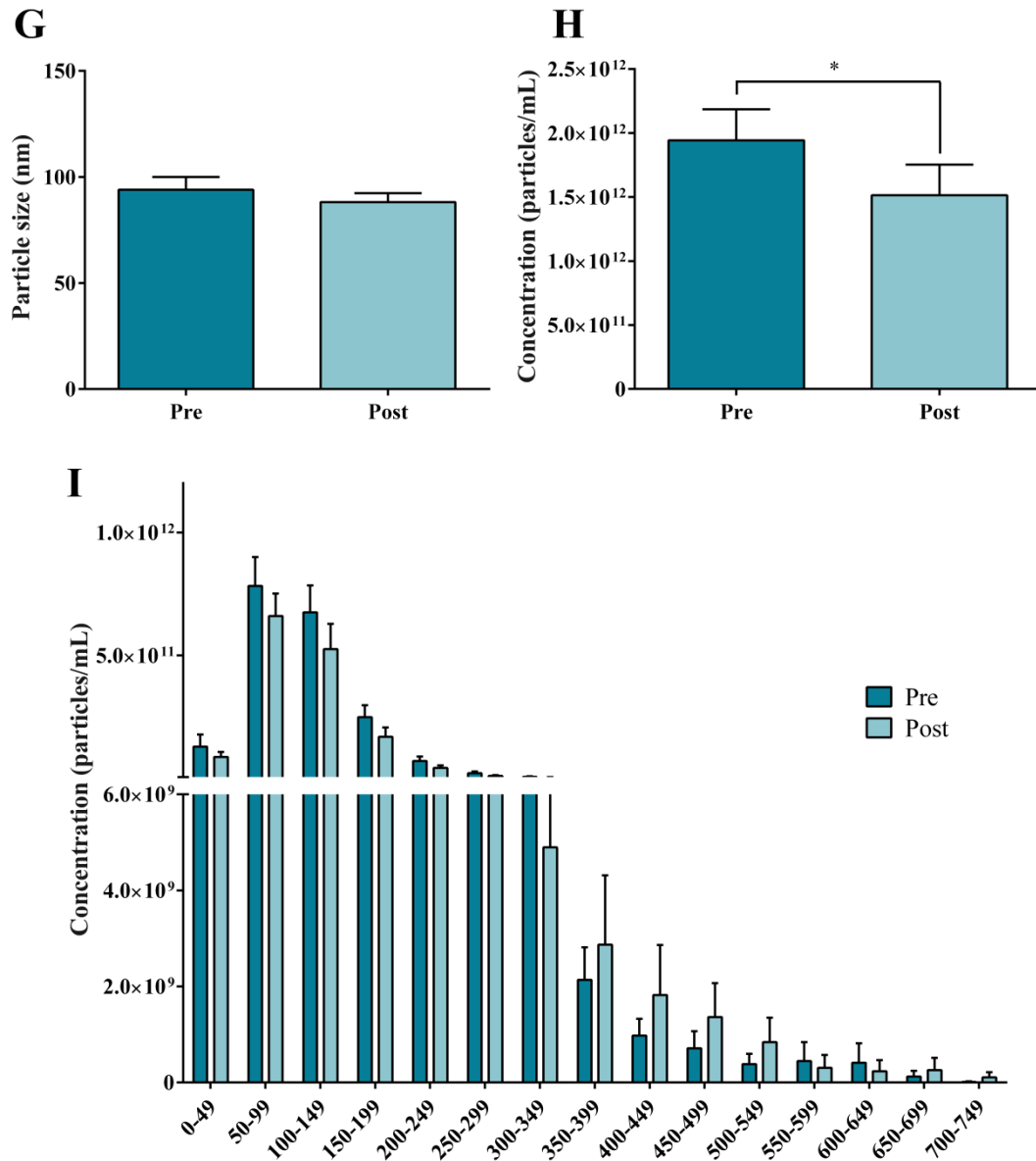
Figure 8.3.2 G-I: NTA EV size and concentration pre- and post-apheresis. EV samples pre- and post-apheresis were measured using NTA. (**G**) Mode size of EVs, (**H**) mean concentration of EVs and (**I**) size distribution of EV concentration *$p<0.05$ (n=12).

Following measurement of all apheresis samples using both techniques, the range of detection of TRPS and NTA was compared using pre-apheresis samples. The range of EVs detected by TRPS (np100 and np200) and NTA were similar (**Figure 8.3.3**), though the reported concentration of EVs varied greatly between the two techniques, and also between TRPS nanopores (**Table 8.3.3**).
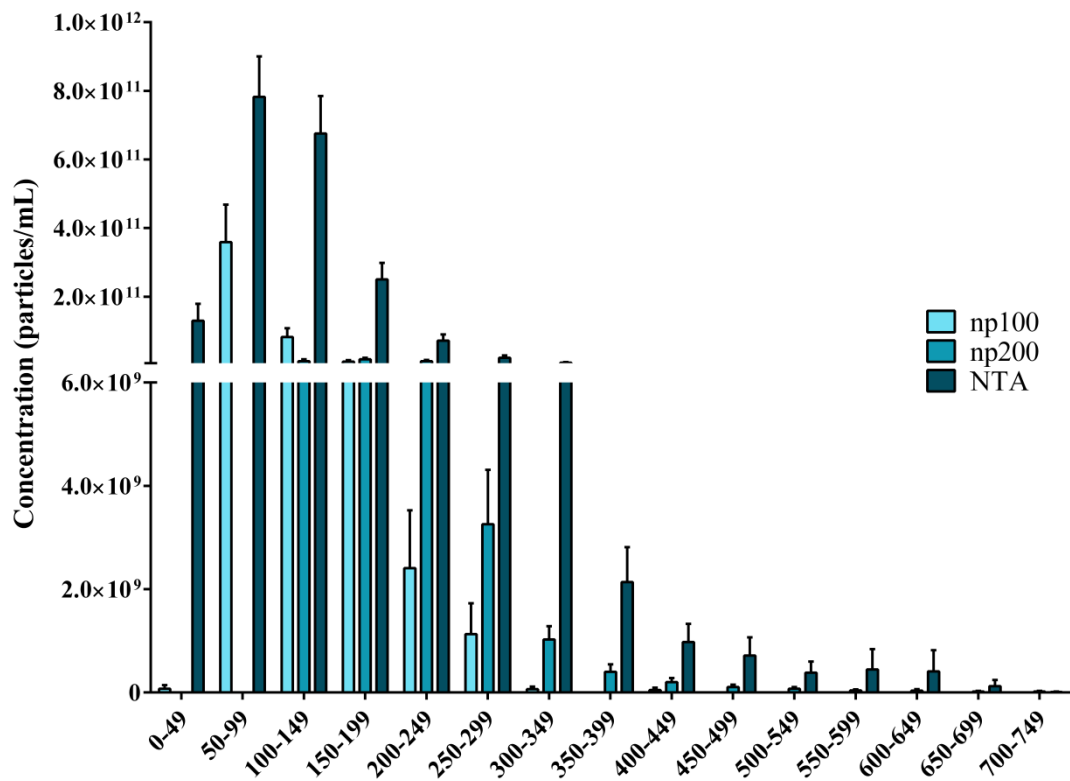
Figure 8.3.3: Range of detection of EV measurement techniques. Comparison of the ranges of detection of TRPS (np100 and np200) and NTA. Data are presented as mean ± SEM, (n=12).

Size range (nm)	np100	np200	NTA
0 – 49	$7.2 \times 10^7 \pm 7.2 \times 10^7$	0	$1.3 \times 10^{11} \pm 4.9 \times 10^{10}$
50 – 99	$3.6 \times 10^{11} \pm 1.1 \times 10^{11}$	0	$7.8 \times 10^{11} \pm 1.2 \times 10^{11}$
100 – 149	$8.25 \times 10^{10} \pm 2.6 \times 10^{10}$	$1.2 \times 10^{10} \pm 5.7 \times 10^9$	$6.8 \times 10^{11} \pm 1.1 \times 10^{11}$
150 – 199	$1.1 \times 10^{10} \pm 4.3 \times 10^9$	$1.8 \times 10^{10} \pm 4.7 \times 10^9$	$2.5 \times 10^{11} \pm 4.8 \times 10^{10}$
200 – 249	$2.4 \times 10^9 \pm 1.1 \times 10^9$	$1.2 \times 10^{10} \pm 3.6 \times 10^9$	$7.2 \times 10^{10} \pm 1.8 \times 10^{10}$
250 - 299	$1.1 \times 10^9 \pm 6.0 \times 10^8$	$3.3 \times 10^9 \pm 1.1 \times 10^9$	$2.2 \times 10^{10} \pm 7.1 \times 10^9$
300 – 349	$6.5 \times 10^7 \pm 4.8 \times 10^7$	$1.0 \times 10^9 \pm 2.6 \times 10^8$	$7.4 \times 10^9 \pm 1.8 \times 10^9$
350 – 399	0	$4.0 \times 10^8 \pm 1.5 \times 10^8$	$2.1 \times 10 \pm 6.8 \times 10^8$
400 – 449	$4.6 \times 10^7 \pm 4.6 \times 10^7$	$2.0 \times 10^8 \pm 7.7 \times 10^7$	$9.8 \times 10^8 \pm 3.5 \times 10^8$
450- 499	0	$1.1 \times 10^8 \pm 4.4 \times 10^7$	$7.1 \times 10^8 \pm 3.5 \times 10^7$
500 -549	0	$7.2 \times 10^7 \pm 3.3 \times 10^7$	$3.8 \times 10^8 \pm 2.1 \times 10^8$
550 -599	0	$4.0 \times 10^7 \pm 1.9 \times 10^7$	$4.5 \times 10^8 \pm 4.0 \times 10^8$
600 – 649	0	$3.5 \times 10^7 \pm 2.8 \times 10^7$	$4.1 \times 10^8 \pm 4.1 \times 10^8$
650 – 699	0	$1.9 \times 10^7 \pm 1.4 \times 10^7$	$1.2 \times 10^8 \pm 1.2 \times 10^8$
700 - 749	0	$1.8 \times 10^7 \pm 1.4 \times 10^7$	$1.0 \times 10^7 \pm 1.0 \times 10^7$

Table 8.3.3: Concentration differences between EV measurement techniques. Differences in detected concentrations of EVs measured by TRPS (np100 and np200) and NTA. Data are presented as mean $\pm$ SEM, (n=12).

8.3.3 Extracellular vesicle origin pre- and post-apheresis

The majority of EVs from both healthy volunteers and individuals with FH (pre-apheresis) were annexin V positive with no difference between healthy volunteers and FH (healthy volunteers: $88.1 \pm 4.8\%$; FH: $88.9 \pm 3.7\%$; **Figure 8.3.4 A**). Individuals with FH had a significantly higher proportion of endothelial-derived EVs (healthy volunteers: $0.4 \pm 0.2\%$; FH: $1.9 \pm 0.6\%$; $p = 0.03$; **Figure 8.3.4 B**). No differences were found in apportions of platelet, monocyte or erythrocyte EVs between healthy volunteers and individuals with FH.
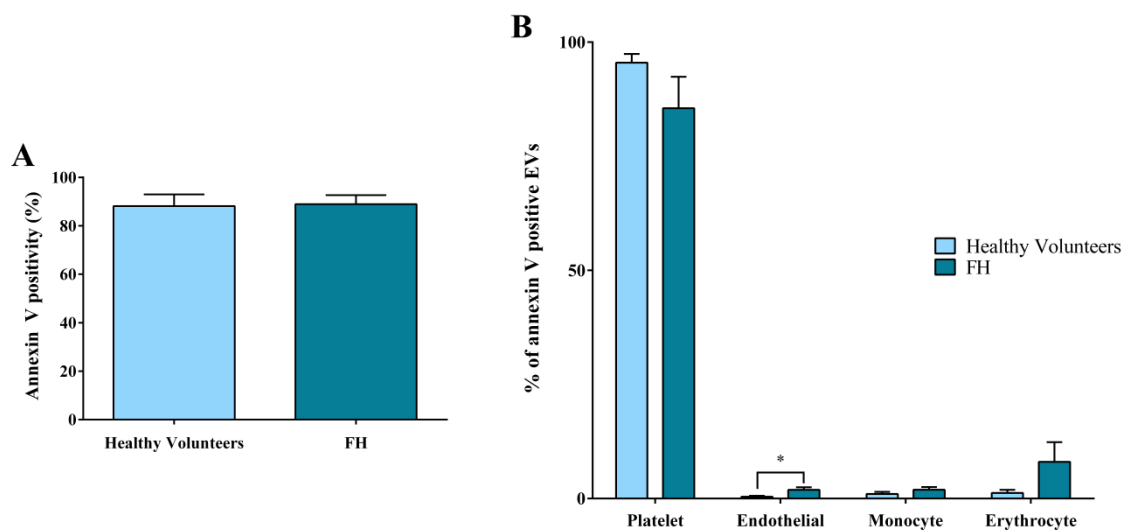
Figure 8.3.4: Flow cytometric analysis of EVs from healthy volunteers and FH. (**A**) EVs from healthy volunteers and individuals with FH were first compared for their annexin V positivity. (**B**) Annexin V positive EVs were then subsequently analysed for positivity of platelet (CD41), endothelial (CD144), monocyte (CD11b) and erythrocyte (CD235a) markers. Healthy volunteers (n=7), FH (n=12),* $p<0.05$.

The gate used to analyse EVs was determined by analysing FSC-A and SSC-A profiles of EVs in relation to platelets in fresh plasma, and was subsequently used to analyse EVs from FH samples pre- and post-apheresis (**Figure 8.3.5 A**). No difference was observed in EV annexin V positivity following apheresis, though the majority of EVs were found to be annexin V positive (pre-apheresis: $88.9 \pm 3.7\%$; post-apheresis: $88.4 \pm 5.1\%$, $p = 0.9$, **Figure 8.3.5 B**). Annexin V positive EVs were then analysed for their expression of platelet (CD41), endothelial (CD144), monocyte (CD11b) and erythrocyte (CD235a) markers (**Figure 8.3.5 C**). No changes

were observed in the markers tested in EVs pre- to post-apheresis. Annexin V-platelet positive EVs occupied the greatest proportion in pre- and post-apheresis samples (~90%).
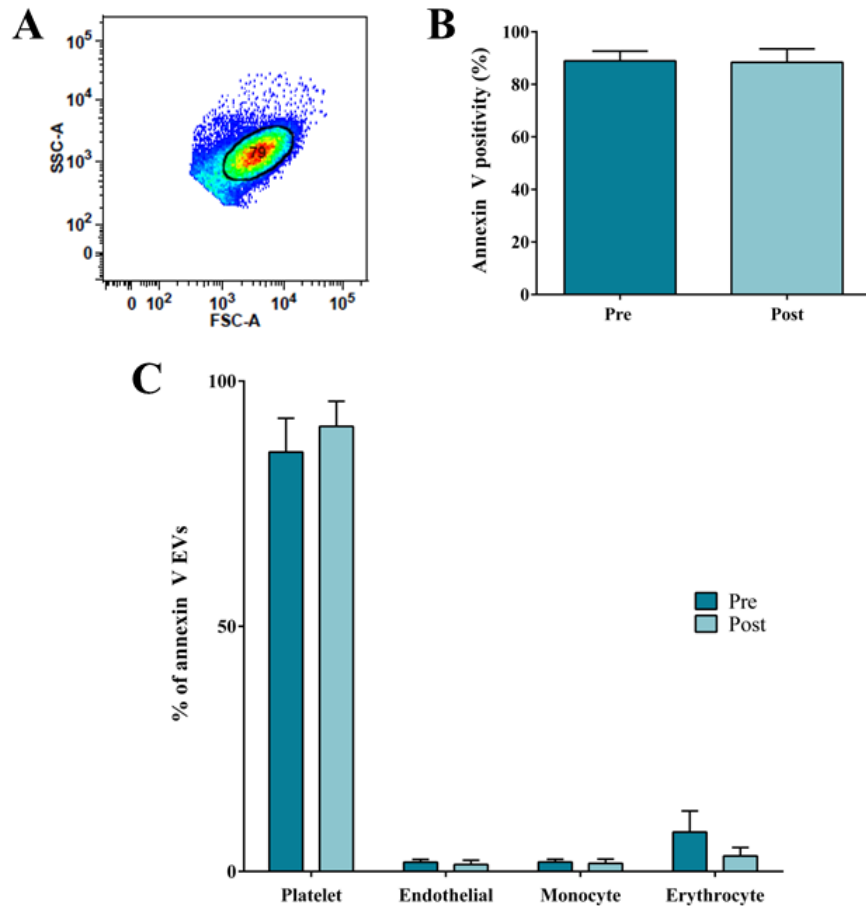
Figure 8.3.5: The effect of apheresis on EV origin. EVs from pre- and post-apheresis samples were analysed using flow cytometry to determine their cellular origin. The FSC-A and SSC-A properties of EVs were compared to those of platelets in fresh plasma in order to define a submicron gate (**A**). (**B**) EVs falling within this gate were then assessed for their annexin V positivity. (**C**) Annexin V positive EVs were then stained for markers of platelets (CD41), endothelial cells (CD144), monocytes (CD11b) and erythrocytes (CD235a). Data are presented as mean ± SEM, (n=12).

8.3.4 Effect of apheresis on fatty acid concentration and composition

GC-FID was used to compare the fatty acids of the EV fraction to those of the surrounding plasma (**Figure 8.3.6**). Total fatty acid concentration was elevated in plasma (healthy volunteers: 1.5 ± 0.2 mg/mL plasma; FH: 2.4 ± 0.4 mg/mL plasma; $p = 0.02$; **A**) and EVs (healthy volunteers: 0.01 ± 0.002 ng/10^6 EVs; FH: 0.03 ± 0.006 ng/10^6 EVs; $p = 0.02$; **C**) in individuals with FH compared to healthy controls.

The composition of several plasma and EV fatty acids differed between healthy volunteers and individuals with FH (**Figure 8.3.6 B/D**). Generally, the same fatty acids were altered in both plasma and EVs. *cis*-vaccenic acid (C18:1n7) and eicosapentaenoic acid (EPA; C20:5n3) were increased in both plasma and EVs of individuals with FH. Stearic acid, docosanoic acid (C22:0), docosapentaenoic acid (C22:5n3) and lignoceric acid (C24:0) were decreased in plasma and EVs of individuals with FH. Whilst palmitoleic acid was increased in plasma of FH individuals, it was decreased in corresponding EVs. Similarly, *cis*-7-hexadecanoic acid (C16:1n9) was decreased in plasma in FH individuals but increased in corresponding EVs. Oleic acid was also decreased specifically within EVs of FH individuals.
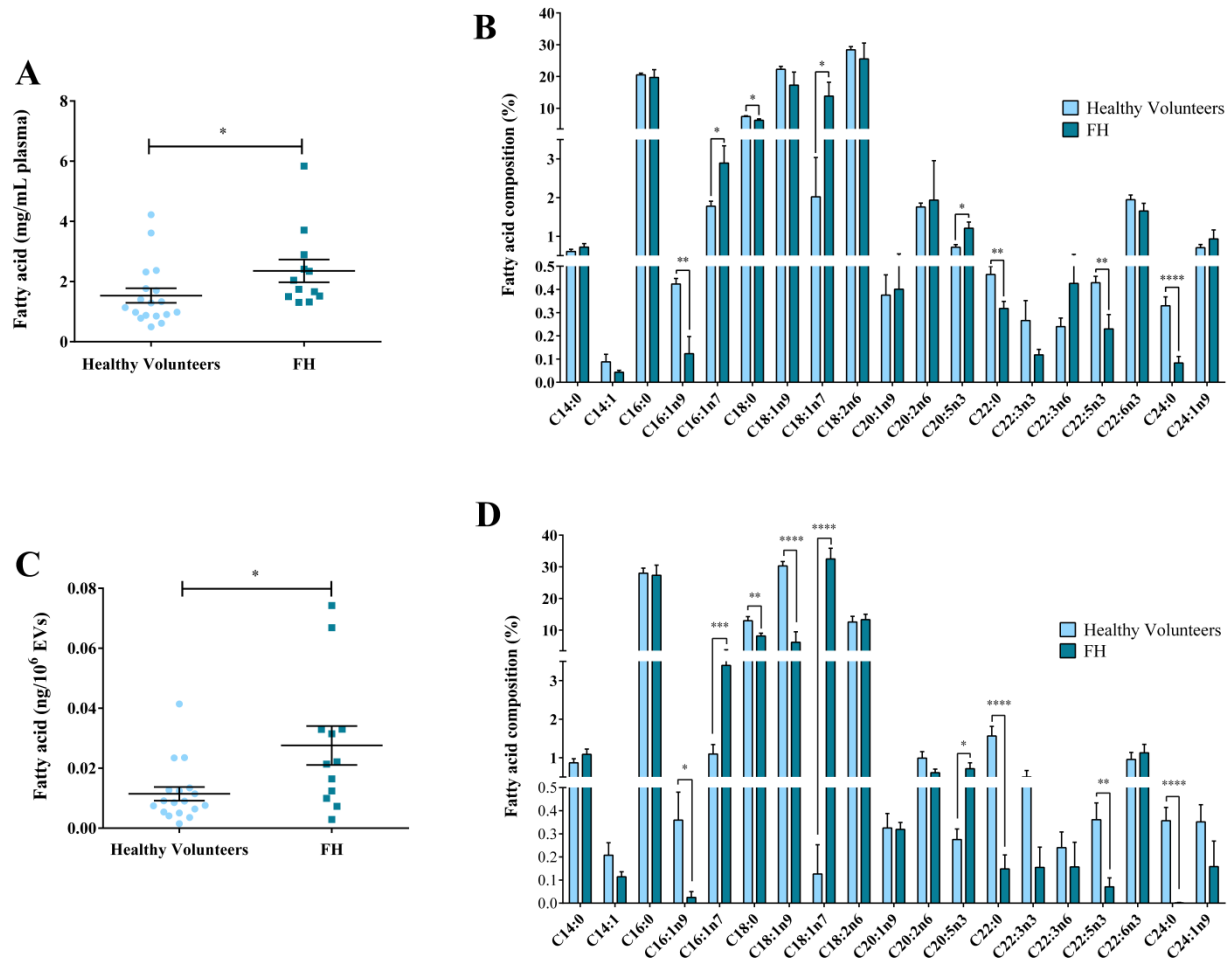
Figure 8.3.6: Fatty acid analysis. Comparison of the total fatty acid concentration of plasma (**A**) and EVs (**C**) and the individual fatty acid composition of plasma (**B**) and EVs (**D**) of healthy volunteers versus FH. Healthy volunteers (n=7), FH (n=12); ****$p<0.00001$, **$p<0.01$, *$p<0.05$.

Total plasma fatty acid concentration was reduced following apheresis (pre: 2.4 ± 1.3 mg/mL to post: 1.3 ± 0.2 mg/mL, $p = 0.01$; **Figure 8.3.7 A**) though this was not mirrored in the EV fraction (pre: 0.03 ± 0.006 ng/10^6 EVs to post: 0.04 ± 0.009 ng/10^6 EVs, $p = 0.2$; **Figure 8.3.7 C**).

The composition of five fatty acids were significantly altered post-apheresis in the plasma (**Figure 8.3.7 B**). Myristic acid (C14:0), *cis*-vaccenic acid, EPA, and docosatrienoic acid (C22:3n3) were increased in post-apheresis plasma samples whilst stearic acid was decreased following apheresis. Three of these fatty acids were also altered in EV samples following apheresis (**Figure 8.3.7 D**). Stearic acid was increased whilst myristic acid and *cis*-vaccenic acid were decreased post-apheresis in EV samples.

A number of significant differences were also observed from directly comparing plasma fatty acid composition with corresponding EV fatty acids (**Table 8.3.4**). Ten fatty acids were compositionally different between plasma and EVs in both pre- and post-apheresis samples. Interestingly, these 10 fatty acids were not the same in pre- and post-apheresis samples.
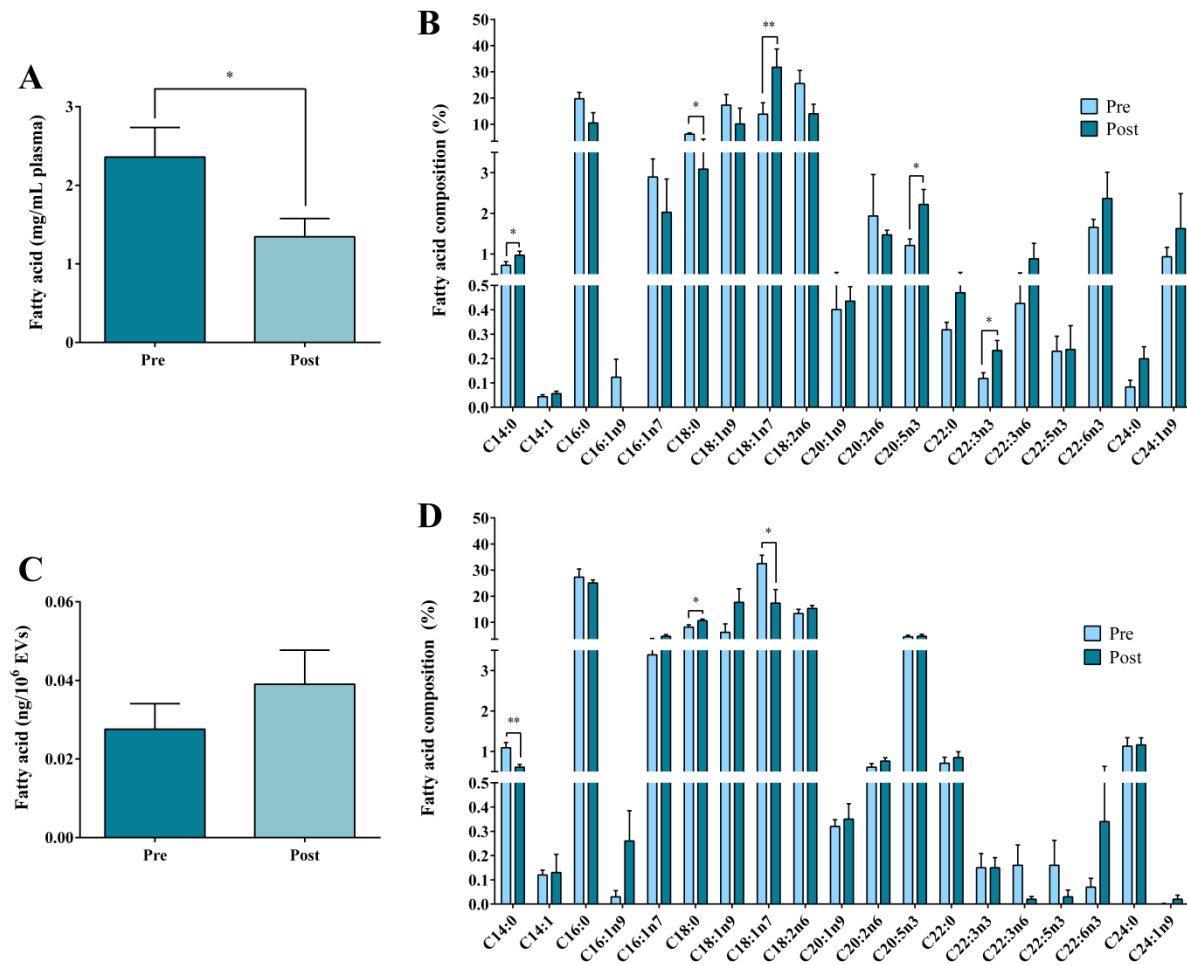
Figure 8.3.7: Effect of apheresis on fatty acids. Comparison of the total fatty acid concentration of plasma (**A**) and EVs (**C**) and the individual fatty acid composition of plasma (**B**) and EVs (**D**) pre- and post-apheresis (n=12); ****$p<0.00001$, **$p<0.01$, *$p<0.05$.

Fatty acid	Pre-apheresis			Post-apheresis		
	Plasma (%)	EVs (%)	*p* value	Plasma (%)	EVs (%)	*p* value
C14:0	0.6 ± 0.1	1.1 ± 0.1	*0.04*	0.9 ± 0.1	0.6 ± 0.07	*0.008*
C14:1	0.04 ± 0.01	0.1 ± 0.02	*0.006*	0.06 ± 0.1	0.1 ± 0.08	*NS*
C16:0	15.7 ± 3.2	27.3 ± 3.2	*NS*	10.5 ± 3.9	25.1 ± 1.2	*0.002*
C16:1n9	2.5 ± 0.6	3.4 ± 0.4	*NS*	2.0 ± 0.8	4.6 ± 0.7	*0.02*
C16:1n7	5.0 ± 0.8	8.2 ± 0.9	*NS*	3.1 ± 1.3	10.6 ± 0.6	*<0.001*
C18:0	15.0 ± 4.2	6.2 ± 3.3	*0.04*	10.1 ± 6.0	17.7 ± 5.4	*NS*
C18:1n9	11.3 ± 4.2	32.5 ± 3.4	*0.003*	31.8 ± 7.0	17.4 ± 5.4	*NS*
C18:1n7	22.2 ± 5.8	13.3 ± 1.7	*0.03*	14.0 ± 3.6	15.3 ± 1.2	*NS*
C20:2n6	1.7 ± 1.0	0.6 ± 0.09	*NS*	1.5 ± 0.1	0.8 ± 0.09	*<0.001*
C20:5n3	0.9 ± 0.2	0.7 ± 0.15	*0.03*	2.2 ± 0.4	0.9 ± 0.15	*0.002*
C22:0	0.3 ± 0.05	0.1 ± 0.06	*0.02*	0.5 ± 0.07	0.1 ± 0.04	*0.001*
C22:3n3	0.1 ± 0.03	0.2 ± 0.09	*NS*	0.2 ± 0.04	0.02 ± 0.01	*<0.001*
C22:3n6	0.4 ± 0.1	0.2 ± 0.1	*NS*	0.9 ± 0.4	0.03 ± 0.03	*0.004*
C22:5n3	0.2 ± 0.06	0.07 ± 0.04	*0.04*	0.2 ± 0.1	0.3 ± 0.3	*NS*
C24:0	0.07 ± 0.03	0.002 ± 0.002	*0.009*	0.2 ± 0.05	0.02 ± 0.02	*0.003*
C24:1n9	0.9 ± 0.2	0.2 ± 0.1	*0.006*	1.6 ± 0.7	0.04 ± 0.02	*NS*

Table 8.3.4: Comparison of plasma and EV fatty acids. Individual fatty acid compositions of plasma and EV samples were directly compared pre- and post-apheresis. Data are presented as mean $\pm$ SEM (n=12), only statistically significant *p* values are given, NS = non-significant.

8.3.5 Extracellular vesicle thrombin generation

Thrombin generation of EVs pre- and post-apheresis was measured using CAT. EV thrombin generation over time was not shown to change following apheresis (pre: 764.8 ± 171.0 area under curve (AUC); to post: 676.0 ± 133.4 AUC; $p = 0.7$; **Figure 8.3.8 A**). However, EV thrombin generation over time showed significant correlation with EV concentration as measured by TRPS (np100) and NTA (r= 0.6, $p = 0.001$ for TRPS np100; **Figure 8.3.8 B**; and r=0.4, $p = 0.04$ for NTA; **Figure 8.3.8 D**). No correlation was found between thrombin generation over time and EV concentration as measured by TRPS using the np200 nanopore (r= -0.1, $p = 0.7$; **Figure 8.3.8 C**).
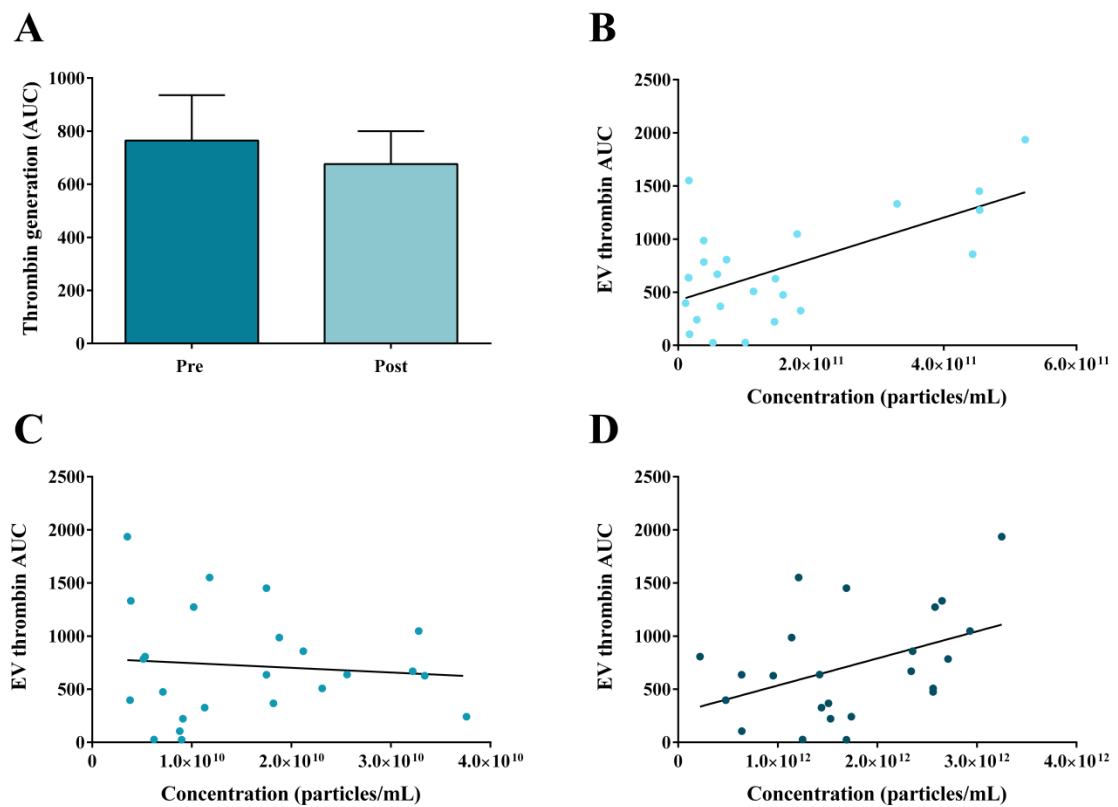
Figure 8.3.8: Thrombin generation potential of EVs in FH. (**A**) Thrombin generation of EVs over time was measured pre- and post-apheresis. EV thrombin generation over time was then correlated against EV concentration measured using TRPS: (**B**) np100, (**C**) np200 and (**D**) NTA; (n=12), AUC = area under curve.

8.4 Discussion

8.4.1 Key findings

The key findings of this chapter were:

1. Circulating exosomes were elevated in individuals with FH compared to healthy volunteers. Apheresis reduced the concentration of EVs, particularly those between 200 – 250 nm.

2. The origin of circulating EVs in individuals with FH was similar to that of healthy volunteers, though endothelial-derived EVs were elevated in FH. Apheresis did not alter the proportion of circulating EVs from a particular cellular origin, the majority of which were annexin V/platelet-positive.

3. Plasma and EV fatty acid concentration was elevated in FH compared to healthy volunteers. Fatty acid composition of plasma and EVs was altered between healthy volunteers and FH. Apheresis reduced plasma fatty acid concentration and altered the composition of certain fatty acids in both plasma and EVs. The fatty acid composition of EVs was different to that of surrounding plasma.

4. The thrombin generation potential of EVs did not differ following apheresis. However, thrombin generation was positively correlated with EV concentration in FH as measured by TRPS np100 and NTA.

8.4.2 Main discussion

Circulating EVs are elevated in a number of diseases including in patients with severe hypercholesterolaemia (541,542). This chapter presents novel data regarding the effects of apheresis on EV size, concentration, origin, fatty acid concentration and thrombin generation in patients with FH. Apheresis reduces the circulating EV concentration, the majority of which are annexin V/platelet-positive EVs.

Several methods exist to measure EVs, though often the technique employed is heavily dictated by the research question and protocol, and each exhibits unique advantages/limitations. Thus two well-established methods for EV measurement were employed in order to capture the full spectrum of EV sizes. At the time, TRPS

and NTA had not previously been subjected to a direct comparison in biological samples. The data presented here illustrate that the range of detectability of TRPS (np100 and np200) and NTA are similar, and although they differ vastly in reported EV concentration reported, taken together there is considerable agreement. This is consistent with bead-based experiments conducted in *Chapter 3*.

No change was observed with TRPS or NTA in mode particle size pre- versus post-apheresis. TRPS using the np200 and NTA both measured a fall in EV concentration pre- versus post-apheresis. EVs within the range of 200-250 nm were reduced the most, which is greater than the size of LDL particles (543), indicating the techniques are measuring a reduction EVs and not LDL. No difference was found in EV concentration with the np100 following apheresis. This further supports that the observed fall in EV concentration by the np200 and NTA was not due to either technique detecting LDL, as the particulate size of LDL lies within the sensitivity of the np100 pore range. Compared to health volunteers, EVs were elevated in the exosomal range in individuals with FH, despite apheresis reducing EVs between 200-250 nm. However, the healthy volunteers used for comparison to FH individuals were not matched for age and BMI and therefore do not represent true matched controls. Total EV concentration was elevated in individuals with FH though this did not quite reach significance.

Flow cytometric measurement of EVs revealed no changes in annexin V positivity or cellular origin following apheresis. In keeping with data at the time (56,542,544), EVs were mostly annexin V positive and of platelet origin (88.9 ± 13%). Taken together with the fall in EV concentration this would suggest that apheresis non-selectively removes EVs, the majority of which are annexin V positive and derived from platelets. These EVs have not only been shown to be elevated in an array of disease states (545–550) but also to promote coagulation (438), atherosclerotic plaque formation (551) and to be associated with atherothrombotic events (547). Non-selective removal of these EVs by apheresis may reduce the risk of thrombus formation by slowing the progression of atherosclerotic lesions thereby complementing the effect of LDL removal. EVs in healthy volunteers were also found to be mainly annexin V positive and of platelet origin, though individuals with FH had a greater concentration of these circulating annexin V/platelet positive EVs compared to healthy volunteers. Individuals with FH had a greater proportion of

endothelial-derived EVs, perhaps suggesting a higher level of endothelial activation compared to healthy volunteers, although the percentage of the total population of EVs was still relatively low (<2%).

GC-FID was used to measure fatty acid concentration and composition of plasma and EVs pre- and post-apheresis. The relative atheroprotective mechanisms of MUFAs and PUFAs are well documented (552) as are the data implicating SFAs in arterial wall lipid accumulation and atherosclerotic plaque formation (553). EVs have been shown to carry a specific cargo of proteins, genetic material and small molecules including fatty acids (554) that can initiate a pro-inflammatory response in target cells (534). Here, concentration of fatty acids was increased in both plasma and EV fractions of FH individuals compared to healthy volunteers. Evidently, individuals with FH have an increased circulating reservoir of lipids compared to healthy volunteers, though intriguingly, some of these excess lipids are incorporated into EVs. Apheresis reduced total fatty acid concentration of plasma. However, this was not reflected in the EV fraction following apheresis. Thus, although the overall number of EVs decreases pre- versus post-apheresis, the fatty acid concentration per EV remains the same. The composition of several fatty acids were different in individuals with FH compared to healthy volunteers in both plasma and EVs, however affected fatty acids and the trends (i.e. increase or decrease) were the same. Surprisingly, plasma and EVs from individuals with FH were more enriched in mono- and polyunsaturated fatty acids such as EPA and contained fewer saturated fatty acids compared to healthy volunteers. However, further work with more reliable healthy controls is needed to confirm these potential differences. EV fatty acids altered following apheresis in FH were the same as those altered in the plasma fraction with apheresis, however the trend of change was specific to EVs or plasma. The physiological relevance of these contradictory changes between plasma and EVs remains to be elucidated. Furthermore, when plasma was directly compared with the EV fraction, the composition of fatty acids was found to be different between compartments. This suggests that the fatty acid composition of EVs is independent to that of surrounding plasma, a concept previously found in a separate cohort of patients with PCOS (76) and data presented in *Chapter 4* (159).

The potential of EVs to generate thrombin was assessed using CAT. No change was observed in EV peak thrombin generation following apheresis. However, total EV

concentration measured by either TRPS (np100) or NTA showed a positive correlation with the total thrombin AUC whereas EV concentration measured by TRPS (np200) showed no correlation. Taken together, this suggests a reduction in EVs is associated with decreased thrombin generation capacity and that smaller EVs, particularly exosomes, are associated with an increased total thrombin generation over time. This conclusion was met based on the fact that both TRPS (np100) and NTA have an increased sensitivity for EVs in the exosomal range compared to TRPS (np200). Furthermore, individuals with FH were shown to have an increased circulating population of smaller EVs compared with healthy volunteers. Both TRPS (np100) and NTA showed a trend towards reduction in exosomal populations of EVs following apheresis, though this did not reach significance. This may suggest that the increased circulating population of exosomes in individuals with FH contributes to a more procoagulant EV fraction. Apheresis treatment non-selectively removes EVs and could potentially reduce the procoagulant potential of exosomes and smaller EVs. In keeping with previous data, (555,556) our results confirm EVs have endogenous TF activity and can stimulate thrombin generation. When exogenous TF was added to EVs to stimulate thrombin generation, the correlation between EV concentration and AUC was lost, indicating saturation of thrombin generation.

8.4.3 Limitations

As this study was an additional part of the normal clinical care received by individuals with FH, three different types of apheresis treatment were used. The present study was not designed to address the effects of the type of apheresis treatment on EVs in FH, though observationally, there were no differences in EV concentration between the techniques. *In vitro* studies have shown that the surface morphology of the adsorbent polymer may effect EV production (557), though this requires confirmation *in vivo*. Having now established that apheresis directly reduces EV concentration, future longitudinal studies should establish whether the reduction in atherogenic EVs is maintained between apheresis treatments and explore the physiological relevance this reduction in EVs has in regards to CVD pathology.

FC measurements to assess cellular origin of EVs pose some potential limitations. EVs were initially gated based on their annexin V positivity meaning only annexin V

positive EVs were analysed for cellular origin. However, not all EVs display annexin V positivity (63). Given the majority of EVs measured in this study were annexin V positive (~90%) and the routine use of annexin V positivity to gate EV populations (56,558,559), these EVs were selected for subsequent staining for markers of cellular origin. In hindsight, the cellular origin of annexin V positive and negative EVs should have been assessed for cellular origin. The rationale at the time however was based on data showing annexin V positive EVs to be more procoagulant (63).

As discussed in previous chapters, many flow cytometers have a practical lower limit of ~300 nm. Therefore smaller EVs, particularly exosomes, are below the detectability of these cytometers, and the fluorescence data obtained from a given sample does not completely reflect the full range of EV sizes observed by NTA and TRPS. Despite this, FC is still one of the most popular techniques to assess surface antigen expression of EVs, mainly because of its wide availability.

Finally, the thrombin generation of patient EV samples was measured in the presence of pooled, healthy plasma to specifically test the activity of EVs as opposed whole patient plasma (that would likely reflect the influence of apheresis). Future studies should assess the procoagulant activity of plasma pre- to post-apheresis to confirm this reduction in atherogenic EVs.

8.4.4 Conclusions

In summary, apheresis reduces the concentration of circulating EVs in patients with FH, the majority of which are annexin V/platelet-positive. Though EV concentration was reduced, apheresis had no effect on the total fatty acid concentration of EVs. Fatty acid composition of EVs is unique and does not reflect that of surrounding plasma. EV concentration (particularly in the exosomal range) positively correlated with total thrombin generation, suggesting that a reduction in EV concentration via apheresis in FH may reduce the ability of EVs to produce thrombin. The removal of EVs that are predominantly annexin V and platelet-derived is a novel finding, supporting the notion that apheresis may have beneficial cardiovascular effects beyond lipoprotein removal. Future work should establish whether EV reduction during apheresis correlates with the longer-term benefits of this treatment.

9. General Discussion

9.1 Thesis overview

The primary aim of this thesis was to explore the characteristics and potential functional applications of adipocyte-derived EVs. Initially, this thesis sought to address issues surrounding methodological and pre-analytic processing of EVs to provide a firm background and understanding which could be applied to the remaining chapters. Adipocyte-derived EV release was then characterised using the well-established adipocyte cell line, 3T3-L1. The physiological characteristics of adipocyte EV release were monitored during adipogenesis. Hypoxia was then used as a pathophysiological stimulus for adipocyte EV generation, and these EVs were characterised according to the methods derived in earlier chapters and assessed for their ability to influence Mϕ function. The potential clinical implication of EVs *in vivo* was then considered. A variety of methodologies were used to assess the presence of adipocyte-derived EVs within plasma EV isolates. Finally, plasma EVs were analysed in a clinical cohort undergoing a routine treatment to determine the profile of EVs in CVD and the effects of an acute treatment modality on circulating EVs.

The promise of EVs as novel circulating biomarkers is great in both physiological and disease states. However, EV research is currently hampered by an overall lack of standardisation in the isolation, storage and measurement of EVs, resulting in gross inconsistencies of reported EV protocols and data. It is important to reflect that during the course of this work, the field has progressed and my work has adapted accordingly – thus practice adopted in earlier experiments may not be mirrored in later chapters. Recent recommendations encourage EV researchers to provide evidence of an EV population from "minimal requirements" outlined in **Table 1.1.2** (16). Currently, these are preferably achieved using isolation techniques such as density ultracentrifugation or SEC to ensure separation of EVs from contaminating materials, particularly in plasma samples. EVs are then typically measured using a combination of TEM to visualise and size EV populations; NTA to determine EV concentration and FC (with micrometre beads) or proteomics/lipidomics to phenotype EVs. However, there are still no gold standard protocols or techniques for EV measurements. As such, different methods of EV detection and pre-analytical processing may be used to achieve these outlined requirements for an EV population; therefore, it is important to understand how these methodologies compare.

Two techniques used for EV size and concentration measurements, NTA and TRPS, were compared in *Chapter 3*. At the time of undertaking this comparison, TRPS was an emerging technique for EV quantification and little was known about how this non-optical, impedance-based method compared with the more popular technique, NTA which uses light scattering. Data presented in this thesis suggest that both NTA and TRPS are able to measure calibration beads over a wide range of concentrations, with TRPS being able to detect beads over a greater size range than NTA. However, to achieve this greater range of detection, TRPS requires the use of multiple nanopores. Not only does this increase the labour intensiveness of sample measurement, but data presented in *Chapter 3* also showed that the detected concentration of the same calibration bead varied between nanopores; a concept since observed by others (407,411). Therefore, the additional time taken and the discrepancy in accuracy between pores may render TRPS less advantageous over NTA, despite the greater range of detection of calibration beads of TRPS. Furthermore, TRPS pores were subject to frequent blocking when using polydisperse samples, making measurements frustrating. NTA and TRPS were also compared in a clinical cohort in *Chapter 8* (discussed below) for their measurement of EV size and concentration in individuals with FH. Interestingly, in contrast to bead measurements in *Chapter 3*, polydisperse plasma EVs were detected over a similar size range using NTA and TRPS (np100 and np200), though the total reported concentration of EVs varied greatly between techniques.

Since the completion of this work, guidelines have been proposed for the use of high and low-sensitivity settings for both NTA and TRPS measurements (149,161,162,407,411). These settings for TRPS involve two different combinations of voltage and stretch being applied to each nanopore to improve accuracy of detection at the extremities of the pore. For NTA, larger particles measured using NTA tend to scatter more light, resulting in a "halo" of scattered light which may be counted by NTA software as smaller particles (**Figure 3.4.1**), perhaps partially explaining the reduced sensitivity of NTA for larger particles. Therefore, recent suggestions to analyse polydisperse samples at two dilutions (high and low sensitivity) with optimised analytical settings may overcome this problem. Furthermore, NTA software has been updated since this work was undertaken to reduce the subjectivity of analytical settings (162).

Despite the limitations of both NTA and TRPS, both techniques were superior at detecting individual populations within polydisperse bead samples compared to FC and DLS (*Chapter 3*). In addition to technical comparisons, *Chapter 3* also addressed a selection of the methodological issues of the EV field by comparing protocols at different stages of pre-analytical processing. As others have since shown, the choice of anticoagulant used to collect blood for EV processing, and subsequent isolation and purification steps (such as filtering) can all impact upon the resultant EV population. As current guidelines are still lacking clarity, the best approach currently seems to be consistency in isolation protocols between samples, and to be clear and honest in reporting of protocols to allow comparison with others in the field. As such, from data presented in *Chapter 3* which showed the negative effects of long-term storage on EV size and concentration, experiments conducted in later chapters (*Chapters 4-7*) aimed to utilise freshly isolated EVs wherever possible.

As outlined in *Chapter 1,* AT is a highly active endocrine organ with diverse roles in regulating lipid metabolism, appetite, blood pressure and androgen levels through the secretion of adipokines (347). EVs have also been implicated in a number of homeostatic mechanisms, though research generally focuses on EVs derived from platelets and endothelial cells. However, little is known about EV release from adipocytes and their potential roles in local and endocrine AT function. Data presented in *Chapter 4* provide a detailed characterisation of EVs released from adipocytes pre- and post-adipogenesis. EVs released from both pre- and mature adipocytes display a classical EV morphology and EV markers including CD9, in accordance with the ISEV minimal requirements for an EV population (16). Adipocyte EVs also bear adipocyte protein markers such as PPARγ and adiponectin that reflect their stage of adipogenesis. Data presented in *Chapter 4* were also the first to show detailed analyses of the lipid composition of adipocyte EVs including fatty acid composition, phospholipid composition and phospholipid fatty acid composition. Interestingly, preadipocytes were shown to release more EVs per cell than mature adipocytes which were enriched in fatty acid signalling entities such as arachidonic acid. This suggests that EVs released from preadipocytes may facilitate communication in the early stages of differentiation; a notion recently supported by evidence from hASCs (441). Data has also shown that adipocyte-derived EVs are

able to modulate lipogenesis in neighbouring adipocytes (388) providing further evidence for a functional role of EVs in adipocyte intercommunication.

In addition to the physiological role of EVs in the cardiovascular system, EVs are also elevated in a number of CVDs, and have been shown to have a detrimental role in atherosclerotic plaque formation (207) and arterial stiffening (213). Obesity is a major risk factor for the development of CVD and other comorbidities due to the dysregulation of adipocyte and AT functioning. *Chapters 5 and 6* exposed adipocytes to hypoxia, a potential instigator of adipocyte dysfunction in obesity, to determine the effects on EV characteristics and function. Hypoxia at 1% O_2 was found to induce a significant increase in EV production, without affecting adipocyte viability, and was therefore selected as the hypoxic stimulus. Previous studies have observed increases in EV release following stimulation with 1% O_2 (241,463,471) though never before in adipocytes, with just one study finding an increase in exosomal protein from adipocytes following a hypoxic insult (390). This hypoxic induction of adipocyte-derived EV release could be mediated via HIF-1α as HIF-1α protein was increased in hypoxic adipocytes and silencing of HIF-1α has previously been shown to abate hypoxia-induced EV secretion (463). However, further work is needed to confirm this in hypoxic adipocyte-derived EV release. *Chapter 5* also presents novel data on the effect of hypoxia on lipid and phospholipid composition of adipocytes and adipocyte-derived EVs. A similar profile of fatty acids was altered in adipocytes and corresponding EVs in hypoxia, suggesting that hypoxia-induced changes in cellular lipid metabolism are transferred to the EV. However, comparison of the fatty acid compositions between hypoxic adipocytes and corresponding EVs highlighted a number of compositional differences, generally suggesting EVs were enriched with a greater repertoire of signalling PUFAs. Therefore a greater number of EVs may be released by adipocytes in hypoxia that have a higher signalling capacity, promoting intercellular communication in AT. Indeed, the monocyte chemoattractant protein, MCP-1 was found to be enriched in hypoxic EVs, suggesting a greater potential of these EVs to communicate with monocytes and Mϕ.

Obese AT is associated with an increased infiltration of proinflammatory Mϕ which feed the inflammation and dysfunction of AT in obesity. Hypoxia is able to induce AT dysfunction (380) and data in this thesis indicates that hypoxia also increases the release of EVs from adipocytes capable of interacting with Mϕ. I therefore

hypothesised that hypoxic adipocyte-derived EVs may participate in this cycle of adipocyte hypoxia and Mϕ inflammation by inducing a phenotypic shift of Mϕ towards a proinflammatory, M1 phenotype and stimulating the migration of additional Mϕ. Unfortunately, due to experimental issues with collaborators, experimental repeats could not be completed. However, preliminary data presented in *Chapter 6* suggest that hypoxic adipocyte-derived EVs may have an alternative motive to that originally hypothesised in Mϕ interaction. The migration of Mϕ indeed looked to be more direct towards hypoxic adipocyte EVs, suggesting a greater chemotactic potential of these EVs. However, the M1 cytokine, IL-1β was decreased and the M2 marker, dectin-1 was increased in Mϕ following incubation with hypoxic adipocyte EVs. This suggests that the initial interaction of hypoxic adipocyte EVs with Mϕ may intend to encourage an M2, anti-inflammatory phenotype, perhaps to promote the resolution of hypoxia-induced damage in AT. However, upon recruitment to hypoxic AT, the local environment of dysfunction and inflammation may stimulate the transition of Mϕ to an M1 phenotype, thereby further exacerbating the metabolic dysregulation. However, further repeats need to be completed to ascertain the true intention of hypoxic adipocyte-derived EVs towards Mϕ.

In vitro experiments played an important part in establishing the characteristics and potential functional interactions of adipocyte-derived EVs in this thesis, enabling the identification of specific markers which may be used to probe for the existence of adipocyte-derived EVs *in vivo*. The metabolic and inflammatory status of adipocytes *in vivo* may dictate the development and severity of obesity-related co-morbidities, and therefore adipocyte-derived EVs may provide a novel circulating biomarker of adipocyte functioning. However, the presence of adipocyte-derived EVs in the circulating plasma EV fraction had not previously been reported. Data presented in *Chapter 7* confirms the presence of adipocyte markers in plasma EV isolates and was used to secure a project grant application. Adiponectin, FABP4 and PPARγ were detected in plasma EVs using a range of techniques from previous chapters in this thesis and others have also confirmed our findings (54,514,515). As discussed in *Section 9.2* below, our group is continuing this work to attempt to isolate adipocyte-derived EVs from circulating plasma EVs in order to investigate these EVs in different patient populations as potential biomarkers of disease.

Alterations in circulating EVs have been associated with a number of diseases, generally manifesting as an increase in circulating EV concentration. Therefore, the therapeutic reduction of EVs in diseases with elevated EV concentrations may help to abate EV-mediated disease progression. Novel data presented in *Chapter 8* show that individuals with FH have higher circulating levels of plasma EVs compared to healthy volunteers. Furthermore, routine apheresis treatment received by these individuals as part of their normal clinical care reduced the concentration of circulating EVs as well as LDL. These EVs were primarily annexin V positive and of platelet origin which, as discussed in *Chapter 1.1.8.2*, can be strongly procoagulant. Additionally, the thrombin generation potential of EVs correlated with EV concentration, which indicates that a reduction in these EVs by apheresis may reduce the EV-mediated procoagulant potential in FH individuals. Intriguingly, apheresis treatment provides a long-term reduction in cardiovascular risk for individuals with FH, though the reduction of LDL following apheresis treatment is transient (526). This suggests that the removal of LDL alone by apheresis does not completely account for the long-term cardiovascular benefits of the treatment. The removal of procoagulant EVs by apheresis may therefore provide additional cardiovascular benefits to individuals with FH, though further work is needed to determine whether this removal of EVs accounts for the long-term benefits of apheresis treatment.

Data presented in this thesis provide new insights into the characteristics and potential functions of adipocyte-derived EVs in normal adipocyte processes such as adipogenesis and in disease-like conditions such as obesity-induced hypoxia. Though the EV field is hampered by a lack of standardisation, EVs are emerging as novel cellular communicators and adipocyte-derived EVs in particular may participate in the autocrine, paracrine and endocrine functions of AT. EVs are therefore likely to feature heavily in future biomarker and therapeutic research in a number of different diseases. As such, adipocyte-derived EVs may become important biomarkers of AT function and metabolic risk in obesity.

9.2 Future research

It is hoped that future research into EVs will resolve many of the standardisation issues in EV isolation and measurement. Although this is a challenging task due to the breadth and variety of research within the EV field, it is essential for progression of the field towards the use of EVs as biomarkers of disease and potentially as therapeutic targets.

From an adipocyte EV perspective, data in this thesis provide a number of interesting opportunities for continuation. For example, *Chapter 4* indicated that preadipocytes were much more active in generating EVs than mature adipocytes. The main focus of the pathological role of adipocyte-derived EVs however focused on EV release from mature adipocytes (*Chapters 5 and 6*). Preadipocytes and adipocyte precursors form an important part of AT, largely accounting for the tissue's innate plasticity. Therefore, the release of preadipocyte-derived EVs may be an interesting avenue of research. For instance, a recent study has observed that exposure of preadipocytes undergoing differentiation to intermittent hypoxia results in a population of mature adipocytes with greater insulin sensitivity and ability to store triglycerides (560).

Our own work with adipocyte-derived EVs will continue with data from *Chapters 5 and 6* currently being extended to analyse the effects of hypoxia and inflammation on adipocyte-derived EV release. It is hypothesised that the combination of hypoxia and inflammation may have a synergistic effect on stimulating adipocyte-derived EV release, which may in turn enhance leukocyte recruitment to AT via breakdown of endothelial barriers. Characterisation of adipocyte-derived EVs will also continue using more primary adipocyte sources; both commercial primary adipocyte cells and those isolated by our group directly from human AT. We hope to continue our characterisation of adipocyte-derived EVs and confirm our results from 3T3-L1 adipocytes, but also to examine adipocyte-derived EVs from adipocytes from patients of varying BMIs and diseases (such as T2D). It may be that adipocyte-derived EVs from obese or metabolically dysfunctional individuals differ to those from healthy individuals, thus potentially leading to the identification of novel biomarkers.

In parallel with this, our *in vivo* research into adipocyte-derived EVs will also continue by applying data from this thesis to attempt to isolate adipocyte-derived

EVs from circulating plasma EV populations. Our group are currently trialling a magnetic bead-based approach to selectively isolate specific populations of EVs, including adipocyte-derived EVs. It is hoped this technique can be combined with other techniques such as FC and TRF to allow for dual staining of adipocyte markers to definitively confirm an adipocyte origin.

References

1.   Wolf P. The nature and significance of platelet products in human plasma. Br J Haematol. 1967 May;13(3):269–88.

2.   Chagraff E, West R. The biological significance of the thromboplastic protein of blood. J Biol Chem. 1946 Nov;166(1):189–97.

3.   Palade GE. A small particulate component of the cytoplasm. J Biophys Biochem Cytol. 1955 Jan;1(1):59–68.

4.   Palade G. Intracellular aspects of the process of protein synthesis. Science. 1975 Sep 12;189(4206):867.

5.   Fries E, Rothman JE. Transport of vesicular stomatitis virus glycoprotein in a cell-free extract. Proc Natl Acad Sci U S A. 1980 Jul;77(7):3870–4.

6.   Rothman JE. Lasker Basic Medical Research Award. The machinery and principles of vesicle transport in the cell. Nat Med. 2002 Oct;8(10):1059–62.

7.   Pan B-T, Johnstone RM. Fate of the transferrin receptor during maturation of sheep reticulocytes in vitro: Selective externalization of the receptor. Cell. 1983 Jul;33(3):967–78.

8.   Pan BT, Teng K, Wu C, et al. Electron microscopic evidence for externalization of the transferrin receptor in vesicular form in sheep reticulocytes. J Cell Biol. 1985 Sep;101(3):942–8.

9.   Webber AJ, Johnson SA. Platelet participation in blood coagulation aspects of hemostasis. Am J Pathol. 1970 Jul;60(1):19–42.

10.   Gould SJ, Raposo G. As we wait: coping with an imperfect nomenclature for extracellular vesicles. J Extracell vesicles. 2013 Jan;2.

11.   van der Pol E, Böing AN, Gool EL, et al. Recent developments on the nomenclature, presence, isolation, detection and clinical impact of extracellular vesicles. J Thromb Haemost. 2015 Nov 12;14(1):48–56.

12.   Ostman S, Taube M, Telemo E. Tolerosome-induced oral tolerance is MHC dependent. Immunology. 2005 Dec;116(4):464–76.

13.   Di Vizio D, Kim J, Hager MH, et al. Oncosome formation in prostate cancer: association with a region of frequent chromosomal deletion in metastatic disease. Cancer Res. 2009 Jul 1;69(13):5601–9.

14.   Ronquist G. Prostasomes: Their Characterisation: Implications for Human Reproduction: Prostasomes and Human Reproduction. Adv Exp Med Biol. 2015 Jan;868:191–209.

15.   Schmidt JR, Kliemt S, Preissler C, et al. Osteoblast-released matrix vesicles - regulation of activity and composition by sulfated and non-sulfated glycosaminoglycans. Mol Cell Proteomics. 2015 Nov 23;

16. Lötvall J, Hill AF, Hochberg F, et al. Minimal experimental requirements for definition of extracellular vesicles and their functions: a position statement from the International Society for Extracellular Vesicles. J Extracell vesicles. 2014 Jan;3:26913.

17. Witwer KW, Buzás EI, Bemis LT, et al. Standardization of sample collection, isolation and analysis methods in extracellular vesicle research. J Extracell vesicles. 2013 Jan;2.

18. Poon IKH, Lucas CD, Rossi AG, et al. Apoptotic cell clearance: basic biology and therapeutic potential. Nat Rev Immunol. 2014 Mar;14(3):166–80.

19. Booth AM. Exosomes and HIV Gag bud from endosome-like domains of the T cell plasma membrane. J Cell Biol. 2006 Mar 6;172(6):923–35.

20. Vanlandingham PA, Ceresa BP. Rab7 regulates late endocytic trafficking downstream of multivesicular body biogenesis and cargo sequestration. J Biol Chem. 2009 May 1;284(18):12110–24.

21. Colombo M, Raposo G, Théry C. Biogenesis, Secretion, and Intercellular Interactions of Exosomes and Other Extracellular Vesicles. Annu Rev Cell Dev Biol. 2014 Oct 11;30(1):255–89.

22. Gruenberg J, Stenmark H. The biogenesis of multivesicular endosomes. Nat Rev Mol Cell Biol. 2004 Apr;5(4):317–23.

23. Colombo M, Moita C, van Niel G, et al. Analysis of ESCRT functions in exosome biogenesis, composition and secretion highlights the heterogeneity of extracellular vesicles. J Cell Sci. 2013 Dec 15;126(Pt 24):5553–65.

24. Möbius W, van Donselaar E, Ohno-Iwashita Y, et al. Recycling compartments and the internal vesicles of multivesicular bodies harbor most of the cholesterol found in the endocytic pathway. Traffic. 2003 Apr;4(4):222–31.

25. Trajkovic K, Hsu C, Chiantia S, et al. Ceramide triggers budding of exosome vesicles into multivesicular endosomes. Science. 2008 Feb 29;319(5867):1244–7.

26. Chairoungdua A, Smith DL, Pochard P, et al. Exosome release of β-catenin: a novel mechanism that antagonizes Wnt signaling. J Cell Biol. 2010 Sep 20;190(6):1079–91.

27. van Niel G, Charrin S, Simoes S, et al. The tetraspanin CD63 regulates ESCRT-independent and -dependent endosomal sorting during melanogenesis. Dev Cell. 2011 Oct 18;21(4):708–21.

28. Charrin S, le Naour F, Silvie O, et al. Lateral organization of membrane proteins: tetraspanins spin their web. Biochem J. 2009 Jun 1;420(2):133–54.

29. Escola J-M, Kleijmeer MJ, Stoorvogel W, et al. Selective Enrichment of Tetraspan Proteins on the Internal Vesicles of Multivesicular Endosomes and on Exosomes Secreted by Human B-lymphocytes. J Biol Chem. 1998 Aug 7;273(32):20121–7.

30. Baietti MF, Zhang Z, Mortier E, et al. Syndecan-syntenin-ALIX regulates the biogenesis of exosomes. Nat Cell Biol. 2012 Jul;14(7):677–85.

31. Ghossoub R, Lembo F, Rubio A, et al. Syntenin-ALIX exosome biogenesis and budding into multivesicular bodies are controlled by ARF6 and PLD2. Nat Commun. 2014 Jan;5:3477.

32. Edgar JR, Eden ER, Futter CE. Hrs- and CD63-dependent competing mechanisms make different sized endosomal intraluminal vesicles. Traffic. 2014 Feb;15(2):197–211.

33. Zerial M, McBride H. Rab proteins as membrane organizers. Nat Rev Mol Cell Biol. Nature Publishing Group; 2001 Feb 1;2(2):107–17.

34. Ostrowski M, Carmo NB, Krumeich S, et al. Rab27a and Rab27b control different steps of the exosome secretion pathway. Nat Cell Biol. 2010 Jan;12(1):19–30; sup pp 1–13.

35. Bobrie A, Krumeich S, Reyal F, et al. Rab27a Supports Exosome-Dependent and -Independent Mechanisms That Modify the Tumor Microenvironment and Can Promote Tumor Progression. Cancer Res. 2012 Aug 3;72(19):4920–30.

36. Webber JP, Spary LK, Sanders AJ, et al. Differentiation of tumour-promoting stromal myofibroblasts by cancer exosomes. Oncogene. 2015 Jan 15;34(3):290–302.

37. Söllner T, Whiteheart SW, Brunner M, et al. SNAP receptors implicated in vesicle targeting and fusion. Nature. 1993 Mar 25;362(6418):318–24.

38. Gao Y, Zorman S, Gundersen G, et al. Single reconstituted neuronal SNARE complexes zipper in three distinct stages. Science. 2012 Sep 14;337(6100):1340–3.

39. Gross JC, Chaudhary V, Bartscherer K, et al. Active Wnt proteins are secreted on exosomes. Nat Cell Biol. 2012 Oct;14(10):1036–45.

40. Hyenne V, Apaydin A, Rodriguez D, et al. RAL-1 controls multivesicular body biogenesis and exosome secretion. J Cell Biol. 2015 Oct 12;211(1):27–37.

41. Nousiainen HO, Quintero IB, Myöhänen TT, et al. Mice deficient in transmembrane prostatic acid phosphatase display increased GABAergic transmission and neurological alterations. PLoS One. 2014 Jan;9(5):e97851.

42. Fader CM, Sánchez DG, Mestre MB, et al. TI-VAMP/VAMP7 and VAMP3/cellubrevin: two v-SNARE proteins involved in specific steps of the autophagy/multivesicular body pathways. Biochim Biophys Acta. 2009 Dec;1793(12):1901–16.

43. Manno S, Takakuwa Y, Mohandas N. Identification of a functional role for lipid asymmetry in biological membranes: Phosphatidylserine-skeletal protein interactions modulate membrane stability. Proc Natl Acad Sci. 2002 Feb 5;99(4):1943–8.

44.   Seigneuret M, Zachowski A, Hermann A, et al. Asymmetric lipid fluidity in human erythrocyte membrane: new spin-label evidence. Biochemistry. 1984 Sep 11;23(19):4271–5.

45.   Daleke DL. Regulation of transbilayer plasma membrane phospholipid asymmetry. J Lipid Res. 2003 Feb 1;44(2):233–42.

46.   Sapet C, Simoncini S, Loriod B, et al. Thrombin-induced endothelial microparticle generation: identification of a novel pathway involving ROCK-II activation by caspase-2. Blood. 2006 Sep 15;108(6):1868–76.

47.   Narumiya S, Ishizaki T, Uehata M. Use and properties of ROCK-specific inhibitor Y-27632. Methods Enzymol. 2000 Jan;325:273–84.

48.   Eguchi A, Mulya A, Lazic M, et al. Microparticles release by adipocytes act as "find-me" signals to promote macrophage migration. PLoS One. 2015 Jan;10(4):e0123110.

49.   Midura EF, Prakash PS, Johnson BL, et al. Impact of caspase-8 and PKA in regulating neutrophil-derived microparticle generation. Biochem Biophys Res Commun. 2015 Dec 17;

50.   Rothmeier AS, Marchese P, Petrich BG, et al. Caspase-1-mediated pathway promotes generation of thromboinflammatory microparticles. J Clin Invest. 2015 Apr;125(4):1471–84.

51.   Chaput N, Théry C. Exosomes: immune properties and potential clinical implementations. Semin Immunopathol. 2011 Sep;33(5):419–40.

52.   Turiák L, Misják P, Szabó TG, et al. Proteomic characterization of thymocyte-derived microvesicles and apoptotic bodies in BALB/c mice. J Proteomics. 2011 Sep 6;74(10):2025–33.

53.   Bobrie A, Colombo M, Krumeich S, et al. Diverse subpopulations of vesicles secreted by different intracellular mechanisms are present in exosome preparations obtained by differential ultracentrifugation. J Extracell vesicles. 2012 Jan;1.

54.   Gustafson CM, Shepherd AJ, Miller VM, et al. Age- and sex-specific differences in blood-borne microvesicles from apparently healthy humans. Biol Sex Differ. 2015 Jan;6:10.

55.   Connolly KD, Willis GR, Datta DBN, et al. Lipoprotein-apheresis reduces circulating microparticles in individuals with familial hypercholesterolemia. J Lipid Res. 2014 Oct;55(10):2064–72.

56.   Christersson C, Johnell M, Siegbahn A. Evaluation of microparticles in whole blood by multicolour flow cytometry assay. Scand J Clin Lab Invest. 2013 Apr;73(3):229–39.

57.   Agouti I, Cointe S, Robert S, et al. Platelet and not erythrocyte microparticles are procoagulant in transfused thalassaemia major patients. Br J Haematol. 2015 Nov;171(4):615–24.

58. Burton JO, Hamali HA, Singh R, et al. Elevated levels of procoagulant plasma microvesicles in dialysis patients. PLoS One. 2013 Jan;8(8):e72663.

59. Jayachandran M, Miller VM, Heit JA, et al. Methodology for isolation, identification and characterization of microvesicles in peripheral blood. J Immunol Methods. 2012 Jan 31;375(1-2):207–14.

60. Shah MD, Bergeron AL, Dong J-F, et al. Flow cytometric measurement of microparticles: pitfalls and protocol modifications. Platelets. 2008 Aug;19(5):365–72.

61. Weiss R, Eichhorn T, Spittler A, et al. Release and cellular origin of extracellular vesicles during circulation of whole blood over adsorbent polymers for lipid apheresis. J Biomed Mater Res B Appl Biomater. 2015 Dec 16;

62. Aleman MM, Gardiner C, Harrison P, et al. Differential contributions of monocyte- and platelet-derived microparticles towards thrombin generation and fibrin formation and stability. J Thromb Haemost. 2011 Nov;9(11):2251–61.

63. Connor DE, Exner T, Ma DDF, et al. The majority of circulating platelet-derived microparticles fail to bind annexin V, lack phospholipid-dependent procoagulant activity and demonstrate greater expression of glycoprotein Ib. Thromb Haemost. 2010 May;103(5):1044–52.

64. Théry C, Regnault A, Garin J, et al. Molecular characterization of dendritic cell-derived exosomes. Selective accumulation of the heat shock protein hsc73. J Cell Biol. 1999 Nov 1;147(3):599–610.

65. Oshima K, Aoki N, Kato T, et al. Secretion of a peripheral membrane protein, MFG-E8, as a complex with membrane vesicles. Eur J Biochem. 2002 Feb;269(4):1209–18.

66. Aoki N, Jin-no S, Nakagawa Y, et al. Identification and characterization of microvesicles secreted by 3T3-L1 adipocytes: redox- and hormone-dependent induction of milk fat globule-epidermal growth factor 8-associated microvesicles. Endocrinology. 2007;148(8):3850–62.

67. Zonneveld MI, Brisson AR, Herwijnen MJC van, et al. Recovery of extracellular vesicles from human breast milk is influenced by sample collection and vesicle isolation procedures. Journal of Extracellular Vesicles. 2014.

68. Hugel B, Martínez MC, Kunzelmann C, et al. Membrane microparticles: two sides of the coin. Physiology (Bethesda). 2005 Feb 1;20(1):22–7.

69. Kalra H, Simpson RJ, Ji H, et al. Vesiclepedia: a compendium for extracellular vesicles with continuous community annotation. PLoS Biol. 2012 Jan;10(12):e1001450.

70. Valadi H, Ekström K, Bossios A, et al. Exosome-mediated transfer of mRNAs and microRNAs is a novel mechanism of genetic exchange between cells. Nat

Cell Biol. 2007 Jun;9(6):654–9.

71. Baj-Krzyworzeka M, Szatanek R, Weglarczyk K, et al. Tumour-derived microvesicles carry several surface determinants and mRNA of tumour cells and transfer some of these determinants to monocytes. Cancer Immunol Immunother. 2006 Jul;55(7):808–18.

72. Ratajczak J, Miekus K, Kucia M, et al. Embryonic stem cell-derived microvesicles reprogram hematopoietic progenitors: evidence for horizontal transfer of mRNA and protein delivery. Leukemia. 2006 May;20(5):847–56.

73. van der Vos KE, Abels ER, Zhang X, et al. Directly visualized glioblastoma-derived extracellular vesicles transfer RNA to microglia/macrophages in the brain. Neuro Oncol. 2015 Oct 3;18(1):nov244.

74. Irmak MK, Oztas Y, Oztas E. Integration of maternal genome into the neonate genome through breast milk mRNA transcripts and reverse transcriptase. Theor Biol Med Model. 2012 Jan;9:20.

75. Pegtel DM, van de Garde MDB, Middeldorp JM. Viral miRNAs exploiting the endosomal-exosomal pathway for intercellular cross-talk and immune evasion. Biochim Biophys Acta. Jan;1809(11-12):715–21.

76. Willis GR, Connolly K, Ladell K, et al. Young women with polycystic ovary syndrome have raised levels of circulating annexin V-positive platelet microparticles. Hum Reprod. 2014 Dec;29(12):2756–63.

77. Alvarez-Erviti L, Seow Y, Yin H, et al. Delivery of siRNA to the mouse brain by systemic injection of targeted exosomes. Nat Biotechnol. 2011 Apr;29(4):341–5.

78. Kreimer S, Belov AM, Ghiran I, et al. Mass Spectrometry-based Molecular Characterization of Extracellular Vesicles: Lipidomics and Proteomics. J Proteome Res. 2015 Apr 30;14(6):2367–84.

79. Laulagnier K, Motta C, Hamdi S, et al. Mast cell- and dendritic cell-derived exosomes display a specific lipid composition and an unusual membrane organization. Biochem J. 2004 May 15;380(Pt 1):161–71.

80. Wubbolts R, Leckie RS, Veenhuizen PTM, et al. Proteomic and biochemical analyses of human B cell-derived exosomes. Potential implications for their function and multivesicular body formation. J Biol Chem. 2003 Mar 28;278(13):10963–72.

81. Llorente A, Skotland T, Sylvänne T, et al. Molecular lipidomics of exosomes released by PC-3 prostate cancer cells. Biochim Biophys Acta. 2013 Jul;1831(7):1302–9.

82. Pienimaeki-Roemer A, Kuhlmann K, Böttcher A, et al. Lipidomic and proteomic characterization of platelet extracellular vesicle subfractions from senescent platelets. Transfusion. 2015 Mar;55(3):507–21.

83. Zakharova L, Svetlova M, Fomina AF. T cell exosomes induce cholesterol accumulation in human monocytes via phosphatidylserine receptor. J Cell

Physiol. 2007 Jul;212(1):174–81.

84. Deregibus MC, Cantaluppi V, Calogero R, et al. Endothelial progenitor cell derived microvesicles activate an angiogenic program in endothelial cells by a horizontal transfer of mRNA. Blood. 2007 Oct 1;110(7):2440–8.

85. Morelli AE, Larregina AT, Shufesky WJ, et al. Endocytosis, intracellular sorting, and processing of exosomes by dendritic cells. Blood. 2004 Nov 15;104(10):3257–66.

86. Rana S, Yue S, Stadel D, et al. Toward tailored exosomes: the exosomal tetraspanin web contributes to target cell selection. Int J Biochem Cell Biol. 2012 Sep;44(9):1574–84.

87. Mulcahy LA, Pink RC, Carter DRF. Routes and mechanisms of extracellular vesicle uptake. J Extracell vesicles. 2014 Jan;3.

88. Escrevente C, Keller S, Altevogt P, et al. Interaction and uptake of exosomes by ovarian cancer cells. BMC Cancer. 2011 Jan;11:108.

89. Tan SS, Yin Y, Lee T, et al. Therapeutic MSC exosomes are derived from lipid raft microdomains in the plasma membrane. J Extracell vesicles. 2013 Jan;2.

90. Tian T, Zhu Y-L, Zhou Y-Y, et al. Exosome Uptake through Clathrin-mediated Endocytosis and Macropinocytosis and Mediating miR-21 Delivery. J Biol Chem. 2014 Jun 20;289(32):22258–67.

91. Barrès C, Blanc L, Bette-Bobillo P, et al. Galectin-5 is bound onto the surface of rat reticulocyte exosomes and modulates vesicle uptake by macrophages. Blood. 2010 Jan 21;115(3):696–705.

92. Nanbo A, Kawanishi E, Yoshida R, et al. Exosomes derived from Epstein-Barr virus-infected cells are internalized via caveola-dependent endocytosis and promote phenotypic modulation in target cells. J Virol. 2013 Oct;87(18):10334–47.

93. Feng D, Zhao W-L, Ye Y-Y, et al. Cellular internalization of exosomes occurs through phagocytosis. Traffic. 2010 May;11(5):675–87.

94. Montecalvo A, Larregina AT, Shufesky WJ, et al. Mechanism of transfer of functional microRNAs between mouse dendritic cells via exosomes. Blood. 2012 Jan 19;119(3):756–66.

95. Parolini I, Federici C, Raggi C, et al. Microenvironmental pH is a key factor for exosome traffic in tumor cells. J Biol Chem. 2009 Dec 4;284(49):34211–22.

96. Del Conde I, Shrimpton CN, Thiagarajan P, et al. Tissue-factor-bearing microvesicles arise from lipid rafts and fuse with activated platelets to initiate coagulation. Blood. 2005 Sep 1;106(5):1604–11.

97. Terrisse AD, Puech N, Allart S, et al. Internalization of microparticles by endothelial cells promotes platelet/endothelial cell interaction under flow. J

Thromb Haemost. 2010 Dec;8(12):2810–9.

98. Tian T, Zhu Y-L, Hu F-H, et al. Dynamics of exosome internalization and trafficking. J Cell Physiol. 2013 Jul;228(7):1487–95.

99. Svensson KJ, Christianson HC, Wittrup A, et al. Exosome uptake depends on ERK1/2-heat shock protein 27 signaling and lipid Raft-mediated endocytosis negatively regulated by caveolin-1. J Biol Chem. 2013 Jun 14;288(24):17713–24.

100. Supplement C. Abstracts from the Fourth International Meeting of ISEV, ISEV2015, Washington, D.C., USA, 23-26 April 2015. Journal of Extracellular Vesicles. 2015.

101. Tushuizen ME, Nieuwland R, Scheffer PG, et al. Two consecutive high-fat meals affect endothelial-dependent vasodilation, oxidative stress and cellular microparticles in healthy men. J Thromb Haemost. 2006 May;4(5):1003–10.

102. Tushuizen ME, Diamant M, Peypers EG, et al. Postprandial changes in the phospholipid composition of circulating microparticles are not associated with coagulation activation. Thromb Res. 2012 Jul;130(1):115–21.

103. Tofler GH, Brezinski D, Schafer AI, et al. Concurrent morning increase in platelet aggregability and the risk of myocardial infarction and sudden cardiac death. N Engl J Med. 1987 Jun 11;316(24):1514–8.

104. Madden LA, Vince R V, Sandström ME, et al. Microparticle-associated vascular adhesion molecule-1 and tissue factor follow a circadian rhythm in healthy human subjects. Thromb Haemost. 2008 May;99(5):909–15.

105. Satsangi J, Jewell DP, Welsh K, et al. Effect of heparin on polymerase chain reaction. Lancet (London, England). 1994 Jun 11;343(8911):1509–10.

106. Maguire CA, Balaj L, Sivaraman S, et al. Microvesicle-associated AAV vector as a novel gene delivery system. Mol Ther. 2012 May;20(5):960–71.

107. Ayers L, Kohler M, Harrison P, et al. Measurement of circulating cell-derived microparticles by flow cytometry: sources of variability within the assay. Thromb Res. 2011 Apr;127(4):370–7.

108. Yuana Y, Bertina RM, Osanto S. Pre-analytical and analytical issues in the analysis of blood microparticles. Thromb Haemost. 2010 Dec 21;105(3):396–408.

109. Yuana Y, Böing AN, Grootemaat AE, et al. Handling and storage of human body fluids for analysis of extracellular vesicles. J Extracell vesicles. 2015 Jan;4:29260.

110. Kubota S, Chiba M, Watanabe M, et al. Secretion of small/microRNAs including miR-638 into extracellular spaces by sphingomyelin phosphodiesterase 3. Oncol Rep. 2015 Jan;33(1):67–73.

111. Kilpinen L, Impola U, Sankkila L, et al. Extracellular membrane vesicles from umbilical cord blood-derived MSC protect against ischemic acute kidney

injury, a feature that is lost after inflammatory conditioning. J Extracell vesicles. 2013 Jan;2.

112. Blanchard N, Lankar D, Faure F, et al. TCR activation of human T cells induces the production of exosomes bearing the TCR/CD3/zeta complex. J Immunol. 2002 Apr 1;168(7):3235–41.

113. Shelke GV, Lässer C, Gho YS, et al. Importance of exosome depletion protocols to eliminate functional and RNA-containing extracellular vesicles from fetal bovine serum. Journal of Extracellular Vesicles. 2014.

114. Eitan E, Zhang S, Witwer KW, et al. Extracellular vesicle-depleted fetal bovine and human sera have reduced capacity to support cell growth. J Extracell vesicles. 2015 Jan;4:26373.

115. Sun L, Wang H, Zhu X, et al. Serum deprivation elevates the levels of microvesicles with different size distributions and selectively enriched proteins in human myeloma cells in vitro. Acta Pharmacol Sin. 2014 Mar;35(3):381–93.

116. Li J, Lee Y, Johansson HJ, et al. Serum-free culture alters the quantity and protein composition of neuroblastoma-derived extracellular vesicles. Journal of Extracellular Vesicles. 2015.

117. Théry C, Amigorena S, Raposo G, et al. Isolation and characterization of exosomes from cell culture supernatants and biological fluids. Curr Protoc Cell Biol. 2006 Apr;Chapter 3:Unit 3.22.

118. Böing AN, van der Pol E, Grootemaat AE, et al. Single-step isolation of extracellular vesicles by size-exclusion chromatography. J Extracell vesicles. 2014 Jan;3.

119. Welton JL, Webber JP, Botos L-A, et al. Ready-made chromatography columns for extracellular vesicle isolation from plasma. J Extracell vesicles. 2015 Jan;4:27269.

120. György B, Módos K, Pállinger E, et al. Detection and isolation of cell-derived microparticles are compromised by protein complexes resulting from shared biophysical parameters. Blood. 2011 Jan 27;117(4):e39–48.

121. Linares R, Tan S, Gounou C, et al. High-speed centrifugation induces aggregation of extracellular vesicles. Journal of Extracellular Vesicles. 2015.

122. van der Pol E, Böing AN, Harrison P, et al. Classification, functions, and clinical relevance of extracellular vesicles. Pharmacol Rev. 2012 Jul;64(3):676–705.

123. Webber J, Clayton A. How pure are your vesicles? J Extracell vesicles. 2013 Jan;2.

124. Heinemann ML, Ilmer M, Silva LP, et al. Benchtop isolation and characterization of functional exosomes by sequential filtration. J Chromatogr A. 2014 Dec 5;1371:125–35.

125. Lamparski HG, Metha-Damani A, Yao J-Y, et al. Production and characterization of clinical grade exosomes derived from dendritic cells. J Immunol Methods. 2002 Dec 15;270(2):211–26.

126. Lobb RJ, Becker M, Wen SW, et al. Optimized exosome isolation protocol for cell culture supernatant and human plasma. Journal of Extracellular Vesicles. 2015.

127. Nordin JZ, Lee Y, Vader P, et al. Ultrafiltration with size-exclusion liquid chromatography for high yield isolation of extracellular vesicles preserving intact biophysical and functional properties. Nanomedicine. 2015 May;11(4):879–83.

128. Raposo G, Nijman HW, Stoorvogel W, et al. B lymphocytes secrete antigen-presenting vesicles. J Exp Med. 1996 Mar 1;183(3):1161–72.

129. Ettelaie C, Collier MEW, Maraveyas A, et al. Characterization of physical properties of tissue factor containing microvesicles and a comparison of ultracentrifuge-based recovery procedures. Journal of Extracellular Vesicles. 2014.

130. Chowdhury R, Webber JP, Gurney M, et al. Cancer exosomes trigger mesenchymal stem cell differentiation into pro-angiogenic and pro-invasive myofibroblasts. Oncotarget. 2015 Jan 20;6(2):715–31.

131. Minciacchi VR, You S, Spinelli C, et al. Large oncosomes contain distinct protein cargo and represent a separate functional class of tumor-derived extracellular vesicles. Oncotarget. 2015 May 10;6(13):11327–41.

132. Aatonen MT, Ohman T, Nyman TA, et al. Isolation and characterization of platelet-derived extracellular vesicles. J Extracell vesicles. 2014 Jan;3.

133. Hong P, Koza S, Bouvier ESP. Size-Exclusion Chromatography for the Analysis of Protein Biotherapeutics and their Aggregates. J Liq Chromatogr Relat Technol. 2012 Nov;35(20):2923–50.

134. Baranyai T, Herczeg K, Onódi Z, et al. Isolation of Exosomes from Blood Plasma: Qualitative and Quantitative Comparison of Ultracentrifugation and Size Exclusion Chromatography Methods. PLoS One. 2015 Jan;10(12):e0145686.

135. de Menezes-Neto A, Sáez MJF, Lozano-Ramos I, et al. Size-exclusion chromatography as a stand-alone methodology identifies novel markers in mass spectrometry analyses of plasma-derived vesicles from healthy individuals. J Extracell vesicles. 2015 Jan;4:27378.

136. Muller L, Hong C-S, Stolz DB, et al. Isolation of biologically-active exosomes from human plasma. J Immunol Methods. 2014 Sep;411:55–65.

137. Clayton A, Court J, Navabi H, et al. Analysis of antigen presenting cell derived exosomes, based on immuno-magnetic isolation and flow cytometry. J Immunol Methods. 2001 Jan 1;247(1-2):163–74.

138. Yuana Y, Osanto S, Bertina RM. Use of immuno-magnetic beads for direct

capture of nanosized microparticles from plasma. Blood Coagul Fibrinolysis. 2012 Apr;23(3):244–50.

139. Shih C-L, Chong K-Y, Hsu S-C, et al. Development of a magnetic bead-based method for the collection of circulating extracellular vesicles. N Biotechnol. 2016 Jan 25;33(1):116–22.

140. Inglis H, Norris P, Danesh A. Techniques for the analysis of extracellular vesicles using flow cytometry. J Vis Exp. 2015 Jan;(97).

141. Van Deun J, Mestdagh P, Sormunen R, et al. The impact of disparate isolation methods for extracellular vesicles on downstream RNA profiling. J Extracell vesicles. 2014 Jan;3.

142. Taylor DD, Zacharias W, Gercel-Taylor C. Exosome isolation for proteomic analyses and RNA profiling. Methods Mol Biol. 2011 Jan;728:235–46.

143. Lőrincz ÁM, Timár CI, Marosvári KA, et al. Effect of storage on physical and functional properties of extracellular vesicles derived from neutrophilic granulocytes. J Extracell vesicles. 2014 Jan;3:25465.

144. supplement C. Abstracts from the Third International Meeting of ISEV 2014 Rotterdam, The Netherlands, April 30th – May 3rd, 2014. Journal of Extracellular Vesicles. 2014.

145. Raynel S, Padula MP, Marks DC, et al. Cryopreservation alters the membrane and cytoskeletal protein profile of platelet microparticles. Transfusion. 2015 Oct;55(10):2422–32.

146. George JN, Pickett EB, Heinz R. Platelet membrane microparticles in blood bank fresh frozen plasma and cryoprecipitate. Blood. 1986 Jul;68(1):307–9.

147. Sokolova V, Ludwig A-K, Hornung S, et al. Characterisation of exosomes derived from human cells by nanoparticle tracking analysis and scanning electron microscopy. Colloids Surf B Biointerfaces. 2011 Oct 1;87(1):146–50.

148. Wu Y, Deng W, Klinke Ii DJ. Exosomes: improved methods to characterize their morphology, RNA content, and surface protein biomarkers. Analyst. 2015 Sep 14;140(19):6631–42.

149. van der Pol E, Hoekstra AG, Sturk A, et al. Optical and non-optical methods for detection and characterization of microparticles and exosomes. J Thromb Haemost. 2010 Dec;8(12):2596–607.

150. Zlotogorski-Hurvitz A, Dayan D, Chaushu G, et al. Human saliva-derived exosomes: comparing methods of isolation. J Histochem Cytochem. 2015 Mar;63(3):181–9.

151. Höög JL, Lötvall J. Diversity of extracellular vesicles in human ejaculates revealed by cryo-electron microscopy. J Extracell vesicles. 2015 Jan;4:28680.

152. Yuana Y, Oosterkamp TH, Bahatyrova S, et al. Atomic force microscopy: a novel approach to the detection of nanosized blood microparticles. J Thromb Haemost. 2010 Mar;8(2):315–23.

153. van der Pol E, Coumans F, Varga Z, et al. Innovation in detection of microparticles and exosomes. J Thromb Haemost. 2013 Jun;11 Suppl 1:36–45.

154. van der Pol E, van Gemert MJC, Sturk A, et al. Single vs. swarm detection of microparticles and exosomes by flow cytometry. J Thromb Haemost. 2012 May;10(5):919–30.

155. van der Vlist EJ, Nolte-'t Hoen ENM, Stoorvogel W, et al. Fluorescent labeling of nano-sized vesicles released by cells and subsequent quantitative and qualitative analysis by high-resolution flow cytometry. Nat Protoc. Nature Publishing Group, a division of Macmillan Publishers Limited. All Rights Reserved.; 2012 Jul;7(7):1311–26.

156. Harshman SW, Canella A, Ciarlariello PD, et al. Proteomic characterization of circulating extracellular vesicles identifies novel serum myeloma associated markers. J Proteomics. 2016 Jan 13;

157. Welton JL, Khanna S, Giles PJ, et al. Proteomics Analysis of Bladder Cancer Exosomes. Mol Cell Proteomics. 2010 Mar 11;9(6):1324–38.

158. Webber J, Stone TC, Katilius E, et al. Proteomics analysis of cancer exosomes using a novel modified aptamer-based array (SOMAscan^{TM}) platform. Mol Cell Proteomics. 2014 Apr;13(4):1050–64.

159. Connolly KD, Guschina IA, Yeung V, et al. Characterisation of adipocyte-derived extracellular vesicles released pre- and post-adipogenesis. Journal of Extracellular Vesicles. 2015.

160. Lawrie AS, Albanyan A, Cardigan RA, et al. Microparticle sizing by dynamic light scattering in fresh-frozen plasma. Vox Sang. 2009 Apr;96(3):206–12.

161. Dragovic RA, Gardiner C, Brooks AS, et al. Sizing and phenotyping of cellular vesicles using Nanoparticle Tracking Analysis. Nanomedicine. 2011 Dec;7(6):780–8.

162. Gardiner C, Ferreira YJ, Dragovic RA, et al. Extracellular vesicle sizing and enumeration by nanoparticle tracking analysis. J Extracell vesicles. 2013 Jan;2.

163. Gercel-Taylor C, Atay S, Tullis RH, et al. Nanoparticle analysis of circulating cell-derived vesicles in ovarian cancer patients. Anal Biochem. 2012 Sep 1;428(1):44–53.

164. Weatherall E, Willmott GR. Applications of tunable resistive pulse sensing. Analyst. 2015 May 21;140(10):3318–34.

165. Coumans FAW, van der Pol E, Böing AN, et al. Reproducible extracellular vesicle size and concentration determination with tunable resistive pulse sensing. J Extracell vesicles. 2014 Jan;3:25922.

166. Vogel R, Anderson W, Eldridge J, et al. A variable pressure method for characterizing nanoparticle surface charge using pore sensors. Anal Chem. 2012 Apr 3;84(7):3125–31.

167. Billinge ER, Broom M, Platt M. Monitoring aptamer-protein interactions using tunable resistive pulse sensing. Anal Chem. 2014 Jan 21;86(2):1030–7.

168. Billinge ER, Platt M. Multiplexed, label-free detection of biomarkers using aptamers and Tunable Resistive Pulse Sensing (AptaTRPS). Biosens Bioelectron. 2015 Jun 15;68:741–8.

169. Yáñez-Mó M, Siljander PR-M, Andreu Z, et al. Biological properties of extracellular vesicles and their physiological functions. J Extracell vesicles. 2015 Jan;4:27066.

170. Saunderson SC, Dunn AC, Crocker PR, et al. CD169 mediates the capture of exosomes in spleen and lymph node. Blood. 2014 Jan 9;123(2):208–16.

171. Willekens FLA, Werre JM, Kruijt JK, et al. Liver Kupffer cells rapidly remove red blood cell-derived vesicles from the circulation by scavenger receptors. Blood. 2005 Mar 1;105(5):2141–5.

172. Rand ML, Wang H, Bang KWA, et al. Rapid clearance of procoagulant platelet-derived microparticles from the circulation of rabbits. J Thromb Haemost. 2006 Jul;4(7):1621–3.

173. Takahashi Y, Nishikawa M, Shinotsuka H, et al. Visualization and in vivo tracking of the exosomes of murine melanoma B16-BL6 cells in mice after intravenous injection. J Biotechnol. 2013 May 20;165(2):77–84.

174. Chen Y-W, Chen Y-C, Wang J-S. Absolute hypoxic exercise training enhances in vitro thrombin generation by increasing procoagulant platelet-derived microparticles under high shear stress in sedentary men. Clin Sci (Lond). 2013 May;124(10):639–49.

175. Suades R, Padró T, Vilahur G, et al. Circulating and platelet-derived microparticles in human blood enhance thrombosis on atherosclerotic plaques. Thromb Haemost. 2012 Dec;108(6):1208–19.

176. Owens AP, Mackman N. Microparticles in hemostasis and thrombosis. Circ Res. 2011 May 13;108(10):1284–97.

177. Perez-Pujol S, Marker PH, Key NS. Platelet microparticles are heterogeneous and highly dependent on the activation mechanism: studies using a new digital flow cytometer. Cytometry A. 2007 Jan;71(1):38–45.

178. Jy W, Johansen ME, Bidot C, et al. Red cell-derived microparticles (RMP) as haemostatic agent. Thromb Haemost. 2013 Oct;110(4):751–60.

179. Schecter AD, Spirn B, Rossikhina M, et al. Release of active tissue factor by human arterial smooth muscle cells. Circ Res. 2000 Jul 21;87(2):126–32.

180. Heijnen HF, Schiel AE, Fijnheer R, et al. Activated platelets release two types of membrane vesicles: microvesicles by surface shedding and exosomes derived from exocytosis of multivesicular bodies and alpha-granules. Blood. 1999 Dec 1;94(11):3791–9.

181. Osterud B. Tissue factor/TFPI and blood cells. Thromb Res. 2012

Mar;129(3):274–8.

182. Lacroix R, Plawinski L, Robert S, et al. Leukocyte- and endothelial-derived microparticles: a circulating source for fibrinolysis. Haematologica. 2012 Dec;97(12):1864–72.

183. Berckmans RJ, Sturk A, van Tienen LM, et al. Cell-derived vesicles exposing coagulant tissue factor in saliva. Blood. 2011 Mar 17;117(11):3172–80.

184. Castaman G, Yu-Feng L, Rodeghiero F. A bleeding disorder characterised by isolated deficiency of platelet microvesicle generation. Lancet (London, England). 1996 Mar 9;347(9002):700–1.

185. Toti F, Satta N, Fressinaud E, et al. Scott syndrome, characterized by impaired transmembrane migration of procoagulant phosphatidylserine and hemorrhagic complications, is an inherited disorder. Blood. 1996 Feb 15;87(4):1409–15.

186. Sheldon H, Heikamp E, Turley H, et al. New mechanism for Notch signaling to endothelium at a distance by Delta-like 4 incorporation into exosomes. Blood. American Society of Hematology; 2010 Sep 30;116(13):2385–94.

187. Rhee J-S, Black M, Schubert U, et al. The functional role of blood platelet components in angiogenesis. Thromb Haemost. 2004 Aug;92(2):394–402.

188. Salomon C, Ryan J, Sobrevia L, et al. Exosomal signaling during hypoxia mediates microvascular endothelial cell migration and vasculogenesis. PLoS One. 2013 Jan;8(7):e68451.

189. Gasser O, Schifferli JA. Activated polymorphonuclear neutrophils disseminate anti-inflammatory microparticles by ectocytosis. Blood. 2004 Oct 15;104(8):2543–8.

190. Dalli J, Serhan CN. Specific lipid mediator signatures of human phagocytes: microparticles stimulate macrophage efferocytosis and pro-resolving mediators. Blood. 2012 Oct 11;120(15):e60–72.

191. Dalli J, Norling L V, Renshaw D, et al. Annexin 1 mediates the rapid anti-inflammatory effects of neutrophil-derived microparticles. Blood. 2008 Sep 15;112(6):2512–9.

192. Lim K, Sumagin R, Hyun Y-M. Extravasating Neutrophil-derived Microparticles Preserve Vascular Barrier Function in Inflamed Tissue. Immune Netw. 2013 Jun;13(3):102–6.

193. Van Niel G, Mallegol J, Bevilacqua C, et al. Intestinal epithelial exosomes carry MHC class II/peptides able to inform the immune system in mice. Gut. 2003 Dec;52(12):1690–7.

194. van Niel G, Raposo G, Candalh C, et al. Intestinal epithelial cells secrete exosome-like vesicles. Gastroenterology. 2001 Aug;121(2):337–49.

195. Qazi KR, Gehrmann U, Domange Jordö E, et al. Antigen-loaded exosomes alone induce Th1-type memory through a B-cell-dependent mechanism.

Blood. 2009 Mar 19;113(12):2673–83.

196. Zhang B, Yin Y, Lai RC, et al. Mesenchymal stem cells secrete immunologically active exosomes. Stem Cells Dev. 2014 Jun 1;23(11):1233–44.

197. Ali SY, Sajdera SW, Anderson HC. Isolation and characterization of calcifying matrix vesicles from epiphyseal cartilage. Proc Natl Acad Sci U S A. 1970 Nov;67(3):1513–20.

198. Anderson HC. The role of matrix vesicles in physiological and pathological calcification. Curr Opin Orthop. 2007;18(5):428–33.

199. Wang W, Kirsch T. Retinoic acid stimulates annexin-mediated growth plate chondrocyte mineralization. J Cell Biol. 2002 Jun 10;157(6):1061–9.

200. Mebarek S, Abousalham A, Magne D, et al. Phospholipases of mineralization competent cells and matrix vesicles: roles in physiological and pathological mineralizations. Int J Mol Sci. 2013 Jan;14(3):5036–129.

201. WHO. World Health Organisation, Cardiovascular diseases [Internet]. Fact sheet #317. 2015 [cited 2016 Feb 5]. Available from: http://www.who.int/mediacentre/factsheets/fs317/en/

202. Mallat Z, Benamer H, Hugel B, et al. Elevated levels of shed membrane microparticles with procoagulant potential in the peripheral circulating blood of patients with acute coronary syndromes. Circulation. 2000 Feb 29;101(8):841–3.

203. Bernal-Mizrachi L, Jy W, Jimenez JJ, et al. High levels of circulating endothelial microparticles in patients with acute coronary syndromes. Am Heart J. 2003 Jun;145(6):962–70.

204. Koga H, Sugiyama S, Kugiyama K, et al. Elevated levels of VE-cadherin-positive endothelial microparticles in patients with type 2 diabetes mellitus and coronary artery disease. J Am Coll Cardiol. 2005 May 17;45(10):1622–30.

205. Pfeifer P, Werner N, Jansen F. Role and Function of MicroRNAs in Extracellular Vesicles in Cardiovascular Biology. Biomed Res Int. 2015 Jan;2015:161393.

206. Jansen F, Yang X, Franklin BS, et al. High glucose condition increases NADPH oxidase activity in endothelial microparticles that promote vascular inflammation. Cardiovasc Res. 2013 Apr 1;98(1):94–106.

207. Rautou P-E, Leroyer AS, Ramkhelawon B, et al. Microparticles from human atherosclerotic plaques promote endothelial ICAM-1-dependent monocyte adhesion and transendothelial migration. Circ Res. 2011 Feb 4;108(3):335–43.

208. Bernal-Mizrachi L, Jy W, Fierro C, et al. Endothelial microparticles correlate with high-risk angiographic lesions in acute coronary syndromes. Int J Cardiol. 2004 Dec;97(3):439–46.

209. O'Rourke M. Arterial stiffness, systolic blood pressure, and logical treatment of arterial hypertension. Hypertension. 1990 Apr;15(4):339–47.

210. Shanahan CM, Cary NRB, Salisbury JR, et al. Medial Localization of Mineralization-Regulating Proteins in Association With Monckeberg s Sclerosis : Evidence for Smooth Muscle Cell-Mediated Vascular Calcification. Circulation. 1999 Nov 23;100(21):2168–76.

211. Luo G, Ducy P, McKee MD, et al. Spontaneous calcification of arteries and cartilage in mice lacking matrix GLA protein. Nature. Nature Publishing Group; 1997 Mar 6;386(6620):78–81.

212. Reynolds JL, Skepper JN, McNair R, et al. Multifunctional roles for serum protein fetuin-a in inhibition of human vascular smooth muscle cell calcification. J Am Soc Nephrol. 2005 Oct 1;16(10):2920–30.

213. Reynolds JL, Joannides AJ, Skepper JN, et al. Human vascular smooth muscle cells undergo vesicle-mediated calcification in response to changes in extracellular calcium and phosphate concentrations: a potential mechanism for accelerated vascular calcification in ESRD. J Am Soc Nephrol. 2004 Nov 1;15(11):2857–67.

214. Kapustin AN, Davies JD, Reynolds JL, et al. Calcium regulates key components of vascular smooth muscle cell-derived matrix vesicles to enhance mineralization. Circ Res. 2011 Jun 24;109(1):e1–12.

215. Mizuno Y, Yagi K, Tokuzawa Y, et al. miR-125b inhibits osteoblastic differentiation by down-regulation of cell proliferation. Biochem Biophys Res Commun. 2008 Apr 4;368(2):267–72.

216. Kapustin AN, Chatrou MLL, Drozdov I, et al. Vascular smooth muscle cell calcification is mediated by regulated exosome secretion. Circ Res. 2015 Apr 10;116(8):1312–23.

217. New SEP, Goettsch C, Aikawa M, et al. Macrophage-derived matrix vesicles: an alternative novel mechanism for microcalcification in atherosclerotic plaques. Circ Res. 2013 Jun 21;113(1):72–7.

218. Maldonado N, Kelly-Arnold A, Vengrenyuk Y, et al. A mechanistic analysis of the role of microcalcifications in atherosclerotic plaque stability: potential implications for plaque rupture. Am J Physiol Heart Circ Physiol. 2012 Sep 1;303(5):H619–28.

219. Krohn JB, Hutcheson JD, Martínez-Martínez E, et al. Extracellular vesicles in cardiovascular calcification: Expanding current paradigms. J Physiol. 2016 Jan 29;

220. Stepanian A, Bourguignat L, Hennou S, et al. Microparticle increase in severe obesity: Not related to metabolic syndrome and unchanged after massive weight loss. Obesity. 2013 Nov 2;21(11):2236–43.

221. Goichot B, Grunebaum L, Desprez D, et al. Circulating procoagulant microparticles in obesity. Diabetes Metab. 2006 Feb;32(1):82–5.

222. Murakami T, Horigome H, Tanaka K, et al. Impact of weight reduction on production of platelet-derived microparticles and fibrinolytic parameters in obesity. Thromb Res. 2007 Jan;119(1):45–53.

223. Esposito K, Ciotola M, Schisano B, et al. Endothelial microparticles correlate with endothelial dysfunction in obese women. J Clin Endocrinol Metab. 2006 Sep;91(9):3676–9.

224. Gündüz Z, Dursun İ, Tülpar S, et al. Increased endothelial microparticles in obese and overweight children. J Pediatr Endocrinol Metab. 2012 Jan;25(11-12):1111–7.

225. Campello E, Zabeo E, Radu CM, et al. Hypercoagulability in overweight and obese subjects who are asymptomatic for thrombotic events. Thromb Haemost. 2015 Jan;113(1):85–96.

226. Koiou E, Tziomalos K, Katsikis I, et al. Platelet-derived microparticles in overweight/obese women with the polycystic ovary syndrome. Gynecol Endocrinol. 2013 Mar;29(3):250–3.

227. Koiou E, Tziomalos K, Katsikis I, et al. Circulating platelet-derived microparticles are elevated in women with polycystic ovary syndrome diagnosed with the 1990 criteria and correlate with serum testosterone levels. Eur J Endocrinol. 2011 Jul;165(1):63–8.

228. Morel O, Luca F, Grunebaum L, et al. Short-term very low-calorie diet in obese females improves the haemostatic balance through the reduction of leptin levels, PAI-1 concentrations and a diminished release of platelet and leukocyte-derived microparticles. Int J Obes (Lond). 2011 Dec;35(12):1479–86.

229. Campello E, Zabeo E, Radu CM, et al. Dynamics of circulating microparticles in obesity after weight loss. Intern Emerg Med. 2016 Feb 2;

230. Webber J, Yeung V, Clayton A. Extracellular vesicles as modulators of the cancer microenvironment. Semin Cell Dev Biol. 2015 Apr;40:27–34.

231. Roccaro AM, Sacco A, Maiso P, et al. BM mesenchymal stromal cell-derived exosomes facilitate multiple myeloma progression. J Clin Invest. American Society for Clinical Investigation; 2013 Apr 1;123(4):1542–55.

232. Webber J, Steadman R, Mason MD, et al. Cancer exosomes trigger fibroblast to myofibroblast differentiation. Cancer Res. 2010 Dec 1;70(23):9621–30.

233. Clayton A, Mitchell JP, Court J, et al. Human tumor-derived exosomes down-modulate NKG2D expression. J Immunol. 2008 Jun 1;180(11):7249–58.

234. Yang C, Kim S-H, Bianco NR, et al. Tumor-derived exosomes confer antigen-specific immunosuppression in a murine delayed-type hypersensitivity model. PLoS One. 2011 Jan;6(8):e22517.

235. Clayton A, Mitchell JP, Court J, et al. Human tumor-derived exosomes selectively impair lymphocyte responses to interleukin-2. Cancer Res. 2007 Aug 1;67(15):7458–66.

236. Taylor DD, Gerçel-Taylor C, Lyons KS, et al. T-cell apoptosis and suppression of T-cell receptor/CD3-zeta by Fas ligand-containing membrane vesicles shed from ovarian tumors. Clin Cancer Res. 2003 Nov 1;9(14):5113–9.

237. Andreola G, Rivoltini L, Castelli C, et al. Induction of lymphocyte apoptosis by tumor cell secretion of FasL-bearing microvesicles. J Exp Med. 2002 May 20;195(10):1303–16.

238. Jubb AM, Turley H, Moeller HC, et al. Expression of delta-like ligand 4 (Dll4) and markers of hypoxia in colon cancer. Br J Cancer. Cancer Research UK; 2009 Nov 17;101(10):1749–57.

239. Al-Nedawi K, Meehan B, Micallef J, et al. Intercellular transfer of the oncogenic receptor EGFRvIII by microvesicles derived from tumour cells. Nat Cell Biol. Nature Publishing Group; 2008 May;10(5):619–24.

240. Skog J, Würdinger T, van Rijn S, et al. Glioblastoma microvesicles transport RNA and proteins that promote tumour growth and provide diagnostic biomarkers. Nat Cell Biol. Nature Publishing Group; 2008 Dec 16;10(12):1470–6.

241. King HW, Michael MZ, Gleadle JM. Hypoxic enhancement of exosome release by breast cancer cells. BMC Cancer. 2012 Jan;12:421.

242. Buzas EI, György B, Nagy G, et al. Emerging role of extracellular vesicles in inflammatory diseases. Nat Rev Rheumatol. 2014 Jun;10(6):356–64.

243. Knijff-Dutmer EAJ, Koerts J, Nieuwland R, et al. Elevated levels of platelet microparticles are associated with disease activity in rheumatoid arthritis. Arthritis Rheum. 2002 Jun;46(6):1498–503.

244. Berckmans RJ, Nieuwland R, Tak PP, et al. Cell-derived microparticles in synovial fluid from inflamed arthritic joints support coagulation exclusively via a factor VII-dependent mechanism. Arthritis Rheum. 2002 Nov;46(11):2857–66.

245. Berckmans RJ, Nieuwland R, Kraan MC, et al. Synovial microparticles from arthritic patients modulate chemokine and cytokine release by synoviocytes. Arthritis Res Ther. 2005 Jan;7(3):R536–44.

246. Bhatnagar S, Shinagawa K, Castellino FJ, et al. Exosomes released from macrophages infected with intracellular pathogens stimulate a proinflammatory response in vitro and in vivo. Blood. 2007 Nov 1;110(9):3234–44.

247. Couper KN, Barnes T, Hafalla JCR, et al. Parasite-derived plasma microparticles contribute significantly to malaria infection-induced inflammation through potent macrophage stimulation. PLoS Pathog. 2010 Jan;6(1):e1000744.

248. Mastronardi ML, Mostefai HA, Meziani F, et al. Circulating microparticles from septic shock patients exert differential tissue expression of enzymes

related to inflammation and oxidative stress. Crit Care Med. 2011 Jul;39(7):1739–48.

249. Shimbo K, Miyaki S, Ishitobi H, et al. Exosome-formed synthetic microRNA-143 is transferred to osteosarcoma cells and inhibits their migration. Biochem Biophys Res Commun. 2014 Mar 7;445(2):381–7.

250. Kim S-H, Lechman ER, Bianco N, et al. Exosomes Derived from IL-10-Treated Dendritic Cells Can Suppress Inflammation and Collagen-Induced Arthritis. J Immunol. American Association of Immunologists; 2005 May 5;174(10):6440–8.

251. Andre F, Schartz NEC, Movassagh M, et al. Malignant effusions and immunogenic tumour-derived exosomes. Lancet (London, England). 2002 Jul 27;360(9329):295–305.

252. Lener T, Gimona M, Aigner L, et al. Applying extracellular vesicles based therapeutics in clinical trials - an ISEV position paper. J Extracell vesicles. 2015 Jan;4:30087.

253. Belting M, Christianson HC. Role of exosomes and microvesicles in hypoxia-associated tumour development and cardiovascular disease. J Intern Med. 2015 Sep;278(3):251–63.

254. Chen L, Wang Y, Pan Y, et al. Cardiac progenitor-derived exosomes protect ischemic myocardium from acute ischemia/reperfusion injury. Biochem Biophys Res Commun. 2013 Feb 15;431(3):566–71.

255. Christianson HC, Svensson KJ, van Kuppevelt TH, et al. Cancer cell exosomes depend on cell-surface heparan sulfate proteoglycans for their internalization and functional activity. Proc Natl Acad Sci U S A. 2013 Oct 22;110(43):17380–5.

256. Liu T, Mendes DE, Berkman CE. Functional prostate-specific membrane antigen is enriched in exosomes from prostate cancer cells. Int J Oncol. 2014 Mar;44(3):918–22.

257. Schindler AE, Ebert A, Friedrich E. Conversion of androstenedione to estrone by human tissue. J Clin Endocrinol Metab. 1972 Oct;35(4):627–30.

258. Zhang Y, Proenca R, Maffei M, et al. Positional cloning of the mouse obese gene and its human homologue. Nature. 1994 Dec 1;372(6505):425–32.

259. Trayhurn P, Wood IS. Adipokines: inflammation and the pleiotropic role of white adipose tissue. Br J Nutr. 2004 Sep;92(3):347–55.

260. Warner A, Mittag J. Breaking BAT: can browning create a better white? J Endocrinol. 2015 Oct 8;228(1):R19–29.

261. Elattar S, Satyanarayana A. Can Brown Fat Win the Battle Against White Fat? J Cell Physiol. 2015 Oct;230(10):2311–7.

262. Trayhurn P. The biology of obesity. Proc Nutr Soc. 2005 Feb;64(1):31–8.

263. Cinti S. The adipose organ at a glance. Dis Model Mech. 2012 Sep;5(5):588–94.

264. Fang L, Guo F, Zhou L, et al. The cell size and distribution of adipocytes from subcutaneous and visceral fat is associated with type 2 diabetes mellitus in humans. Adipocyte. Jan;4(4):273–9.

265. Wree A, Schlattjan M, Bechmann LP, et al. Adipocyte cell size, free fatty acids and apolipoproteins are associated with non-alcoholic liver injury progression in severely obese patients. Metabolism. 2014 Dec;63(12):1542–52.

266. Skurk T, Alberti-Huber C, Herder C, et al. Relationship between adipocyte size and adipokine expression and secretion. J Clin Endocrinol Metab. 2007 Mar;92(3):1023–33.

267. Cannon B, Nedergaard J. Brown adipose tissue: function and physiological significance. Physiol Rev. 2004 Jan;84(1):277–359.

268. Cypess AM, Lehman S, Williams G, et al. Identification and importance of brown adipose tissue in adult humans. N Engl J Med. 2009 Apr 9;360(15):1509–17.

269. Feldmann HM, Golozoubova V, Cannon B, et al. UCP1 ablation induces obesity and abolishes diet-induced thermogenesis in mice exempt from thermal stress by living at thermoneutrality. Cell Metab. 2009 Feb;9(2):203–9.

270. Wang QA, Tao C, Gupta RK, et al. Tracking adipogenesis during white adipose tissue development, expansion and regeneration. Nat Med. 2013 Oct;19(10):1338–44.

271. Wu J, Boström P, Sparks LM, et al. Beige adipocytes are a distinct type of thermogenic fat cell in mouse and human. Cell. Elsevier; 2012 Jul 20;150(2):366–76.

272. Vegiopoulos A, Muller-Decker K, Strzoda D, et al. Cyclooxygenase-2 Controls Energy Homeostasis in Mice by de Novo Recruitment of Brown Adipocytes. Science (80-). 2010 May 6;328(5982):1158–61.

273. Roberts LD, Ashmore T, Kotwica AO, et al. Inorganic nitrate promotes the browning of white adipose tissue through the nitrate-nitrite-nitric oxide pathway. Diabetes. 2015 Feb;64(2):471–84.

274. Cornelius P, MacDougald OA, Lane MD. Regulation of Adipocyte Development. Annu Rev Nutr. 1994 Jul;14(1):99–129.

275. Seale P, Bjork B, Yang W, et al. PRDM16 controls a brown fat/skeletal muscle switch. Nature. 2008 Aug 21;454(7207):961–7.

276. Barbatelli G, Murano I, Madsen L, et al. The emergence of cold-induced brown adipocytes in mouse white fat depots is determined predominantly by white to brown adipocyte transdifferentiation. Am J Physiol Endocrinol Metab. 2010 Jun;298(6):E1244–53.

277. Frayn KN, Karpe F. Regulation of human subcutaneous adipose tissue blood flow. Int J Obes (Lond). 2014 Aug;38(8):1019–26.

278. Kissebah AH, Krakower GR. Regional adiposity and morbidity. Physiol Rev. 1994 Oct;74(4):761–811.

279. Spalding KL, Arner E, Westermark PO, et al. Dynamics of fat cell turnover in humans. Nature. 2008 May 4;453(7196):783–7.

280. Wajchenberg BL. Subcutaneous and Visceral Adipose Tissue: Their Relation to the Metabolic Syndrome. Endocr Rev. 2000 Dec;21(6):697–738.

281. Ibrahim MM. Subcutaneous and visceral adipose tissue: structural and functional differences. Obes Rev. 2010 Jan;11(1):11–8.

282. Wildman RP, Muntner P, Reynolds K, et al. The obese without cardiometabolic risk factor clustering and the normal weight with cardiometabolic risk factor clustering: prevalence and correlates of 2 phenotypes among the US population (NHANES 1999-2004). Arch Intern Med. American Medical Association; 2008 Aug 11;168(15):1617–24.

283. Fried SK, Lee M-J, Karastergiou K. Shaping fat distribution: New insights into the molecular determinants of depot- and sex-dependent adipose biology. Obesity (Silver Spring). 2015 Jul;23(7):1345–52.

284. Björntorp P. Metabolic implications of body fat distribution. Diabetes Care. 1991 Dec;14(12):1132–43.

285. Thomou T, Tchkonia T, Kirkland JL. Adipose Tissue in Health and disease: Cellular and Molecular Basis of Functional Differences amoung Fat Depots. Leff T, Granneman JG, editors. Wiley-Blackwell; 2010. 21-47 p.

286. Britton KA, Fox CS. Perivascular adipose tissue and vascular disease. Clin Lipidol. 2011 Feb;6(1):79–91.

287. Soltis EE, Cassis LA. Influence of perivascular adipose tissue on rat aortic smooth muscle responsiveness. Clin Exp Hypertens A. 1991 Jan;13(2):277–96.

288. Löhn M, Dubrovska G, Lauterbach B, et al. Periadventitial fat releases a vascular relaxing factor. FASEB J. 2002 Jul;16(9):1057–63.

289. Gollasch M. Vasodilator signals from perivascular adipose tissue. Br J Pharmacol. 2012 Feb;165(3):633–42.

290. Gao Y-J, Lu C, Su L-Y, et al. Modulation of vascular function by perivascular adipose tissue: the role of endothelium and hydrogen peroxide. Br J Pharmacol. 2007 Jun;151(3):323–31.

291. Meyer MR, Fredette NC, Barton M, et al. Regulation of vascular smooth muscle tone by adipose-derived contracting factor. PLoS One. Public Library of Science; 2013 Jan 11;8(11):e79245.

292. Lehman SJ, Massaro JM, Schlett CL, et al. Peri-aortic fat, cardiovascular

disease risk factors, and aortic calcification: the Framingham Heart Study. Atherosclerosis. 2010 Jun;210(2):656–61.

293. Greenstein AS, Khavandi K, Withers SB, et al. Local inflammation and hypoxia abolish the protective anticontractile properties of perivascular fat in obese patients. Circulation. 2009 Mar 31;119(12):1661–70.

294. Ntambi JM, Young-Cheul K. Adipocyte differentiation and gene expression. J Nutr. 2000 Dec;130(12):3122S – 3126S.

295. Green H, Kehinde O. Spontaneous heritable changes leading to increased adipose conversion in 3T3 cells. Cell. 1976 Jan;7(1):105–13.

296. Green H, Kehinde O. An established preadipose cell line and its differentiation in culture. II. Factors affecting the adipose conversion. Cell. 1975 May;5(1):19–27.

297. Doi H, Masaki N, Takahashi H, et al. A new preadipocyte cell line, AP-18, established from adult mouse adipose tissue. Tohoku J Exp Med. 2005 Nov;207(3):209–16.

298. Wabitsch M, Brenner RE, Melzner I, et al. Characterization of a human preadipocyte cell strain with high capacity for adipose differentiation. Int J Obes Relat Metab Disord. 2001 Jan;25(1):8–15.

299. Négrel R, Grimaldi P, Ailhaud G. Establishment of preadipocyte clonal line from epididymal fat pad of ob/ob mouse that responds to insulin and to lipolytic hormones. Proc Natl Acad Sci U S A. 1978 Dec;75(12):6054–8.

300. Forest C, Grimaldi P, Czerucka D, et al. Establishment of a preadipocyte cell line from the epididymal fat pad of the lean C57 BL/6J mouse--long term effects of insulin and triiodothyronine on adipose conversion. In Vitro. 1983 Apr;19(4):344–54.

301. Gregoire FM, Smas CM, Sul HS. Understanding adipocyte differentiation. Physiol Rev. 1998 Jul;78(3):783–809.

302. Morrison S, McGee SL. 3T3-L1 adipocytes display phenotypic characteristics of multiple adipocyte lineages. Adipocyte. Jan;4(4):295–302.

303. Draman MS, Grennan-Jones F, Zhang L, et al. Effects of prostaglandin F(2α) on adipocyte biology relevant to graves' orbitopathy. Thyroid. 2013 Dec;23(12):1600–8.

304. Rodbell M. Metabolism of isolated fat cells. I. Effects of hormones on glucose metabolism and lipolysis. J Biol Chem. 1964 Feb;239:375–80.

305. Alessi MC, Peiretti F, Morange P, et al. Production of plasminogen activator inhibitor 1 by human adipose tissue: possible link between visceral fat accumulation and vascular disease. Diabetes. 1997 May;46(5):860–7.

306. Kranendonk MEG, Visseren FLJ, van Balkom BWM, et al. Human adipocyte extracellular vesicles in reciprocal signaling between adipocytes and macrophages. Obesity (Silver Spring). 2014 May;22(5):1296–308.

307. Kranendonk MEG, Visseren FLJ, van Herwaarden JA, et al. Effect of extracellular vesicles of human adipose tissue on insulin signaling in liver and muscle cells. Obesity (Silver Spring). 2014 Oct;22(10):2216–23.

308. García-Fuentes E, Santiago-Fernández C, Gutiérrez-Repiso C, et al. Hypoxia is associated with a lower expression of genes involved in lipogenesis in visceral adipose tissue. J Transl Med. 2015 Jan;13:373.

309. Pittenger MF, Mackay AM, Beck SC, et al. Multilineage potential of adult human mesenchymal stem cells. Science. 1999 Apr 2;284(5411):143–7.

310. Ahfeldt T, Schinzel RT, Lee Y-K, et al. Programming human pluripotent stem cells into white and brown adipocytes. Nat Cell Biol. 2012 Feb;14(2):209–19.

311. Xiong C, Xie C-Q, Zhang L, et al. Derivation of adipocytes from human embryonic stem cells. Stem Cells Dev. 2005 Dec;14(6):671–5.

312. Farooqi IS, Matarese G, Lord GM, et al. Beneficial effects of leptin on obesity, T cell hyporesponsiveness, and neuroendocrine/metabolic dysfunction of human congenital leptin deficiency. J Clin Invest. 2002 Oct;110(8):1093–103.

313. Kobayashi K, Forte TM, Taniguchi S, et al. The db/db mouse, a model for diabetic dyslipidemia: molecular characterization and effects of Western diet feeding. Metabolism. 2000 Jan;49(1):22–31.

314. Maffei M, Fei H, Lee GH, et al. Increased expression in adipocytes of ob RNA in mice with lesions of the hypothalamus and with mutations at the db locus. Proc Natl Acad Sci. 1995 Jul 18;92(15):6957–60.

315. Moitra J, Mason MM, Olive M, et al. Life without white fat: a transgenic mouse. Genes Dev. 1998 Oct 15;12(20):3168–81.

316. Ahima RS. Adipose tissue as an endocrine organ. Obesity (Silver Spring). 2006 Aug;14 Suppl 5:242S – 249S.

317. Pajvani UB, Hawkins M, Combs TP, et al. Complex distribution, not absolute amount of adiponectin, correlates with thiazolidinedione-mediated improvement in insulin sensitivity. J Biol Chem. 2004 Mar 26;279(13):12152–62.

318. Yamauchi T, Kamon J, Ito Y, et al. Cloning of adiponectin receptors that mediate antidiabetic metabolic effects. Nature. 2003 Jun 12;423(6941):762–9.

319. Combs TP, Berg AH, Obici S, et al. Endogenous glucose production is inhibited by the adipose-derived protein Acrp30. J Clin Invest. American Society for Clinical Investigation; 2001 Dec 15;108(12):1875–81.

320. Rosen ED, MacDougald OA. Adipocyte differentiation from the inside out. Nat Rev Mol Cell Biol. 2006 Dec;7(12):885–96.

321. Janani C, Ranjitha Kumari BD. PPAR gamma gene--a review. Diabetes Metab Syndr. Jan;9(1):46–50.

322. Yang W-S, Jeng C-Y, Wu T-J, et al. Synthetic Peroxisome Proliferator- Activated Receptor- Agonist, Rosiglitazone, Increases Plasma Levels of Adiponectin in Type 2 Diabetic Patients. Diabetes Care. 2002 Feb 1;25(2):376–80.

323. Baxa CA, Sha RS, Buelt MK, et al. Human adipocyte lipid-binding protein: purification of the protein and cloning of its complementary DNA. Biochemistry. 1989 Oct 31;28(22):8683–90.

324. Hotamisligil GS, Johnson RS, Distel RJ, et al. Uncoupling of Obesity from Insulin Resistance Through a Targeted Mutation in aP2, the Adipocyte Fatty Acid Binding Protein. Science (80-). American Association for the Advancement of Science; 1996 Nov 22;274(5291):1377–9.

325. Ikeda Y, Tsuchiya H, Hama S, et al. Resistin affects lipid metabolism during adipocyte maturation of 3T3-L1 cells. FEBS J. 2013 Nov;280(22):5884–95.

326. Fukuhara A, Matsuda M, Nishizawa M, et al. Visfatin: a protein secreted by visceral fat that mimics the effects of insulin. Science. American Association for the Advancement of Science; 2005 Jan 21;307(5708):426–30.

327. Ouchi N, Parker JL, Lugus JJ, et al. Adipokines in inflammation and metabolic disease. Nat Rev Immunol. 2011 Feb;11(2):85–97.

328. Boydens C, Maenhaut N, Pauwels B, et al. Adipose Tissue as Regulator of Vascular Tone. Curr Hypertens Rep. 2012 Mar 14;14(3):270–8.

329. Loskutoff DJ, Samad F. The adipocyte and hemostatic balance in obesity: studies of PAI-1. Arterioscler Thromb Vasc Biol. 1998 Jan;18(1):1–6.

330. Ikeda Y, Tsuchiya H, Hama S, et al. Resistin regulates the expression of plasminogen activator inhibitor-1 in 3T3-L1 adipocytes. Biochem Biophys Res Commun. 2014 May 30;448(2):129–33.

331. Samad F, Pandey M, Loskutoff DJ. Tissue factor gene expression in the adipose tissues of obese mice. Proc Natl Acad Sci U S A. 1998 Jun 23;95(13):7591–6.

332. Adya R, Tan BK, Punn A, et al. Visfatin induces human endothelial VEGF and MMP-2/9 production via MAPK and PI3K/Akt signalling pathways: novel insights into visfatin-induced angiogenesis. Cardiovasc Res. 2008 May 1;78(2):356–65.

333. Crandall DL, Hausman GJ, Kral JG. A review of the microcirculation of adipose tissue: anatomic, metabolic, and angiogenic perspectives. Microcirculation. 1997 Jun;4(2):211–32.

334. Rupnick MA, Panigrahy D, Zhang C-Y, et al. Adipose tissue mass can be regulated through the vasculature. Proc Natl Acad Sci U S A. 2002 Aug 6;99(16):10730–5.

335. Sierra-Honigmann MR, Nath AK, Murakami C, et al. Biological action of leptin as an angiogenic factor. Science. 1998 Sep 11;281(5383):1683–6.

336. Cassis LA, Police SB. Adipose Tissue in Health and Disease: Adipose Tissue and Blood Pressure Regulation. Leff T, Granneman JG, editors. Wiley-Blackwell; 2010. 245-263 p.

337. Exley MA, Hand L, O'Shea D, et al. Interplay between the immune system and adipose tissue in obesity. J Endocrinol. 2014 Nov;223(2):R41–8.

338. Lumeng CN, Bodzin JL, Saltiel AR. Obesity induces a phenotypic switch in adipose tissue macrophage polarization. J Clin Invest. 2007 Jan;117(1):175–84.

339. Wu D, Molofsky AB, Liang H-E, et al. Eosinophils Sustain Adipose Alternatively Activated Macrophages Associated with Glucose Homeostasis. Science (80-). American Association for the Advancement of Science; 2011 Mar 24;332(6026):243–7.

340. Cartwright MJ, Tchkonia T, Kirkland JL. Aging in adipocytes: potential impact of inherent, depot-specific mechanisms. Exp Gerontol. 2007 Jun;42(6):463–71.

341. Rosen CJ, Bouxsein ML. Mechanisms of disease: is osteoporosis the obesity of bone? Nat Clin Pract Rheumatol. 2006 Jan;2(1):35–43.

342. Karagiannides I, Tchkonia T, Dobson DE, et al. Altered expression of C/EBP family members results in decreased adipogenesis with aging. Am J Physiol Regul Integr Comp Physiol. 2001 Jun;280(6):R1772–80.

343. Makowski L, Boord JB, Maeda K, et al. Lack of macrophage fatty-acid-binding protein aP2 protects mice deficient in apolipoprotein E against atherosclerosis. Nat Med. 2001 Jun;7(6):699–705.

344. WHO. World Health Organisation, Obesity and overweight [Internet]. Fact Sheet #311. 2015. Available from: http://www.who.int/mediacentre/factsheets/fs311/en/

345. Banks WA, DiPalma CR, Farrell CL. Impaired transport of leptin across the blood-brain barrier in obesity. Peptides. 1999 Nov;20(11):1341–5.

346. Weyer C, Funahashi T, Tanaka S, et al. Hypoadiponectinemia in obesity and type 2 diabetes: close association with insulin resistance and hyperinsulinemia. J Clin Endocrinol Metab. 2001 May;86(5):1930–5.

347. Trayhurn P, Beattie JH. Physiological role of adipose tissue: white adipose tissue as an endocrine and secretory organ. Proc Nutr Soc. 2001 Aug;60(3):329–39.

348. Fisher RM, Eriksson P, Hoffstedt J, et al. Fatty acid binding protein expression in different adipose tissue depots from lean and obese individuals. Diabetologia. 2001 Oct;44(10):1268–73.

349. Xu A, Wang Y, Xu JY, et al. Adipocyte fatty acid-binding protein is a plasma biomarker closely associated with obesity and metabolic syndrome. Clin Chem. 2006 Mar;52(3):405–13.

350. Furuhashi M, Tuncman G, Görgün CZ, et al. Treatment of diabetes and atherosclerosis by inhibiting fatty-acid-binding protein aP2. Nature. 2007 Jun 21;447(7147):959–65.

351. Samad F, Ruf W. Inflammation, obesity, and thrombosis. Blood. 2013 Nov 14;122(20):3415–22.

352. Berg AH, Scherer PE. Adipose tissue, inflammation, and cardiovascular disease. Circ Res. 2005 May 13;96(9):939–49.

353. Samad F, Yamamoto K, Loskutoff DJ. Distribution and regulation of plasminogen activator inhibitor-1 in murine adipose tissue in vivo. Induction by tumor necrosis factor-alpha and lipopolysaccharide. J Clin Invest. 1996 Jan 1;97(1):37–46.

354. Nakata M, Yada T, Soejima N, et al. Leptin promotes aggregation of human platelets via the long form of its receptor. Diabetes. 1999 Feb;48(2):426–9.

355. Berndt J, Klöting N, Kralisch S, et al. Plasma visfatin concentrations and fat depot-specific mRNA expression in humans. Diabetes. 2005 Oct;54(10):2911–6.

356. Kim S-R, Bae Y-H, Bae S-K, et al. Visfatin enhances ICAM-1 and VCAM-1 expression through ROS-dependent NF-kappaB activation in endothelial cells. Biochim Biophys Acta. 2008 May;1783(5):886–95.

357. Dahl TB, Yndestad A, Skjelland M, et al. Increased expression of visfatin in macrophages of human unstable carotid and coronary atherosclerosis: possible role in inflammation and plaque destabilization. Circulation. 2007 Feb 27;115(8):972–80.

358. Elias I, Franckhauser S, Ferré T, et al. Adipose tissue overexpression of vascular endothelial growth factor protects against diet-induced obesity and insulin resistance. Diabetes. 2012 Jul;61(7):1801–13.

359. Sun K, Wernstedt Asterholm I, Kusminski CM, et al. Dichotomous effects of VEGF-A on adipose tissue dysfunction. Proc Natl Acad Sci U S A. 2012 Apr 10;109(15):5874–9.

360. Sung H-K, Doh K-O, Son JE, et al. Adipose vascular endothelial growth factor regulates metabolic homeostasis through angiogenesis. Cell Metab. 2013 Jan 8;17(1):61–72.

361. García de la Torre N, Rubio MA, Bordiú E, et al. Effects of weight loss after bariatric surgery for morbid obesity on vascular endothelial growth factor-A, adipocytokines, and insulin. J Clin Endocrinol Metab. 2008 Nov;93(11):4276–81.

362. Tan CY, Vidal-Puig A. Adipose tissue expandability: the metabolic problems of obesity may arise from the inability to become more obese. Biochem Soc Trans. 2008 Oct;36(Pt 5):935–40.

363. Brahimi-Horn MC, Pouysségur J. Oxygen, a source of life and stress. FEBS Lett. 2007 Jul 31;581(19):3582–91.

364. Wood IS, de Heredia FP, Wang B, et al. Cellular hypoxia and adipose tissue dysfunction in obesity. Proc Nutr Soc. 2009 Nov;68(4):370–7.

365. Goossens GH, Bizzarri A, Venteclef N, et al. Increased adipose tissue oxygen tension in obese compared with lean men is accompanied by insulin resistance, impaired adipose tissue capillarization, and inflammation. Circulation. 2011 Jul 5;124(1):67–76.

366. Frayn KN, Humphreys SM. Metabolic characteristics of human subcutaneous abdominal adipose tissue after overnight fast. Am J Physiol Endocrinol Metab. 2012 Feb 15;302(4):E468–75.

367. Rausch ME, Weisberg S, Vardhana P, et al. Obesity in C57BL/6J mice is characterized by adipose tissue hypoxia and cytotoxic T-cell infiltration. Int J Obes (Lond). 2008 Mar;32(3):451–63.

368. Yin J, Gao Z, He Q, et al. Role of hypoxia in obesity-induced disorders of glucose and lipid metabolism in adipose tissue. Am J Physiol Endocrinol Metab. 2009 Feb;296(2):E333–42.

369. Ye J, Gao Z, Yin J, et al. Hypoxia is a potential risk factor for chronic inflammation and adiponectin reduction in adipose tissue of ob/ob and dietary obese mice. AJP Endocrinol Metab. 2007 Jul 24;293(4):E1118–28.

370. Cancello R, Henegar C, Viguerie N, et al. Reduction of macrophage infiltration and chemoattractant gene expression changes in white adipose tissue of morbidly obese subjects after surgery-induced weight loss. Diabetes. 2005 Aug;54(8):2277–86.

371. Hosogai N, Fukuhara A, Oshima K, et al. Adipose Tissue Hypoxia in Obesity and Its Impact on Adipocytokine Dysregulation. Diabetes. 2007 Mar 29;56(4):901–11.

372. Varia MA, Calkins-Adams DP, Rinker LH, et al. Pimonidazole: A Novel Hypoxia Marker for Complementary Study of Tumor Hypoxia and Cell Proliferation in Cervical Carcinoma. Gynecol Oncol. 1998 Nov;71(2):270–7.

373. Kabon B, Nagele A, Reddy D, et al. Obesity decreases perioperative tissue oxygenation. Anesthesiology. 2004 Feb;100(2):274–80.

374. Fleischmann E, Kurz A, Niedermayr M, et al. Tissue oxygenation in obese and non-obese patients during laparoscopy. Obes Surg. Jan;15(6):813–9.

375. Hiltebrand LB, Kaiser HA, Niedhart DJ, et al. Subcutaneous oxygen pressure in spontaneously breathing lean and obese volunteers: a pilot study. Obes Surg. 2008 Jan;18(1):77–83.

376. Pasarica M, Rood J, Ravussin E, et al. Reduced oxygenation in human obese adipose tissue is associated with impaired insulin suppression of lipolysis. J Clin Endocrinol Metab. 2010 Aug;95(8):4052–5.

377. Zhang L, Ebenezer PJ, Dasuri K, et al. Aging is associated with hypoxia and oxidative stress in adipose tissue: implications for adipose function. Am J Physiol Endocrinol Metab. 2011 Oct;301(4):E599–607.

378. Goossens GH. The role of adipose tissue dysfunction in the pathogenesis of obesity-related insulin resistance. Physiol Behav. 2008 May 23;94(2):206–18.

379. Yuan F, Guo Z-Z, Ji W-J, et al. BOLD-MRI evaluation of subcutaneous and visceral adipose tissue oxygenation status: effect of dietary salt intake. Am J Transl Res. 2015 Jan;7(3):598–606.

380. Wang B, Wood IS, Trayhurn P. Dysregulation of the expression and secretion of inflammation-related adipokines by hypoxia in human adipocytes. Pflugers Arch. 2007 Dec;455(3):479–92.

381. Yun Z, Maecker HL, Johnson RS, et al. Inhibition of PPAR gamma 2 gene expression by the HIF-1-regulated gene DEC1/Stra13: a mechanism for regulation of adipogenesis by hypoxia. Dev Cell. 2002 Mar;2(3):331–41.

382. Regazzetti C, Peraldi P, Grémeaux T, et al. Hypoxia decreases insulin signaling pathways in adipocytes. Diabetes. 2009 Jan;58(1):95–103.

383. Kralisch S, Ebert T, Lossner U, et al. Adipocyte fatty acid-binding protein is released from adipocytes by a non-conventional mechanism. Int J Obes (Lond). 2013 Dec 13;

384. DeClercq V, d'Eon B, McLeod RS. Fatty acids increase adiponectin secretion through both classical and exosome pathways. Biochim Biophys Acta. 2015 Sep;1851(9):1123–33.

385. Ertunc ME, Sikkeland J, Fenaroli F, et al. Secretion of fatty acid binding protein aP2 from adipocytes through a nonclassical pathway in response to adipocyte lipase activity. J Lipid Res. 2015 Feb;56(2):423–34.

386. Ferrante SC, Nadler EP, Pillai DK, et al. Adipocyte-derived exosomal miRNAs: a novel mechanism for obesity-related disease. Pediatr Res. 2015 Mar;77(3):447–54.

387. Müller G, Jung C, Straub J, et al. Induced release of membrane vesicles from rat adipocytes containing glycosylphosphatidylinositol-anchored microdomain and lipid droplet signalling proteins. Cell Signal. 2009 Feb;21(2):324–38.

388. Müller G, Schneider M, Biemer-Daub G, et al. Upregulation of lipid synthesis in small rat adipocytes by microvesicle-associated CD73 from large adipocytes. Obesity (Silver Spring). 2011 Aug;19(8):1531–44.

389. Müller G, Schneider M, Biemer-Daub G, et al. Microvesicles released from rat adipocytes and harboring glycosylphosphatidylinositol-anchored proteins transfer RNA stimulating lipid synthesis. Cell Signal. 2011 Jul;23(7):1207–23.

390. Sano S, Izumi Y, Yamaguchi T, et al. Lipid synthesis is promoted by hypoxic adipocyte-derived exosomes in 3T3-L1 cells. Biochem Biophys Res Commun. 2014 Mar 7;445(2):327–33.

391. Koeck ES, Iordanskaia T, Sevilla S, et al. Adipocyte exosomes induce transforming growth factor beta pathway dysregulation in hepatocytes: a novel paradigm for obesity-related liver disease. J Surg Res. 2014

Dec;192(2):268–75.

392. Deng Z -b., Poliakov A, Hardy RW, et al. Adipose Tissue Exosome-Like Vesicles Mediate Activation of Macrophage-Induced Insulin Resistance. Diabetes. 2009 Aug 12;58(11):2498–505.

393. Aoki N, Yokoyama R, Asai N, et al. Adipocyte-derived microvesicles are associated with multiple angiogenic factors and induce angiogenesis in vivo and in vitro. Endocrinology. 2010 Jun;151(6):2567–76.

394. Martin PJ, Haren N, Ghali O, et al. Adipogenic RNAs are transferred in osteoblasts via bone marrow adipocytes-derived extracellular vesicles (EVs). BMC Cell Biol. 2015 Jan;16:10.

395. Harding C, Heuser J, Stahl P. Receptor-mediated endocytosis of transferrin and recycling of the transferrin receptor in rat reticulocytes. J Cell Biol. 1983 Aug;97(2):329–39.

396. Inokawa A, Inuzuka T, Takahara T, et al. Tubby-like protein superfamily member PLSCR3 functions as a negative regulator of adipogenesis in mouse 3T3-L1 preadipocytes by suppressing induction of late differentiation stage transcription factors. Biosci Rep. 2015 Jan;36(1).

397. Gernapudi R, Yao Y, Zhang Y, et al. Targeting exosomes from preadipocytes inhibits preadipocyte to cancer stem cell signaling in early-stage breast cancer. Breast Cancer Res Treat. 2015 Apr;150(3):685–95.

398. Fauré J, Lachenal G, Court M, et al. Exosomes are released by cultured cortical neurones. Mol Cell Neurosci. 2006 Apr;31(4):642–8.

399. Lai RC, Chen TS, Lim SK. Mesenchymal stem cell exosome: a novel stem cell-based therapy for cardiovascular disease. Regen Med. 2011 Jul;6(4):481–92.

400. Tanaka M, Nozaki M, Fukuhara A, et al. Visfatin is released from 3T3-L1 adipocytes via a non-classical pathway. Biochem Biophys Res Commun. 2007 Jul 27;359(2):194–201.

401. Kozak D, Anderson W, Vogel R, et al. Advances in Resistive Pulse Sensors: Devices bridging the void between molecular and microscopic detection. Nano Today. 2011 Oct 1;6(5):531–45.

402. Garbus J, Deluca HF, Loomans ME, et al. The rapid incorporation of phosphate into mitochondrial lipids. J Biol Chem. 1963;238:59–63.

403. Tatischeff I, Larquet E, Falcón-Pérez JM, et al. Fast characterisation of cell-derived extracellular vesicles by nanoparticles tracking analysis, cryo-electron microscopy, and Raman tweezers microspectroscopy. J Extracell vesicles. 2012 Jan;1.

404. Gardiner C, Harrison P, Belting M, et al. Extracellular vesicles, tissue factor, cancer and thrombosis - discussion themes of the ISEV 2014 Educational Day. J Extracell vesicles. 2015 Jan;4:26901.

405. Filipe V, Hawe A, Jiskoot W. Critical evaluation of Nanoparticle Tracking Analysis (NTA) by NanoSight for the measurement of nanoparticles and protein aggregates. Pharm Res. 2010 May;27(5):796–810.

406. Vogel R, Willmott G, Kozak D, et al. Quantitative sizing of nano/microparticles with a tunable elastomeric pore sensor. Anal Chem. 2011 May 1;83(9):3499–506.

407. van der Pol E, Coumans FAW, Grootemaat AE, et al. Particle size distribution of exosomes and microvesicles determined by transmission electron microscopy, flow cytometry, nanoparticle tracking analysis, and resistive pulse sensing. J Thromb Haemost. 2014 Jul;12(7):1182–92.

408. Orozco AF, Lewis DE. Flow cytometric analysis of circulating microparticles in plasma. Cytometry A. 2010 Jun;77(6):502–14.

409. van Ierssel SH, Van Craenenbroeck EM, Conraads VM, et al. Flow cytometric detection of endothelial microparticles (EMP): effects of centrifugation and storage alter with the phenotype studied. Thromb Res. 2010 Apr;125(4):332–9.

410. Vasudev R, Mathew S, Afonina N. Characterization of submicron (0.1-1 μm) particles in therapeutic proteins by nanoparticle tracking analysis. J Pharm Sci. 2015 May;104(5):1622–31.

411. Maas SLN, de Vrij J, van der Vlist EJ, et al. Possibilities and limitations of current technologies for quantification of biological extracellular vesicles and synthetic mimics. J Control Release. 2015 Feb 28;200:87–96.

412. Maas SLN, De Vrij J, Broekman MLD. Quantification and Size-profiling of Extracellular Vesicles Using Tunable Resistive Pulse Sensing. J Vis Exp. 2014 Oct 19;(92):e51623.

413. Dieckmann Y, Cölfen H, Hofmann H, et al. Particle size distribution measurements of manganese-doped ZnS nanoparticles. Anal Chem. 2009 May 15;81(10):3889–95.

414. Anderson W, Kozak D, Coleman VA, et al. A comparative study of submicron particle sizing platforms: accuracy, precision and resolution analysis of polydisperse particle size distributions. J Colloid Interface Sci. 2013 Sep 1;405:322–30.

415. Xu Y, Nakane N, Maurer-Spurej E. Novel test for microparticles in platelet-rich plasma and platelet concentrates using dynamic light scattering. Transfusion. 2011 Feb;51(2):363–70.

416. Roberts GS, Kozak D, Anderson W, et al. Tunable nano/micropores for particle detection and discrimination: scanning ion occlusion spectroscopy. Small. 2010 Dec 6;6(23):2653–8.

417. Willmott GR, Chaturvedi R, Cummins SJW, et al. Actuation of Tunable Elastomeric Pores: Resistance Measurements and Finite Element Modelling. Exp Mech. 2013 Sep 10;54(2):153–63.

418. Varga Z, Yuana Y, Grootemaat AE, et al. Towards traceable size determination of extracellular vesicles. J Extracell vesicles. 2014 Jan;3.

419. Lacroix R, Robert S, Poncelet P, et al. Standardization of platelet-derived microparticle enumeration by flow cytometry with calibrated beads: results of the International Society on Thrombosis and Haemostasis SSC Collaborative workshop. J Thromb Haemost. 2010 Nov 2;8(11):2571–4.

420. van der Pol E, Coumans FAW, Sturk A, et al. Refractive index determination of nanoparticles in suspension using nanoparticle tracking analysis. Nano Lett. 2014 Nov;14(11):6195–201.

421. Stoner SA, Duggan E, Condello D, et al. High sensitivity flow cytometry of membrane vesicles. Cytom Part A. 2015 Oct 20;n/a – n/a.

422. Freyssinet J-M, Toti F. Membrane microparticle determination: at least seeing what's being sized! J Thromb Haemost. 2010 Feb;8(2):311–4.

423. Gardiner C, Shaw M, Hole P, et al. Measurement of refractive index by nanoparticle tracking analysis reveals heterogeneity in extracellular vesicles. J Extracell vesicles. 2014 Jan;3:25361.

424. Chandler WL, Yeung W, Tait JF. A new microparticle size calibration standard for use in measuring smaller microparticles using a new flow cytometer. J Thromb Haemost. 2011 Jun 6;9(6):1216–24.

425. Nolte-'t Hoen ENM, van der Vlist EJ, de Boer-Brouwer M, et al. Dynamics of dendritic cell-derived vesicles: high-resolution flow cytometric analysis of extracellular vesicle quantity and quality. J Leukoc Biol. 2013 Mar;93(3):395–402.

426. Patil R, Ghosh K, Damania K, et al. Effect of anticoagulant therapy on cell-derived microparticles and pregnancy outcome in women with pregnancy loss. Br J Haematol. 2015 Apr 28;

427. Macey M, McCarthy D, Azam U, et al. Ethylenediaminetetraacetic acid plus citrate-theophylline-adenosine-dipyridamole (EDTA-CTAD): a novel anticoagulant for the flow cytometric assessment of platelet and neutrophil activation ex vivo in whole blood. Cytometry B Clin Cytom. 2003 Jan;51(1):30–40.

428. Yuana Y, Koning RI, Kuil ME, et al. Cryo-electron microscopy of extracellular vesicles in fresh plasma. J Extracell vesicles. 2013 Dec 31;2.

429. György B, Pálóczi K, Kovács A, et al. Improved circulating microparticle analysis in acid-citrate dextrose (ACD) anticoagulant tube. Thromb Res. 2014 Feb;133(2):285–92.

430. Davies RT, Kim J, Jang SC, et al. Microfluidic filtration system to isolate extracellular vesicles from blood. Lab Chip. 2012 Dec 21;12(24):5202–10.

431. Trummer A, De Rop C, Tiede A, et al. Recovery and composition of microparticles after snap-freezing depends on thawing temperature. Blood Coagul Fibrinolysis. 2009 Jan;20(1):52–6.

432. Weber H, Kollars M, Kyrle PA, et al. Comparison of different methods for isolation and storage of microparticles from human blood. J Thromb Haemost JTH [ABSTRACT]. 2007;5 (Supplem.

433. Greenberg AS, Obin MS. Obesity and the role of adipose tissue in inflammation and metabolism. Am J Clin Nutr. 2006;83(2):461S – 465S.

434. Kershaw EE, Flier JS. Adipose tissue as an endocrine organ. J Clin Endocrinol Metab. 2004 Jun;89(6):2548–56.

435. Bernlohr DA, Bolanowski MA, Kelly TJ, et al. Evidence for an increase in transcription of specific mRNAs during differentiation of 3T3-L1 preadipocytes. J Biol Chem. American Society for Biochemistry and Molecular Biology; 1985 May 10;260(9):5563–7.

436. Noda N, Honma S, Ohmiya Y. Hes1 is required for contact inhibition of cell proliferation in 3T3-L1 preadipocytes. Genes to Cells. 2011 Jun 12;16(6):704–13.

437. Azarnia R, Russell TR. Cyclic AMP effects on cell-to-cell junctional membrane permeability during adipocyte differentiation of 3T3-L1 fibroblasts. J Cell Biol. 1985 Jan;100(1):265–9.

438. Sinauridze EI, Kireev DA, Popenko NY, et al. Platelet microparticle membranes have 50- to 100-fold higher specific procoagulant activity than activated platelets. Thromb Haemost. 2007 Mar;97(3):425–34.

439. Gurr MI, Harwood JL, Frayn KN. Lipid Biochemistry. 5th ed. Blackwell Science; 2002. 95 p.

440. Zhou X, Wu W, Chen J, et al. AMP-activated protein kinase is required for the anti-adipogenic effects of alpha-linolenic acid. Nutr Metab (Lond). 2015 Jan;12:10.

441. Kyoung S, In J, Seong H, et al. Exosomes secreted during adipogenic differentiation of human adipose-derived stem cells induce adipogenesis of human adipose-derived stem cells. J Extracell vesicles [ABSTRACT]. 2015;PXIV2.

442. Zeghari N, Vidal H, Younsi M, et al. Adipocyte membrane phospholipids and PPAR-gamma expression in obese women: relationship to hyperinsulinemia. Am J Physiol Endocrinol Metab. 2000 Oct 1;279(4):E736–43.

443. Losito I, Patruno R, Conte E, et al. Phospholipidomics of Human Blood Microparticles. Anal Chem. 2013 Jul 2;85(13):6405–13.

444. Arisawa K, Ichi I, Yasukawa Y, et al. Changes in the phospholipid fatty acid composition of the lipid droplet during the differentiation of 3T3-L1 adipocytes. J Biochem. 2013 Sep;154(3):281–9.

445. Madsen L, Petersen RK, Kristiansen K. Regulation of adipocyte differentiation and function by polyunsaturated fatty acids. Biochim Biophys Acta. 2005 May 30;1740(2):266–86.

446. Ramstedt B, Slotte JP. Membrane properties of sphingomyelins. FEBS Lett. 2002 Oct;531(1):33–7.

447. Smith ER, Storch J. The adipocyte fatty acid-binding protein binds to membranes by electrostatic interactions. J Biol Chem. 1999 Dec 10;274(50):35325–30.

448. Gericke A, Smith ER, Moore DJ, et al. Adipocyte Fatty Acid-Binding Protein: Interaction with Phospholipid Membranes and Thermal Stability Studied by FTIR Spectroscopy †. Biochemistry. 1997 Jul 8;36(27):8311–7.

449. Blouin CM, Le Lay S, Eberl A, et al. Lipid droplet analysis in caveolin-deficient adipocytes: alterations in surface phospholipid composition and maturation defects. J Lipid Res. 2010 May;51(5):945–56.

450. Vance JE, Tasseva G. Formation and function of phosphatidylserine and phosphatidylethanolamine in mammalian cells. Biochim Biophys Acta. 2013 Mar;1831(3):543–54.

451. Jong OG de, Verhaar MC, Chen Y, et al. Cellular stress conditions are reflected in the protein and RNA content of endothelial cell-derived exosomes. Journal of Extracellular Vesicles. 2012.

452. Smas CM, Sul HS. Pref-1, a protein containing EGF-like repeats, inhibits adipocyte differentiation. Cell. 1993 May 21;73(4):725–34.

453. Park SY, Lee JH, Kim KY, et al. Cilostazol increases 3T3-L1 preadipocyte differentiation with improved glucose uptake associated with activation of peroxisome proliferator-activated receptor-gamma transcription. Atherosclerosis. 2008 Dec;201(2):258–65.

454. Lihn AS, Pedersen SB, Richelsen B. Adiponectin: action, regulation and association to insulin sensitivity. Obes Rev. 2005 Feb;6(1):13–21.

455. Hertzel A V, Bernlohr DA. The mammalian fatty acid-binding protein multigene family: molecular and genetic insights into function. Trends Endocrinol Metab. 2000 Jul;11(5):175–80.

456. Lee J-E, Moon P-G, Lee I-K, et al. Proteomic Analysis of Extracellular Vesicles Released by Adipocytes of Otsuka Long-Evans Tokushima Fatty (OLETF) Rats. Protein J. 2015 May 22;34(3):220–35.

457. Ramteke A, Ting H, Agarwal C, et al. Exosomes secreted under hypoxia enhance invasiveness and stemness of prostate cancer cells by targeting adherens junction molecules. Mol Carcinog. 2015 Jul;54(7):554–65.

458. Björntorp P. Adipose tissue distribution and function. Int J Obes. 1991 Sep;15 Suppl 2:67–81.

459. Trayhurn P, Wang B, Wood IS. Hypoxia in adipose tissue: a basis for the dysregulation of tissue function in obesity? Br J Nutr. 2008 Apr 9;100(02):227–35.

460. Xu H, Barnes GT, Yang Q, et al. Chronic inflammation in fat plays a crucial

role in the development of obesity-related insulin resistance. J Clin Invest. 2003 Dec;112(12):1821–30.

461. Frayn KN. Adipose tissue and the insulin resistance syndrome. Proc Nutr Soc. 2001 Aug;60(3):375–80.

462. Hosogai N, Fukuhara A, Oshima K, et al. Adipose tissue hypoxia in obesity and its impact on adipocytokine dysregulation. Diabetes. 2007 Apr;56(4):901–11.

463. Wang T, Gilkes DM, Takano N, et al. Hypoxia-inducible factors and RAB22A mediate formation of microvesicles that stimulate breast cancer invasion and metastasis. Proc Natl Acad Sci U S A. 2014 Aug 5;111(31):E3234–42.

464. Zhang H-C, Liu X-B, Huang S, et al. Microvesicles derived from human umbilical cord mesenchymal stem cells stimulated by hypoxia promote angiogenesis both in vitro and in vivo. Stem Cells Dev. 2012 Dec 10;21(18):3289–97.

465. Aga M, Bentz GL, Raffa S, et al. Exosomal HIF1α supports invasive potential of nasopharyngeal carcinoma-associated LMP1-positive exosomes. Oncogene. 2014 Mar 24;33(37):4613–22.

466. Fan G-C. Hypoxic exosomes promote angiogenesis. Blood. 2014 Dec 11;124(25):3669–70.

467. Hashimoto T, Yokokawa T, Endo Y, et al. Modest hypoxia significantly reduces triglyceride content and lipid droplet size in 3T3-L1 adipocytes. Biochem Biophys Res Commun. 2013 Oct 11;440(1):43–9.

468. Boden G. Role of fatty acids in the pathogenesis of insulin resistance and NIDDM. Diabetes. 1997 Jan;46(1):3–10.

469. Snodgrass RG, Boß M, Zezina E, et al. Hypoxia Potentiates Palmitate-induced Pro-inflammatory Activation of Primary Human Macrophages. J Biol Chem. 2015 Nov 17;

470. Aldridge A, Kouroupis D, Churchman S, et al. Assay validation for the assessment of adipogenesis of multipotential stromal cells--a direct comparison of four different methods. Cytotherapy. 2013 Jan;15(1):89–101.

471. Wysoczynski M, Ratajczak MZ. Lung cancer secreted microvesicles: underappreciated modulators of microenvironment in expanding tumors. Int J Cancer. 2009 Oct 1;125(7):1595–603.

472. Vince R V, Chrismas B, Midgley AW, et al. Hypoxia mediated release of endothelial microparticles and increased association of S100A12 with circulating neutrophils. Oxid Med Cell Longev. Jan;2(1):2–6.

473. Salomon C, Kobayashi M, Ashman K, et al. Hypoxia-induced changes in the bioactivity of cytotrophoblast-derived exosomes. PLoS One. 2013 Jan;8(11):e79636.

474. Milane L, Singh A, Mattheolabakis G, et al. Exosome Mediated Communication within the Tumor Microenvironment. J Control Release. 2015 Jul 2;219:278–94.

475. Weidemann A, Breyer J, Rehm M, et al. HIF-1α activation results in actin cytoskeleton reorganization and modulation of Rac-1 signaling in endothelial cells. Cell Commun Signal. 2013 Jan;11:80.

476. Burger D, Schock S, Thompson CS, et al. Microparticles: biomarkers and beyond. Clin Sci (Lond). 2013 Apr;124(7):423–41.

477. Duivenvoorde LPM, van Schothorst EM, Swarts HM, et al. A Difference in Fatty Acid Composition of Isocaloric High-Fat Diets Alters Metabolic Flexibility in Male C57BL/6JOlaHsd Mice. PLoS One. 2015 Jan;10(6):e0128515.

478. Bolsoni-Lopes A, Festuccia WT, Chimin P, et al. Palmitoleic acid (n-7) increases white adipocytes GLUT4 content and glucose uptake in association with AMPK activation. Lipids Health Dis. 2014 Jan;13:199.

479. Ackerman D, Simon MC. Hypoxia, lipids, and cancer: surviving the harsh tumor microenvironment. Trends Cell Biol. 2014 Aug;24(8):472–8.

480. Scoditti E, Massaro M, Carluccio MA, et al. Additive regulation of adiponectin expression by the mediterranean diet olive oil components oleic Acid and hydroxytyrosol in human adipocytes. PLoS One. 2015 Jan;10(6):e0128218.

481. Galindo-Hernandez O, Serna-Marquez N, Castillo-Sanchez R, et al. Extracellular vesicles from MDA-MB-231 breast cancer cells stimulated with linoleic acid promote an EMT-like process in MCF10A cells. Prostaglandins Leukot Essent Fatty Acids. 2014 Dec;91(6):299–310.

482. Alessi M-C, Poggi M, Juhan-Vague I. Plasminogen activator inhibitor-1, adipose tissue and insulin resistance. Curr Opin Lipidol. 2007 Jun;18(3):240–5.

483. Morange PE, Lijnen HR, Alessi MC, et al. Influence of PAI-1 on adipose tissue growth and metabolic parameters in a murine model of diet-induced obesity. Arterioscler Thromb Vasc Biol. 2000 Apr;20(4):1150–4.

484. Zhao G, Etherton TD, Martin KR, et al. Dietary alpha-linolenic acid reduces inflammatory and lipid cardiovascular risk factors in hypercholesterolemic men and women. J Nutr. 2004 Nov;134(11):2991–7.

485. O'Donnell VB, Murphy RC. New families of bioactive oxidized phospholipids generated by immune cells: identification and signaling actions. Blood. 2012 Sep 6;120(10):1985–92.

486. Marconescu A, Thorpe PE. Coincident exposure of phosphatidylethanolamine and anionic phospholipids on the surface of irradiated cells. Biochim Biophys Acta. 2008 Oct;1778(10):2217–24.

487. Li Z, Zhang H, Liu J, et al. Reducing plasma membrane sphingomyelin

increases insulin sensitivity. Mol Cell Biol. 2011 Oct 15;31(20):4205–18.

488. Higgins LH, Withers HG, Garbens A, et al. Hypoxia and the metabolic phenotype of prostate cancer cells. Biochim Biophys Acta. 2009 Dec;1787(12):1433–43.

489. Lamounier-Zepter V, Look C, Alvarez J, et al. Adipocyte fatty acid-binding protein suppresses cardiomyocyte contraction: a new link between obesity and heart disease. Circ Res. 2009 Aug 14;105(4):326–34.

490. Peeters W, de Kleijn DP V, Vink A, et al. Adipocyte fatty acid binding protein in atherosclerotic plaques is associated with local vulnerability and is predictive for the occurrence of adverse cardiovascular events. Eur Heart J. 2011 Jul;32(14):1758–68.

491. Wood IS, Stezhka T, Trayhurn P. Modulation of adipokine production, glucose uptake and lactate release in human adipocytes by small changes in oxygen tension. Pflugers Arch. 2011 Sep;462(3):469–77.

492. Wang B, Wood IS, Trayhurn P. Hypoxia induces leptin gene expression and secretion in human preadipocytes: differential effects of hypoxia on adipokine expression by preadipocytes. J Endocrinol. 2008 Jul;198(1):127–34.

493. Arita Y, Kihara S, Ouchi N, et al. Paradoxical Decrease of an Adipose-Specific Protein, Adiponectin, in Obesity. Biochem Biophys Res Commun. 1999 Apr;257(1):79–83.

494. Yu J, Shi L, Wang H, et al. Conditioned medium from hypoxia-treated adipocytes renders muscle cells insulin resistant. Eur J Cell Biol. 2011 Dec;90(12):1000–15.

495. Seo M-J, Lee Y-J, Hwang J-H, et al. The inhibitory effects of quercetin on obesity and obesity-induced inflammation by regulation of MAPK signaling. J Nutr Biochem. 2015 Nov;26(11):1308–16.

496. Whitlock G, Lewington S, Sherliker P, et al. Body-mass index and cause-specific mortality in 900 000 adults: collaborative analyses of 57 prospective studies. Lancet. 2009 Mar 28;373(9669):1083–96.

497. Calle EE, Rodriguez C, Walker-Thurmond K, et al. Overweight, obesity, and mortality from cancer in a prospectively studied cohort of U.S. adults. N Engl J Med. 2003 Apr 24;348(17):1625–38.

498. Shaikh SR, Haas KM, Beck MA, et al. The effects of diet-induced obesity on B cell function. Clin Exp Immunol. 2015 Jan;179(1):90–9.

499. Gordon S, Taylor PR. Monocyte and macrophage heterogeneity. Nat Rev Immunol. 2005 Dec;5(12):953–64.

500. Weisberg SP, McCann D, Desai M, et al. Obesity is associated with macrophage accumulation in adipose tissue. J Clin Invest. 2003 Dec;112(12):1796–808.

501. Gordon S. The role of the macrophage in immune regulation. Res Immunol.

Jan;149(7-8):685–8.

502. Oliveira AG, Araujo TG, Carvalho BM, et al. Acute exercise induces a phenotypic switch in adipose tissue macrophage polarization in diet-induced obese rats. Obesity. 2013 Dec 11;21(12):2545–56.

503. Elcombe SE, Naqvi S, Van Den Bosch MWM, et al. Dectin-1 Regulates IL-10 Production via a MSK1/2 and CREB Dependent Pathway and Promotes the Induction of Regulatory Macrophage Markers. Lang R, editor. PLoS One. Public Library of Science; 2013 Mar 22;8(3):e60086.

504. Willment JA, Lin H-H, Reid DM, et al. Dectin-1 expression and function are enhanced on alternatively activated and GM-CSF-treated macrophages and are negatively regulated by IL-10, dexamethasone, and lipopolysaccharide. J Immunol. 2003 Nov 1;171(9):4569–73.

505. Neels JG, Olefsky JM. Inflamed fat: what starts the fire? J Clin Invest. 2006 Jan;116(1):33–5.

506. Cinti S. Adipocyte death defines macrophage localization and function in adipose tissue of obese mice and humans. J Lipid Res. 2005 Sep 8;46(11):2347–55.

507. Aprahamian TR. Elevated adiponectin expression promotes adipose tissue vascularity under conditions of diet-induced obesity. Metabolism. 2013 Dec;62(12):1730–8.

508. Mosser DM, Edwards JP. Exploring the full spectrum of macrophage activation. Nat Rev Immunol. 2008 Dec;8(12):958–69.

509. Dayer J-M, Chicheportiche R, Juge-Aubry C, et al. Adipose tissue has anti-inflammatory properties: focus on IL-1 receptor antagonist (IL-1Ra). Ann N Y Acad Sci. 2006 Jun;1069:444–53.

510. Weisberg SP, Hunter D, Huber R, et al. CCR2 modulates inflammatory and metabolic effects of high-fat feeding. J Clin Invest. 2006 Jan;116(1):115–24.

511. Arner E, Mejhert N, Kulyté A, et al. Adipose tissue microRNAs as regulators of CCL2 production in human obesity. Diabetes. 2012 Aug;61(8):1986–93.

512. Kirk EA, Sagawa ZK, McDonald TO, et al. Monocyte chemoattractant protein deficiency fails to restrain macrophage infiltration into adipose tissue [corrected]. Diabetes. 2008 May;57(5):1254–61.

513. Jiang M, Zhang L, Ma X, et al. Tamoxifen inhibits macrophage FABP4 expression through the combined effects of the GR and PPARγ pathways. Biochem J. 2013 Sep 15;454(3):467–77.

514. Phoonsawat W, Aoki-Yoshida A, Tsuruta T, et al. Adiponectin is partially associated with exosomes in mouse serum. Biochem Biophys Res Commun. 2014 Jun 6;448(3):261–6.

515. Looze C, Yui D, Leung L, et al. Proteomic profiling of human plasma exosomes identifies PPARgamma as an exosome-associated protein. Biochem

Biophys Res Commun. 2009 Jan 16;378(3):433–8.

516. Ogawa R, Tanaka C, Sato M, et al. Adipocyte-derived microvesicles contain RNA that is transported into macrophages and might be secreted into blood circulation. Biochem Biophys Res Commun. 2010 Aug 6;398(4):723–9.

517. David S, Kümpers P, van Slyke P, et al. Mending leaky blood vessels: the angiopoietin-Tie2 pathway in sepsis. J Pharmacol Exp Ther. 2013 Apr;345(1):2–6.

518. Goldstein JL, Brown MS. The LDL receptor locus and the genetics of familial hypercholesterolemia. Annu Rev Genet. 1979 Jan;13:259–89.

519. Goldstein JL, Hobbs H, Brown M. Familial Hypercholesterolemia. 8th editio. Valle D, Scriver C, Beaudet A, editors. The metabolic and molecular basis of inherited disease. New York: McGraw-Hill; 2001. 2863-2913 p.

520. Grundy SM, Cleeman JI, Merz CNB, et al. Implications of recent clinical trials for the National Cholesterol Education Program Adult Treatment Panel III guidelines. Circulation. 2004 Jul 13;110(2):227–39.

521. Orsoni A, Villard EF, Bruckert E, et al. Impact of LDL apheresis on atheroprotective reverse cholesterol transport pathway in familial hypercholesterolemia. J Lipid Res. 2012 Apr;53(4):767–75.

522. Stoffel W, Borberg H, Greve V. Application of specific extracorporeal removal of low density lipoprotein in familial hypercholesterolaemia. Lancet. 1981 Nov 7;2(8254):1005–7.

523. Eisenhauer T, Armstrong VW, Wieland H, et al. Selective removal of low density lipoproteins (LDL) by precipitation at low pH: first clinical application of the HELP system. Klin Wochenschr. 1987 Feb 16;65(4):161–8.

524. Agishi T, Kaneko I, Hasuo Y, et al. Double filtration plasmapheresis. 1980. Ther Apher. 2000 Feb;4(1):29–33.

525. Otto C, Kern P, Bambauer R, et al. Efficacy and safety of a new whole-blood low-density lipoprotein apheresis system (Liposorber D) in severe hypercholesterolemia. Artif Organs. 2003 Dec;27(12):1116–22.

526. Kroon AA, Demacker PN, Kleinveld HA, et al. The rebound of lipoproteins after LDL-apheresis. Effects on chemical composition and LDL-oxidizability. Atherosclerosis. 1999 Nov 1;147(1):105–13.

527. Kroon AA, Aengevaeren WR, van der Werf T, et al. LDL-Apheresis Atherosclerosis Regression Study (LAARS). Effect of aggressive versus conventional lipid lowering treatment on coronary atherosclerosis. Circulation. 1996 May 15;93(10):1826–35.

528. Thompson GR, Miller JP, Breslow JL. Improved survival of patients with homozygous familial hypercholesterolaemia treated with plasma exchange. Br Med J (Clin Res Ed). 1985 Dec 14;291(6510):1671–3.

529. Seidel D. H.E.L.P. apheresis therapy in the treatment of severe

hypercholesterolemia: 10 years of clinical experience. Artif Organs. 1996 May;20(4):303–10.

530. Mabuchi H, Koizumi J, Shimizu M, et al. Long-term efficacy of low-density lipoprotein apheresis on coronary heart disease in familial hypercholesterolemia. Hokuriku-FH-LDL-Apheresis Study Group. Am J Cardiol. 1998 Dec 15;82(12):1489–95.

531. Gordon BR, Kelsey SF, Dau PC, et al. Long-term effects of low-density lipoprotein apheresis using an automated dextran sulfate cellulose adsorption system. Liposorber Study Group. Am J Cardiol. 1998 Mar 15;81(4):407–11.

532. Katopodis JN, Kolodny L, Jy W, et al. Platelet microparticles and calcium homeostasis in acute coronary ischemias. Am J Hematol. 1997 Feb;54(2):95–101.

533. Nomura S, Komiyama Y, Kagawa H, et al. Microparticles and coronary artery disease. Am J Hematol. 1997;56(4):296.

534. Barry OP, Kazanietz MG, Praticò D, et al. Arachidonic acid in platelet microparticles up-regulates cyclooxygenase-2-dependent prostaglandin formation via a protein kinase C/mitogen-activated protein kinase-dependent pathway. J Biol Chem. 1999 Mar 12;274(11):7545–56.

535. Hjuler Nielsen M, Irvine H, Vedel S, et al. Elevated atherosclerosis-related gene expression, monocyte activation and microparticle-release are related to increased lipoprotein-associated oxidative stress in familial hypercholesterolemia. PLoS One. 2015 Jan;10(4):e0121516.

536. Suades R, Padró T, Alonso R, et al. Lipid-lowering therapy with statins reduces microparticle shedding from endothelium, platelets and inflammatory cells. Thromb Haemost. 2013 Aug;110(2):366–77.

537. Umekita K, Hidaka T, Ueno S, et al. Leukocytapheresis (LCAP) decreases the level of platelet-derived microparticles (MPs) and increases the level of granulocytes-derived MPs: a possible connection with the effect of LCAP on rheumatoid arthritis. Mod Rheumatol. 2009 Jan;19(3):265–72.

538. Abdelhafeez AH, Jeziorczak PM, Schaid TR, et al. Clinical CVVH model removes endothelium-derived microparticles from circulation. J Extracell vesicles. 2014 Jan;3.

539. Lee WP, Datta BN, Ong BB, et al. Defining the role of lipoprotein apheresis in the management of familial hypercholesterolemia. Am J Cardiovasc Drugs. 2011 Dec 1;11(6):363–70.

540. Collins PW, Macchiavello LI, Lewis SJ, et al. Global tests of haemostasis in critically ill patients with severe sepsis syndrome compared to controls. Br J Haematol. 2006 Oct;135(2):220–7.

541. Georgescu A, Alexandru N, Andrei E, et al. Circulating microparticles and endothelial progenitor cells in atherosclerosis: pharmacological effects of irbesartan. J Thromb Haemost. 2012 Apr;10(4):680–91.

542. Suades R, Padró T, Alonso R, et al. Circulating CD45+/CD3+ lymphocyte-derived microparticles map lipid-rich atherosclerotic plaques in FH patients. Thromb Haemost. 2013 Oct 2;111(1).

543. Krauss RM, Burke DJ. Identification of multiple subclasses of plasma low density lipoproteins in normal humans. J Lipid Res. 1982 Jan;23(1):97–104.

544. Robert S, Poncelet P, Lacroix R, et al. Standardization of platelet-derived microparticle counting using calibrated beads and a Cytomics FC500 routine flow cytometer: a first step towards multicenter studies? J Thromb Haemost. 2009 Jan;7(1):190–7.

545. Ichijo M, Ishibashi S, Ohkubo T, et al. Elevated Platelet Microparticle Levels after Acute Ischemic Stroke with Concurrent Idiopathic Thrombocytopenic Purpura. J Stroke Cerebrovasc Dis. 2013 Jun 6;

546. Pereira J, Alfaro G, Goycoolea M, et al. Circulating platelet-derived microparticles in systemic lupus erythematosus. Association with increased thrombin generation and procoagulant state. Thromb Haemost. 2006 Jan;95(1):94–9.

547. Namba M, Tanaka A, Shimada K, et al. Circulating platelet-derived microparticles are associated with atherothrombotic events: a marker for vulnerable blood. Arterioscler Thromb Vasc Biol. 2007 Jan;27(1):255–6.

548. Nomura S, Suzuki M, Katsura K, et al. Platelet-derived microparticles may influence the development of atherosclerosis in diabetes mellitus. Atherosclerosis. 1995 Aug;116(2):235–40.

549. Sabatier F, Darmon P, Hugel B, et al. Type 1 and type 2 diabetic patients display different patterns of cellular microparticles. Diabetes. 2002 Sep;51(9):2840–5.

550. Tan KT, Tayebjee MH, Lim HS, et al. Clinically apparent atherosclerotic disease in diabetes is associated with an increase in platelet microparticle levels. Diabet Med. 2005 Dec;22(12):1657–62.

551. Nomura S, Tandon NN, Nakamura T, et al. High-shear-stress-induced activation of platelets and microparticles enhances expression of cell adhesion molecules in THP-1 and endothelial cells. Atherosclerosis. 2001 Oct;158(2):277–87.

552. Hansen SN, Harris WS. New evidence for the cardiovascular benefits of long chain omega-3 fatty acids. Curr Atheroscler Rep. 2007 Dec;9(6):434–40.

553. De Pascale C, Avella M, Perona JS, et al. Fatty acid composition of chylomicron remnant-like particles influences their uptake and induction of lipid accumulation in macrophages. FEBS J. 2006 Dec;273(24):5632–40.

554. Deng Z-B, Zhuang X, Ju S, et al. Exosome-like nanoparticles from intestinal mucosal cells carry prostaglandin E2 and suppress activation of liver NKT cells. J Immunol. 2013 May 1;190(7):3579–89.

555. Nielsen MH, Beck-Nielsen H, Andersen MN, et al. A flow cytometric method

for characterization of circulating cell-derived microparticles in plasma. J Extracell vesicles. 2014 Jan;3.

556.   Novelli F, Neri T, Tavanti L, et al. Procoagulant, tissue factor-bearing microparticles in bronchoalveolar lavage of interstitial lung disease patients: an observational study. PLoS One. 2014 Jan;9(4):e95013.

557.   Weiss R, Spittler A, Schmitz G, et al. Thrombocyte Adhesion and Release of Extracellular Microvesicles Correlate with Surface Morphology of Adsorbent Polymers for Lipid Apheresis. Biomacromolecules. 2014 May 30;

558.   Larson MC, Woodliff JE, Hillery CA, et al. Phosphatidylethanolamine is externalized at the surface of microparticles. Biochim Biophys Acta. 2012 Dec;1821(12):1501–7.

559.   Al Kaabi A, Traupe T, Stutz M, et al. Cause or effect of arteriogenesis: compositional alterations of microparticles from CAD patients undergoing external counterpulsation therapy. PLoS One. 2012 Jan;7(10):e46822.

560.   Lu H, Gao Z, Zhao Z, et al. Transient hypoxia reprograms differentiating adipocytes for enhanced insulin sensitivity and triglyceride accumulation. Int J Obes (Lond). 2016 Jan;40(1):121–8.

Appendices

Fatty acid	DAY 0			DAY 15		
	Cells (%)	EVs (%)	*p value*	Cells (%)	EVs (%)	*p value*
SFA	**39.96 ± 1.55**	**53.42 ± 4.49**	*<0.0001*	**51.81 ± 1.64**	**34.89 ± 4.65**	*<0.0001*
C14:0	0.43 ± 0.05	0.16 ± 0.13	*0.003*	3.27 ± 0.27	0.34 ± 0.16	*<0.0001*
C15:0	0.36 ± 0.07	0.67 ± 0.11	*0.0004*	0.36 ± 0.02	0.24 ± 0.08	*0.03*
C16:0	16.81± 0.47	23.45 ± 2.08	*0.0004*	44.22 ± 1.16	17.51 ± 3.67	*<0.0001*
C18:0	20.82 ± 0.70	26.12 ± 1.76	*0.0003*	3.79 ± 0.18	15.79 ± 0.65	*<0.0001*
C20:0	0.72 ± 0.18	2.19 ± 0.28	*<0.0001*	0.10 ± 0.00	0.79 ± 0.04	*<0.0001*
C24:0	0.82 ± 0.08	0.83 ± 0.13	*ns*	0.07 ± 0.01	0.22 ± 0.05	*0.003*
MUFA	**23.38 ± 1.39**	**24.75 ± 5.51**	*<0.0001*	**39.33 ± 1.35**	**26.51 ± 6.23**	*<0.001*
C14:1	0.15 ± 0.09	0.05 ± 0.09	*ns*	0.10 ± 0.02	0.04 ± 0.04	*0.02*
C16:1n9	1.88 ± 0.17	2.37 ± 0.31	*0.0004*	23.39 ± 0.67	7.21 ± 3.37	*<0.0001*
C16:1n7	1.31 ± 0.10	2.16 ± 0.67	*0.03*	ND	ND	-
C18:1n9	14.02 ± 0.65	11.63 ± 1.35	*0.006*	12.86 ± 0.51	14.96 ± 0.89	*0.003*
C18:1n7	3.69 ± 0.21	3.66 ± 0.16	*ns*	2.80 ± 0.13	1.11 ± 0.78	*0.008*
C20:1n9	0.74 ± 0.07	0.44 ± 0.11	*0.0004*	0.13 ± 0.01	2.98 ± 1.00	*0.003*
C22:1n9	ND	3.15 ± 2.58	-	ND	ND	-
C24:1n9	1.38 ± 0.10	1.29 ± 0.24	*ns*	0.05 ± 0.01	0.21± 0.15	*ns*
PUFA	**32.13 ± 2.39**	**19.34 ± 6.99**	*<0.0001*	**1.1 ± 0.1**	**37.54 ± 8.76**	*<0.0001*
C18:2n6	2.63 ± 0.37	12.05 ± 4.44	*0.003*	0.23 ± 0.01	32.80 ± 7.77	*0.0007*
C18:3n3	1.02 ± 0.60	1.09 ± 1.11	*ns*	0.05 ± 0.01	3.63 ±0.38	*<0.0001*
C20:2n6	3.57 ± 0.10	0.96 ± 0.18	*<0.0001*	0.12 ± 0.01	0.15 ± 0.05	*ns*
C20:3n3	1.40 ± 0.07	0.60 ± 0.13	*<0.0001*	ND	ND	-
C20:4n6	13.92 ± 0.68	2.91 ± 0.52	*<0.0001*	0.56 ± 0.04	0.63 ± 0.33	*ns*
C22:2	0.88 ± 0.04	0.28 ± 0.09	*<0.0001*	ND	ND	-
C22:3	1.81 ± 0.10	ND	-	ND	ND	-
C22:5n3	2.66 ± 0.19	0.63 ± 0.34	*<0.0001*	0.13 ± 0.01	0.21 ± 0.09	*ns*
C22:6n3	4.14 ± 0.24	0.82 ± 0.18	*<0.0001*	0.01 ± 0.02	0.15 ± 0.14	*ns*
Other	**2.93 ± 0.55**	**2.12 ± 0.38**	*ns*	**0.92 ± 0.05**	**0.74 ± 0.17**	*ns*
C16 Ac	2.18 ± 0.31	1.76 ± 0.30	*0.04*	0.53 ± 0.03	0.43 ± 0.13	*0.15*
C18 Ac	0.75 ± 0.24	0.36 ± 0.08	*0.009*	0.39 ± 0.02	0.31 ± 0.04	*0.009*

Table I: Cell to EV fatty acid analysis. Comparison of individual fatty acid proportions of 3T3-L1 cells and their corresponding EVs at day 0 (n=6) and day 15 (n=5). Ac = acetals; SFA = saturated fatty acid; MUFA = monounsaturated fatty acid; PUFA = polyunsaturated fatty acid; ND = not detected, ns = non-significant.

A

Fatty acids (% of total)	Day 0		Day 15	
	Cells	**EVs**	**Cells**	**EVs**
Phosphatidylethanolamine				
SFA	*16.6*	*32.5*	*25.6*	*37.9*
C16:0	3.2	11.0	15.7	16.4
C18:0	13.4	**20.9**	9.9	**17.8**
C20:0	-	0.6	-	0.9
C24:0	-	-	-	2.8
MUFA	*11.0*	*24.3*	*38.3*	*34.3*
C16:1n9	0.8	3.3	-	6.4
C16:1n7	0.7	1.3	**21.7**	11.5
C18:1n9	7.4	15.1	12.6	13.1
C18:1n7	2.1	3.8	4.0	3.3
C20:1n9	-	0.8	-	-
PUFA	*66.9*	*37.9*	*28.2*	*23.0*
C18:2n6	0.9	1.7	0.8	0.7
C18:3n3	0.7	5.2	-	8.8
C20:2n6	7.4	4.3	1.4	1.3
C20:3n6	1.5	1.7	-	0.6
C20:4n6	**37.7**	13.5	13.9	7.8
C20:5n3	5.4	1.5	3.1	1.4
C22:2n6	2.1	1.3	-	-
C22:3n3	4.2	2.5	-	-
C22:4n6	0.9	-	-	-
C22:5n3	6.1	3.0	2.6	-
C22:6n3	-	3.2	6.4	2.4
Other	*4.2*	*4.6*	*5.0*	*3.9*
C16 acetals	4.2	4.6	5.0	3.9

B

Fatty acids (% of total)	Day 0		Day 15	
	Cells	EVs	Cells	EVs
Sphingomyelin				
SFA	*67.3*	*62.6*	*81.3*	*61.8*
C14:0	-	0.7	0.6	0.9
C16:0	26.9	**34.8**	**44.4**	**31.6**
C18:0	15.1	17.7	16.1	16.9
C20:0	4.9	3.3	5.8	2.8
C22:0	8.9	6.1	10.5	4.9
C24:0	11.5	-	3.9	4.7
MUFA	*30.9*	*6.2*	*12.6*	*14.1*
C16:1n9	0.9	4.4	1.9	7.9
C16:1n7	0.6	-	1.4	-
C18:1n9	0.6	1.8	0.9	1.9
C24:1n9	**28.8**	-	8.4	4.3
PUFA	*1.9*	*31.4*	*5.8*	*24.0*
C18:2n6	-	0.7	-	0.6
C18:3n3	-	0.8	1.7	-
C18:3n6	1.9	7.7	2.9	8.7
C20:2n6	-	1.6	-	2.2
C20:3n6	-	-	-	0.6
C20:4n6	-	-	-	-
C22:3n3	-	-	1.2	3.8
C22:4n6	-	-	-	8.1
C22:5n3	-	8.2	-	-
C22:6n3	-	12.4	-	-

C

Fatty acids (% of total)	Day 0		Day 15	
	Cells	EVs	Cells	EVs
Phosphatidylcholine				
SFA	*37.3*	*52.1*	*41.1*	*48.7*
C14:0	-	0.7	-	0.6
C16:0	**21.8**	**37.8**	29.7	**30.9**
C18:0	15.5	13.6	11.4	17.2
MUFA	*30.3*	*36.4*	*52.9*	*43.1*
C16:1n9	2.3	3.9	0.6	2.1
C16:1n7	1.6	1.9	**32.1**	20.6
C18:1n9	18.4	22.9	15.0	14.8
C18:1n7	7.4	7.1	5.2	5.6
C20:1n9	0.6	0.6	-	-
PUFA	*28.9*	*9.6*	*4.6*	*6.3*
C18:2n6	2.7	1.8	0.5	0.7
C18:3n3	-	1.2	0.3	2.9
C20:2n6	3.6	1.0	0.5	-
C20:3n6	1.8	0.9	0.3	-
C20:4n6	13.6	2.9	2.0	1.4
C20:5n3	2.1	-	0.5	-
C22:2n6	-	-	0.0	-
C22:3n3	1.0	-	0.1	-
C22:5n3	1.5	0.9	0.3	0.6
C22:6n3	2.6	0.9	0.6	0.7
Other	*1.1*	*-*	*-*	*-*
C16 acetals	1.1	-	-	-

D

Fatty acids (% of total)	Day 0 Cells	Day 15 Cells
Cardiolipin		
SFA	*26.7*	*11.3*
C16:0	12.1	7.4
C18:0	14.6	3.9
MUFA	*35.4*	*79.0*
C16:1n9	2.4	-
C16:1n7	2.6	**54.6**
C18:1n9	**19.4**	14.1
C18:1n7	11.0	10.3
PUFA	*36.3*	*7.2*
C18:2n6	9.6	2.2
C18:3n3	4.3	1.6
C20:2n6	2.3	-
C20:3n6	4.2	0.8
C20:4n6	9.9	1.7
C20:5n3	1.5	-
C22:3n3	0.9	-
C22:4n6	-	-
C22:5n3	1.3	-
C22:6n3	2.3	0.9
Other	*0.8*	*0.8*
C16 acetals	0.8	0.8

E

Fatty acids (% of total)	Day 0		Day 15	
	Cells	EVs	Cells	EVs
Phosphatidylserine				
SFA	*46.0*	*59.0*	*49.3*	*62.5*
C14:0	-	-	-	1.5
C16:0	1.0	13.0	7.3	22.9
C18:0	**43.8**	**44.2**	**42.0**	**33.4**
C20:0	-	1.1	-	-
C22:0	0.6	-	-	-
C24:0	0.6	0.7	-	4.7
MUFA	*22.3*	*24.5*	*33.7*	*18.2*
C16:1n9	0.7	3.4	0.7	7.0
C16:1n7	-	-	15.7	3.9
C18:1n9	18.6	16.4	12.8	7.3
C18:1n7	2.4	3.5	3.8	-
C20:1n9	0.6	-	-	-
C24:1n9	-	1.2	0.7	-
PUFA	*30.2*	*14.9*	*15.1*	*19.3*
C18:2n6	1.3	1.3	0.9	1.1
C18:3n6	-	0.9	-	-
C18:3n3	0.7	6.8	1.6	13.1
C20:2n6	2.2	0.6	-	4.4
C20:3n6	3.3	1.8	0.6	-
C20:4n6	8.1	1.4	3.2	0.7
C20:5n3	0.6	-	-	-
C22:2n6	1.3	0.6	-	-
C22:3n3	3.0	-	0.9	-
C22:5n3	4.5	0.7	2.8	-
C22:6n3	5.2	0.8	5.1	-

F

Fatty acids(% of total)	Day 0		Day 15	
	Cells	EVs	Cells	EVs
Phosphatidylinositol				
SFA	*43.1*	*54.9*	*39.3*	*65.1*
C14:0	-	0.6	-	0.8
C16:0	1.6	17.5	**19.9**	21.5
C18:0	**41.5**	**36.8**	19.4	**34.3**
C20:0	-	-	-	1.6
C24:0	-	-	-	6.9
MUFA	*7.1*	*19.5*	*33.1*	*11.2*
C16:1n9	-	8.9	-	3.8
C16:1n7	-	-	7.6	-
C18:1n9	5.5	8.9	18.3	7.4
C18:1n7	1.6	1.7	7.2	-
PUFA	*49.2*	*25.2*	*26.0*	*23.7*
C18:2n6	-	1.1	0.7	0.8
C18:3n3	1.1	17.1	1.0	15.2
C20:2n6	9.9	2.4	3.2	4.5
C20:3n6	1.1	-	0.7	1.2
C20:4n6	30.0	4.6	14.9	2.0
C20:5n3	1.4	-	1.9	-
C22:2n6	0.6	-	-	-
C22:3n3	1.3	-	0.6	-
C22:5n3	2.2	-	1.5	-
C22:6n3	1.6	-	1.5	-

Table II: Phospholipid fatty acid compositions following adipogenesis. Individual phospholipids from cells and EVs pre- and post-adipogenesis were separated using 2D-TLC and then subjected to GC. Compositions of individual fatty acids are presented for (**A**) phosphatidylethanolamine; (**B**) sphingomyelin; (**C**) phosphatidylcholine; (**D**) cardiolipin; (**E**) phosphatidylserine; and (**F**) phosphatidylinositol. Only fatty acids >0.5% are presented. Totals of saturated, monounsaturated and polyunsaturated fatty acids (SFA, MUFA and PUFA respectively) are given (n=1).

Fatty acid	O₂ condition					
	Normoxia	**1%**	**2%**	**5%**	**10%**	**21%**
SFA	48.1 ± 2.6	*52.6 ± 1.2*	50.7 ± 0.2	*52.2 ± 2.4*	45.1 ± 0.8	*43.1 ± 1.4*
C14:0	2.9 ± 0.3	3.2 ± 0.2	2.5 ± 0.09	3.2 ± 0.3	3.0 ± 0.03	2.8 ± 0.2
C16:0	42.0 ± 2.0	*45.2 ± 0.9*	*44.0 ± 0.07*	*45.4 ± 2.0*	41.9 ± 0.8	*37.2 ± 1.2*
C18:0	3.1 ± 0.2	*4.3 ± 0.05*	*4.3 ± 0.07*	3.6 ± 0.2	3.2 ± 0.02	3.1 ± 0.1
MUFA	49.2 ± 2.9	*41.4 ± 1.2*	*45.6 ± 0.2*	*45.2 ± 2.1*	49.0 ± 0.6	*53.1 ± 1.7*
C14:1	0.6 ± 0.1	0.5 ± 0.1	0.5 ± 0.02	0.3 ± 0.1	0.5 ± 0.03	0.8 ± 0.2
C16:1n9	0.6 ± 0.1	0.9 ± 0.01	0.7 ± 0.03	0.4 ± 0.06	0.5 ± 0.02	0.8 ± 0.05
C16:1n7	32.9 ± 1.5	*27.8 ± 0.9*	*27.6 ± 0.1*	*29.4 ± 1.2*	33.3 ± 0.4	*35.5 ± 0.9*
C18:1n9	12.1 ± 0.8	12.3 ± 0.1	*13.6 ± 0.08*	11.9 ± 0.4	11.4 ± 0.06	11.9 ± 0.2
C18:1n7	3.2 ± 0.5	2.9 ± 0.1	3.2 ± 0.02	3.2 ± 0.3	3.4 ± 0.1	4.2 ± 0.4
PUFA	1.4 ± 0.4	1.3 ± 0.03	1.9 ± 0.04	1.4 ± 0.2	1.6 ± 0.1	1.9 ± 0.2
C18:3n3	0.3 ± 0.06	0.3 ± 0.01	0.3 ± 0.01	0.2 ± 0.04	0.3 ± 0.02	0.4 ± 0.05
C20:4n6	0.6 ± 0.2	0.6 ± 0.01	0.9 ± 0.03	0.6 ± 0.07	0.7 ± 0.04	0.8 ± 0.08
C20:5n3	0.2 ± 0.05	0.2 ± 0.00	0.2 ± 0.01	0.2 ± 0.03	0.2 ± 0.02	0.2 ± 0.02
C22:5n3	0.1 ± 0.05	0.1 ± 0.01	0.2 ± 0.01	0.1 ± 0.01	0.1 ± 0.01	0.2 ± 0.02
C22:6n3	0.3 ± 0.06	0.2 ± 0.01	0.4 ± 0.03	0.3 ± 0.02	0.3 ± 0.02	0.3 ± 0.02

Table III: Fatty acid composition of hypoxic cells. Compositional changes in cellular fatty acids between normoxic controls and hypoxic conditions. Data are presented as the mean percentage composition ± standard deviation. Significant changes ($p<0.05$) from normoxic values are in bold italics. Normoxia (n=15), 1, 2, 5, 10, 21% O_2 (n=3). SFA = saturated fatty acids; MUFA = monounsaturated fatty acids; PUFA = polyunsaturated fatty acids.

Fatty acid	O₂ condition					
	Normoxia	**1%**	**2%**	**5%**	**10%**	**21%**
SFA	51.2 ± 6.9	59.1 ± 0.1	46.3 ± 0.02	48.0 ± 0.06	49.7 ± 0.02	56.8 ± 8.3
C14:0	0.6 ± 0.6	1.5 ± 0.0	1.6 ±0.0	ND	ND	0.5 ± 0.9
C16:0	36.2 ± 2.6	*40.5 ± 0.1*	34.3 ± 0.01	32.7 ± 0.03	37.3 ± 0.01	*45.1 ± 3.0*
C18:0	14.5 ± 3.7	17.1 ± 0.1	*10.3 ± 0.0*	15.3 ± 0.03	12.4 ± 0.01	11.2 ± 4.4
MUFA	39.1 ± 12.1	31.6 ± 0.2	46.1 ± 0.03	44.2 ± 0.06	44.0 ± 0.03	37.7 ± 4.6
C14:1	0.1 ± 0.2	0.4 ± 0.0	0.9 ± 0.01	ND	ND	0.1 ± 0.2
C16:1n9	0.6 ± 0.5	0.4 ± 0.01	1.0 ± 0.0	ND	0.4 ± 0.0	0.2 ± 0.4
C16:1n7	19.2 ± 6.4	*8.3 ± 0.1*	*26.2 ± 0.01*	20.7 ± 0.03	*23.8 ± 0.01*	20.6 ± 2.6
C18:1n9	13.1 ± 2.4	*16.9 ± 0.03*	13.1 ± 0.01	15.0 ± 0.01	13.4 ± 0.01	11.5 ± 0.5
C18:1n7	4.6 ± 1.4	5.0 ± 0.01	4.5 ± 0.0	6.1 ± 0.01	4.9 ± 0.0	4.4 ± 0.3
C20:1n9	1.5 ± 1.3	0.7 ± 0.0	0.4 ± 0.0	2.5 ± 0.01	1.4 ± 0.0	0.9 ± 0.6
PUFA	8.6 ± 12.6	7.4 ± 0.02	5.1 ± 0.01	6.9 ± 0.01	4.7 ± 0.01	3.9 ± 1.5
C18:2n6	0.6 ± 0.5	1.3 ± 0.0	ND±	0.7 ± 0.0	0.5 ± 0.0	0.3 ± 0.2
C18:3n3	2.4 ± 1.3	3.6 ± 0.01	2.0 ± 0.0	2.5 ± 0.01	1.3 ± 0.0	1.0 ± 0.6
C20:2n6	0.4 ± 0.3	0.6 ± 0.0	0.3 ± 0.0	0.5 ±0.0	0.5 ± 0.0	0.5 ± 0.1
C20:4n6	1.6 ± 0.6	1.4 ± 0.0	2.0 ± 0.0	2.3 ± 0.01	1.9 ± 0.0	1.7 ± 0.4
C20:5n3	2.1 ± 5.5	0.6 ± 0.0	0.3 ± 0.0	0.6 ± 0.0	0.5 ± 0.0	0.4 ± 0.1
C22:6n3	1.9 ± 4.6	ND	0.5 ± 0.0	0.4 ± 0.0	0.03 ± 0.0	ND

Table IV: EV fatty acid composition. Compositional changes in EV fatty acids between normoxia and hypoxia. Data are presented as the mean percentage composition ± SD. Significant changes ($p<0.05$) from normoxic values are in bold italics. Normoxia (n=15), 1, 2, 5, 10, 21% O₂ (n=3), ND = not detected; SFA = saturated fatty acids; MUFA = monounsaturated fatty acids; PUFA = polyunsaturated fatty acids.

Fatty acid	Normoxia			Hypoxia (1% O₂)		
	Cells (%)	EVs (%)	*p value*	Cells (%)	EVs (%)	*p value*
SFA	48.1 ± 2.6	51.2 ± 6.9	-	52.6 ± 1.2	59.1 ± 0.1	****
C14:0	2.9 ± 0.3	0.6 ± 0.6	*	3.2 ± 0.2	1.5 ± 0.0	****
C16:0	42.0 ± 2.0	36.2 ± 2.6	****	45.2 ± 0.9	40.5 ± 0.1	****
C18:0	3.1 ± 0.2	14.5 ± 3.7	****	4.3 ± 0.1	17.1 ± 0.1	****
MUFA	49.2 ± 2.9	39.1 ± 12.1	**	41.4 ± 1.2	31.6 ± 0.2	****
C16:1n7	32.9 ± 1.5	19.2 ± 6.4	****	27.8 ± 0.9	8.3 ± 0.1	****
C18:1n9	-	-	-	12.3 ± 0.1	16.9 ± 0.0	****
C18:1n7	-	-	-	2.9 ± 0.1	5.0 ± 0.0	****
C20:1n9	ND	1.5 ± 1.3	-	ND	0.7 ± 0.0	**
PUFA	1.4 ± 0.4	9.0 ± 12.6	*	1.3 ± 0.0	7.4 ± 0.0	****
C18:2n6	ND	0.6 ± 0.5	-	ND	1.3 ± 0.0	****
C18:3n3	-	-	-	0.3 ± 0.0	3.6 ± 0.0	****
C20:2n6	ND	0.4 ± 0.3	-	ND	0.6 ± 0.0	*
C20:4n6	-	-	-	0.6 ± 0.0	1.4 ± 0.0	***
C22:5n3	0.1 ± 0.1	ND	-	0.1 ± 0.0	ND	-

Table V: Composition of cell versus EVs in hypoxia. Significant changes in fatty acid composition of normoxic and hypoxic cells versus their corresponding EVs. Values are given as a percentage of the total fatty acid composition. *$p<0.05$, **$p<0.01$, ***$p<0.001$, ****$p<0.0001$. Normoxia (n=15), hypoxia (n=3), '-' indicates no change, ND = not detected (or below 0.05%).

A

Fatty acid (% total)	Cells		EVs	
	Normoxia	Hypoxia	Normoxia	Hypoxia
Phosphatidylethanolamine				
SFA	*23.10*	*22.04*	***43.38***	*27.51*
C15:0	-	-	0.99	0.51
C16:0	13.36	11.23	**27.49**	11.91
C18:0	9.74	10.81	14.38	**15.09**
C20:0	-	-	0.52	-
MUFA	*34.54*	*32.25*	*37.39*	*29.79*
C16:1n9	-	-	1.67	1.63
C16:1n7	**20.73**	**17.65**	18.37	13.21
C18:1n9	9.41	9.05	12.33	11.12
C18:1n7	4.40	5.55	5.02	3.83
PUFA	*28.11*	*31.24*	*14.18*	*31.84*
C18:2n6	0.81	1.00	0.74	-
C18:3n3	-	0.61	6.32	5.60
C20:2n6	1.33	1.80	4.50	1.95
C20:3n3	-	-	-	0.73
C20:4n6	12.38	13.76	-	11.96
C20:5n3	4.53	4.71	1.48	3.79
C22:2n6	-	0.53	-	-
C22:5n3	2.26	2.61	-	2.96
C22:6n3	6.80	6.22	1.14	4.85
Acetals	11.46	12.00	3.26	8.78
C16 acetals	8.22	8.22	2.26	7.84
C18 acetals	3.24	3.78	1.00	0.94

B

Fatty acid (% total)	Cells		EVs	
	Normoxia	Hypoxia	Normoxia	Hypoxia
Sphingomyelin				
SFA	*78.85*	*74.42*	*65.79*	*71.41*
C14:0	0.64	0.68	-	-
C15:0	0.50	0.59	1.23	0.57
C16:0	**43.68**	**38.99**	**31.80**	**34.53**
C18:0	10.68	11.70	21.23	13.38
C20:0	4.51	3.87	-	3.90
C22:0	9.94	9.55	6.45	9.83
C24:0	8.90	9.04	5.26	9.20
MUFA	*12.87*	*16.26*	*19.76*	*13.60*
C16:1n9	0.53	0.80	2.84	1.53
C16:1n7	2.19	4.24	4.61	-
C18:1n9	1.02	1.85	6.05	1.19
C18:1n7	0.59	1.00	1.52	0.57
C24:1n9	8.54	8.37	4.74	10.31
PUFA	*7.40*	*7.06*	*13.45*	*13.76*
C18:3n6	1.41	0.95	-	1.25
C18:3n3	3.80	4.05	11.68	9.29
C20:2n6	0.72	0.79	1.77	2.12
C22:3n3	1.47	1.27	-	1.10
Acetals	*-*	*0.71*	*-*	*-*
C16 acetals	-	0.71	-	-

C

Fatty acid (% total)	Cells		EVs	
	Normoxia	Hypoxia	Normoxia	Hypoxia
Phosphatidylcholine				
SFA	*37.22*	*40.88*	***44.06***	*41.90*
C14:0	0.42	0.72	-	-
C16:0	28.15	29.98	**25.86**	**28.42**
C18:0	8.65	10.18	15.50	13.48
MUFA	*53.89*	*49.34*	*43.55*	***44.91***
C16:1n9	-	-	2.00	1.30
C16:1n7	**34.81**	**30.57**	17.65	20.30
C18:1n9	12.42	11.12	15.74	15.31
C18:1n7	6.66	7.65	8.16	8.00
PUFA	*5.37*	*5.59*	*12.46*	*10.07*
C18:2n6	0.63	0.76	0.95	0.88
C18:3n3	-	-	5.48	1.83
C20:2n6	0.52	0.52	-	0.57
C20:3n3	-	-	0.87	0.78
C20:4n6	2.42	2.60	2.31	2.66
C20:5n3	1.03	0.93	0.64	0.71
C22:5n3	-	-	1.12	1.21
C22:6n3	0.77	0.78	1.09	1.43
Acetals	*0.72*	*0.99*	*0.90*	*0.61*
C16 acetals	0.72	0.99	0.90	0.61

D

Fatty acid (% total)	Cells		EVs	
	Normoxia	Hypoxia	Normoxia	Hypoxia
Cardiolipin				
SFA	*15.01*	**69.11**	*46.51*	*58.35*
C14:0	0.81	-	0.83	0.54
C15:0	0.74	1.03	1.89	1.29
C16:0	9.01	19.56	**29.71**	18.22
C18:0	3.45	**45.87**	11.52	**24.70**
C20:0	-	1.25	0.79	0.90
C22:0	-	1.40	-	-
C24:0	-	-	1.77	12.70
MUFA	*75.78*	*22.71*	*35.22*	*23.61*
C14:1	-	0.93	-	-
C16:1n9	-	-	3.25	5.47
C16:1n7	**59.42**	6.97	19.61	12.43
C18:1n9	9.10	6.55	10.35	5.71
C18:1n7	7.26	6.14	2.01	-
C24:1n9	-	2.12	-	-
PUFA	*6.99*	*5.75*	*15.79*	*16.56*
C18:2n6	1.45	1.12	0.64	-
C18:3n3	4.07	2.18	12.82	13.07
C20:2n6	-	1.89	2.33	2.70
C20:3n3	0.57	-	-	-
C20:4n6	0.90	0.56	-	0.79

E

Fatty acid (% total)	Cells		EVs	
	Normoxia	Hypoxia	Normoxia	Hypoxia
Phosphatidylserine				
SFA	*42.20*	*49.34*	*39.75*	*49.06*
C15:0	-	0.54	1.75	1.91
C16:0	10.35	7.28	17.14	18.04
C18:0	**31.83**	**40.96**	20.86	**27.99**
C20:0	-	-	-	1.12
C22:0	-	0.56	-	-
MUFA	*31.78*	*26.52*	*26.94*	*27.31*
C16:1n9	0.64	1.08	5.38	6.51
C16:1n7	14.04	12.66	4.88	3.33
C18:1n9	12.49	9.12	12.17	13.95
C18:1n7	4.61	3.66	4.51	3.52
PUFA	*22.69*	*21.11*	*31.88*	*22.53*
C18:2n6	0.95	0.80	0.68	1.16
C18:3n3	3.18	6.53	**21.07**	9.73
C20:2n6	1.63	1.89	4.00	2.85
C20:3n3	0.85	0.80	-	-
C20:4n6	8.35	4.28	6.13	7.52
C20:5n3	1.69	0.79	-	1.27
C22:2n6	0.60	0.63	-	-
C22:5n3	2.11	2.14	-	-
C22:6n3	3.33	3.25	-	-

F

Fatty acid	Cells		EVs	
(% total)	Normoxia	Hypoxia	Normoxia	Hypoxia
Phosphatidylinositol				
SFA	*34.41*	*39.08*	*51.91*	*50.89*
C14:0	-	2.25	-	-
C15:0	1.10	0.71	1.25	0.88
C16:0	16.36	16.85	12.88	11.69
C18:0	**16.95**	**19.27**	**37.78**	**37.72**
C20:0	-	-	-	0.60
MUFA	*28.43*	*29.17*	*24.26*	*29.29*
C16:1n9	-	-	4.57	1.88
C16:1n7	7.24	8.79	7.36	11.72
C18:1n9	15.86	13.14	10.26	11.56
C18:1n7	5.33	7.24	2.07	4.13
PUFA	*34.80*	*27.29*	*21.71*	*18.24*
C18:2n6	-	1.38	-	0.56
C18:3n3	9.31	6.96	16.51	9.01
C20:2n6	3.33	2.74	2.86	1.42
C20:3n3	0.75	0.85	-	-
C20:4n6	15.16	10.01	2.34	3.32
C20:5n3	3.16	2.30	-	-
C22:3n3	-	0.82	-	-
C22:5n3	1.39	1.07	-	1.90
C22:6n3	1.70	1.16	-	2.03

Table VI: Phospholipid fatty acid composition of hypoxic and normoxic adipocytes. Individual fatty acids compositions of (**A**) PE; (**B**) sphingomyelin; (**C**) PC; (**D**) cardiolipin; (**E**) PS; and (**F**) PI. Only fatty acids >0.5% are presented. The most abundant individual fatty acid and class are highlighted in bold for each sample. Totals of saturated, monounsaturated and polyunsaturated fatty acids (SFA, MUFA and PUFA respectively) are given (n=1).

Gene	Forward primer sequence	Reverse primer sequence
GAPDH	5'-CATTGACCTCAACTACATG-3'	5'-TCTCCATGGTGGTGAAGAC-3'
IL-10	5'-ACGGCGCTGTCATCGATT-3'	5'- TGGAGCTTATTAAAGGCATTCTTC-3'
IL-1Ra	5'- GGCCTCCGCAGTCACC-TAATCAC-3'	5'- GGACAGGCACATCTTCCCTCCAT-3'
Dectin-1	5'-GGAAGCAACACATTGGAGAATGG-3'	5'-CTTTGGTAGGAGTCACACTGTC-3'

Table VII: qRT-PCR primers. Details of the primers used for qRT-PCR.